Real-time Characterization of Transcription Initiation Intermediates for *E. coli* RNA Polymerase Using Fast Footprinting and Equilibrium and Stopped-flow Fluorescence

By

Sara Elizabeth Heitkamp

A dissertation submitted in partial fulfillment of

the requirements for the degree of

Doctor of Philosophy

(Biochemistry)

at the

UNIVERSITY OF WISCONSIN-MADISON

2012

Date of final oral examination: 07/26/2012

Final Oral Committee:

Dr. M. Thomas Record, Jr., Professor, Chemistry and Biochemistry
Dr. Tricia Kiley, Professor, BMC
Dr. Robert Landick, Professor, Biochemistry
Dr. Sam Butcher, Biochemistry
Dr. Michael Cox, Biochemistry

Abstract

The pathway by which *E. coli* RNA polymerase (RNAP) forms initiation-capable open complexes (I_3 and RP_o) at the bacteriophage λP_R promoter involves at least two key intermediates (designated I_1, I_2). We used equilibrium and time-resolved footprinting and fluorescence assays to characterize these intermediates and to dissect the detailed mechanism of initiation at λP_R. HO• snapshots show that I_1 forms rapidly (in < 0.1 s); however, fast MnO_4^- footprinting at 19°C reveals no reactivity of any DNA bases in I_1, indicating that promoter DNA in the cleft is still duplex.

We report FRET-monitored equilibrium titrations at 2°C where I_1 is the only promoter complex, and at 10, 19 and 37°C to compare FRET effects in open complexes at these temperatures. Both equilibrium FRET measurements on I_1 at 2°C and the initial phase of real-time association kinetic experiments at 19°C exhibit large FRET effects, providing compelling evidence for bending and wrapping of both upstream and downstream duplex promoter DNA on RNAP in the initial closed intermediate. Our results suggest that upstream wrapping occurs soon after formation of the HO•-detected I_1 complex but before base-flipping of -11A and DNA opening in the cleft. We also monitored changes in stopped-flow fluorescence of the σ^{70} subunit during transcription initiation at the λP_R promoter using intrinsic and "beacon" probes. From comparisons of the two assays, we deduce that the two exponential phases in intrinsic and TMR fluorescence represent the decay-to-equilibrium formation of a late species of I_1 in which the -11 A base is flipped out of the bent duplex; the slow phase represents the conversion of these I_1 species to open complexes.

These results support the proposal that RNAP is a molecular isomerization machine that, after initial specific binding, first bends the DNA duplex toward the cleft to form a bent closed intermediate $I_{1,B}$ detected by fast HO• footprinting. Subsequent upstream bending and wrapping converts $I_{1,B}$ to $I_{1,W}$. Next, base flipping converts $I_{1,W}$ to $I_{1,F}$. $I_{1,F}$ is poised to open in the rate-determining step in the cleft to form the initial, relatively unstable open intermediate I_2. Finally, assembly of downstream mobile elements on the downstream DNA duplex form the more stable open complexes (I_3, RP_o), which are also wrapped.

Table of Contents

Abstract..... i

Table of Contents..... iii

List of Tables.....viii

List of Figures.....ix

Acknowledgements.....xii

Chapter 1: Introduction.....1

Basics of Transcription.....2

Structure and Function of RNAP.....3

Interactions of RNAP σ^{70} Holoenzyme and Promoter DNA.....5

Isomerization Steps for Transcription Initiation.....6

Use of Footprinting to Characterize RNAP- DNA Conformational Changes.....9

Role of Upstream Promoter DNA in Early RNAP-DNA Interactions and During Formation of RP_o.....12

Upstream DNA Wrapping Around RNAP.....13

Sigma Region 2 Mediates DNA Binding and Opening.....16

Insights Provided by Fluorescence Assays.....18

Transcription Initiation, Elongation, and Termination.....24

Upstream Binding Transcription Factors.....25

Significance of the Work Presented Here.....26

References.....31

Figures.....39

Chapter 2: Characterization of Key Closed and Open *Escherichia coli* RNA Polymerase– Promoter Intermediate Complexes in Transcription Initiation Using Real-Time Fast Footprinting.....48

Preface……48

Abstract……49

Introduction……51

Results

Fast HO• Footprints Demonstrate that the I_1 Intermediate Forms in ≤ 0.1 s and Persists For ~15 s After Mixing RNAP and λP_R……...55

Simulation of the Population Distribution of Free and Complexed Promoter DNA as a Function of Time after Mixing, with Input from HO• Footprinting……56

~10 bp Periodicity in Downstream Region (~ -10 to +20) of Both HO• Footprints of Both Strands of I_1 but not Open Complex HO• Footprints……..57

Fast MnO_4^- Footprinting Demonstrates that I_1 is Closed, and that Opening Occurs at the Rate of Formation of I_2 and Subsequent Open Complexes……..59

Real-time HO• Snapshots of a Burst of the Initial Open Intermediate I_2……..61

Discussion……65

Burst Experiments and Fast Footprinting Provide Structural and Kinetic Information About Key Transcription Initiation Intermediates……65

Order of the Steps that Recognize the -10 Region, Put Downstream DNA in the Cleft, and Open It……..67

Materials and Methods……71

References……79

Tables……..85

Figures…….88

Chapter 3: Real-time and Equilibrium FRET Characterization of Promoter DNA Wrapping and Unwrapping in *E. coli* RNAP Transcription Initiation Intermediates.....101

Preface……..101

Abstract……102

Introduction……....103

Results……..……106

Design of Promoter DNA FRET Constructs……107

Equilibrium FRET demonstrates promoter DNA wrapping around RNAP in the closed complex I_1……108

FRET Shows that Open Complexes are Also Wrapped……...110

Real-time Wrapping of the λP_R Promoter around RNAP……..……. 112

Real-time Dissociation FRET Experiments Utilizing a High [Salt] Upshift Rapidly Disrupt Promoter DNA Wrapping……..118

Discussion……...120

Materials and Methods……123

References……...127

Tables……133

Figures……..134

Chapter 4: Real-time Studies of -11A Base Flipping and Opening of the -10 Region of Promoter DNA Monitored by Intrinsic and Beacon Fluorescence of the Sigma-70 Subunit of *E. coli* RNA Polymerase.....154

Preface……..154

Abstract……..……..155

Introduction……..……...157

Results……..164

Changes in Intrinsic and Beacon (Tetramethyl Rhodamine Adduct) RNAP Fluorescence on the Time Course of Open Complex Formation……164

Analysis of Rate Constants k_{fast} and k_{slow} from the Two- Exponential Fits…….167

Studies of the Role of W433 in Intrinsic RNAP Fluorescence……170

Real-time Fluorescence Salt Upshift Experiments on Stable Open Complexes Show That the Fluorescence Change Occurs With The Same Rate as DNA Closing……..172

Discussion……..…….175

Characterization of the interaction of σ_2 with -10 promoter DNA elements…...176

DNA Closing……178

Comparison of RNAP Beacon and Intrinsic Fluorescence Results to Previous 2-AP Fluorescence Studies……..…….179

Comparison with Previous Intrinsic Fluorescence Studies on the T7A1 Promoter……..…180

Role of W433…….……...……..182

Conclusion……..183

Materials and Methods…….……184

References…….……..190

Tables…….……...194

Figures…….…….197

Chapter 5: Summary.....212

Figure……...217

References……..……220

Appendices……..222

Appendix 1: Temperature Dependence of Equilibrium "Beacon" RNAP Fluorescence and of Permanganate Reactivity for RNAP-λP_R Promoter DNA Complexes at a Range of Temperatures from 2-37°C……..224

Appendix 2: Preliminary Determinations of the Association Kinetics of RNAP with the λP_R Promoter Utilizing Cy3 Fluorescent Probes located at (-100), (+14) or (+29) Relative to the Start Site of Transcription…….....…….231

Appendix 3: Preliminary Determinations of the Association and Dissociation Kinetics of RNAP with the T7A1 Promoter at 19°C and 37°C using the RNAP "Beacon" Assay……..223

Appendix 4: Preliminary Determinations of the Association Kinetics of RNAP with the rrnb P1 Promoter in the Presence and Absence of Initiating Nucleotides ATP and CTP at 37°C Using the RNAP "beacon" Assay……..…246

Appendix 5: Determination of the Rates of GTP Incorporation at the +3 Position at the λP_R promoter at 5, 10, 25, and 37°C using Thin Layer Chromatography……..251

Appendix 6: Effect of Nucleotides and of Heparin on Promoter DNA Wrapping Around RNAP as Monitored by Equilibrium and Real-time FRET……..…260

Appendix 7: Comparison of Amounts of Long and Short Transcripts Produced by WT RNAP at the λP_R promoter Under Single Round Conditions at 10°C and 37°C……..270

References……...279

List of Tables

Chapter 2

Table 1. Local Maxima and Minima of DNA in I_1 and Stable Open Complexes (I_3, RP_o)……..…..85

Table 2: Predicted Fractions of Promoter DNA in Intermediate (I_1 or I_2) and Stable (I_3, RP_o) Complexes vs. Time in Burst Experiments Simulated in Fig. 3……...87

Chapter 3

Kinetic rate constants for real-time FRET experiments……133

Chapter 4

Rate and Equilibrium Constants for the Beacon and Intrinsic Fluorescence Assays During Formation of Open Complexes at the λP_R Promoter…….194

Table 2. Dissociation Rates for RNAP "Beacon" Open Complexes (I_3, RP_o) Upshifted to 1.1M Salt…….....195

Table 3. Dissociation Rates for RNAP Open Complexes (I_3, RP_o) Upshifted to 1.1M Salt as Monitored By Intrinsic RNAP Fluorescence…...……..196

Supplemental Table 1. Compiled Kinetic Data for Intrinsic Fluorescence Experiments…….210

Supplemental Table 2. Compiled Kinetic Data for Beacon Fluorescence Experiments ……211

List of Figures

Chapter 1

Figure 1. The Kinetic Pathway for Formation of Open Complexes at the λP_R Promoter……42

Figure 2. Architecture of Bacterial *Thermus thermophilis* RNA polymerase Holoenzyme……43

Figure 3. Model of the Stable Open Complex Formed by E. coli RNAP……..44

Figure 4. Interactions of the RNAP Subunits with Promoter DNA Elements…...45

Figure 5. Model of the Upstream Wrap for I_1……..……..46

Figure 6. Structure of Region 2.3 of σ^{70}……47

Chapter 2

Figure 1. Lanes From Representative Sequencing Gels Showing Distributions of Promoter Fragments Obtained From Single-hit HO• Snapshots of The Nontemplate and Template Strand Backbone……...92

Figure 2. Phosphoimager Line Scans of Gel Lanes Quantifying Relative HO• Reactivities of the DNA Backbone at Each Position (from -70 to +30) of the Nontemplate and Template Strands……93

Figure 3. Berkeley Madonna™ Simulations of Bursts of the Key Intermediates I_1 and I_2……94

Figure 4. Corrected Line Scans of Lanes of the Sequencing Gel Lanes in Figs. 1 and 2 to Show the Predicted Nontemplate and Template Strand Footprints of Homogeneous Populations of I_1……...95

Figure 5. Periodic Protection is Observed in the Backbone of the Downstream Duplex of I_1 But Not Open Complexes……96

Figure 6. Slow Kinetics of Development of MnO_4^- Reactivity of Single Stranded Thymines in the Vicinity of the Transcription Start Site During Association initiated by Fast Mixing of Excess RNAP (55 nM) with λP_R Promoter DNA at 19 ºC……97

Figure 7. Lanes from a Representative Gel of Single-hit HO• Footprinting Experiments (5 mM $FeEDTA^{2-}$) Probing the Nontemplate Strand of λP_R after An Upshift of (I_3, RP_o) Complexes to 1.1 M NaCl at 10 ºC…….....98

Figure 8. Phosphoimager Line Scans of Lanes of Sequencing Gels Resolving DNA Fragments From Replicate Single-hit HO• Footprints (5 mM $FeEDTA^{2-}$) of The Nontemplate DNA Strand……..99

Figure 9. Testing the Possible [Salt] Effect on HO• Cleavage of Free DNA…..100

Chapter 3

Figure 1. Representative Equilibrium FRET Experiments for RNAP- Promoter DNA Cy3 (-100) Cy5 (+14) complexes at 2, 10, 19, and 37°C……137

Figure 2. Representative Equilibrium FRET Control Experiments at 2°C……...139

Figure 3. Representative Equilibrium FRET Experiments with Dyes in the Opposite Orientation (Cy3 (+14) Cy5 (-100))……..141

Figure 4. Temperature Dependence of Cy3 and Cy5 Emission……..143

Figure 5. Temperature dependence of equilibrium FRET measurements…….153

Figure 6. Real-time DNA Bending Monitored by Stopped-flow Fluorescence at 19°C Using 100nM Cy3 (-100) Cy5 (+14) λP_R Promoter DNA……147

Figure 7. Reversal of FRET Dye Positions For Real-time DNA Bending Monitored By Stopped-flow Fluorescence at 19°C [Cy3 (+14) Cy5 (-100) λP_R Promoter DNA]……..……149

Figure 8. Equilibrium and Real-time FRET Experiments for RNAP- $\lambda P_R P_{RM}$ promoter complexes……..……151

Figure 9. Rapid Salt Upshift “Burst” Experiment for Characterizing the Dissociation of the Highly Wrapped Open Complexes at 19°C……153

Chapter 4

Figure 1. Cartoon Model and Structural Model Based on PDB 3YID Depicting the RNAP “Beacon” Assay……200

Figure 2. Representative Kinetic Data for Formation of Open Complexes at the λP_R Promoter……202

Figure 3. Rate Constants k_{fast} and k_{slow} Quantifying the Fast and Slow Components of Two Exponential Fits to the Intrinsic and TMR Kinetic Data Plotted as a Function of the Promoter DNA Concentration (50-300 nM)……203

Figure 4. Permanganate Reactivity of Wild Type and W433A RNAP- Promoter DNA Complexes at 19°C…….204

Figure 5. Representative Kinetic Data for the Association of 10nM RNAP σ^{70}-W433A with 100nM λP_R promoter DNA……205

Figure 6. Representative Kinetic Data for Dissociation of Beacon RNAP σ^{70}211-Cys-TMR Open Complexes (I_3, RP_o) following a 1.1M NaCl upshift……...206

Figure 7. Representative Kinetic Data for Dissociation of RNAP σ^{70} Open Complexes (I_3, RP_o) Following a 1.1M NaCl Upshift as Monitored by Intrinsic RNAP Fluorescence……208

Chapter 5

Figure 1. Mechanism of Formation and Stabilization of Open Complexes Between E. coli RNA polymerase and Promoter DNA……...…….....217

Acknowledgements

I would like to thank Dr. Tom Record for allowing me to work in his lab both as an undergraduate researcher for four years and as a graduate student for 2 years. Without his support, I would never have gone to graduate school or finished my PhD.

I would like to thank my labmates Ben Knowles, Amanda Drennan, Raashi Sreenivasan, and Emily Guinn for being both great colleagues and also great friends during my time in graduate school.

I would also like to thank all of the undergraduates that I worked with: Dana Bellissimo, Mikaela Poulos, Emily Lingeman, Mark Kraemer, Kristin Zorn, Even Buechel, and Natalie Gaio. You are my superstars! I appreciate all of your help tremendously.

I would like to thank my parents Gary and Roberta Heitkamp and my boyfriend Zach Brown for their constant support and encouragement.

I would like to thank my committee members: Dr. Robert Landick, Dr. Tricia Kiley, Dr. Sam Butcher and Dr. Michael Cox. I would also like to thank my unofficial committee members Dr. Irina Artsimovich, Dr. Aaron Hoskins, Dr. Rick Gourse and Dr. Wilma Ross for their suggestions and discussion.

I would like to thank the National Science Foundation for my Graduate Research Fellowship award, the Department of Biochemistry for a graduate Travel Award, and the Wisconsin Alumni Research Foundation for an Ambassador travel award.

xoxo,
Gossip Girl

Chapter 1

Introduction

Preface

This introduction briefly outlines the major advances in understanding the mechanism of isomerization of the *E. coli* RNAP- promoter DNA closed complex to the transcriptionally active open complex. At the end of the introduction, I highlight how my research has developed testable hypotheses regarding the kinetic mechanism of transcription initiation, including the timing of DNA opening, the role of promoter DNA wrapping around RNAP, the interactions of sigma region 2.3 with -10 promoter DNA elements, and the transcription activities for complexes formed at different temperatures. Many excellent reviews provide more in-depth coverage of transcription initiation topics that are not discussed here (Browning and Busby, 2004; Haugen *et al.* 2008; Wigneshweraraj *et al.* 2008; de Haseth *et al.* 2008; Gruber and Gross, 2003; Paget and Helmann, 2003; Borukhov and Nudler, 2008).

Introduction

Transcription of RNA from DNA is the first step in gene expression and is carried out by RNA polymerase (RNAP). Transcription can be broken down into four stages: (i) recognition of promoter DNA by RNAP followed by isomerization steps resulting in the formation of the open complex in which the two DNA strands are melted to form an ~14 nontemplate transcription bubble (Figure 1); (ii) binding of NTPs and initial production of short, abortive RNA transcripts 2-11nts in length; (iii) promoter clearance and the transition to productive RNA elongation; and (iv) termination of elongation and the release of RNAP from the DNA.

Most studies of bacterial transcription initiation have been performed with *Escherichia coli* RNAP. The *E. coli* RNA polymerase core enzyme (E) is comprised of five subunits ($\alpha_2\beta\beta'\omega$, ~380 kDa). Core RNAP requires a specificity subunit (most commonly σ^{70}) in order to form the RNAP holoenzyme and to specifically recognize promoter DNA sequences (Figure 2, Burgess *et al.* 1969, Travers and Burgess, 1969). In *E. coli*, σ^{70} is the "housekeeping" or primary promoter specificity factor which directs RNAP to many promoters during nutrient-rich conditions of log phase growth. σ^{70} plays an essential role in promoter recognition and RP_o formation as well as in the early steps of RNA synthesis. Alternative σ factors are used by the cell to respond to stress conditions including high external osmolalities and for nitrogen fixation (Gruber and Gross, 2003).

Members of the "σ^{70} family" have a conserved sequence containing four regions, numbered 1-4 and subdomains (1.1, 1.2, etc; here referred to as $\sigma_{1.1}$, $\sigma_{1.2}$, etc; Lonetto *et al*. 1992). σ^{70} is comprised of several independently folded domains ($\sigma_{1.2}$, σ_2, σ_4)

connected to flexible domains ($\sigma_{3.2}$ and $\sigma_{1.1}$) (Schwartz *et al.* 2008). In free sigma, $\sigma_{1.1}$ and σ_4 are thought to interact, causing autoinhibition of binding to promoter DNA (Schwartz *et al.* 2008, Camarero *et al.* 2002). Binding of RNAP to σ^{70} causes a large conformation change in σ^{70}, relieving this autoinhibition (Callaci *et al.* 1999). However, recent evidence from fluorescence binding experiments suggests that large conformation changes in sigma are not required for recognition of the single-stranded nontemplate region of the -10 element (Mekler *et al.* 2011a). $\sigma_{1.1}$ and $\sigma_{1.2}$ are also thought to provide the main contacts with RNAP core by interacting with an evolutionarily conserved coiled-coil element in β' (Vassylyev *et al.* 2002).

Structure and Function of RNA Polymerase

E. coli RNAP has been notoriously difficult to crystallize and therefore most of the available structures have been obtained from the thermophilic eubacteria *Thermus aquaticus* and *Thermus thermophilis*. *E. coli* RNAP holoenzyme is also too large (~450kDa) for NMR characterization, thus prohibiting solution-state structural studies. Eukaryotic and archeal core RNAPs contain the same basic five subunit structure as *E. coli* RNAP plus 5-8 additional subunits. T7 RNAP contains only a single subunit and is much smaller than the other RNAP cores (~99kDa).

Bacterial core RNAP (~390 kDa, 150 Å long x 115 Å tall x 120 Å wide) resembles a "crab claw" containing a wide internal channel made up of the β and β' subunits tethered by a flexible domain, (Zhang *et al.* 1999; Murakami *et al.* 2002a, b; Vassylyev *et al.* 2002) similar to that of the archaeal core (Cramer *et al.* 2000, 2001). At the base of the channel is the catalytic Mg^{2+} which is chelated by the Asp residues of the absolutely conserved -NADFDGD- motif of β'. The ~27Å cleft of β and β′ binds the

transcription bubble (Zhang *et al.* 1999). At the downstream end of the cleft, the flexible domains of β and β′ are proposed to assemble on the downstream duplex DNA to stabilize the open complexes. The αCTDs serve as a platform for the β and β' subunits (Zhang *et al.* 1999). The αCTDs are flexibly tethered to the αNTDs via 14-residue flexible linkers (Blatter *et al.* 1994) and can bind nonspecifically to upstream DNA as far as approximately position -90 (Gourse *et al.* 2000). The small ω subunit is bound on the exterior of the β' subunit (Ghosh *et al.* 2003).

Opalka *et al.* (2010) were able to generate molecular models for the *E. coli* core RNAP and ternary complex by using a combination of approaches (X-ray crystallography, ab initio structural prediction, homology modeling, and single-particle cryo-electron microscopy). The β and β' subunits of all bacterial RNAPs are highly conserved sequence and expected to have nearly identical structure. However, the *E. coli* RNAP contains large β and β' sequence insertions whose function has remained elusive, due to the lack of complete structural and biochemical data. Opalka and colleagues were able to generate high-resolution structural information for the *Eco* lineage-specific inserts βi4, βi9, and βi11, and in the context of core RNAP and the TEC.

Figure 3 depicts a model of the *E. coli* Eσ^{70} RNAP open complex structure (PDB 3YID). This figure highlights the arrangement of σ^{70} on core and the interaction of the promoter DNA and σ_2, σ_3 and σ_4 (Lonetto *et al*. 1992). The $\sigma_{3.2}$ linker is buried in the RNA exit channel. σ_{NCD} is a nonconserved region that connects $\sigma_{1.2}$ and σ_2. The β and β′ subunits form a deep, wide cleft that binds the transcription bubble. At the bottom of the cleft is a hinge formed by the N-terminal domains of the α subunits. At the downstream

end of the cleft, the flexible domains of β and β′ are proposed to assemble on the downstream duplex DNA to stabilize the open complexes. Promoter DNA binds in the cleft with the +1 start site near the active site Mg^{2+}.

Interactions of RNAP σ^{70} holoenzyme and promoter DNA

The consensus recognition sequence for RNAP σ^{70} contains sequence elements centered at -10 and -35 upstream of the transcription start site (See Figure 4). In the crystal structure for *T. aquaticus* σ^{A}, $\sigma_{4.2}$ was found to interact with the -35 promoter DNA element by utilizing a helix-turn-helix motif that interacts with the major groove (Campbell *et al.* 2002). $\sigma_{2.3}$ interacts with the nontemplate single strand of the -10 recognition element (-12 to -7, consensus TATAAT) In addition, σ^{70} factors also recognize a TG sequence upstream of − 10 (called the extended – 10, not present in all promoters) via $\sigma_{3.0}$ (Barne *et al.* 1997, Mitchell *et al.* 2003). The discriminator sequence is thought to be involved in promoter melting and isomerization to form the open complex. The discriminator region (~-6 to -1) interacts with $\sigma_{1.2}$ (Haugen *et al.* 2008). The spacer length is the number of base pairs separating the − 10 and − 35 elements, and is optimally 17 bp (Feklistov *et al.* 2006, Haugen *et al.* 2006). Many promoters also contain an AT-rich sequence upstream of the -35 region known as the UP element that has been shown to interact with the C-terminal domain of the alpha subunits (αCTD) during promoter binding (Estrem *et al.* 1998, Aiyar *et al.* 1998). The full UP element contains two adjacent subsites, optimally centered at the −53 and −43 positions, and the presence of the UP element has been shown to stimulate transcription up to ~90-fold.

Isomerization Steps for Transcription Initiation

The bacteriophage λ promoter (λP_R) has been extensively investigated by kinetic, equilibrium, and DNA footprinting studies as a model system to characterize the steps in transcription initiation. The near-consensus -35 and -10 elements of λP_R (Figure 4) are each only one base-pair different that the consensus promoter sequence; it forms stable open complexes relatively rapidly, and initiates abortive or productive transcripts relatively rapidly, and so is considered a "strong" promoter. Wild type λP_R does not have an UP element, but does have two AT-rich tracks positioned from − 36 to – 59 and from − 80 to – 100.

Binding of the RNAP holoenzyme to promoter DNA triggers a series of large-scale conformational changes in both biopolymers leading to the formation of open complexes (Figure 1). The current minimal kinetic mechanism for formation of transcriptionally-competent open complexes at λP_R involves at least three kinetically-significant on-pathway intermediates (Figure 1). In the first step of initiation, RNA polymerase recognizes promoter DNA and binds to form the advanced closed complex, I_1 (Roe *et al.* 1984, Roe *et al.* 1985). At other promoters evidence exists for a less-advanced early intermediate, RP_c (Sclavi *et al*. 2005, Rogozina *et al.* 2009) Although a RP_c –like complex almost certainly forms before I_1 at λP_R, it has not been observed in kinetic experiments. In I_1, the duplex DNA is bent and wrapped around RNAP, but not yet opened (Figure 5, Davis *et al.* 2007). At λP_R, the DNA in I_1 is continuously protected from ·OH and DNase I on both strands from − 11 to positions + 20–25, but is not MnO_4^- reactive (Davis *et al.* 2007).

E.coli RNAP requires no helicase cofactor to open the promoter DNA duplex. When is the DNA opened during transcription initiation and is it opened in one step or many? How does RNAP screen for non-promoter DNA and prevent it from accessing the active site cleft? The arrangement of sigma on core and the interactions of sigma regions 2 and 4 with the -10 and -35 elements define a promoter DNA trajectory in the early closed complex RP_c in which the DNA is at 90° with respect to the cleft. Based on the holoenzyme structures, we proposed that protection of both strands from − 11 to + 15 results from a sharp ~ 90° bend at the upstream end of the − 10 element that directs downstream duplex DNA into the active-site cleft (Davis *et al.* 2007). Movement of mobile elements at the downstream end of the cleft that block early access to the DNA provide the additional protection to + 20 and + 25. Conversion of RP_c to a more I_1-like complex appears to be driven by increasing temperature, by favoring the bend at − 11/− 12 and/or the interactions that stabilize the bend (Figure 3).

The architecture of the RNAP itself may play a role in discriminating promoter DNA from nonpromoter DNA during early initiation steps. In σ^{70}, the acidic N-terminal domain of σ^{70}, region 1.1 provides an additional block to nonspecific DNA binding. Region 1.1 is a single-stranded DNA mimic and binds in the cleft near the active site Mg^{2+}; 1.1 must be repositioned in order for the template strand of promoter DNA to access the active site and be properly positioned for binding of NTPs and transcription initiation (Nagai and Shimamoto, 1997, Mekler *et al.* 2002).

Initial structural studies suggested that the DNA binding cleft was too narrow to accommodate duplex DNA; therefore it was postulated that promoter DNA could only access the active site as single stranded DNA (Vassylyev *et al.* 2002; Murakami *et al.*

2002). However, more recent work has shown that the width of the RNAP active site cleft is dynamic and is sufficient to allow duplex DNA binding. Recent single molecule experiments have shown that the clamp is able to adopt multiple open and closed states, consistent with the model that the “hinges” in β and β′ at the base of the cleft are flexible in solution.

After formation of I_1, the RNAP-DNA complex undergoes isomerization to open the transcription bubble (-11 to +3) and load the single stranded template DNA into the active site. During the conversion of I_1 to I_2, the DNA is opened in a single, rate-limiting step (Gries *et al*. 2010). This step is strongly temperature dependent and the 34 kcal activation energy is consistent with the cooperative opening of at least 6–7 bp in the I_1–I_2 transition state. High concentrations of salt and solutes have very small effects on this step, consistent with DNA opening occurring within the RNAP cleft (Kontur *et al.* 2008, Gries *et al.* 2010). This step is the bottleneck in the forward direction. Because of this, use of high [RNAP] and rapid mixing in the association direction allow one to generate a “burst” of I_1 for characterization by fast footprinting or fluorescence (Gries *et al*. 2010, Kontur *et al.* 2010) Importantly, this initial unstable open complex has the template strand +1 start site correctly positioned in the active site; however the nontemplate strand has not yet occupied its final binding track. These studies, carried out at λP_R, led us to propose that RNAP is a molecular isomerization machine that uses promoter DNA binding energy to actively open the DNA within the cleft after loading of the duplex DNA during formation of I_1.

After the DNA is opened, I_2 rapidly converts to I_3 and then to the most stable open complex, RP_o. I_2 differs from RP_o in the amount of permanganate reactivity of the

nontemplate strand, indicating that movements of the nontemplate strand are coupled to conversion of I_2 to RP_o (Gries *et al.* 2010, Kontur *et al*. 2008). During this transition there is also a large-scale assembly of the downstream mobile elements (DMEs) including the β' mobile jaw on the downstream DNA (See Figure 2, Kontur *et al.* 2010, Drennan *et al.* unpublished). These conformational changes convert the unstable open complexes I_2 and I_3 to the final form of the open complex, RP_o. However, although there are clear differences between I_2 and RP_o, the breakdown of when these changes occur (whether during the conversion of I_2 to I_3 or of I_3 to RP_o) is currently ambiguous.

Use of footprinting to characterize RNAP- DNA conformational changes

"Footprinting" is the method whereby binding of ligands or structural changes in a biopolymer (such as RNA, DNA, or a protein) protects regions of the molecule from cleavage or modification by the footprinting reagent. DNA footprinting allows one to probe the accessibility of the individual residues and create a structural "map" of regions of the DNA that are protected. Footprinting can be used in either equilibrium or kinetic assays to compare different populations of RNAP-DNA complexes. By using temperature shifts (at equilibrium) or using fast-mixing kinetic "burst" experiments, one can shift the population of RNAP-DNA complexes to be studied. In our lab, low temperature shifts have been used to characterize the closed complex I_1 and rapid mixing of open complexes with a high [salt] upshift were used to characterize the first open complex, I_2.

Hydroxyl radical and DNase I footprints probe the extent of protection of DNA by RNAP. Fe-EDTA footprinting generates HO• in solution via the Fenton reaction (Fenton, 1894), and was previously shown to be able to cleave DNA within 5 milliseconds (ms)

(Shcherbakova and Brenowitz, 2008). The extent of DNase I protection in I_1 complexes formed with an upstream-truncated promoter DNA fragment is short downstream as compared to I_1 complexes formed with a full length DNA fragment (Davis *et al.* 2005). Permanganate (MnO_4^-) footprinting, which probes the exposure of single-stranded or unstacked thymine residues, was used to determine that the duplex DNA is bent and wrapped around RNAP in I_1, but not yet opened (Davis *et al.* 2007). However, these experiments were only able to sample times as short as 15 seconds after mixing RNAP and promoter DNA. Quantitative analysis of permanganate footprints was also used to determine that the template strand is loaded in the RNAP active site upon formation of the I_2 intermediate, but that the nontemplate strand continues to rearrange during the conversion of I_2 to RP_o (Gries *et al.* 2010).

Our lab has proposed that RNAP binds and bends promoter DNA to form the closed complex I_1 prior to the rate-liming conversion of I_1 to I_2 open complexes (Figure 1; Davis *et al.* 2007). An alternative model for DNA opening has been proposed by Sclavi and coworkers (Sclavi *et al.* 2005, Rogozina *et al.* 2009). They proposed that the DNA opens before the rate-limiting step and that the transcription bubble opens before contacts are formed between the RNAP active site cleft and positions -12 to +20 in the downstream DNA. Fast •OH and MnO_4^- footprinting was used to characterize complexes populated during the formation of RP_o at the T7A1 promoter. In these experiments, the •OH are generated by irradiating the sample with synchrotron radiation X-ray beams, which allows for reaction times as short as 10 ms. Sclavi *et al* (2005) found that at early times (0.2 to 1s) the RNAP first contacts the upstream promoter DNA region (-55 to +43), whereas protection of downstream DNA (-9 to +20) develops later

(1 to 200 s). The authors analyzed the protection of different regions (upstream and downstream) of promoter DNA as a function of time and found that most promoter DNA positions exhibited biphasic protection kinetics. The authors fit the protection data to a sum of two exponentials and the observed rates were used to develop a kinetic model consisting of a series of equilibrating intermediates on the pathway to open complex formation at the T7A1 promoter. These intermediates were proposed to differ in the position of insertion into the RNAP active site cleft.

Rogozina *et al.* 2009 used fast •OH footprinting at both 20°C and 37°C and MnO_4^- footprinting at 37°C to characterize the kinetic pathway for T7A1. They also characterized a mutant T7A1 promoter with a consensus -10 region at 37°C. Following the same method as their earlier work, the authors monitored the kinetics of protection from •OH cleavage for different regions of the promoter to modify their kinetic model such that it included additional intermediates and an off-pathway complex.

However, there are some issues with this analysis that prevent an unambiguous analysis of the footprinting data, in particular the •OH footprinting. Without prior knowledge of the kinetic mechanism of T7A1 or the relative populations of intermediates sampled at a given time and set of experimental conditions, it is difficult to assign identities to each of the relative hydroxyl radical protection amplitudes or to determine at which step(s) in the mechanism that opening occurs. It is also unclear how the authors can compare the kinetics of •OH protection and MnO_4^- cleavage when the earliest time point for MnO_4^- is an order of magnitude slower than that for •OH protection.

At the time my thesis research was initiated, evidence existed that I_1 at λP_R was an extensively-wrapped, probably-closed complex with far-upstream promoter DNA (to -

80 or farther) wrapped on the “back” side of RNAP (Figure 5, Davis *et al.* 2007) far downstream DNA (to +20 or +25) in or near the active site cleft (Craig *et al.* 1998; Saecker *et al.* 2002). But the evidence that I_1 is a closed complex with an extended downstream footprint was indirect and in particular was not obtained in real-time; the real-time characterization of I_1 by fast hydroxyl radical and permanganate footprinting is the subject of **Chapter 2** of this thesis.

I**n Chapter 2, we used rapid kinetic footprinting experiments to characterize the rate of protection from •OH cleavage during formation of I_1 and to map changes in the reactivity of the downstream DNA during open complex formation. Kinetic permanganate footprinting experiments in the forward direction demonstrate that the DNA is still closed in I_1, and opens during the I_1 to I_2 transition.**

Role of Upstream Promoter DNA in Early RNAP-DNA Interactions and During Formation of RP_o

Interactions of the αCTDs with upstream promoter DNA were found to mediate a stable wrap around RNAP within RNAP-promoter DNA open complexes (Cellai *et al.* 2007). The presence of DNA upstream of the − 35 element at λP_R increases the rate of the bottleneck DNA opening isomerization step; k_2 (conversion of I_1 into I_2) for full-length λP_R is~ 50-fold larger than that for λP_R promoter DNA truncated at − 47 (UT-47). However, deletion of the upstream DNA has little effect to no effect on the stability of I_1. Deletion of upstream DNA leads to a “less advanced” closed complex that only protects downstream DNA to + 2 (template)/+ 7 (nontemplate) relative to ~ + 20 observed for the

full-length λP_R promoter (Davis *et al*. 2005). Clearly, the interactions of upstream promoter DNA with RNAP regulate DNA opening, however the underlying mechanism of this regulation remains unclear. One possibility is that upstream DNA mediates transcription bubble opening by defining the trajectory of the upstream DNA wrap; this DNA wrapping may bend the promoter DNA in the upstream -35 and -10 regions, thereby allowing the -11A base to flip out of the duplex stack. Flipping of the -11A base then nucleates DNA melting. Work described in this thesis directly tests these hypotheses.

Upstream DNA Wrapping Around RNAP

Footprinting at the full-length λP_R promoter defined the upstream boundary of protection from cleavage by DNase I or ·OH cleavage to be ~ − 65 in RP_o. However, ·OH footprints of I_1 reveal modest protection of the DNA backbone on both strands to at least – 85 (Davis *et al.* 2007). DNA upstream of -65 is thought to stabilize the upstream wrap of DNA around RNAP by providing a stable interaction with the αCTDs and also increasing the bend angle of the DNA so that it can enter the RNAP active site cleft (Davis *et al.* 2005, Davis *et al.* 2007). Hypersensitive DNase I sites in I_1 indicate that a bend occurs just upstream of the − 35 element. Based on our kinetic and footprinting data, we proposed that σ_4 induces a bend in the upstream DNA and the two αCTDs place far upstream DNA near the downstream end of the cleft (Figure 5). We proposed that the upstream DNA is directed into a surface groove formed by β′ and the N-terminal domain of the associated α subunit. This positioning would place the upstream DNA near a conserved mobile element in β′, termed the upstream clamp. We hypothesize that interactions between upstream DNA and upstream clamp restrain the movements

of mobile elements at the downstream end of the cleft. In the absence of this constraint, these elements could interfere with the loading of the downstream DNA into the cleft.

We have mapped the I_1 protection pattern and the inferred bend onto available X-ray structures (Figure 5). These models suggest that RNAP wraps DNA around the "back" of the β′ subunit; alternatively, the mobile αCTDs could mediate these upstream interactions. In this model, the αCTDs accelerate the DNA melting step by setting the trajectory for wrapping interactions. However, crosslinking studies of RP_o indicated that the αCTDs are mobile and can occupy multiple sites on the upstream DNA (Haugen *et al.* 2008 and references therein).

Various models for wrapping promoter DNA on *E. coli* RNAP in I_1 and RP_o complexes have been proposed (for a review on promoter DNA wrapping around RNAP see Coulombe and Burton, 1999). *E. coli* RNAP has been found to induce bending of T7A1 promoter DNA in both open complexes and during transcription of RNA products up to 11 bases in length (Heuman *et al.* 1988a). Based off of this work and evidence from neutron scattering and quantitative electrooptics, the DNA bend in RP_o at T7A1 was proposed to be centered at position -3 with regard to the +1 start site of transcription, with a bend angle 45° ± 5° (Heuman *et al.* 1988b, Meyer-Alme *et al.* 1994). RNAP-induced bending has also been demonstrated for RP_o formed by $E\sigma^{70}$ at the *gal* (Kuhnke *et al.* 1989) and λP_L (Rees *et al.* 1993) promoters and for σ^{54} RP_o at the *glnA* promoter (Rippe *et al.* 1997). Open complexes of σ^{54} RP_o at the *glnA* promoter exhibited DNA contour lengths significantly shorter than that of free promoter DNA, suggesting that promoter DNA must wrap around the back side of RNAP (Rippe *et al.* 1997).

Atomic force microscopy studies from the Rivetti lab indicated that the sequence of the upstream promoter DNA regulated the extent of stable wrapping of λP_R DNA around RNAP in RP_o as measured by DNA contour length (Mangiarotti *et al.* 2009). Replacement of upstream λP_R DNA with heterologous sequence between positions −463 and −36 decreased the extend of DNA compaction in RP_o from 30±0.4 nm for the wild-type sequence to only 6±0.8 nm for that of the substituted λ P_R DNA (Mangiarotti *et al.* 2009).

Promoter DNA has been proposed to remain wrapped during transcription initiation (Heuman *et al.* 1988a) and elongation (Rivetti *et al.* 2003) for *E. coli* RNAP. Transcription ternary complexes of *E. coli* RNAP stalled at positions +24, +70 and +379 had an average compaction of 22 nm as measured by AFM and a DNA deformation compatible with an approximate 180° DNA wrap around the enzyme. However, this extent of wrapping was deduced to be less than that of open complexes.

T7 and eukaryotic RNAP enzymes have also been observed to bend promoter DNA. Fluorescence assays demonstrated that rapid binding of T7 RNAP is followed by bending and opening of the DNA; opening was found to be coupled to bending (Tang and Patel 2006a and 2006b). Circular permutation assays provide confirmation of this DNA bending (Ujvári and Martin 2000). Yeast pol III stalled at position +377 showed a DNA compaction of 30 nm (Rivetti *et al.* 2003). **Although many studies have sought to determine the mechanism and role of promoter DNA wrapping during transcription initiation, it was unclear how the trajectory of the promoter DNA wrap regulates initiation and elongation (See Chapter 3 and Appendices). In this thesis, we used equilibrium and real-time stopped flow fluorescence assays to**

show that promoter DNA is highly wrapped in I_1 and that the wrap persists during open complex formation.

Sigma Region 2 Mediates DNA Binding and Opening

σ_2 is highly conserved and has been subdivided into four regions: 2.2, 2.2, 2.3, and 2.4 (Lonetto *et al.* 1992, Gribskov and Burgess 1986). σ_2 is involved in recognition of the -10 promoter DNA element ($\sigma_{2.4}$), nucleation of strand separation ($\sigma_{2.3}$), and formation of the open complex (Tomsic *et al.* 2001). Interactions of σ_2 with -10 promoter DNA elements play a critical role in recognizing and stabilizing the upstream single stranded nontemplate strand. De Haseth and coworkers first proposed that several basic residues in $\sigma_{2.3}$ (K414, K418, R423, and K426) are involved in promoter DNA binding (De Haseth and Tsujikawa, 2003). The four residues Y425, Y430, W433, and W434 are positioned on the same face of the protein, where they can interact with promoter DNA (See Figure 6, Malhotra *et al*, 1996, Murakami *et al.* 2002). In the co-crystal structure, Y430 and W433 are positioned near the double-stranded- single stranded junction of the forked DNA template (Murakami *et al.* 2002). Y430 has been found to flip the -11A out of the DNA helix during DNA opening and therefore both Y430 and W433 likely play crucial roles during nucleation (Schroeder *et al.* 2009). Alanine substitutions for basic and aromatic amino acids in $\sigma_{2.3}$ render RNAP cold sensitive for DNA opening and transcription initiation. DNA opening is less favored at lower temperatures, and therefore this suggests a model whereby key amino acids in $\sigma_{2.3}$ mediate DNA opening. Of all the single substitutions, Y430A had the greatest decrease in stability (Panaghie *et al.* 2000, De Haseth and Tsujikawa, 2003). At 20°C, the

mutants also had reduced transcription levels, consistent with the model that open complex formation is disfavored in the substituted RNAP.

Recently, the structure of a *T. aquaticus* σ^A (a σ^{70} homolog) fragment comprising σ^A regions 2 and 3 bound to a single-stranded DNA fragment containing the -10 nt strand sequence was determined (Feklistov and Darst, 2011). The authors concluded from the structure and from biochemical data that σ^A region 2.3 captures the nontemplate strand after the DNA is opened. In their model, the nontemplate strand within the -10 promoter element is specifically recognized by $\sigma_{2.3}$ via direct interactions with the DNA bases. The -11A and -7A bases are flipped out of the DNA base stack and buried in hydrophobic pockets on σ. Under the conditions for which the authors perform equilibrium binding studies, specific recognition of the -10 promoter DNA occurs only upon strand separation, with little to no specific recognition of the duplex -10 element.

Clearly, interactions of $\sigma_{2.3}$ with the -10 promoter DNA element are important for opening and stabilization of the transcription bubble during initiation; however the timing of these steps and the specific role of each amino acid during the process of promoter DNA bending and opening is unclear. Both RNAP and promoter DNA must undergo a series of conformational changes in order to open the DNA and properly load the +1 transcription start site of the DNA into the RNAP active site cleft. How do interactions of σ_2 with the -10 element regulate this process? What is the timing of bending of duplex DNA, base flipping of the -11 and -7 nontemplate strand bases and opening of the transcription bubble? How do the aromatic amino acids in $\sigma_{2.3}$ contribute to the process of binding, bending and opening of the DNA? **Until recently (see Chapter 4 of this**

work), the timing and mechanism of these events has remained ambiguous, due to the lack of specific probes on the RNAP and/ or DNA in this region. Here, we have used the RNAP beacon and intrinsic fluorescence assays in order to monitor the kinetics of -11A base flipping and the interactions of $\sigma_{2.3}$ with -10 promoter DNA elements during isomerization of RNAP to open complexes.

Insights Provided by Fluorescence Assays

Numerous fluorescence techniques have been used to investigate conformational changes in bacterial RNAP and promoter DNA. Some of the earliest fluorescence work came out of the Patel lab; the authors used 2-aminopurine (2-AP), fluorescence anisotropy, and FRET tags in steady state and time-resolved transient kinetic experiments for the phage T7 RNAP (Tang and Patel, 2006a; Tang and Patel, 2006b). The observed rate constants of the FRET and 2-aminopurine fluorescence changes were indistinguishable, indicating that the DNA bending and opening processes are temporally coupled and these DNA conformational changes take place after the DNA-binding step. The results are consistent with the mechanism in which the initial binding of T7 RNAP to the promoter results in a closed complex, which is then converted into an open complex in which the promoter is both sharply bent and melted (Tang and Patel, 2006a). In the closed complex, promoter DNA is bent slightly by <40 degrees but bent more sharply by 86 degrees in the open complex. The authors proposed that that a significant part of the available free energy from promoter DNA binding is utilized in DNA bending and/or untwisting (Tang and Patel, 2006b).

FRET studies have also been used to investigate the movement of σ^{70} regions 1.1, 2, 3.1, 3.2, and 4 upon formation of the holoenzyme-DNA binary complex (Mekler *et al.* 2002) and to study the release of σ^{70} during transcription elongation (Mukhopadhyay *et al.* 2001). In the first study, Mekler *et al.* found that σ^{70} undergoes a large conformation change upon association with RNAP core. In the second study, Mukhopadhyay *et al.* found that σ^{70} can in some cases remain bound to RNAP during transcription elongation. Single molecule FRET has been used to monitor changes between the RNAPII closed, open, and elongation complexes (Treutlein *et al.* 2012). **In this thesis, we use equilibrium and stopped-flow bulk kinetic FRET experiments to characterize the extent of promoter DNA wrapping around RNAP during transcription initiation and expand on previous proposals for upstream DNA wrapping. We find that the I_1 closed complex is highly wrapped and that the wrap persist during open complex formation.**

Single molecule nanomanipulation of promoter DNA allowed Revyakin *et al.* (2004) to monitor the end-to-end extension of a mechanically stretched, supercoiled, single DNA molecule. In this assay, the authors were able directly to observe the change in extension associated with unwinding of approximately one turn of promoter DNA by RNAP. By averaging over a 20 second time window, extents of unwinding were determined to within ±1 base pair. Using the consensus promoter lac_{CONS}, the authors found that, for negatively supercoiled DNA, there were only two unwinding states: an initial state prior to unwinding, and a final state after unwinding with no other intermediates observed within the temporal resolution of their system (1 second). Experiments performed at low temperatures exhibited no unwinding, consistent with

previous findings that complexes formed at low temperature are not open (*Craig et al.* 1998, de Haseth *et al.* 1998).

Fluorescent dyes have also been inserted into promoter DNA in order to characterize the kinetics of DNA opening by *E. coli* RNAP. Schroeder, de Haseth and collaborators utilized 2-AP substitutions in the upstream transcription bubble region (positions -11, -8, -4) to monitor conformational changes in a 65 bp (-45 to + 20) consensus promoter DNA during association with RNAP (Schroeder *et al.* 2011). Rate constants determined by 2-AP fluorescence (whether the 2-AP substitution is at −4, −8 or −11), were at least seven-fold greater than those detected by electrophoretic mobility shift assays (EMSA) for heparin-resistant complex formation, regardless of whether fit to single or double exponentials. The authors concluded that the 2-AP assay detected a DNA conformational change that preceded formation of the EMSA-detected stable open complexes. Since 2-AP fluorescence emission reports on changes in the local environment of DNA bases, including the unstacking and melting of duplex DNA, the authors concluded that they were detecting movements of the duplex DNA (bending and/or base flipping) prior to formation of the fully open transcription bubble. Work with 2-AP dyes inserted into the downstream transcription bubble region of the λP_R promoter (-4, +1 or +2 relative to the start site of transcription) in our lab required high concentrations of DNA (>250 nM) and exhibited a very small change (<0.5 fold) in fluorescence emission upon formation of open complexes (Heitkamp, unpublished). Therefore, we sought to find other fluorescence assays that could be used to monitor conformation changes in RNAP and DNA during transcription bubble opening.

Recently an assay for detecting the interaction of sigma region 2 with promoter DNA, known as the RNAP "beacon" method, was developed (Mekler *et al.* 2011a). The assay takes advantage of the multiple aromatic amino acids of σ^{70} that change their environment upon interaction with DNA. The RNAP beacon assay detects changes in the fluorescence emission of a site-specifically attached probe near σ_2. The σ^{70} derivative is labeled at amino acid position 211 with tetramethylrhodamine-5-maleimide (211Cys-TMR). This position is spatially close to the highly conserved Trp and Tyr residues (W433, W434, Y425, Y430) of $\sigma_{2.3}$. In free RNAP, these aromatic amino acids participate in photo-electron transfer to the dye, resulting in fluorescence quenching. However, specific binding of promoter DNA -10 elements within the DNA-binding track of $\sigma_{2.3}$ relieves the quenching reaction, causing a large increase in fluorescence intensity. This assay has been used to monitor RNAP interactions with both upstream and downstream fork junction promoter fragments and to investigate the role of Gp2 in regulating interactions of the *E. coli* RNAP β' jaw with downstream promoter DNA (Mekler *et al.* 2011a, Mekler *et al.* 2011b, Mekler *et al.* 2011c). **However, until this work (Chapter 4), the RNAP "beacon" assay had never been used in real-time kinetic experiments. We find that the RNAP 'beacon" assay monitors real-time base flipping of -11A into a pocket on $\sigma_{2.3}$.**

In Mekler *et al.* 2011a, both free σ^{70} and RNAP σ^{70} holoenzyme recognized the -10 promoter element with the same efficiency and specificity. This suggests that a conformational change is not required for σ^{70} to recognize ssDNA. In the holoenzyme, contacts with DNA downstream of the -10 element strengthen the interaction of σ with nontemplate DNA in the transcription bubble. They also found that binding of the β'

RNAP subunit is sufficient to allow specific recognition of the TG motif of the extended -10 promoter element by σ^{70}.

In Mekler *et al.* 2011b, the authors designed new model downstream fork junction promoter fragments that specifically bind RNAP to mimic the downstream segment of promoter complexes. DNA opening is coupled to RNAP binding to downstream fork junctions; these interactions stabilize the energetically unfavorable transcription bubble. Because of this, the downstream duplex must exceed a critical length for efficient formation of transcription competent open promoter complex.

In Mekler *et al.* 2011c, binding of the RNAP-gp2 complex to promoter DNA and various promoter fragments was monitored using the RNAP "beacon" assay. The RNAP affinity to downstream promoter duplex and also to promoter fragments that lacked downstream promoter DNA was inhibited in the presence of gp2. Gp2 was found to decrease the RNAP binding affinity to template and nontemplate strand segments of the transcription bubble downstream of the -10 promoter element. The authors propose that this inhibition occurs via allosteric mechanism that is set in motion by the gp2 binding to the β' jaw.

In addition to extrinsic fluorophores on RNAP, the intrinsic fluorescence of tryptophans and/or tyrosines on RNAP have been used to monitor RNAP interactions with promoter DNA. Johnson and Chester (1998) used intrinsic RNAP fluorescence to investigate the kinetics of association of *E. coli* RNAP with the T7A1 promoter. They found that association assays above 20°C exhibited biphasic kinetics that were best fit to the sum of two exponentials (referred to here as k_{fast} and k_{slow}). Below 20°C, the association kinetics were best fit to a single exponential. At all temperatures, k_{fast} was

promoter DNA-concentration dependent, and when detected, k_{slow} was promoter [DNA] independent. The authors concluded that these results are best explained by a two-step association mechanism in which RNAP and promoter DNA are in rapid equilibrium (k_{fast}) with the first closed intermediate and then slowly isomerize to form open complexes (k_{slow}). Below 20°C, the T7A1 promoter does not form open complexes at any detectable levels, and therefore only k_{fast} is monitored. In this study, the authors had limited information about which specific tryptophans (and possibly tyrosines) were being reported on in the intrinsic fluorescence assay and therefore they concluded that the assay monitored global effects arising from many tryptophan residues on RNAP. **In this thesis, I use the RNAP "beacon" and intrinsic fluorescence assays to characterize the rates of -11A base flipping and of interactions of $\sigma_{2.3}$ with the -10 element of promoter DNA in real-time.**

Most recently, co-localization single-molecule spectroscopy (CoSMoS), was used to define the initiation pathway at an activator-dependent bacterial σ^{54} promoter. The reversible formation of two closed complexes with greatly differing stabilities was observed, along with multiple attempts for each successful formation of an open complex. σ^{54} was released from the polymerase core during transcription initiation. Such experimental systems are powerful but are currently limited in their temporal resolution to ~1 second, and are unable to provide the rapid mixing needed for transient "burst" kinetics experiments. Further development of new fluorescence techniques will provide a greater understanding of the interactions of RNAP with promoter DNA during transcription initiation.

Transcription Initiation, Elongation, and Termination

As introduced above, the four stages of transcription initiation are: binding of promoter DNA and RNAP-DNA isomerization steps that lead to formation of open complexes; binding of NTPs and reiterative synthesis of short “abortive” RNA transcripts; promoter clearance and transition to productive elongation; and finally, transcription termination and the release of RNAP from the DNA.

RNAP catalyzes the addition of nucleotides to a growing RNA chain by attaching a nucleotide monophosphate to the 3’-OH group of the RNA chain and releasing PP_i. In *E. coli*, the preferred start site nucleotide is ATP followed by GTP. However, U or C start sites have also been identified. At many promoters, RNAP undergoes numerous rounds of “abortive” cycling, whereby short RNA products are produced and released while the RNAP is still bound to the promoter. This process occurs both *in vitro* and *in vivo* (Goldman *et al.* 2009). Goldman *et al* were able to directly measure abortive transcription products 11-15 nt long *in vivo* using linked nucleic acid (LNA) probes. These probes, originally designed for detection of microRNAs, are small LNA-modified oligonucleotide probes that are hybridized to the abortive RNA generated during transcription from a plasmid-borne copy of the N25anti promoter in *E. coli*. Interestingly, Goldman *et al* (2009) hypothesized that the finding that these abortive RNAs accumulate to detectable levels *in vivo* suggests that these abortive transcripts may have a functional role, such as serving as a sequence-specific primer for transcription initiation.

During this initial transcription, RNAP maintains the original contacts with the promoter elements while downstream DNA is unwound and pulled into the active site.

This DNA “scrunching” causes a buildup of stress, leading to rewinding of upstream DNA and a release of energy that allows RNAP to escape the promoter (Revyakin *et al.* 2006, Kapanidis *et al.* 2006). σ^{70} is not required for elongation and is typically released from the transcription complex during this process (Mooney *et al.* 2005). However, σ^{70} can sometimes be retained beyond the transition from initiation to elongation (Mukhopadhyay *et al.* 2001). When this happens, σ_2 can induce a promoter-proximal pause at promoters with a -10 element-like sequence in the nontemplate strand downstream of the +1 start site (Ring *et al.* 1996).

Although promoter sequence and experimental conditions are known to affect the abortive to processive ratio of RNAP transcription, questions still remain regarding the biological function of abortive transcripts and the molecular mechanisms modulating the conversion from abortive to productive transcription by RNAP (Deuschle *et al.* 1986, Hsu *et al.* 2006).

Upstream Binding Transcription Factors

Many transcription factors bind upstream of the promoter where they can interact with the α-CTDs and bend far upstream DNA. Catabolite gene activating protein (CAP) is a far upstream-binding transcription factor that recognizes the promoter DNA minor via a helix-turn-helix DNA binding motif (Kolb *et al.* 1993). Binding of CAP to upstream promoter DNA creates and extensive DNA wrap around both CAP and RNAP. The α-CTDs are required for CAP-mediated transcription activation and must be in the proper orientation for transcription activation to occur (Zhou *et al.* 1994). Factor for inversion stimulation (Fis) is another upstream-binding transcription factor that interacts with promoter DNA via a helix-turn-helix motif (Ross *et al.* 1990). Fis also bends DNA and

the magnitude of the bend is dependent upon the DNA sequences flanking the transcription factor (Pan *et al.* 1996).

Significance of the Work Presented Here

Transcription initiation is regulated by σ factors, accessory protein transcription factors, ligands including NTPs, promoter DNA sequence identity, and RNAP isomerization steps. Although transcription initiation and elongation steps have been extensively studied using biochemical, structural, and molecular genetics methods, it is still unclear how RNAP is able to respond to these various types of regulation to adjust transcription levels at different promoters. It has become increasingly clear that the sequence of the DNA promoter and the resulting RNAP isomerization steps that occur as a result of interactions with the nontemplate and template DNA strands play an important role in the biological activity of the RNAP molecular machine. However, due to the difficulty of characterizing transient intermediates and of obtaining high quality structural information about those intermediates, most research in the field has focused on other dimensions of regulation, including protein regulators, such as transcription factors and σ factors, or on the effects of initiating NTPs.

At the λP_R promoter, there are at least three steps required to convert the initial closed complex to RP_o (Figure 1). However, these intermediates are highly transient and only populated on the millisecond (or faster) time scale. Therefore, there has been a need to develop techniques that are capable of characterizing the kinetically-significant, but transiently populated and unstable intermediates on the RNAP-DNA isomerization pathway.

Here I present my dissertation work on characterization of the unstable intermediates during RNAP transcription initiation at the λP_R promoter. This work expands upon the previous work in the field by providing new information about the DNA opening step, the timing of loading of duplex DNA into the RNAP active site cleft during formation of the first intermediate I_1, the interactions of σ_2 with the -10 element during promoter DNA bending and opening, and the timing of wrapping of promoter DNA around RNAP during transcription initiation. I have also investigated the kinetic pathway of transcription initiation at the T7A1 promoter and the effect of different forms of the open complex at λP_R on the abortive to productive ratios for transcription. These studies provide new information about the regulatory roles of the different intermediates during cellular RNAP activities. An outline of the research questions and my contributions to developing testable hypothesis for each are presented below:

When does the DNA open? Does it open in a single step or multiple? What is the boundary of the downstream footprint for I_1? What are the key structural features of the first open complex I_2? How does the footprint of I_2 compare to the late open complexes RP_o and I_3?

In Chapter Two, I present a draft of my co-first author paper with Amanda Drennan and Ted Gries. In this work, we use real-time permanganate and •OH footprinting to show that duplex DNA is bound in the RNAP active site cleft as early as 100 ms but is not yet opened. In I_1, promoter DNA is periodically protected from ~-60 to +20, suggesting that the DNA is still in a duplex form and is wrapped in the upstream

region. During the conversion of I_1 to I_2, the DNA is opened and periodicity of the downstream DNA goes away.

Does promoter DNA wrap around RNAP during transcription initiation, and how stable is the wrap during each step of initiation (I_1, I_2, I_3, RP_o)? When does unwrapping occur during dissociation (before or after DNA closing)? How does DNA wrapping change upon addition of nucleotides?

Chapter Three is a draft of my first-author paper using equilibrium and real-time stopped flow fluorescence to characterize the formation of a stable promoter DNA wrap around RNAP. For these experiments, I utilized Cy3 and Cy5 FRET dyes placed on the upstream and downstream ends of λP_R promoter DNA in order to directly monitor when the ends of the DNA are brought close together during transcription initiation. By monitoring the extent of wrapping as a function of temperature at equilibrium and in real-time association assays, we can determine which intermediates on the pathway to formation of the stable open complex (I_1, I_2, I_3, and RP_o) are wrapped and estimate the extent of DNA bending in each step.

What is the rate of formation of I_1? When are specific contacts formed between $\sigma_{2.3}$ and promoter DNA (with duplex DNA or the single strands after opening?) How do interactions of $\sigma_{2.3}$ with promoter DNA stabilize the open complex? When are contacts between $\sigma_{2.3}$ and promoter DNA broken during dissociation (before or after DNA closing)?

In Chapter Four, I present a draft of my first author paper using stopped-flow fluorescence to monitor the association kinetics of RNAP with λP_R promoter DNA. For these experiments, I use both the RNAP "beacon" assay and changes in RNAP intrinsic fluorescence to monitor the association of RNAP with LPR promoter DNA in real-time at 19°C. I also use high salt upshift "burst" experiments to destabilize the open complexes formed at 10, 19 and 37°C and to characterize when contacts are broken between $\sigma_{2.3}$ and the promoter DNA with regards to the timing of DNA closing and dissociation of RNAP-promoter DNA complexes to free RNAP and DNA.

Which open complex is responsible for processive transcription elongation? How do conformational changes in RNAP prior to the transition to elongation regulate transcription? What are the affinities of different open complexes for NTPs and what is the initial rate of NTP incorporation? Is the kinetic mechanism for association of RNAP with promoter DNA conserved across all promoters, i.e., is the mechanism a general feature of transcription initiation?

The Final Appendices present unfinished work on transcription initiation for the different open complexes. In Appendix 1, I present preliminary data on the temperature dependence of "beacon" RNAP fluorescence and of permanganate reactivity of RNAP-λP_R promoter DNA complexes formed at wide range of temperatures from 2-37°C.

In Appendix 2, I report preliminary determinations of the association kinetics of RNAP with the λP_R promoter utilizing Cy3 fluorescent probes located at (-100), (+14) or (+29) relative to the start site of transcription

In Appendix 3, I present real-time RNAP “beacon” fluorescence stopped-flow assays to characterize the kinetic pathway for association of RNAP with the T7A1 promoter at 19°C and 37°C. These experiments were designed to provide a direct comparison of the kinetic mechanisms for LPR and the T7A1 promoter.

In Appendix 4, I present a preliminary determination of the association kinetics of RNAP with the *rrnB* P1 promoter using the RNAP “beacon” assay under transcription salt conditions (120mM KCl), and in the presence and absence of the initiating nucleotides ATP and CTP (+1 and +2). This work was performed in collaboration with Jared Winkelman from the Gourse laboratory.

In Appendix 5, I present a preliminary characterization of the rate of NTP incorporation at the +3 position at the λP_R promoter during transcription initiation at 5, 10, 25, and 37°C using thin layer chromatography.

In Appendix 6, I describe preliminary data on the effect of nucleotides on promoter DNA wrapping around RNAP in open complexes at 19°C as monitored by real-time FRET. I also present a preliminary investigation of the effect of heparin on RNAP-DNA complexes at 2, 10 and 19°C.

In Appendix 7, I compare the amounts of long and short transcripts produced by wild-type RNAP at the λP_R promoter under single round conditions at 10°C and 37°C. This work was done in collaboration with Mike Capp.

References

Anand, V. S., and Patel, S. S. 2006. Transient state kinetics of transcription elongation by T7 RNA polymerase. *J Biol Chem.* **281:** 35677-85.

Aiyar, S.E., Gourse, R. L., and Ross, W. 1998. Upstream A-tracts increase bacterial promoter activity through interactions with the RNA polymerase alpha subunit. *Proc Natl Acad Sci U S A.* **95:**14652-7.

Barne, K. A., Bown, J.A., Busby, S.J., Minchin, S. D. 1997. Region 2.5 of the *Escherichia coli* RNA polymerase σ^{70} subunit is responsible for the recognition of the 'extended - 10' motif at promoters *EMBO J.* **16:** 4034–4040.

Blatter, E. E., Ross, W., Tang, H., Gourse, R. L., and Ebright, R. H. 1994. Domain organization of RNA polymerase alpha subunit: C- terminal 85 amino acids constitute a domain capable of dimerization and DNA binding. *Cell.* **78:** 889–896.

Borukhov, S and Nudler, E. 2008. RNA polymerase: the vehicle of transcription. *Trends. Microbiol*. **16:** 126-134.

Brodolin, K., Zenkin, N. & Severinov, K. 2005. Remodeling of the σ70 subunit non-template DNA strand contacts during the final step of transcription initiation. *J. Mol. Biol.* **350:** 930–937.

Browning, D. F., and Busby, S. J. 2004. The regulation of bacterial transcription initation. *Nat. Rev. Microbiol.* **2:** 57-65.

Buc, H. and McClure, W.R. 1985. Kinetics of open complex formation between *Escherichia coli* RNA polymerase and the *lac* UV5 promoter. Evidence for a sequential mechanism involving three steps. *Biochemistry*. **24**: 2712-2723.

Burgess, R. R., Travers, A. A., Dunn, J. J., and Bautz, E. K. F. 1969. Factor stimulating transcription by RNA polymerase. *Nature* **221**: 43-44.

Callaci, S., Heyduk, E., and Heyduk, T. Core RNA polymerase from E. coli induces a major change in the domain arrangement of the σ^{70} subunit. *Cell.* **3:** 229- 238.

Camarero, J. A., Shekhtman, A., Campbell, E. A., Chlenov, M., Gruber, T. M., Bryant, D. A. et al. 2002. Autoregulation of a bacterial sigma factor explored by using segmental isotopic labeling and NMR. *Proc. Natl Acad. Sci. USA.* **99:** 8536–8541.

Campbell, E. A., Muzzin, O., Chlenov, M., Sun, J. L., Olson, A., Weinman, O., Trester-Zedlitz, M. L., and Darst, S. A. 2002. Structure of the bacterial RNA polymerase promoter specificity σ subunit. *Mol. Cell*. **9:** 527-539.

Cellai, S., Mangiarotti, L., Vannini, N., Naryshkin, N., Kortkhonjia, E., Ebright, R.H., and Rivetti C. 2007. Upstream promoter sequences and alphaCTD mediate stable DNA wrapping within the RNA polymerase-promoter open complex. *EMBO.* **3:** 271-8.

Craig, M. L., Suh, W. C., and Record, M. T., Jr. 1995. HO• and DNase I probing of $E\sigma^{70}$ RNA polymerase-λP_R promoter open complexes: Mg^{2+} binding and its structural consequences at the transcription start site. *Biochemistry* **34:** 15624–15632.

Craig, M. L., Tsodikov, O. V., McQuade, K. L., Schlax, P. E., Jr., Capp, M. W., Saecker, R. M., and Record, M. T., Jr. 1998. DNA footprints of the two kinetically significant intermediates in formation of an RNA polymerase-promoter open complex: Evidence that interactions with start site and downstream DNA induce sequential conformational changes in polymerase and DNA. *J Mol Biol* **283:** 741–756.

Davis, C. A., Bingman, C. A., Landick, R., Record M. T., Jr., and Saecker, R. M. 2007. Real-time footprinting of DNA in the first kinetically significant intermediate in open complex formation by *Escherichia coli* RNA polymerase. *Proc Natl Acad Sci* (USA) **104:** 7833- 7838.

Davis, C. A., Capp, M. W., Record, M. T., Jr., and Saecker, R. M. 2005. The effects of upstream DNA on open complex formation by *Escherichia coli* RNA polymerase. *Proc Natl Acad Sci (USA)* **102:** 285–290.

de Haseth, P. L., Zupancic, M. L., and Record, M. T. Jr. 1998. RNA polymerase-promoter interactions: the comings and goings of RNA polymerase. *J. Bacteriol.* **180:** 3019-3025.

Deuschle, U., Kammerer, W., Gentz, R., and Bujard, H. 1986. Promoters of *Escherichia coli*: a hierarchy of *in vivo* strength indicates alternate structures. *EMBO J.* **5:** 2987–2994

Ederth, J., Artsimovitch, I., Isaksson, L. A., and Landick, R. 2002. The downstream DNA jaw of bacterial RNA polymerase facilitates both transcriptional initiation and pausing. *J Biol Chem* **277:** 37456–37463.

Estrem, S.T., Gaal, T., Ross, W., and Goursde, R. L. 1998. Identification of an UP element consensus sequence for bacterial promoters. *Proc Natl Acad Sci U S A.* **95:** 9761-6.

Feklistov, A., Barinova, N., Sevostyanova, A., Heyduk, E., Bass, I., Vvedenskaya, I. et al. 2006. A basal promoter element recognized by free RNA polymer- ase sigma subunit determines promoter recognition by RNA polymerase holoenzyme. *Mol. Cell.* **23:** 97–107.

Feklistov A., and Darst S. A. 2011. Structural basis for promoter-10 element recognition by the bacterial RNA polymerase σ subunit. *Cell.* **147:** 1257-69.

Goldman, S. R., Ebright, R. H., and Nickels, B. E. 2009. Direct detection of abortive RNA transcripts *in vivo. Science* **324:** 927–928.

Gourse, R. L., Ross, W., and Gaal, T. 2000. UPs and downs in bacterial transcription initiation the role of the α subunit of RNA polymerase in promoter recognition. *Mol. Microbiol.* **37:** 687-695.

Gruber, T. M., and Gross, C. A. 2003. Multiple sigma subunits and the partitioning of the bacterial transcriptional space. *Annu. Rev. Microbiol.* **57:** 441-466.

Gribskov M., and Burgess, R. R. 1986. Sigma factors from E. coli, B. subtilis, phage SP01, and phage T4 are homologous proteins. *Nucleic Acids Res 14:* 6745.

Gries, T. J., Kontur, W. S., Capp, M. W., Saecker, R. M., and Record, M. T., Jr. 2010. One-step DNA melting in the RNA polymerase cleft opens the initiation bubble to form an unstable open complex. *Proc Natl Acad Sci (USA)* **107:** 10418-10423.

Gruber, T. M., Gross, C. A. 2003. Multiple sigma subunits and the partitioning of bacterial transcription space *Annu. Rev. Microbiol.,* **57:** 441–466.

Haugen, S. P., Berkmen, M. B., Ross, W., Gaal, T., Ward, C. & Gourse, R. L. 2006. rRNA promoter regulation by nonoptimal binding of sigma region 1.2: an additional recognition element for RNA polymerase. *Cell.* **125:** 1069–1082.

Haugen, S. P., Ross, W., and Gourse, R. L. 2008. Advances in bacterial promoter recognition and its control by factors that do not bind DNAa. *Nat. Rev. Microbial.* **6:** 507-519.

Haugen, S. P., Ross, W., Manrique, M. & Gourse, R. L. 2008b. Fine structure of the promoter–sigma region 1.2 interaction. *Proc. Natl Acad. Sci. USA.* **105:** 3292–3297.

Helmann, J. D. and deHaseth, P. L. 1999. Protein-nucleic acid interactions during open complex formation investigated by systematic alteration of the protein and DNA binding partners. *Biochemistry* **38:** 5959–5967.

Hsu, L. M., Cobb, I. M., Ozmore, J. R., Khoo, M., Nahm, G., Xia, L., *et al.* 2006. Initial transcribed sequence mutations specifically affect promoter escape properties. *Biochemistry* **45:** 8841–8854

Johnson R. S., and Chester R.E. 1998. Stopped-flow kinetic analysis of the interaction of Escherichia coli RNA polymerase with the bacteriophage T7 A1 promoter. *J Mol Biol.* **283:** 353-70.

Kapanidis, A. N., Margeat, E., Ho, S. O., Kortkhonjia, E., Weiss, S., and Ebright, R. H. 2006. Initial transcription by RNA polymerase proceeds through a DNA-scrunching mechanism. *Science* **314:** 1144-1147.

Kontur W.S., Capp, M.W., Gries, T.J., Saecker, R.M., and Record, M.T., Jr. 2010. Probing DNA binding, DNA opening, and assembly of a downstream clamp/jaw in Escherichia coli RNA polymerase-lambdaP(R) promoter complexes using salt and the physiological anion glutamate. *Biochemistry.* **49:** 4361-73.

Kontur, W. S., Saecker, R. M., Capp, M. W., and Record, M. T., Jr. 2008. Late steps in the formation of *E. coli* RNA polymerase-λP_R promoter open complexes: Characterization of conformational changes by rapid [perturbant] upshift experiments. *J Mol Biol* **376:** 1034–1047.

Kontur, W. S., Saecker, R. M., Davis, C. A., Capp, M. W., and Record, M. T., Jr. 2006. Solute probes of conformational changes in open complex (RP_o) formation by

Escherichia coli RNA polymerase at the λP_R promoter: Evidence for unmasking of the active site in the isomerization step and for large-scale coupled folding in the subsequent conversion to RP_o. *Biochemistry* **45:** 2161–2177.

Lane, W. J. and Darst, S. A. 2010a. Molecular evolution of multisubunit RNA polymerases: Sequence analysis. *J Mol Biol* **395:** 671–685.

Lane, W. J. and Darst, S. A. 2010b. Molecular evolution of multisubunit RNA polymerases: Structural analysis. *J Mol Biol* **395:** 686–704.

Li, X. Y. and McClure, W. R. 1998. Characterization of the closed complex intermediate formed during transcription initiation by by *Escherichia coli* RNA polymerase. *J Biol Chem* **273:** 23549-23557.

Lonetto M., Gribskov M., Gross C.A. The sigma 70 family: sequence conservation and evolutionary relationships*. J Bacteriol.***174:** 3843-9.

Mangiarotti L, Cellai S, Ross W, Bustamante C, Rivetti C. 2009. Sequence-dependent upstream DNA-RNA polymerase interactions in the open complex with lambdaP_R and lambdaP_{RM} promoters and implications for the mechanism of promoter interference. *J Mol Biol.* **385:**748-60.

Mekler, V., Kortkhonjia, E., Mukhopadhyay, J., Knight, J., Revyakin, A., Kapanidis, A. N., Niu, W., Ebright, Y. W., Levy, R., and Ebright, R. H. 2002. Structural organization of bacterial RNA polymerase holoenzyme and the RNA polymerase-promoter open complex. *Cell* **108:** 599–614.

Mekler V., Pavlova O., and Severinov K. 2011a. Interaction of Escherichia coli RNA polymerase σ70 subunit with promoter elements in the context of free σ70, RNA polymerase holoenzyme, and the β'-σ70 complex. *J Biol Chem.* **286:** 270-9.

Mekler V., Minakhin L., and Severinov K. 2011b. A critical role of downstream RNA polymerase-promoter interactions in the formation of initiation complex. *J Biol Chem.* **286:** 22600-8

Mekler V., Minakhin L., Sheppard C., Wigneshweraraj S., and Severinov K. 2011c. Molecular mechanism of transcription inhibition by phage T7 gp2 protein. *J Mol Biol.* **413:** 1016-27.

Mitchell, J. E., Zheng, D., Busby, S. J., and Minchin, S. D. 2003. Identification and analysis of 'extended - 10' promoters in *Escherichia coli*. *Nucleic Acids Res.* **31:** 4689–4695

Mukhopadhyay, J., Kapanidis, A. N., Mekler, V., Kortkhonjia, E., Ebright, Y. W., and Ebright, R. H. 2001. Translocation of σ^{70} with RNA polymerase during transcription: fluorescence resonance energy transfer assay for movement relative to DNA. *Cell* **106:** 453–463

Murakami, K. S. and Darst, S. A. 2003. Bacterial RNA polymerases: The wholo story. *Curr Opin Struct Biol* **13:** 31–39.

Murakami, K. S., Masuda, S., Campbell, E. A., Muzzin, O., and Darst, S. A. 2002a. Structural basis of transcription initiation: An RNA polymerase holoenzyme-DNA complex. *Science* **296:** 1285–1290.

Murakami, K. S., Masuda, S., and Darst, S. A. 2002b. Structural basis of transcription initiation: RNA polymerase holoenzyme at 4 Å resolution. *Science* **296:** 1280–1284.

Nagai, H. and Shimamoto, N. 1997 Regions of the *Escherichia coli* primary sigma factor σ^{70} that are involved in interaction with RNA polymerase core enzyme. *Genes Cells* **2:** 725–734.

Paget, M. S., and Helmann, J. D. 2003. The sigma^{70} family of sigma factors. *Genome Biol.* **4:** 203.

Panaghie, G., Aiyar, S. E., Bobb, K.L., Hayward, R.S., and de Haseth, P.L. 2000. Aromatic amino acids in region 2.3 of Escherichia coli sigma 70 participate collectively in the formation of an RNA polymerase-promoter open complex. *J Mol Biol.* **200:**1217-30.

Revyakin, A., Ebright, R.H., Strick, T.R. 2004. Promoter unwinding and promoter clearance by RNA polymerase: Detection by single-molecule DNA nanomanipulation. *Proc. Natl Acad. Sci. USA.* **101:** 4776–4780.

Revyakin, A., Liu C., Ebright, R.H., Strick, T.R. 2006. Abortive initiation and productive initiation by RNA polymerase involve DNA scrunching. *Science* **314:** 1139-43.

Ring, B. Z., Yarnell, W. S., and Roberts, J. W. 2006. Function of *E. coli* RNA polymerase sigma factor σ^{70} in promoter-proximal pausing. *Cell* **86:** 485–493.

Roberts, C. W., Roberts, J. W. 1996. Base-specific recognition of the nontemplate strand of promoter DNA by *E. coli* RNA polymerase. *Cell* **86:** 495–501

Roe, J. H., Burgess, R. R., and Record, M. T., Jr. 1984. Kinetics and mechanism of the interaction of *Escherichia coli* RNA polymerase with the λP_R promoter. *J Mol Biol* **176:** 495–522.

Rogozina, A., Zaychikov, E., Buckle, M., Heumann, H., and Sclavi, B. 2009. DNA melting by RNA polymerase at the T7A1 promoter precedes the rate-limiting step at 37 °C and results in the accumulation of an off-pathway intermediate. *Nucleic Acids Res* **37:** 5390–5404.

Saecker, R. M. and Record, M. T., Jr. 2002. Protein surface salt bridges and paths for DNA wrapping. *Curr Opin Struct Biol* 12: 311–319.

Saecker, R. M. Record, M. T., and de Haseth, P. L. 2010. Mechanism of Bacterial Transcription Initiation: RNA Polymerase - Promoter Binding, Isomerization to Initiation-Competent Open Complexes, and Initiation of RNA Synthesis. *J Mol Biol* **4:** 754–771

Saecker, R. M., Tsodikov, O. V., McQuade, K. L., Schlax, P. E., Jr., Capp, M. W., and Record, M. T., Jr. 2002. Kinetic studies and structural models of the association of *E. coli* σ^{70} RNA polymerase with the λP_R promoter: Large scale conformational changes in forming the kinetically significant intermediates. *J Mol Biol* **319:** 649–671.

Scherbakova, I. Mitra, S. Beer, R. H. and Brenowitz, M. 2006. Fast Fenton footprinting: a laboratory-based method for the time-resolved analysis of DNA, RNA, and protein. **34:** e48.

Schroeder, L. A., Gries, T. J., Saecker, R. M., Record, M. T., Jr., Harris, M. E., and DeHaseth, P. L. 2009. Evidence for a tyrosine-adenine stacking interaction and for a short-lived open intermediate subsequent to initial binding of *Escherichia coli* RNA polymerase to promoter DNA. *J Mol Biol* **385:** 339–349.

Schroeder, L. A., Karpen, M. E., and deHaseth, P. L. 2008. Threonine 429 of *Escherichia coli* σ^{70} is a key participant in promoter DNA melting by RNA

polymerase. *J Mol Biol* **376:** 153–165.

Schwartz, E. C., Shekhtman, A., Dutta, K., Pratt, M. R, Cowburn, D., Darst, S., and Muir, T. W. 2008. A full-length group 1 bacterial sigma factor adopts a compact structure incompatible with DNA binding. *Chem. Biol.* **15:** 1091-1103.

Sclavi, B., Zaychikov, E., Rogozina, A., Walther, F., Buckle, M., and Heumann, H. 2005. Real-time characterization of intermediates in the pathway to open complex formation by *Escherichia coli* RNA polymerase at the T7A1 promoter. *Proc Natl Acad Sci (USA)* **102:** 4706–4711.

Travers, A. A. and Burgess, R. R. 1969. Cyclic re-use of the RNA polymerase sigma factor. *Nature* **222:** 537-540.

Tomsic, M., Tsujikawa, L., Panaghie, G., Wang, Y., Azok, J., and deHaseth, P. L. 2001. Different roles for basic and aromatic amino acids in conserved region 2 of *Escherichia coli* σ^{70} in the nucleation and maintenance of the single-stranded DNA bubble in open RNA polymerase-promoter complexes. *J Biol Chem* **276:** 31891–31896.

Tsodikov, O. V. and Record, M. T., Jr. 1999. General method of analysis of kinetic equations for multistep reversible mechanisms in the single-exponential regime: Application to kinetics of open complex formation between $E\sigma^{70}$ RNA polymerase and λP_R promoter DNA. *Biophys J* **76:** 1320–1329.

Vassylyev, D. G., Sekine, S., Laptenko, O., Lee, J., Vassylyeva, M. N., Borukhov, S., and Yokoyama, S. 2002. Crystal structure of a bacterial RNA polymerase holoenzyme at 2.6 Å resolution. *Nature* **417:** 712–719.

Vassylyev, D. G., Vassylyeva, M. N., Perederina, A., Tahirov, T. H., and Artsimovitch, I. 2007. Structural basis for transcription elongation by bacterial RNA polymerase. *Nature* **448:** 157–162.

Wigneswaraj, S., Bose, D., Burrows, P. C, Joly, N., Schumacher, J., Rappas, M., *et al.* 2008. Modus operandi of the bacterial RNA polymerase containing the σ^{54} promoter-specificity factor. *Mol. Microbiol.* **68:** 538-546.

Yin, Y.W., and Steitz, T.A. 2002. Structural basis for the transition from initiation to elongation transcription in T7 RNA polymerase. *Science* **298:**1387-95.

Zhang, G., Campbell, E. A., Minakhin, L., Richter, C., Severinov, K., and Darst, S. A.

1999. Crystal structure of *Thermus aquaticus* core RNA polymerase at 3.3A resolution. *Cell* **98:** 811-824.

Figure Captions

Figure 1. The kinetic pathway for formation of open complexes at the LPR promoter (Figure created by Ruth Saecker and Irina Artsimovich). RNAP and promoter DNA rapidly equilibrate to form the first kinetically-significant intermediate, I_1. The DNA is then opened in a single, rate-limiting step during the conversion of I_1 to I_2. I_2 is unstable and rapidly equilibrates to I_3 and then to the final form of the open complex, RP_o. During the conversion of I_2 to RP_o, the downstream clamp/jaw of RNAP is assembled on the downstream DNA from +10 to +20.

Figure 2. Architecture of bacterial *Thermus thermophilis* RNA polymerase holoenzyme (PDB 1IW7). Core RNAP has five subunits ($\alpha_2\beta\beta'\omega$, 450kDa) and associates with the σ^{70} specificity subunit in order to specifically recognize promoter DNA. The active site is positioned at the bottom of the cleft formed by the β and β' subunits. (Murakami, *et al*. 2002b).

Figure 3. Model of the Stable Open Complex formed by E. coli RNAP. Model of the RNAP- promoter DNA open complex. Downstream mobile elements (DMEs) assemble on downstream DNA during the conversion of I_2 to RP_o. Figure created from PDBs 3IYD and 3LU0 and published in Saecker *et al.* 2010.

Figure 4. Interactions of the RNAP subunits with promoter DNA elements. (Figure created by Ruth Saecker and Irina Artsimovich). σ_2 and σ_4 recognize the -10 and -35 promoter elements. σ^{70} factors also recognize a TG sequence upstream of −10 called the extended −10 and guanines in the discriminator region at −6 and −5. Another region of interest on promoter DNA is the spacer length, which is the number of base pairs separating the −10 and −35 elements, and is optimally 17 bp. Many promoters also contain an AT-rich sequence upstream of the -35 region known as the UP element that has been shown to interact with the c-terminus of the alpha subunits (αCTD) during

promoter binding. The greatest differences between the LPR and T7A1 promoters are in the discriminator region.

Figure 5. Model of the Upstream Wrap for I_1. Model of the first kinetically significant intermediate I_1 preceding formation of the open complex RP_o. The conformation of RNAP (beige) is based on the x-ray crystal structure of the homologous *T. thermophilus* enzyme (PDB 1IW7). The modeled position of promoter DNA in I_1 is based on DNase I, ·OH and $KMnO_4$ footprinting and relevant crystal structures. Figure from Davis *et al.* 2007.

Figure 6. Structure of region 2.3 of σ^{70}. The side chains of K414, K418, Y425, T429, Y430, W433, W434, and Q437 (Lys, green; Tyr, red; Thr, blue; Trp, purple; Gln, pink) are aligned on approximately the same face of the protein, where they can interact with promoter DNA. Y430 has been shown to stack with − 11A of the − 10 region. Figure from Saecker *et al.* 2010.

Figure 1.

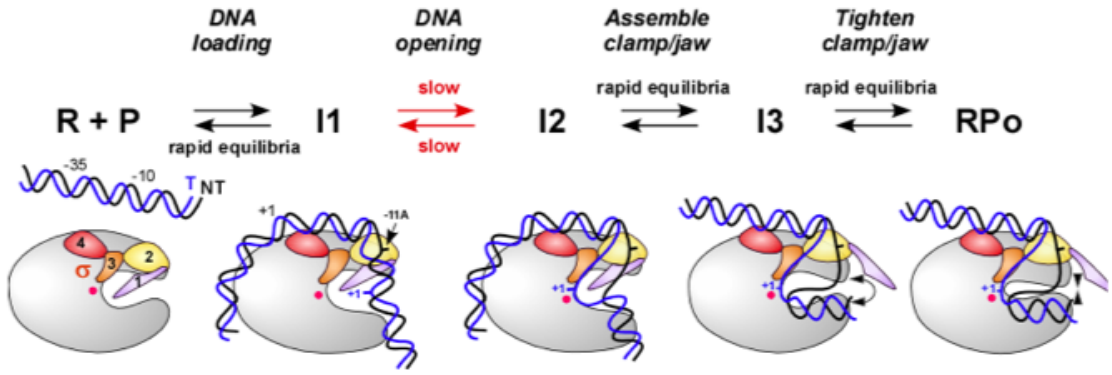
DNA loading
DNA opening
Assemble clamp/jaw
Tighten clamp/jaw
slow
rapid equilibria
rapid equilibria
R + P
rapid equilibria
I1
slow
I2
I3
RPo
-35
-10
T
NT
σ
4
3
2
1
+1
-11A

Figure 2.

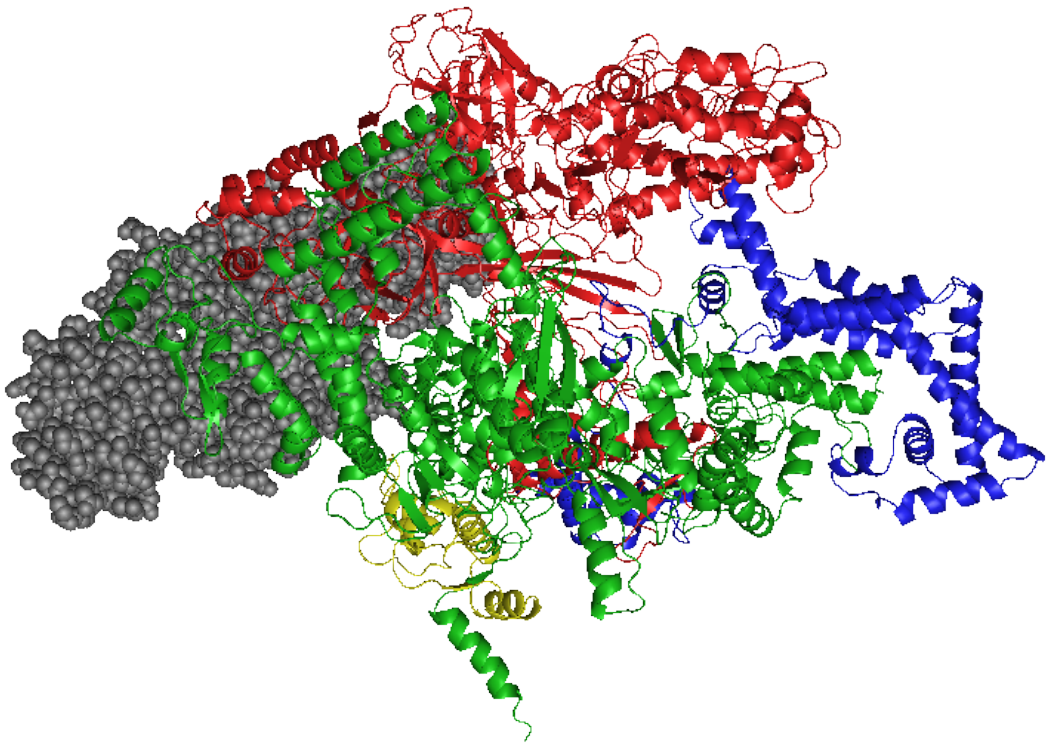

Figure 3.

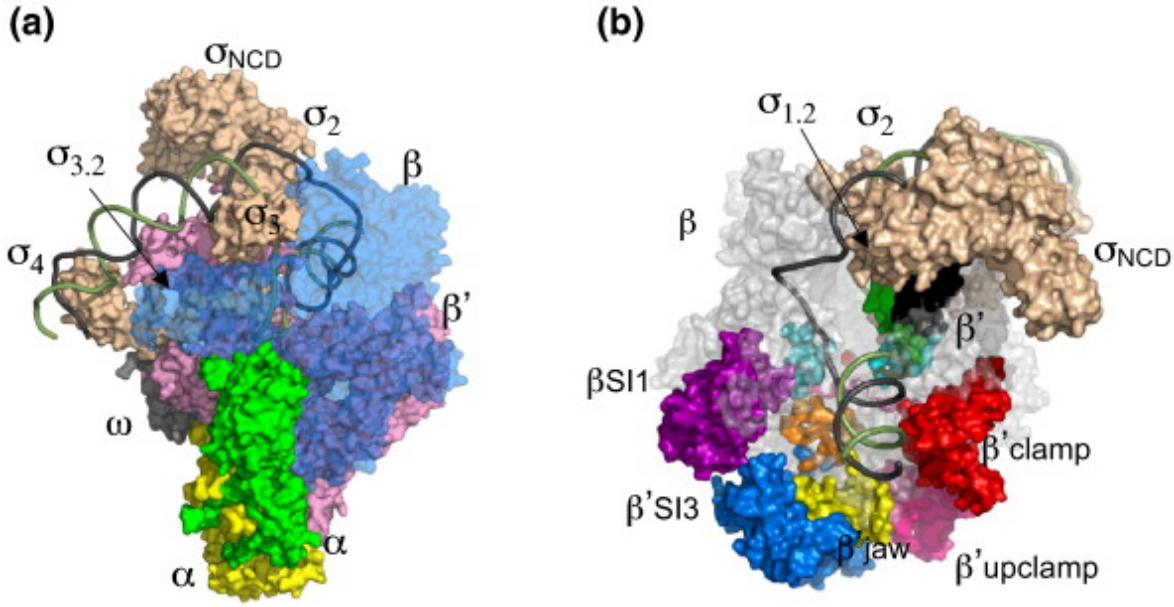
(a)
σNCD
σ2
σ3.2
β
σ3
σ4
β'
ω
α
α
(b)
σ1.2
σ2
β
σNCD
β'
βSI1
β'clamp
β'SI3
β' jaw
β'upclamp

Figure 4.

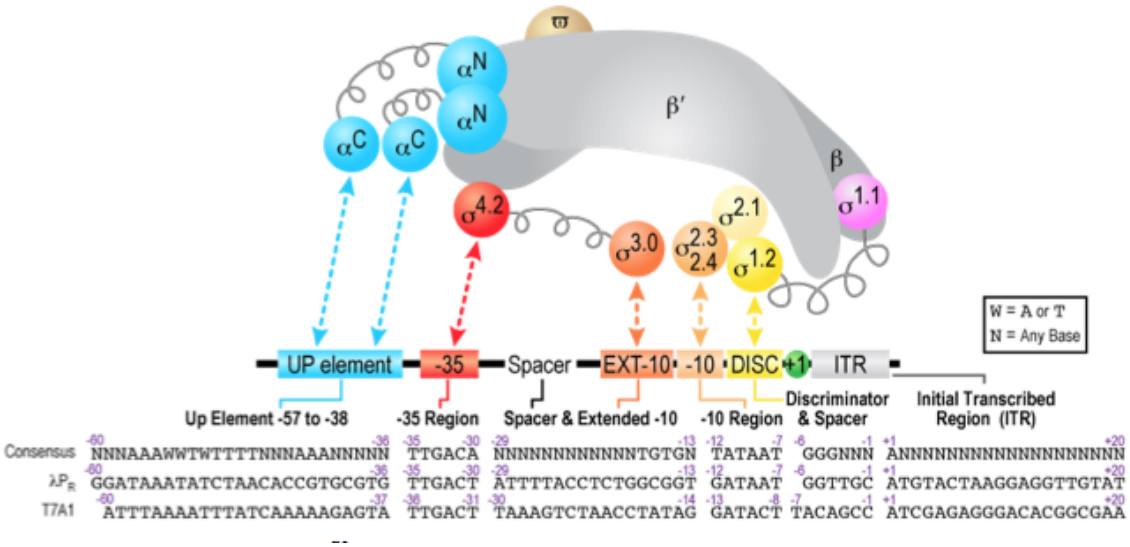
ω
αN
αN
αC
αC
β′
β
σ4.2
σ3.0
σ2.1
σ2.3
2.4
σ1.2
σ1.1
W = A or T
N = Any Base
UP element
-35
Spacer
EXT-10
-10
DISC
+1
ITR
Up Element -57 to -38
-35 Region
Spacer & Extended -10
-10 Region
Discriminator & Spacer
Initial Transcribed Region (ITR)
Consensus NNNAAAWWTWTTTTNNNAAANNNNN TTGACA NNNNNNNNNNNNNTGTGN TATAAT GGGNNN ANNNNNNNNNNNNNNNNNNN
λP_R GGATAAATATCTAACACCGTGCGTG TTGACT ATTTTACCTCTGGCGGT GATAAT GGTTGC ATGTACTAAGGAGGTTGTAT
T7A1 ATTTAAAATTTATCAAAAAGAGTA TTGACT TAAAGTCTAACCTATAG GATACT TACAGCC ATCGAGAGGGACACGGCGAA

Figure 5.

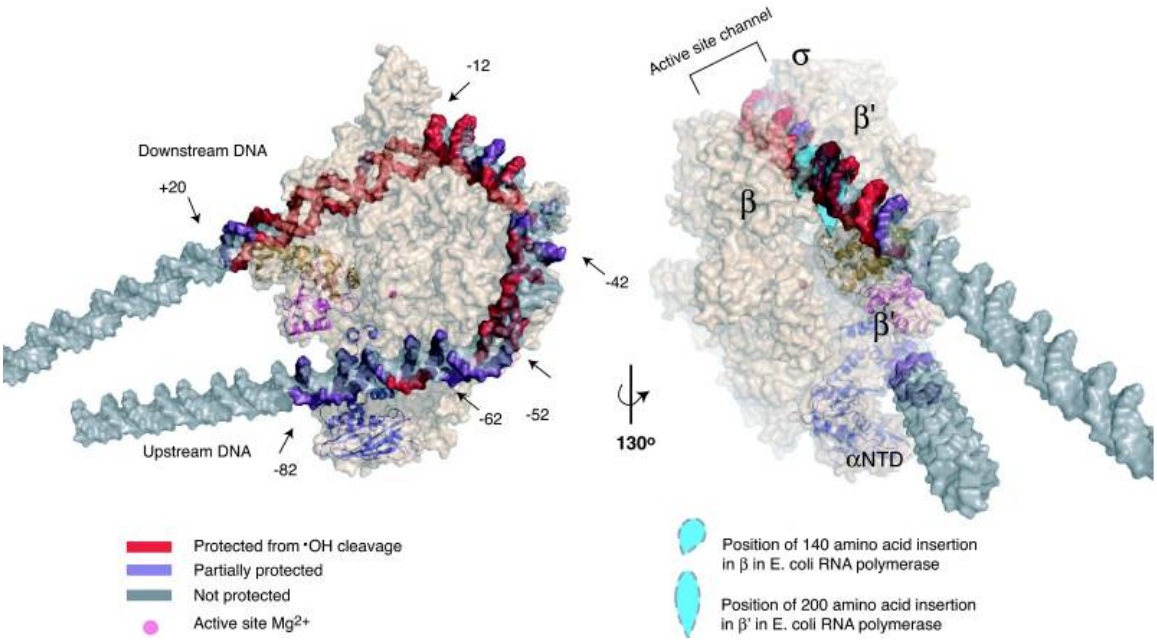
Active site channel
σ
β'
β
β'
αNTD
-12
Downstream DNA
+20
-42
-62
-52
Upstream DNA
-82
130°
Protected from •OH cleavage
Partially protected
Not protected
Active site Mg2+
Position of 140 amino acid insertion in β in E. coli RNA polymerase
Position of 200 amino acid insertion in β' in E. coli RNA polymerase

Figure 6.

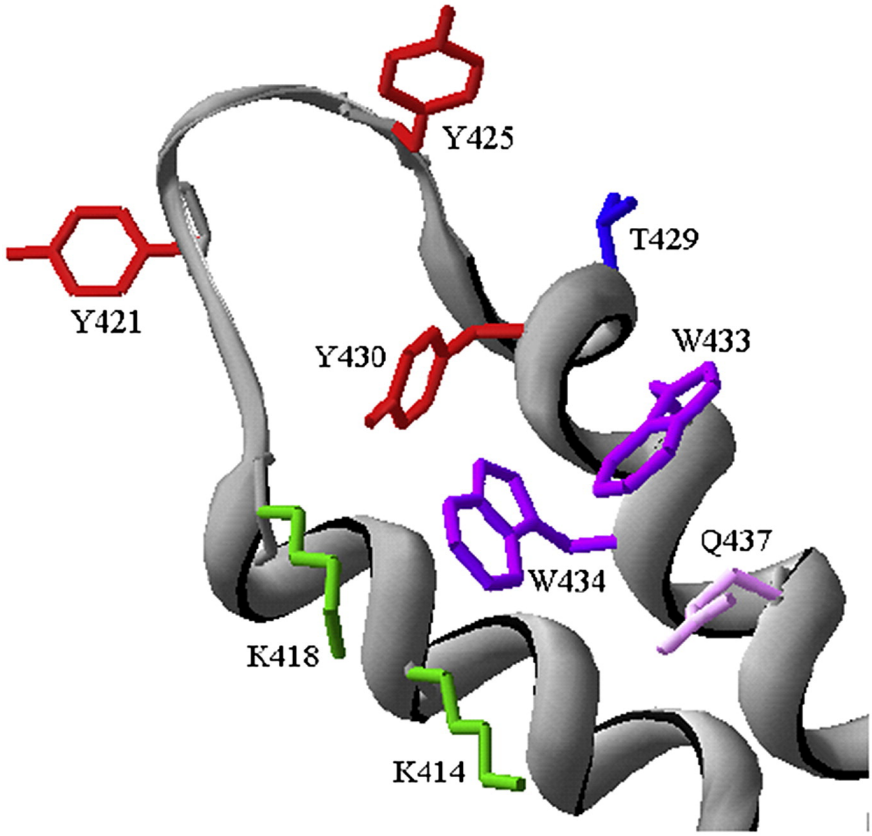

Chapter 2:

Characterization of Key Closed and Open *Escherichia coli* RNA Polymerase– Promoter Intermediate Complexes in Transcription Initiation Using Real-Time Fast Footprinting

Preface: This chapter is in preparation for publication with co-first authors (Amanda Drennan, Theodore Gries, and Sara Heitkamp). My contributions to this research included: collection and analysis of I_1 footprinting data and preparation of the figures, tables, and text. I thank Dr. Theodore Gries, Dr. Amanda Drennan, and Dana Bellissimo for their significant experimental contributions. I also thank Dr. Amanda Drennan for her significant contributions to preparation of the manuscript and figures. I thank Dr. Ted Gries for kinetic simulations. I thank Dr. Ruth Saecker for discussion.

Abstract

The pathway by which *E. coli* RNA polymerase (RNAP) forms initiation-capable open complexes at promoter DNA involves two key intermediates (designated I_1, I_2). Here, we compare real-time fast footprinting snapshots of the DNA backbones (taken by hydroxyl radical, HO•) and open thymine bases (by permanganate, MnO_4^-) of I_1 and I_2 at the λP_R promoter, and compare these two intermediates with free DNA and more stable open complexes (I_3, RP_o). HO• snapshots show that the I_1 intermediate forms rapidly (in < 0.1 s), with as strong protection upstream of the -10 region as in stable open complexes, and somewhat weaker, periodic protection from the -10 region to +25. We conclude that in I_1, one face of the downstream DNA duplex is protected by insertion into the RNAP cleft, but that the DNA strand backbones are not yet engulfed by the RNAP cleft as is characteristic of late open complexes (I_3, RP_o). Fast MnO_4^- footprinting reveals no reactivity of any DNA bases in I_1, indicating that promoter DNA in the cleft is still duplex; furthermore, the rate of DNA opening determined by MnO_4^- footprinting is the same as is obtained by filter binding for formation of competitor-resistant (i.e., open) complexes, three orders of magnitude slower than the rate of formation of I_1 at 55 nM RNAP. Real-time MnO_4^- footprints of I_2 revealed that the entire initiation bubble (-11 to +2) is open, but that the nontemplate (nt) strand is not in its final track, because single stranded thymines (-4, -3, +2) are only half as reactive in I_2 as in (I_3, RP_o) (1). Here, HO• footprints of the nt strand in I_2 reveal that the transcription bubble (-11 to +2) and downstream DNA duplex (+3 to ~ +20) are less strongly protected than in (I_3, RP_o), indicating the nt strand is not yet placed and that downstream mobile elements are not yet fully assembled on this DNA. These results

support the proposal that RNAP is a molecular isomerization machine that bends the DNA duplex into the cleft in the formation of I_1, opens it in the formation of I_2, and then assembles downstream mobile elements on the downstream DNA duplex to form the final open complexes I_3 and RP_o.

Introduction

To better understand regulation of bacterial transcription initiation by promoter sequence, factors, and ligands, it is necessary to understand the series of large-scale conformational changes triggered by initial binding of RNA polymerase holoenzyme (RNAP) to promoter DNA (P) that lead to the formation of transcriptionally-competent open complexes. The current status of the (minimal) mechanism of formation of initiation competent open complexes is:

$$R + P \underset{fast}{\overset{K_1}{\rightleftharpoons}} I_1 \underset{slow}{\overset{k_2}{\underset{k_{-2}}{\rightleftharpoons}}} I_2 \underset{K_{-3}}{\overset{fast}{\rightleftharpoons}} I_3, RP_o \qquad \text{(Mechanism 1)}$$

In this mechanism, RNAP (R) binds to λP_R promoter DNA (P) to form the first kinetically significant intermediate I_1, in which duplex DNA is bent upstream of -35 and -10 promoter regions in order to wrap DNA upstream to ~ -80 (relative to the transcription start site +1) (2), and to direct the downstream duplex (~ -10 to +20) into the downstream DNA binding channel (Davis *et al.* 2007; Saecker *et al.* 2002). In the subsequent bottleneck (slow) step in this mechanism, 13 base pairs of promoter DNA (-11 to +2) are opened in the cleft by RNAP using binding free energy to form the first open intermediate I_2 (Gries *et al.* 2010). In this step the +1 base of the template (t) strand may be specifically loaded into the RNAP active site. The open intermediate I_2 rapidly converts to the late open complexes (I_3, RP_o) by rearrangement of the downstream region of the nontemplate (nt) strand bubble (i.e., the discriminator region) (1) and folding/assembly of downstream mobile elements (DMEs) onto downstream

DNA (Drennan *et al.* unpublished). Hydroxyl radical (HO•) footprinting evidence indicates that DNA in the final open complex (RP_o at 37 ºC) is periodically protected upstream (-70 to -13) and fully protected downstream (-12 to +25) (Craig *et al.* 1995).

To date, the transient noncovalent intermediates of transcription initiation have not been successfully stabilized (e.g., using heteroduplexes) for characterization by high-resolution structural methods. Footprinting studies at temperatures below the transition from closed to open complexes (in the range of 0 ºC to 20 ºC, depending on the promoter) have been used to characterize closed complexes at λP_R (Craig *et al.* 1998), λP_{RM} (upstream variant) (Li and McClure, 1998), *rrnB* P1 (Rutherford *et al.* 2009), T7A1 (Schickor *et al.* 1990), *lac*UV5 (Spassky *et al.* 1985), and groE (Cowing *et al.* 1989) promoters. Extrapolation of stability data from higher temperature indicated that the λP_R closed complex at 2ºC was the I_1 intermediate. Closed complexes in σ^{54}-dependent transcription initiation were trapped and characterized by withholding the activator protein (Popham *et al.* 1989; Sasse-Dwight and Gralla, 1988; Sasse-Dwight and Gralla, 1989). Friedman and Gelles (2012), using a novel multiwavelength single-molecule fluorescence colocalization (CoSMoS) method, demonstrated that there were at least two on-pathway closed complexes and obtained rate and equilibrium constants for formation of these closed complexes by σ^{54} RNAP. Revyakin *et al*. (2004) investigated *E. coli* RNAP binding and subsequent DNA opening (unwinding) at a "consensus" variant of the lac promoter (*lacCONS*) using micromagnets magnets to apply torsional force and hold linear promoter DNA in a negatively or positively supercoiled state, and obtained thermodynamic and kinetic information about these steps as a function of torsional stress (Revyakin *et al.* 2004).

Real-time HO• and permanganate (MnO_4^-) fast footprinting are high resolution methods with excellent time resolution that have been used to obtain both structural and kinetic information about (*i*) transient on-pathway intermediates in RNA folding (Shcherbakova and Brenowitz, 2008), (*ii*) early intermediates in open complex formation by RNAP at T7A1 (Rogozina *et al.* 2009; Sclavi B*, et al.* 2005) and λP_R (Davis *et al.* 2007) promoters, and (*iii*) the initial (intermediate) open complex at the λP_R promoter (Gries *et al.* 2010).

Here, we present real-time single-hit HO• and MnO_4^- fast footprinting experiments that characterize the protection of each base of the promoter DNA backbone and the extent of opening of thymines in the initiation DNA bubble prior to and following DNA opening in transcription initiation. By combining burst experiments to generate relatively homogeneous populations of transcription intermediates with fast footprinting chemistry (Davis *et al.* 2007; Kontur *et al.* 2010; Kontur *et al.* 2008; Saecker *et al.* 2002), we are able to trap and characterize the short-lived closed intermediate I_1 and the short-lived first open intermediate I_2. Fast footprinting of these intermediates provides kinetic information about their rates of formation and conversion, and characterizes the differences in HO• protection in the upstream, transcription bubble, and downstream regions as RNAP binds free promoter DNA and transforms the promoter DNA and itself into the stable open complexes (I_3, RP_o). We find that RNAP is a molecular isomerization machine that inserts the downstream DNA duplex into the RNAP active site cleft in the formation of I_1, opens it using binding free energy in the conversion of I_1 to I_2, and then stabilizes the initial open complex by folding/assembly of

DMEs on the downstream duplex DNA, consistent with previous results (Gries *et al.* 2010; Davis *et al.* 2007; Kontur *et al.* 2008; Kontur *et al.* 2010).

Results

Fast HO• Footprints Demonstrate that the I_1 Intermediate Forms in ≤ 0.1 s and Persists For ~15 s After Mixing RNAP and λP_R

To obtain structural and kinetic information for the first transcription initiation intermediate I_1, we rapidly mix RNAP and λP_R promoter and take fast (< 10 ms time scale) chemical "snapshots" of the backbones of both DNA strands at different times after mixing to characterize changes in their HO• reactivity during open complex formation. For these experiments, a < 10 ms-duration pulse of HO• is generated by the Fenton reaction; Fe(II)-EDTA is rapidly mixed with a preformed RNAP-promoter DNA mixture containing H_2O_2, using a multi-syringe quench flow rapid mixer (Shcherbakova and Brenowitz 2008; Shcherbakova *et al.* 2006). In some previous applications of fast footprinting, synchrotron radiation was used to generate HO• (Rogozina *et al.* 2009; Sclavi *et al*. 2005).

To be quantitatively interpretable, footprinting experiments must be performed in the single-hit regime, in which no more that one-third of promoter DNA molecules have reacted with HO• (Shcherbakova *et al.* 2006; Brenowitz *et al.* 1986). This constraint, together with the need to obtain single base resolution over a span of 100 bases on the sequencing gel, makes detailed visual comparisons of sequencing gels like that shown in Fig. 1 difficult. However, normalized line scans of representative gels (Fig. 2) clearly demonstrate global protection of both the t and nt strands as early as 0.1 s after mixing.

The most important conclusions from analysis of the line scans in Fig. 2 are that (*i*) both nt and t strand promoter DNA backbones from approximately -60 to +25 are protected from HO• cleavage as early as 0.1 s after mixing, (*ii*) the downstream

protection of both strands (-10 to +20 or more) in this time range is non-uniform, with periodic maxima and minima, and (*iii*) neither boundaries, pattern, nor the degree of HO• protection changes greatly between 0.1 s and 15 s (Fig. 2). These data indicate that a large fraction of promoter DNA forms an intermediate complex with an extended, periodic downstream footprint (*i.e.,* I_1) in the first 0.1 s after mixing. Since the protection pattern (and therefore the fraction of promoter DNA which is I_1) remains nearly constant over a time window of two orders of magnitude (0.1 s to 10 s), we conclude that this represents an equilibrium between I_1 and reactants which is rapidly established on the time scale of the conversion of I_1 to I_2 (which requires about 100 s at 19 ºC (Saecker *et al*. 2002; see below). An increase in downstream protection and a reduction in downstream periodicity is observed at long time points, where all promoter DNA has been converted to stable open complexes (I_3, RP_o).

Simulation of the Population Distribution of Free and Complexed Promoter DNA as a Function of Time after Mixing, with Input from HO• Footprinting

Previously, the kinetics of formation of open complexes at the λP_R promoter, as determined by filter binding, were found to involve at least one intermediate, but were single exponential, indicating that the intermediate (I_1) was in rapid equilibrium with free promoter on the time-scale of the subsequent DNA opening step ($k_{-1} >> k_2$; cf. Mech. 1). Analysis of these data yielded the equilibrium constant for forming the closed complex I_1 ($K_1 = k_1/k_{-1}$) and the rate constant for the conversion of I_1 to I_2 (k_2) as a function of temperature (Saecker *et al.* 2002), but provided no information about individual values of k_1 and k_{-1}. From the observation that I_1 forms in less than 0.1 s after mixing 55 nM excess RNAP with promoter DNA, a lower bound on the pseudo-first order rate constant

for forming I_1 is 24.2 s^{-1}, and a lower bound on the second order rate constant k_1 is 4.4 x 10^8 M^{-1} s^{-1}. Given the I_1 binding constant (4.4 x 10^7 M^{-1} at 19 ºC), we conclude that k_{-1} is 10 s^{-1}, which indeed is much larger than k_2 (0.01 s^{-1} at 19 ºC) as required for rapid equilibrium (Saecker *et al.* 2002). Therefore, the footprinting results in Fig. 2 are completely consistent with the expectation based on filter binding: I_1 is in rapid equilibrium with reactants on the 100 s time scale required to form open complexes. Using these parameters, a simulation of the burst of I_1, its persistence in equilibrium with free promoter, and its eventual decay to form stable open complexes is shown in Fig. 3A. This simulation predicts a population distribution of approximately 70% I_1 and 30% free promoter DNA over the time interval from 0.1 s to 1 s; small reductions in the population fractions of I_1 and free promoter as open complexes (I_2, I_3, RP_o) are produced (starting in the time range 1 – 10 s); and larger reductions in these population fractions beyond 15 s as the population of open complexes increases. This simulation provides the information needed to correct the HO• footprints in Fig. 2 for the significant (~30%) subpopulation of free promoter DNA and small population of open complexes (I_2, I_3, RP_o) at each time; these corrected footprints of I_1 (Fig. 4) reveal no major conformational changes of promoter DNA occur between 0.1 s and 15 s.

~10 bp Periodicity in Downstream Region (~ -10 to +20) of Both HO• Footprints of Both Strands of I_1 but not Open Complex HO• Footprints

HO• snapshots of I_1 and open complexes (I_3, RP_o) in Figs. 2 and 4 exhibit clear periodicity. Local maxima and minima identified visually (see arrows Figs. 4C and D) are listed in Table 1 and plotted on structural models of these complexes in Fig. 5, discussed below. This periodic protection does not result from some periodic variation

of the HO• reactivity of free DNA that is independent of and unrelated to binding of RNAP, since the observed periodicities persist even in the “difference” line scans obtained by dividing the line scans of the complexes by that of free DNA (see Materials and Methods).

Most significantly, the downstream regions (-12 to +25) of both strands of I_1 exhibit periodic variations between strong and weak protection with a 10 bp repeat and a 3-4 bp offset between nt and t strands, while late open complexes (I_3, RP_o exhibit uniformly strong protection and no periodicity in this region (Figs. 2 and 4; also (Craig *et al.* 1995). Observation of periodic HO• protection patterns of DNA backbones of both strands in a protein complex with a ~10 bp repeat and 3-4 bp offset indicates that one face of the DNA duplex is protected because it is bound on the protein surface, while the other side of the duplex is exposed. Local maxima and minima in HO• reactivity of both strands of mononucleosomal DNA are periodic (10.2 bp repeat) over the full 146 bp protected, and the patterns of the two strands are offset by 3-4 base pairs, the minor groove width (Hayes *et al*. 1990). The crystal structure of the nucleosome confirms this pattern: the DNA duplex lies in a shallow surface groove, wrapping 1¾ turns around the nucleosome core (Richmond *et al.* 1984; Davey *et al.* 2002). The HO• protection pattern of the I_1 complex between RNAP and λP_R is therefore very similar to that of the nucleosome.

For the upstream region (~ -58 to -12), Table 1 demonstrates that the maxima, minima, and periodicity are the same for I_1 and open complexes (I_3, RP_o). This correspondence between upstream HO• footprints indicates that upstream interactions are formed early and maintained throughout the steps of open complex formation. The

periodic patterns for t and nt strands of open complexes are very similar to those obtained in TB by (Craig *et al.* 1995). A refinement of the previous model (Davis *et al.* 2007) for the wrapping of the observed region (>70 bp) of DNA (-50 to +20) on the surface of RNAP in the I_1 complex is shown in Fig. 5A. The stable open complex (I_3, RP_o, Fig. 5B) has the same HO• protection pattern, and so must have the same upstream contacts and wrapping surface as I_1. Downstream, the uniformly strong protection and absence of periodicity in open complexes results from the conformational changes that engulf both strands in the initiation bubble in the cleft and from the folding/assembly of DMEs to engulf the downstream duplex (+3 to +20 or beyond) in the conversion of I_2 to RP_o (Saecker *et al.* 2002; Kontur *et al.* 2010; Kontur *et al.* 2008; Kontur *et al.* 2006; Drennan *et al.* unpublished).

Fast MnO_4^- Footprinting Demonstrates that I_1 is Closed, and that Opening Occurs at the Rate of Formation of I_2 and Subsequent Open Complexes

MnO_4^- footprinting is a powerful probe of single-stranded or unstacked thymine bases (Sasse-Dwight and Gralla, 1989). Rogazina *et al.* (2009) recently used a combination of fast HO• and MnO_4^- footprinting to take snapshots of the condition of promoter DNA on the time course of open complex formation by RNAP at the T7A1 promoter, and to compare the time evolution of DNA backbone protection and DNA opening. Gries *et al.* (2010) rapidly destabilized the final 10ºC λP_R open complex with a high salt upshift to obtain a transient (0.25 s – 1 s) burst of the intermediate I_2 (simulated in Fig. 3B). Using high concentrations (66.7 M) of MnO_4^-, Gries *et al.* obtained moderate-exposure (150 ms), single-hit snapshots during the burst and decay of the population of I_2, and discovered that I_2 was open at all positions of the initiation

bubble. Here, we apply this method to take shorter-exposure 50 ms duration MnO_4^- snapshots during a burst of I_1 and its subsequent conversion to open complexes. Experiments are performed for the conditions simulated in Fig. 3A (19 ºC, 55 nM RNAP), where a burst of I_1 forms in <0.1 s and persists for >10 s before the population of I_2 and subsequent open complexes increases significantly.

Gel lanes in the insets to Figs. 6A and B show the kinetics of development of MnO_4^- reactivity in the region of the initiation bubble on both nt (Fig. 6A) and t (Fig. 6B) strands. In the first 10 s, where I_1 is the predominant promoter complex, these 50 ms MnO_4^- snapshots detect no reactive (open) thymines. Development of MnO_4^- reactivity at all positions detected with this MnO_4^- dose (i.e., -4/-3 and +2 on the nt strand; -11 and -9/-8 on the t strand) occurs on a much slower timescale. MnO_4^- reactivity is visually detectable in these 50 ms snapshots only after 15 – 25 s, increasing to a plateau at times exceeding 200 s. The time evolution of MnO_4^- reactivity corresponds to that in the simulation of Fig. 3A for the formation of post-I_1 (open) complexes. The observation of substantial MnO_4^- reactivity in 50 ms snapshots at these longer times demonstrates that the dose of MnO_4^- used is sufficient to observe opening; the lack of reactivity in the time window of the burst of I_1 (0.1 s to 10 s) demonstrates that I_1 is not MnO_4^- reactive and hence, by this operational definition, is closed. Base-flipping at -11 (Schroeder *et al.* 2009; Feklistov and Darst, 2011), thought to occur in I_1 (Gries *et al.* 2010), does not expose the thymine at -11 (t strand) to MnO_4^-; nt strand thymines at -10 and -7 in the upstream part of the open region of the nt strand are not detected in either I_1 or subsequent open complexes (Gries *et al.* 2010).

Data for all MnO_4^--reactive positions were analyzed (see Materials and Methods) to obtain the fraction reacted as a function of time, normalized by the average maximum (plateau) reactive fraction for that position, and plotted together for each strand in Figs. 6A and B. Single exponential fits to these data yield values of k_{obs}, the observed rate constant for the formation of MnO_4^--detected complexes at 55 nM excess RNAP; for both t and nt strands, $k_{obs} = 0.01\ s^{-1}$. This k_{obs} is related to k_2, the rate constant of the rate-determining DNA opening step, by $k_{obs} = (K_1[RNAP]/(1+K_1[RNAP]))k_2$. For the conditions of Fig. 6, $(K_1[RNAP]/(1+K_1[RNAP])) = 0.7$, so $k_{obs} = 0.7(k_2) = 0.01\ s^{-1}$, and $k_2 = 0.014\ s^{-1}$. (The uncertainty in k_2 is approximately +/- 50%.) These determinations of k_{obs} at 55 nM RNAP and of the DNA opening rate constant k_2 agree quantitatively with the values predicted from interpolation of filter binding kinetic results at 19 ºC ($k_{obs} = 0.009\ s^{-1}$ at 55 nM RNAP; $k_2 = 0.013\ s^{-1}$) (Saecker *et al*. 2002). Indeed, both MnO_4^- and filter binding assays detect the same population of open, competitor-resistant complexes.

Real-time HO• Snapshots of a Burst of the Initial Open Intermediate I_2

I_2 is the initial, relatively unstable open complex, formed in the rate-determining, DNA-opening step from the closed intermediate I_1 (cf. Mech. 1.; (Gries *et al.* 2010)). Because I_2 is formed in and not before the rate-determining step in the forward (association) direction and, once formed, immediately converts to the more stable open complexes I_3 and RP_o, a sufficient population of I_2 cannot be obtained in association experiments to footprint. However, Kontur *et al.* (2008) and Gries *et al.* (2010) discovered that the RP_o and I_3 open complexes are very rapidly destabilized by an upshift from 0.12 M NaCl to 1.1 M NaCl at 10 ºC, forming a transient burst of the initial

open complex I_2 approximately 0.25 s after the upshift. A majority population of I_2, formed by this upshift in about 0.1 s (cf. Fig. 3B), persists for about 1 s because the DNA closing step converting I_2 to I_1 is the bottleneck step in dissociation, and its rate constant (k_{-2}) is found to be independent of salt concentration. From the kinetic data (Gries *et al.* 2010; Kontur *et al.* 2008), the time evolution of the population of promoter complexes after the salt upshift is simulated in Fig. 3B. This simulation shows that a majority (80%) of promoter DNA, initially present as (I_3, RP_o) open complexes, has been converted to I_2 open complexes in the first 0.25 s after the upshift, whereas 100% of promoter DNA has dissociated from RNAP by 5 – 10 s after the upshift (Fig. 3B, Table 2). Gries *et al.* (2010) found that the entire initiation bubble (-11 to +2) was open in I_2, although MnO_4^- reactivities of all thymines detected (except the t strand +1 T) are less than in I_3/RP_o open complexes.

To detect differences in the extent of DNA backbone protection in I_2 as compared to I_3/RP_o open complexes, fast (<10 ms) HO• footprinting snapshots were taken during the burst of I_2 and its decay to I_1. Sequencing gels showing representative time series of these experiments with the nt strand (labeled upstream) are shown in Fig. 7. As in the HO• footprinting during the burst of I_1 (Fig. 1), these experiments were performed at concentrations of $FeEDTA^{2-}$ (5 mM) and H_2O_2 (0.059 m) chosen to give single-hit product distributions (>70% uncut), so features of the footprints are not visually apparent from Fig. 7. Appropriately normalized line scans of these gel lanes are shown in Fig. 8.

Yellow line scans in Fig. 8 show that, 0.25 s after the salt upshift, where the promoter population is 80% I_2, the entire downstream region (~ -30 to +25) of the nt

strand, from the spacer to the downstream boundary of the footprint, is less protected from HO• attack than in the initial (I_3, RP_o) open complex (red line scans in Fig. 8). This result is not an artifact of footprinting at high salt concentrations; control experiments (Fig. 9) show that the HO• reactivity of free DNA is not a function of salt concentration over this range. (Hence, HO• snapshots of (I_3, RP_o) open complexes obtained at low salt concentration prior to the upshift can be directly compared to those for I_2 and free DNA obtained after the salt upshift). Nor is the higher reactivity of I_2 than I_3/RP_o it an artifact from the delay time in the reaction loop, as control HO• snapshots of I_3/RP_o taken 0.25 s and 10 s after dilution with low salt buffer exhibit no difference in HO• reactivity over this time range. Using the population distribution predicted from the kinetics simulation at 0.25 s (81% I_2, 9% (I_3/RP_o), 11% free DNA; Table 2) and the line scans of free DNA and (I_3, RP_o) (Fig. 8), the I_2 line scan was corrected to obtain the predicted 100% I_2 line scan (black traces in Fig. 8). Line scans before and after correction superimpose within the uncertainty, so the uncorrected (yellow) line scan is also an accurate depiction of the HO• reactivity profile of the nt strand of I_2.

Comparison of HO• snapshots of I_2 with those of (I_3, RP_o) and free DNA reveals the same degree of protection of nt promoter DNA upstream of -30. In this far upstream region, HO• footprints of I_1 and (I_3, RP_o) are nearly superimposable as well (Fig. 4). Together, these data demonstrate that upstream contacts of RNAP with the nt strand (beginning with the -35 region) are formed in I_1 and maintained in I_2 and I_3/RP_o. Preliminary data with the t strand exhibit the same behavior of the upstream region. Downstream of the -35 element, both the spacer region (-30 to -12) and the region in the cleft or contacting the DMEs (-12 to +25) of the nt HO• footprint are less protected in

I_2 than in I_3/RP_o. These data are consistent with the proposal, based on MnO_4^- footprinting, that the discriminator region of the nt strand rearranges in the conversion of the initial open complex (I_2) to the more stable open complexes (I_3, RP_o) (Gries *et al.* 2010).

Discussion

Burst Experiments and Fast Footprinting Provide Structural and Kinetic Information about Key Transcription Initiation Intermediates

Structural and kinetic information about intermediates in a process like open complex formation and transcription initiation is necessary in order to determine the mechanism and characterize the nature and sequence of large-scale conformational changes that occur after initial specific binding of RNAP to promoter DNA. This information is required to understand how these steps are regulated by promoter sequence, factors, ligands, and solution variables. Typically during the time course of any process, as products accumulate and reactants are consumed, mixtures of the various intermediates are present at low concentrations relative to those of reactants and products. However, once the kinetics and thermodynamics of the process have been investigated, and some information has been obtained about the rate-limiting step in each direction, experiments can be designed to obtain a transient burst of the key intermediate that precedes the rate-determining step.

In an optimally designed burst, a near-homogeneous population of the intermediate is obtained which persists for a long enough time to permit characterization. Bursts of the key I_1 and I_2 intermediates, which bracket the slow DNA opening – DNA closing step of this process, meet these criteria as shown in Fig. 3. Filter binding kinetic data predict the conditions that are optimal to obtain a relatively homogeneous population of I_1. At 19 ºC, the equilibrium constant for forming I_1 from promoter DNA is a maximum; at short times after mixing with a large excess (55 nM) of RNAP, 70% of the population of promoter DNA is predicted to be I_1, and 30% unbound

promoter DNA. This population is relatively stable for about 10 s before significant conversion to the subsequent (open, competitor resistant) complexes occurs. However, the filter binding data predict only the I_1 equilibrium constant, and not how rapidly this population of I_1 is established. Fast HO• footprinting snapshots (Figs. 1 and 2) show that a complex with an extended downstream footprint (to +25; i.e., I_1) forms in 0.1 s. The combination of filter binding and fast HO• footprinting snapshots establishes both the amplitude of the burst (70% I_1) and a lower bound for the bimolecular rate constant for forming I_1 from free promoter DNA ($k_1 \geq 4.4 \times 10^8$ M^{-1} s^{-1}). This rate constant is only one order of magnitude less than the diffusion limit, indicating that the process of bending the upstream and downstream duplex to wrap DNA around RNAP in I_1 (subsequent to formation of the initial specific contacts with the promoter) is very efficient. This transient population of I_1 is stable over a time window of about two orders of magnitude (0.1 to 10 s).

To generate a burst population of the I_2 intermediate to study, it is necessary to rapidly destabilize the open complex (I_3, RP_o). Kontur *et al.* (2008) discovered that molar concentrations of urea and salt were excellent destabilizing agents that cause immediate conversion of I_3/RP_o to I_2 but do not affect the kinetics of conversion of I_2 to I_1, for which the rate constant is approximately 0.7 s^{-1} at 10 ºC. The simulation (Fig. 3B) based on the kinetic data of Kontur *et al.* (2008) predicts that after an upshift to 1.1 M salt, a burst of I_2 is generated with the maximum population occurring 0.25 s after initiation of the upshift. In this 0.25 s, the initial population of open complexes at 10 ºC, assumed to be an equilibrium mixture of RP_o and I_3, converts entirely to I_3 and then to I_2 by disassembling DMEs from the downstream DNA. The ability of molar concentrations

of urea and salt to drive conversion of (I_3, RP_o) to I_2 is readily explained: disassembly of DMEs is favored by high urea and high salt. Little information is available about the relative amounts of I_3 and RP_o in equilibrium mixtures of open complexes at different temperatures, and the differences in assembly and binding of DMEs to downstream promoter DNA between these complexes have not been determined. The RNAP jaw deletion variant studied in (Drennan *et al.* unpublished) may be a model for I_3, and exhibits a similar increase in HO• reactivity of the entire downstream region of promoter DNA to that observed here for I_2.

Order of the Steps that Recognize the -10 Region, Put Downstream DNA in the Cleft, and Open It

Unlike eukaryotic polymerases, the *E. coli* σ^{70} RNAP holoenzyme is able to open the DNA transcription bubble without the aid of a helicase cofactor or the energy of ATP hydrolysis. This raises interesting questions about the molecular mechanism of DNA opening during transcription initiation. Is RNAP a molecular machine that actively opens double stranded DNA after it has been loaded into the RNAP cleft (Gries *et al.* 2010, Davis *et al.* 2007; Saecker *et al.* 2011; Saecker *et al*. 2002)? Or, does RNA polymerase take advantage of transient DNA 'breathing" to passively but selectively load the t strand into the enzyme active site (Rogozina *et al.* 2009; Murakami *et al.* 2002; Chen *et al.* 2010)? Crystal structures of the free holoenzyme in the absence of promoter DNA revealed a narrow active site cleft (~15 Å (Murakami *et al.* 2002; Belogurov *et al*. 2009) that appears to be too small for double stranded DNA (~22 Å diameter) to enter, suggesting that the DNA must be opened prior to entering the RNAP

cleft. However, other RNAP studies suggest that flexibility of the RNAP cleft provides opportunities for duplex DNA to enter (Cramer *et al.* 2001; Gnatt *et al.* 2001).

Sclavi and collaborators (Rogozina *et al.* 2009; Sclavi *et al*. 2005) used time-resolved x-ray-generated HO• and fast MnO_4^- footprinting to characterize transcription initiation intermediates for *E. coli* RNAP on the T7A1 promoter. However, without prior knowledge of the kinetic mechanism of T7A1 or the relative populations of intermediates sampled at a given time and set of experimental conditions, it is difficult to assign identities to each of the relative HO• protection amplitudes or to determine the step(s) in the mechanism where opening occurs.

Recently, the structure of a Taq σ^A fragment comprising σ^A regions 2 and 3 bound to a single stranded DNA fragment containing the -10 nt strand sequence was determined (Feklistov and Darst, 2011). The authors concluded from the structure and from biochemical data that σ^A region 2.3 captures the nt strand after the DNA is opened. In their model, the nt strand within the -10 promoter element is specifically recognized by σ region 2.3 via direct interactions with the DNA bases. The -11A and -7A nt strand bases are flipped out of the DNA base stack and buried in hydrophobic pockets on RNAP. Under the conditions for which the authors perform equilibrium binding studies, specific recognition of the -10 promoter DNA occurs only upon strand separation, with little to no specific recognition of the duplex -10 element. However, we provide footprinting evidence that duplex DNA is bent and loaded into the RNAP active site in I_1, and, more specifically, that the -10 element is as protected in I_1 as it is in (I_3, RP_o), indicative that specific contacts between the -10 element and σ region 2 are formed before the DNA is opened. In our model, -11A is flipped out of the DNA base stack prior

to DNA opening; however -7A is not flipped out into a hydrophobic pocket on RNAP until the DNA becomes melted in the I_1 to I_2 transition. While the contacts downstream in I_1 strengthen during the conversion to RP_o, the upstream contacts are formed in I_1 and persist.

Interactions of RNAP with the duplex DNA downstream of the start site are required for stabilization of the open transcription bubble in RP_o, as heteroduplex probes lacking downstream DNA were found to bind much weaker than those with DNA downstream to +12 (Mekler *et al.* 2011). Interactions of RNAP with the open bubble are weak in the context of model promoter fragments therefore formation of the upstream interactions alone may be unable overcome the unfavorable energetic barrier on the pathway to formation of the final open complex, RP_o. Here, we have shown that the first open complex I_2 is weakly and partially protected from cleavage by HO• both in the RNAP cleft and in the downstream DNA binding channel. I_2 is highly unstable relative to I_1 and (I_3, RP_o) at all temperatures, and rapidly converts to (I_3, RP_o) during transcription initiation. Assembly of the downstream RNAP elements around the duplex downstream DNA likely stabilizes the energetically unfavorable open DNA bubble.

In our model (Fig. 5), consistent with Davis *et al.* 2007 and as proposed in Gries *et al.* 2010 and Saecker *et al.* 2011, weak contacts between RNAP and downstream DNA are initially formed when duplex DNA is bent and loaded into the RNAP active site cleft during formation of I_1. In I_1, promoter DNA is periodically protected downstream (~-10 to +25), consistent with wrapping around the exterior of RNAP. During formation of I_2, the DNA is opened, but the downstream DNA is only weakly contacted by RNAP DMEs. However, the downstream protection is no longer periodic, indicating that all faces of the

DNA are interacting with RNAP. Upon conversion to RP_o, the downstream DNA duplex becomes engulfed by RNAP DMEs, which stabilize the open transcription bubble. In RP_o, downstream DNA is highly protected from HO• cleavage and the open complex is extremely stable, with a dissociation constant of 6.2×10^{-5} s^{-1} at 17 ºC (Kontur *et al.* 2006). Therefore, we propose that both specific interactions with both the single stranded upstream region of the transcription bubble and the downstream DNA duplex are required for formation of the late open complexes (I_3, RP_o).

Materials and Methods

Buffers– Storage buffer for RNAP at -80 °C (SB) contained 10 mM Tris (pH 7.5 at 4°C), 6.85 M glycerol, 100 mM NaCl, 100 nM Na_2EDTA, and 100 nM DTT. Binding buffer used in HO• footprinting experiments (HO• BB) was 1 mM Na_2HPO_4 (pH 8.0 at the temperature of the experiment), 10 mM $MgCl_2$, 120 mM NaCl, and 100 μg/ml BSA. Binding buffer used in MnO_4^- footprinting experiments (MnO_4^- BB) was 40 mM Tris (pH 8.0 at the temperature of the experiment), 10 mM $MgCl_2$, 120 mM NaCl, and 100 μg/ml BSA. Urea loading buffer, used to resuspend footprinting samples, contained 8 M urea, 0.5 x TBE, 0.05% xylene cyanol, and 0.05% bromophenol blue.

RNAP preparation and purification– *E. coli* σ^{70} RNA polymerase was prepared, purified, and stored as described in (Gries *et al.* 2010). Stable open complexes between RNAP holoenzyme and λP_R promoter DNA were formed at room temperature by incubating RNAP in SB with ^{32}P-DNA for ~90 minutes. For forward direction association experiments, the final (I_3, RP_o) solution contained 55 nM active RNAP, < 1 nM DNA, 4% SB (from the RNAP solution), and HO• BB or MnO_4^- BB components at the listed concentrations. For back direction dissociation experiments, the final (I_3, RP_o) solution contained 20 nM active RNAP, < 1 nM DNA, 4% SB (from the RNAP solution), and HO• BB or MnO_4^- BB components at the listed concentrations.

λP_R promoter DNA preparation and purification– λP_R promoter duplex DNA fragments for I_1 (~180 bp long) were PCR-amplified from plasmid pPR59 (λP_R (-59 to +34) (37), a gift from Dr. Wilma Ross) and isolated using the Qiagen QIAquick PCR Purification Kit. For t strand downstream kinase label, duplex fragments were cleaved

with BssHII (NEB); 5' phosphates were removed with Antarctic Phosphatase (NEB); 5' phosphates were replaced with ^{32}P ([γ-^{32}P] ATP was added via T4 polynucleotide kinase (NEB)); 3' ends were filled in via Sequenase (USB) with 1 mM cold dGTP + dCTP; and the upstream end was cut with EcoRV to remove the upstream label. For nt strand downstream fill-in label, duplex fragments were cleaved with EcoRV and BssHII, and then filled in downstream with [α-^{32}P] dCTP (along with 1 mM cold dGTP + dCTP) via Sequenase. Labeled fragments were purified on a 5% acrylamide gel and isolated using an Elutip-d Purification Minicolumn (Whatman).

λP_R promoter DNA for I_2 footprints (wild type λP_R sequence -60 to +20) was prepared, purified and labeled as in (Gries *et al.* 2010).

Fast HO• footprinting: I_1– RNAP in HO• BB (also contained 4% SB, see above) and λP_R promoter DNA + 0.4 % H_2O_2 in HO• BB were independently loaded into a KinTek Corporation RQF-3 Rapid Chemical Quench-Flow instrument and cooled to 19°C using an attached circulating water bath. Whenever possible, the amount of glycerol present was kept at a minimum because glycerol is a potent HO• scavenger (Shcherbakova and Brenowitz, 2008).

For single-hit HO• reactions, *push syringe C* was loaded with HO• BB supplemented with 16.5 mM EDTA and 15 mM $(NH_4)_2Fe(SO_4)_2$. The quench-flow instrument was operated in a *push-pause-push* mode. The first push rapidly mixed RNAP with λP_R promoter DNA, and this solution was held in the *T-loop* for the desired perturbation time. The second push subjected the contents of the *T-loop* to 5 mM $FeEDTA^{2-}$. (Note that this produces a burst of HO•s that react on the order of ~10 ms.) During the second push, the sample was expelled into a collection tube containing 500

µl ethanol to quench the reaction. By using reaction times between 0.1 s and 600 s, only *reaction loop 7* was used. Quenched reactions were immediately ethanol precipitated and purified by Illumina Microspin GE-25 columns or Chroma Spin™+ TE-10 columns. Purified DNA fragments were concentrated by ethanol precipitation, resuspended in urea loading buffer, and resolved on an 8% acrylamide sequencing gel. Only a subset of these footprints was of sufficient quality to perform advanced analysis.

Fast HO• footprinting: I_2– Pre-formed RP_o complexes in HO• BB (also contained 4% SB, see above) were loaded into the *sample A* tube of a KinTek Corporation RQF-4 Rapid Chemical Quench-Flow instrument, cooled to 10 ºC by a circulating water bath. The *sample B* tube was loaded with HO• BB (without SB) supplemented with additional NaCl to 2.08 M, 400 µg/ml heparin, and 0.4% H_2O_2. *Push syringe A* was loaded with HO• BB, while *push syringe B* was loaded with HO• BB supplemented with additional NaCl to 2.08 M and 400 µg/ml heparin. For HO• footprinting experiments, only the pre-formed RP_o solution (*sample A tube*) and not the *push syringe* solutions contained SB (to minimize the final glycerol concentration). For single-hit HO• reactions, *push syringe C* was loaded with HO• BB supplemented with additional NaCl to 1.1 M, 400 µg/ml heparin, 16.5 mM EDTA, and 15 mM $(NH_4)_2FE(SO_4)_2$. *Push syringe D* was loaded with a quench solution containing 120 mM thiourea, 80 mM EDTA, and 800 mM NaCl.

The quench-flow instrument was operated in a *push-pause-push-pause-push* mode. The first push rapidly mixed the pre-formed open complexes with the high salt solution, resulting in a final [NaCl] of 1.1 M and 0.2% H_2O_2. This solution was held in the *T-loop* for the desired perturbation time. The second push mixed the contents of the *T-loop* with the solution in *push syringe C*, resulting in a final $[FeEDTA]^{2-}$ of 5 mM. This

solution was held in the *reaction loop 3* for 10 ms before the final push mixed the contents of *reaction loop 3* with the quench solution from *push syringe D* and expelled the solution into the collection tube. By using reaction times between 0.25 s and 10 s, only *reaction loop 3* was used. Quenched reactions were immediately ethanol precipitated and purified by Chroma Spin™ TE+10 columns. Purified DNA fragments were concentrated by ethanol precipitation, resuspended in urea loading buffer, and resolved on an 8% acrylamide gel.

Each load-reaction cycle took 250 seconds. Low salt RP_o control reactions (isotonic dilution of RP_o) were performed as above, except that the NaCl supplement was omitted to maintain [NaCl] at 120 mM.

HO• footprinting analysis– Footprinting gels were dried and exposed to a storage phosphoimager screen. The screen was read by a Typhoon 9410 scanner. Line scans for HO• footprints were obtained by drawing a line down each lane (ImageQuant version 5.1) and creating a plot of signal intensity (directly proportional to radioactive counts) versus run length (Microsoft Excel). Plots for each lane of an experiment were normalized by dividing the signal for each position by the average signal from a limited region of the footprint (excluding the uncut band) constituting several long DNA fragments (in the compression region of the gel; ~ -70 to -60 for downstream labeled fragments).

After normalization to a short upstream region outside of the known DNA footprint, a moving average of 10 was applied to each data set to decrease the noise within the line scans. When indicated, the line scans for a specific complex (I_1, I_2) were corrected for the calculated population of respective complexes. The HO• reactivity (r_{obs}) of a

position within the promoter DNA backbone is the sum of contributions from each species at any time during the formation of I_3/RP_o:

$$r_{obs}^{t} = \theta_{I_3/RP_o}^{t} r_{I_3/RP_o} + \theta_{I_1}^{t} r_{I_1} + \theta_{FreeDNA}^{t} r_{FreeDNA} \qquad \text{(Equation 1)}$$

or during the dissociation of I_3/RP_o:

$$r_{obs}^{t} = \theta_{I_3/RP_o}^{t} r_{I_3/RP_o} + \theta_{I_2}^{t} r_{I_2} + \theta_{FreeDNA}^{t} r_{FreeDNA} \qquad \text{(Equation 2)}$$

where θ_i^t is the fraction of total promoters predicted to be in species *i* (where *i* = I_3/RP_o, I_2, I_1, or free DNA; see Fig. 3 and Table 2) at a given time (t) after mixing, and r_i is the corresponding intrinsic reactivity of a position in species *i*. This population fraction analysis can be applied to obtain the intrinsic reactivity of each position in I_1 complexes (where t = 0.1 s to 15 s):

$$r_{I_1} = \frac{(r_{obs}^{t} - \theta_{I_3/RPo}^{t} r_{I_3/RPo} - \theta_{FreeDNA}^{t} r_{FreeDNA})}{\theta_{I_1}^{t}} \qquad \text{(Equation 3)}$$

or in I_2 complexes:

$$r_{I_2} = \frac{(r_{obs}^{t} - \theta_{I_3/RPo}^{t} r_{I_3/RPo} - \theta_{FreeDNA}^{t} r_{FreeDNA})}{\theta_{I_2}^{t}} \qquad \text{(Equation 4)}$$

The intrinsic reactivity of I_3/RP_o ($r_{I3/RPo}$) and of free DNA ($r_{FreeDNA}$) were determined from control footprints known to contain either only I_3/RP_o or only free DNA, as previously determined by nitrocellulose filter binding experiments (20, 21). The calculated values of r_{I_1} and r_{I_2} have large uncertainty because the calculation involves differences between terms with quite large uncertainties (calculated uncertainty from replicates within a single experiment is ±10%).

For analysis of periodic protection, HO• line scans of I_3/RP_o footprints and corrected I_1 footprints were fit in Excel to a moving average (10 per moving average) to decrease noise and thus clarify the local maxima and local minima according to the respective sequencing lanes within a footprint. The local maxima and minima from two independent line scans for both the t and nt strands were mapped onto the working model of I_1 (Table 1; Fig. 5). The periodicities observed in the I_1 line scans are preserved in the "difference" line scans obtained by dividing the line scans of the complexes by that of free DNA:

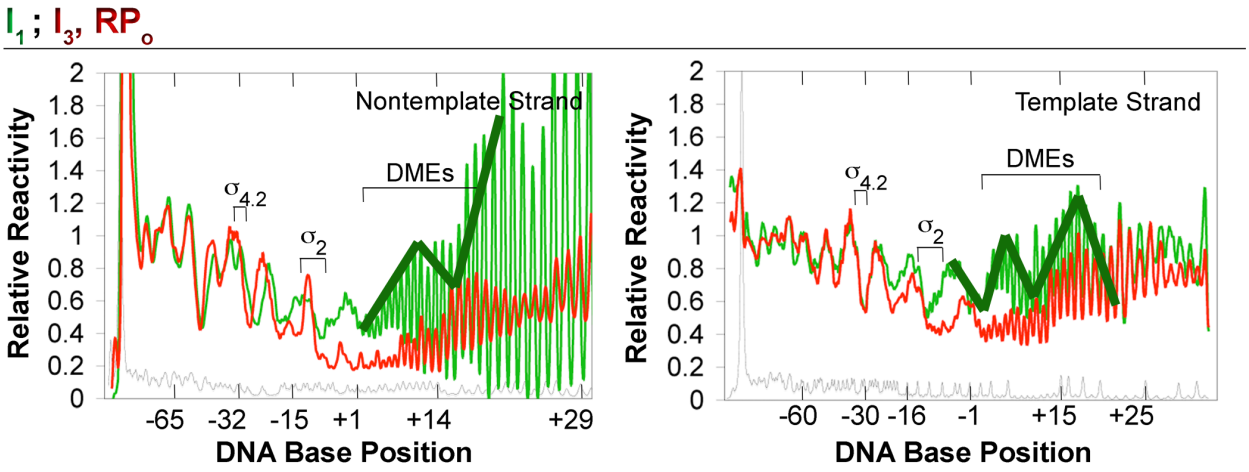

Fast MnO_4^- footprinting: I_1– RNAP in MnO_4^- BB (also contained 4% SB, see above) and λP_R promoter DNA in MnO_4^- BB were independently loaded into a KinTek Corporation RQF-3 Rapid Chemical Quench-Flow instrument, and cooled to 19°C by a circulating water bath within the instrument. The solutions of RNAP and promoter DNA were mixed and held in *reaction loop 7* for varying times before the final push mixed the complexes with 66.7 mM $NaMnO_4$ for 50 ms. Following MnO_4^- modification, samples were expelled into a collection tube containing a 500 µl ethanol quench. Quenched reactions were immediately ethanol precipitated and washed. Modified fragments were cleaved by 1 M piperidine at 90°C. Reactions were evaporated and resuspended in TE buffer (10 mM Tris, 1 mM EDTA, pH 8.0) twice. After a third evaporation cycle, the purified DNA fragments were resuspended in urea loading buffer and resolved on an 8% acrylamide sequencing gel.

Here, we used a high concentration of MnO_4^- (66.7 M) in order to ensure that our ability to detect the rate of formation of open complexes was not limited by the rate of reactivity of the MnO_4^-. Control reactions with RP_o show that the reactivity of single stranded DNA bases mixed with MnO_4^- (~ 1 $M^{-1}s^{-1}$, (38)) for 50 ms (~ 0.07 s^{-1}) is identical to that observed for complexes mixed with MnO_4^- for longer times. Therefore, we are able to detect a rate of formation of open complexes that accurately reflects the real-time rate of opening.

MnO_4^- footprinting analysis– Each lane and reactive band of a given MnO_4^- footprint was boxed using ImageQuant TL, and the total intensity within each box quantified. The intensity of each uncut and reactive band was divided by the sum of the intensities of the uncut and reactive bands within a given lane, thus providing the fraction of promoter

DNA that is modified at a given position. Values of these intensities for the free DNA lanes were subtracted from those of each sample lane to correct for background. These corrected intensities were plotted vs. time and fit to a single exponential time course. To construct Fig. 6, all corrected intensities were normalized by the appropriate fitted plateau intensity and platted as normalized reactivities vs. time.

References

Belogurov, G.A.*, et al*. 2009. Transcription inactivation through local refolding of the RNA polymerase structure*. Nature.* **457:** 332-335.

Brenowitz, M., Senear, D. F., Shea, M. A. and Ackers, G. K. 1986. Quantitative DNase footprint titration: A method for studying protein-DNA interactions*. Methods Enzymol.* **130:** 132-181.

Chen, J., Darst, S. A. and Thirumalai, D. 2010. Promoter melting triggered by bacterial RNA polymerase occurs in three steps*. Proc Natl Acad Sci U S A.* **107:** 12523-12528.

Cowing, D.W., Mecsas, J., Record, M.T., Jr, and Gross, C.A. 1989. Intermediates in the formation of the open complex by RNA polymerase holoenzyme containing the sigma factor sigma 32 at the groE promoter*. J Mol Biol.* **210:** 521-530.

Craig, M.L., Suh, W.C., and Record M.T., Jr. 1995. HO and DNase I probing of E sigma 70 RNA polymerase--lambda PR promoter open complexes: Mg2+ binding and its structural consequences at the transcription start site*. Biochemistry.* **34:** 15624-15632.

Craig, M. L.*, et al*. 1998. DNA footprints of the two kinetically significant intermediates in formation of an RNA polymerase-promoter open complex: Evidence that interactions with start site and downstream DNA induce sequential conformational changes in polymerase and DNA*. J Mol Biol.* **283:** 741-756.

Cramer, P., Bushnell, D. A. and Kornberg, R. D. 2001. Structural basis of transcription: RNA polymerase II at 2.8 angstrom resolution*. Science.* **292:** 1863-1876.

Davey, C. A., Sargent, D. F., Luger, K., Maeder, A. W. and Richmond, T. J. 2002. Solvent mediated interactions in the structure of the nucleosome core particle at 1.9 a resolution. *J Mol Biol.* **319:** 1097-1113.

Davis, C.A., Bingman, C.A., Landick, R., Record, M.T., Jr and Saecker, R.M. 2007. Real-time footprinting of DNA in the first kinetically significant intermediate in open complex formation by escherichia coli RNA polymerase. *Proc Natl Acad Sci U S A.* **104:** 7833-7838.

Feklistov, A., and Darst, S.A. 2011. Structural basis for promoter-10 element recognition by the bacterial RNA polymerase sigma subunit. *Cell.* **147:** 1257-1269.

Friedman, L. J., and Gelles, J. 2012. Mechanism of transcription initiation at an activator-dependent promoter defined by single-molecule observation. *Cell.* **148:** 679-689.

Gnatt, A. L., Cramer, P., Fu, J., Bushnell, D. A. and Kornberg, R. D. 2001. Structural basis of transcription: An RNA polymerase II elongation complex at 3.3 A resolution. *Science.* **292:** 1876-1882.

Gries, T. J., Kontur, W. S., Capp, M. W., Saecker, R. M., and Record, M.T., Jr. 2010. One-step DNA melting in the RNA polymerase cleft opens the initiation bubble to form an unstable open complex. *Proc Natl Acad Sci U S A.* **107:** 10418-10423.

Hayes, J. J., Tullius, T. D., and Wolffe, A. P. 1990. The structure of DNA in a nucleosome. *Proc Natl Acad Sci U S A.* **87:** 7405-7409.

Hudson, B. P., *et al*. 2009. Three-dimensional EM structure of an intact activator-dependent transcription initiation complex. *Proc Natl Acad Sci U S A .* **106:** 19830-19835.

Kontur, W. S., Capp, M. W., Gries, T. J., Saecker, R. M., and Record, M. T., Jr. 2010. Probing DNA binding, DNA opening, and assembly of a downstream clamp/jaw in *Escherichia coli* RNA polymerase-lambda P_R promoter complexes using salt and the physiological anion glutamate*. Biochemistry.* **49:** 4361-4373.

Kontur, W. S., Saecker, R. M., Capp, M.W., and Record, M. T., Jr. 2008. Late steps in the formation of E. coli RNA polymerase-lambda P R promoter open complexes: Characterization of conformational changes by rapid [perturbant] upshift experiments*. J Mol Biol.* **376:** 1034-1047.

Kontur, W. S., Saecker, R. M., Davis, C. A., Capp, M. W., and Record, M.T., Jr. 2006. Solute probes of conformational changes in open complex (RP_o) formation by escherichia coli RNA polymerase at the lambdaPR promoter: Evidence for unmasking of the active site in the isomerization step and for large-scale coupled folding in the subsequent conversion to RPo*. Biochemistry* **45:** 2161-2177.

Li, X. Y., and McClure, W.R. 1998. Characterization of the closed complex intermediate formed during transcription initiation by *Escherichia coli* RNA polymerase*. J Biol Chem* **273:** 23549-23557.

Mangiarotti, L., Cellai, S., Ross, W., Bustamante, C., and Rivetti, C. 2009. Sequence-dependent upstream DNA-RNA polymerase interactions in the open complex with lambdaPR and lambdaPRM promoters and implications for the mechanism of promoter interference*. J Mol Biol.* **385:** 748-760.

Mekler, V., Minakhin, L. and Severinov, K. 2011. A critical role of downstream RNA polymerase-promoter interactions in the formation of initiation complex*. J Biol Chem.* **286:** 22600-22608.

Murakami, K. S., Masuda, S., and Darst, S. A. 2002. Structural basis of transcription initiation: RNA polymerase holoenzyme at 4 Å resolution. *Science.* **296:** 1280-1284.

Murakami, K. S., Masuda, S., Campbell, E. A., Muzzin, O., and Darst, S.A. 2002. Structural basis of transcription initiation: An RNA polymerase holoenzyme-DNA complex. *Science.* **296:** 1285-1290.

Opalka, N.*, et al*. 2010. Complete structural model of escherichia coli RNA polymerase from a hybrid approach. *PLoS Biol.* **8:** e1000483.

Popham, D. L., Szeto, D., Keener, J., and Kustu, S. 1989. Function of a bacterial activator protein that binds to transcriptional enhancers. *Science.* **243:** 629-635.

Revyakin, A., Ebright, R. H., and Strick, T. R. 2004. Promoter unwinding and promoter clearance by RNA polymerase: Detection by single-molecule DNA nanomanipulation. *Proc Natl Acad Sci U S A.* **101:** 4776-4780.

Richmond, T. J., Finch, J. T., Rushton, B., Rhodes, D., and Klug, A. 1984. Structure of the nucleosome core particle at 7 A resolution. *Nature.* **311:** 532-537.

Rogozina, A., Zaychikov, E., Buckle, M., Heumann, H., and Sclavi, B. 2009. DNA melting by RNA polymerase at the T7A1 promoter precedes the rate-limiting step at 37 degrees C and results in the accumulation of an off-pathway intermediate. *Nucleic Acids Res.* **37:** 5390-5404.

Rutherford, S.T., Villers, C.L., Lee, J.H., Ross, W. and Gourse, R.L. 2009. Allosteric control of escherichia coli rRNA promoter complexes by DksA. *Genes Dev.* **23:** 236-248.

Saecker, R. M.*, et al*. 2002. Kinetic studies and structural models of the association of E. coli sigma(70) RNA polymerase with the lambdaP(R) promoter: Large scale conformational changes in forming the kinetically significant intermediates*. J Mol Biol.* **319:** 649-671.

Saecker, R.M., Record, M.T., Jr and Dehaseth, P.L. 2011. Mechanism of bacterial transcription initiation: RNA polymerase - promoter binding, isomerization to initiation-competent open complexes, and initiation of RNA synthesis*. J Mol Biol.* **412:** 754-71.

Sasse-Dwight, S., and Gralla, J. D. 1988. Probing the escherichia coli glnALG upstream activation mechanism in vivo*. Proc Natl Acad Sci U S A.* **85:** 8934-8938.

Sasse-Dwight, S., and Gralla, J. D. 1989. KMnO4 as a probe for lac promoter DNA melting and mechanism in vivo*. J Biol Chem.* **264:** 8074-8081.

Schickor, P., Metzger, W., Werel, W., Lederer, H. and Heumann, H. 1990. Topography of intermediates in transcription initiation of *E.coli. EMBO J.* **9:** 2215-2220.

Schroeder, L. A.*, et al*. 2009. Evidence for a tyrosine-adenine stacking interaction and for a short-lived open intermediate subsequent to initial binding of escherichia coli RNA polymerase to promoter DNA*. J Mol Biol.* **385:** 339-349.

Sclavi, B.*, et al*. 2005. Real-time characterization of intermediates in the pathway to open complex formation by escherichia coli RNA polymerase at the T7A1 promoter*. Proc Natl Acad Sci U S A.* **102:** 4706-4711.

Shcherbakova, I., and Brenowitz, M. 2008. Monitoring structural changes in nucleic acids with single residue spatial and millisecond time resolution by quantitative hydroxyl radical footprinting*. Nat Protoc.* **3:** 288-302.

Shcherbakova, I., Mitra, S., Beer, R. H., and Brenowitz, M. 2006. Fast fenton footprinting: A laboratory-based method for the time-resolved analysis of DNA, RNA and proteins. *Nucleic Acids Res.* **34:** e48.

Spassky, A., Kirkegaard, K. and Buc, H. 1985. Changes in the DNA structure of the lac UV5 promoter during formation of an open complex with *Escherichia coli* RNA polymerase. *Biochemistry.* **24:** 2723-2731.

Tsodikov, O. V., Craig, M. L., Saecker, R. M., and Record, M. T., Jr. 1998. Quantitative analysis of multiple-hit footprinting studies to characterize DNA conformational changes in protein-DNA complexes: Application to DNA opening by E sigma70 RNA polymerase. *J Mol Biol.* **283:** 757-769.

Table 1. Local Maxima and Minima of DNA in I_1 and Stable Open Complexes (I_3, RP_o).

	I_1[a,b] **(0.1, 1, 10, 15 s)**	**(I_3, RPo)**[b,c] **(200, 600 s)**
Local Maxima t strand	-47.5	-47.5
	-35.5	-37
	-24.5	-26
	-14.5	-14.5
	-5.5	
	+5.5	
	+16.5	
Local Minima t strand	-54	-52
	-43	-42
	-30.5	-31
	-20	-19.5
	-10	-9
	+0.5	
	+10	
	+21	
Local Maxima nt strand	-56.5[d]	-55
	-44.5	-44.5
	-34	-34
	-23	-24
	-10	-10
	-2	
	+10	
	+21	
Local minima	-50	-49.5

nt strand	-40	-40.5
	-27.5	-28.5
	-18.5	-19
	-6.5	
	+5	
	+15	

[a] Local maxima and minima were averaged from at least 3 of 4 lanes at 4 time points (nt) or 6 lanes at 2 time points (t).

[b] Positions are reported as averages to the nearest 0.5 bp. Average uncertainty is ±1 bp unless noted otherwise.

[c] Local maxima and minima were averaged from two independent time points. Data agree with previous HO• periodicity map of RP_o (4).

[d] Uncertainty is ± 1.5 bp.

Table 2: Predicted Fractions of Promoter DNA in Intermediate (I_1 or I_2) and Stable (I_3, RP_o) Complexes vs. Time in Burst Experiments Simulated in Fig. 3.

	Time (s)	**I_1**	**Free DNA**	**I_3, RP_o**
I_1 Footprinting	(-) RNAP	0.00	1.00	0.00
	0.1	0.68	0.32	0.00
	1	0.70	0.29	0.01
	7	0.65	0.27	0.08
	10	0.63	0.26	0.11
	15	0.60	0.25	0.16
	200, 600	0.00	0.00	1.00
	Time (s)	**I_2**	**Free DNA**	**I_3, RP_o**
I_2 Footprinting	10	0.000	1.000	0.00
	0.25	0.807	0.109	0.08
	(-) Salt Upshift	0.000	0.000	1.00

Figure Captions

Figure 1. Lanes from representative sequencing gels showing distributions of promoter fragments obtained from single-hit HO• snapshots of the nt (**A**) and t (**B**) strand backbones taken at the indicated times during open complex formation. All reactions are initiated by mixing 55 nM excess RNAP with < 1 nM ^{32}P downstream-labeled λP_R promoter DNA (containing 0.2 % H_2O_2) at 19 ºC. After the reaction time indicated on the gel lane (0.1 s to 200 s in these examples), 10 ms HO• snapshots were taken by addition of $FeEDTA^{2-}$ (5 mM) before a thiourea quench. Lines drawn down each lane (shown in red) are used to determine the relative HO• reactivity at each DNA base position according to the A/G sequence lanes (Materials and Methods; Fig. 2). In panel **A**, lanes have been rearranged to consolidate the figure.

Figure 2. Phosphoimager line scans of gel lanes (Fig. 1) quantifying relative HO• reactivities of the DNA backbone at each position (from -70 to +30) of the nt (**A**) and t (**B**) strands of λP_R promoter DNA at the indicated times in a burst association experiment designed to characterize I_1. All lanes were normalized by setting the relative reactivity of the group of bands upstream of the footprint (positions -60 to -70) equal to 1.0. Reactivities of the nt strand of DNA (panel **A**) at 0.1 s (gray), 1 s (pale green), 7 s (dark green), and 15 s (green) and of the t strand (panel **B**) at 0.1 s (gray) and 15 s (green) are compared to reactivities of free promoter DNA (blue) and of the final open complex at 200 s ((I_3, RP_o); red). Key features of results in 0.1 – 15 s line scans were reproduced in at least 3 of 4 lanes at 4 time points (nt) or 6 lanes at 2 time points (t). For reference, brackets on the line scans indicate the regions of RNAP that interact with key regions of promoter DNA, including region 4.2 of σ (which interacts with the -35 element (-30 to -35)); region 2 of σ (which interacts with the -10 element (-7 to -12)); downstream mobile elements of core RNAP (DMEs) including regions of the β lobe and SI1, the β' clamp, the β' jaw, and β' SI3 (proposed to interact with downstream DNA (~ +3 to +20).

Figure 3. Berkeley Madonna™ simulations of bursts of the key intermediates I_1 (**A**; green) and I_2 (**B**; gold), and the corresponding time courses for free promoter DNA (blue) and open complexes (red) (see also Table 2). **A.** Creation of a burst of I_1 by rapid mixing of λP_R promoter DNA with large excess of RNAP (55 nM active) in TB at 19 ºC (K_1 for I_1 formation is ~4.4 x 10^7 M^{-1}, therefore K_1 [RNAP] = 2.4, or the fraction of I_1 is 2.4/ 3.4 = 0.7). For this population distribution of I_1 and free DNA to be established in 0.1 s, as observed in Fig. 2, the pseudo first-order rate constant k_1 must exceed 24.2 s^{-1}, and the first-order rate constant k_{-1} must exceed 10 s^{-1}; the simulation was performed for these lower bounds. **B.** Creation of a burst of the first open intermediate I_2 by a rapid upshift of (I_3, RP_o) open complexes to 1.1 M NaCl in TB at 10 ºC. The simulation was performed for rate constants determined by (20) at 10 ºC.

Figure 4. Corrected line scans of lanes of the sequencing gel lanes in Figs. 1 and 2 to show the predicted nt (**A**) and t (**B**) strand footprints of homogeneous populations of I_1. Simulations results from Fig. 3A (and Table 2) and control scans of free DNA (blue) and (I_3, RP_o) (red) were used for these corrections. Black arrows indicate local maxima and minima determined for both strands in the downstream region of the I_1 footprints (~ -10 to +20) (see Table 1, Fig. 5). Local maxima and minima shown are consistent with replicate experiments (see Table 1). Conditions and normalization are as described in Figs. 1-3.

Figure 5. Periodic protection is observed in the backbone of the downstream duplex of I_1 (green) but not open (red) complexes. All local maxima (blue) and local minima (orange) observed in HO• line scans of I_1 and (I_3, RP_o) footprints (Table 1) are mapped on DNA (Figs. 1 and 4, Table 1; see Materials and Methods). Periodic protection of the DNA backbone upstream of ~ -10 is the same in I_1 and open complexes. **A**. Periodic protection of the DNA backbone of I_1 extends downstream to ~ +20. **B**. The DNA backbones of open complexes are periodically protected until ~ -10; from -10 to +20 the DNA backbone is fully protected by binding of both single strands of the initiation bubble in the cleft and folding/assembly of DMEs onto the downstream duplex (**Chapter 3**, (19)), in agreement with the previous HO• periodicity map of RP_o (4). Both panels are

modeled from a combination of the *E. coli* RNAP core model and *E. coli* RNAP holoenzyme low-resolution EM structure (PDB ID 3LU0 and 3IYD (39, 40)). DNA placement is modeled largely in accordance with that in Davis *et al.* 2007 (2).

Figure 6. Slow kinetics of development of MnO_4^- reactivity of single stranded thymines in the vicinity of the transcription start site during association initiated by fast mixing of excess RNAP (55 nM) with λP_R promoter DNA at 19 ºC. Representative gels are provided as insets. Thymine residues of the λP_R promoter that are known to react to MnO_4^- during DNA opening are plotted for the nt strand (+2 (⊕, ●) and -4/-3 (☒, ■)) and **B.** the t strand (-9/-8 (⊕, ●) and -11 (☒, ■)). Free DNA control lanes were obtained under conditions identical to samples. Indicated times for each lane are times after mixing RNAP with DNA at which the 50 ms MnO_4^- snapshot was taken, followed by a quench (see Materials and Methods). Gels were quantified and results normalized as described in Materials and Methods.

Figure 7. Lanes from a representative gel of single-hit HO• footprinting experiments (5 mM $FeEDTA^{2-}$) probing the nt strand of λP_R after an upshift of (I_3, RP_o) complexes to 1.1 M NaCl at 10 ºC. HO• snapshots (10 ms) were taken at the predicted peak of the burst of I_2 (0.25 s) and after decay of I_2 to free promoter DNA (10 s). For the "RP_o control" lanes, open complexes at 10 ºC were mixed with 0.120 M NaCl and footprinted at the indicated times. In all cases, the time of reaction with HO• was 10 ms before application of a thiourea quench. Inapplicable lanes have been omitted, and lanes shown here have been rearranged to consolidate the figure.

Figure 8. Phosphoimager line scans of lanes of sequencing gels (e.g. Fig. 7), resolving DNA fragments from replicate single-hit HO• footprints (5 mM $FeEDTA^{2-}$) of the nt DNA strand. Panels **A** and **B** are replicate experiments. The reactivity of DNA in the late open complexes (I_3, RP_o) (red) is compared to that of 0.25 s after 1.1 M NaCl upshift (I_2; gold) and 10 s after upshift (free DNA; blue) (Table 2). Correction for the mixed population (i.e. free DNA and I_3/RP_o), performed as in Fig. 4, is shown in black.

Regions of promoter contacted by σ and DMEs (bracketed) are defined in Fig. 2. Line scans are normalized as described in Materials and Methods.

Figure 9. Testing the possible [salt] effect on HO• cleavage of free DNA. These control reactions were performed in the multi-syringe fast mixer, wherein 10 ms HO• snapshots were taken by addition of $FeEDTA^{2-}$ (20 mM) before a thiourea quench. (**A**) Gel comparing HO• reactivity of free DNA in solutions containing increasing (indicated) concentrations of NaCl. (**B**) The fraction of total promoter fragments cleaved at least once by HO• from (**A**) is plotted versus [NaCl].

Figure 1.

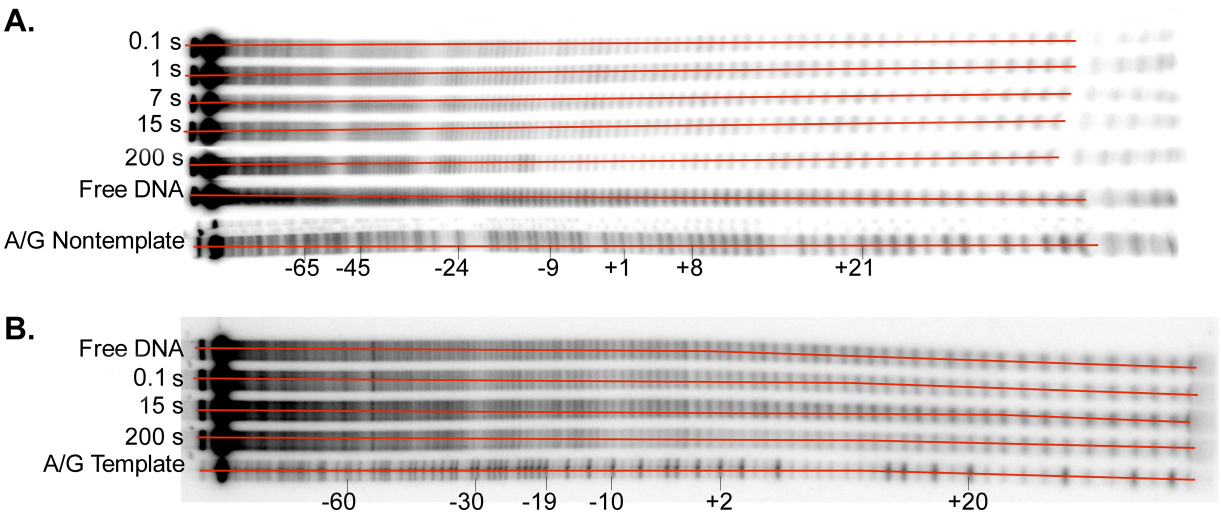
A.
0.1 s
1 s
7 s
15 s
200 s
Free DNA
A/G Nontemplate
-65
-45
-24
-9
+1
+8
+21
B.
Free DNA
0.1 s
15 s
200 s
A/G Template
-60
-30
-19
-10
+2
+20

Figure 2.

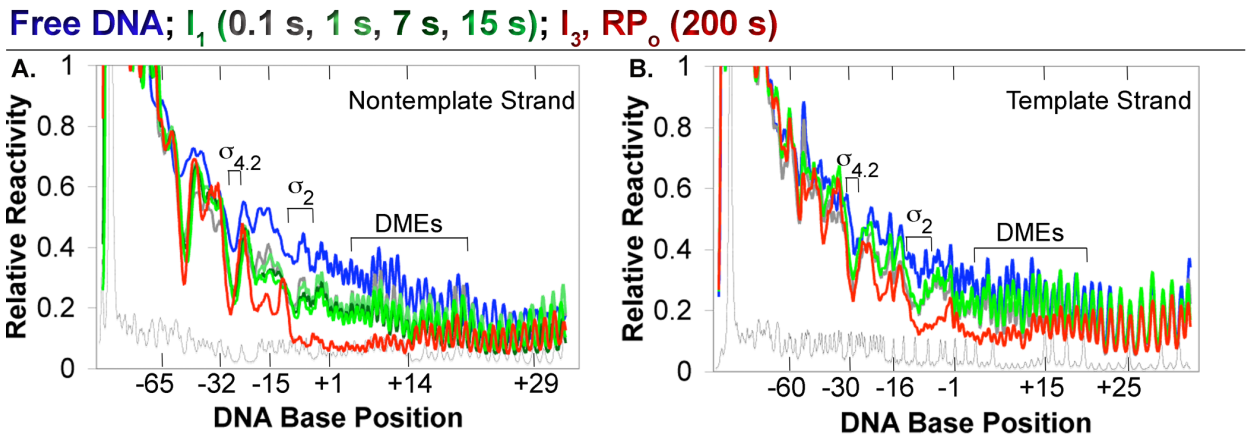
Free DNA; I1 (0.1 s, 1 s, 7 s, 15 s); I3, RPo (200 s)
A.
Nontemplate Strand
Relative Reactivity
σ4.2
σ2
DMEs
-65 -32 -15 +1 +14 +29
DNA Base Position
B.
Template Strand
Relative Reactivity
σ4.2
σ2
DMEs
-60 -30 -16 -1 +15 +25
DNA Base Position

Figure 3.

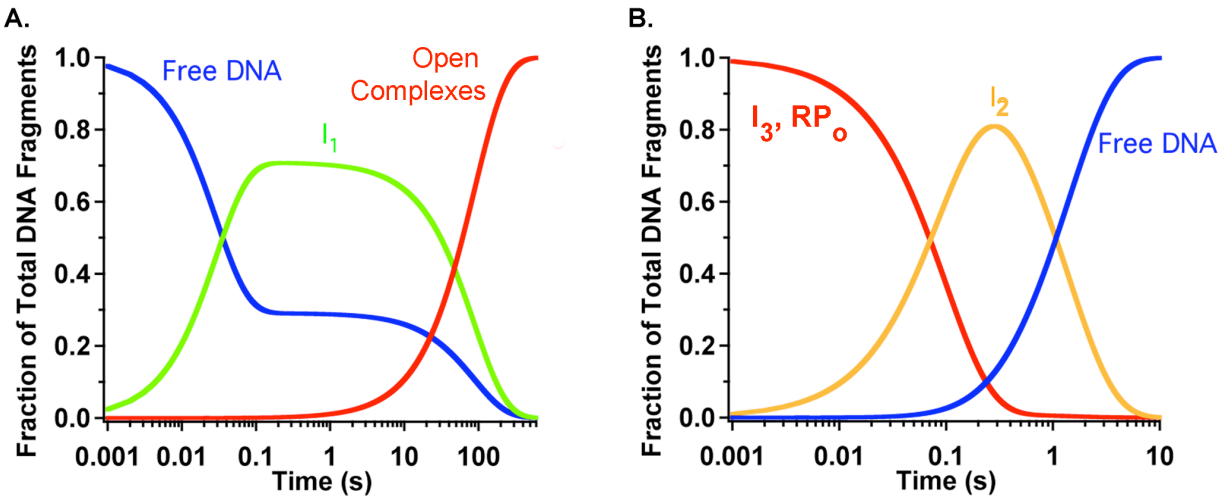
A.
Fraction of Total DNA Fragments
1.0
0.8
0.6
0.4
0.2
0.0
Free DNA
Open
Complexes
I1
0.001
0.01
0.1
1
10
100
Time (s)
B.
Fraction of Total DNA Fragments
1.0
0.8
0.6
0.4
0.2
0.0
I3, RPo
I2
Free DNA
0.001
0.01
0.1
1
10
Time (s)

Figure 4.

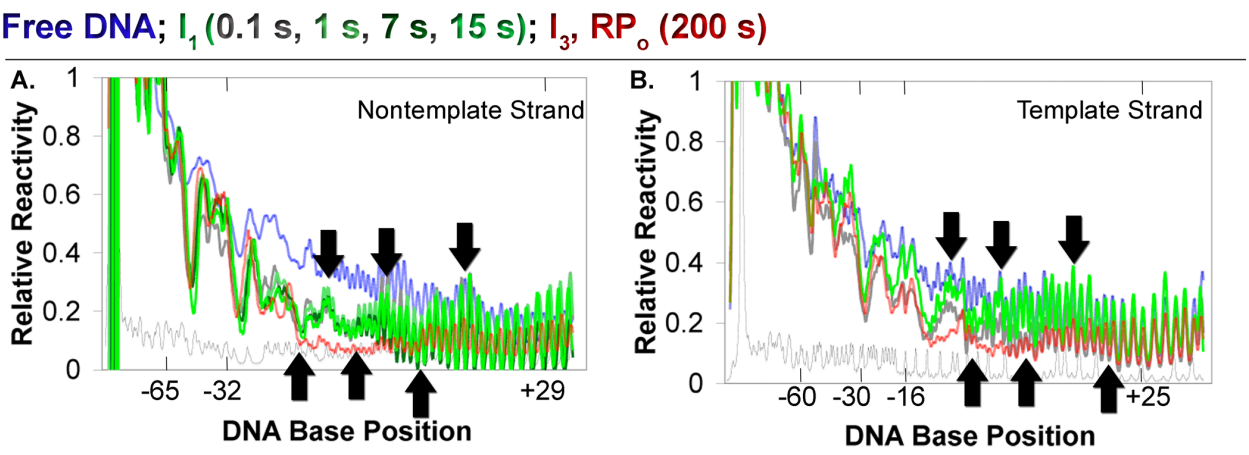
Free DNA; I1 (0.1 s, 1 s, 7 s, 15 s); I3, RPo (200 s)
A.
Nontemplate Strand
Relative Reactivity
1
0.8
0.6
0.4
0.2
0
-65
-32
+29
DNA Base Position
B.
Template Strand
Relative Reactivity
1
0.8
0.6
0.4
0.2
0
-60
-30
-16
+25
DNA Base Position

Figure 5.

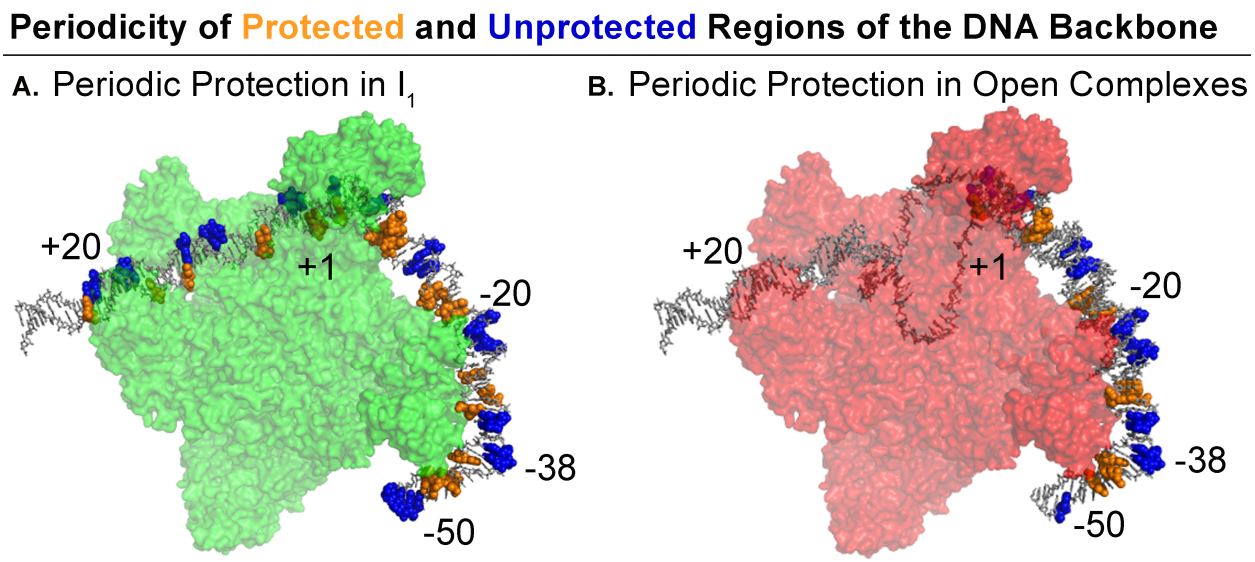
Periodicity of Protected and Unprotected Regions of the DNA Backbone
A. Periodic Protection in I1
+20
+1
-20
-38
-50
B. Periodic Protection in Open Complexes
+20
+1
-20
-38
-50

Figure 6.

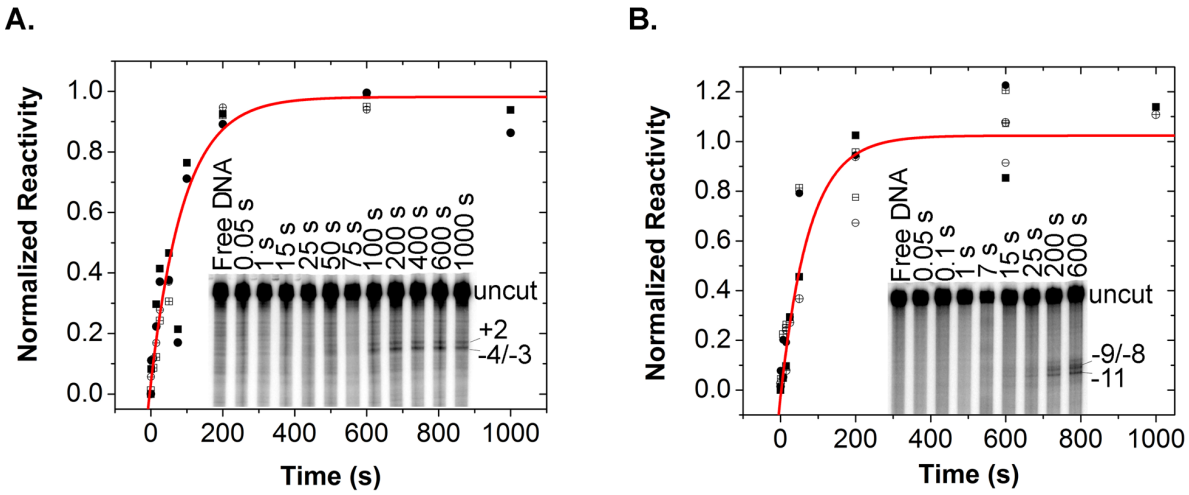
A.
Normalized Reactivity
Time (s)
Free DNA
0.05 s
1 s
15 s
25 s
50 s
75 s
100 s
200 s
400 s
600 s
1000 s
uncut
+2
-4/-3
B.
Normalized Reactivity
Time (s)
Free DNA
0.05 s
0.1 s
1 s
7 s
15 s
25 s
200 s
600 s
uncut
-9/-8
-11

Figure 7.

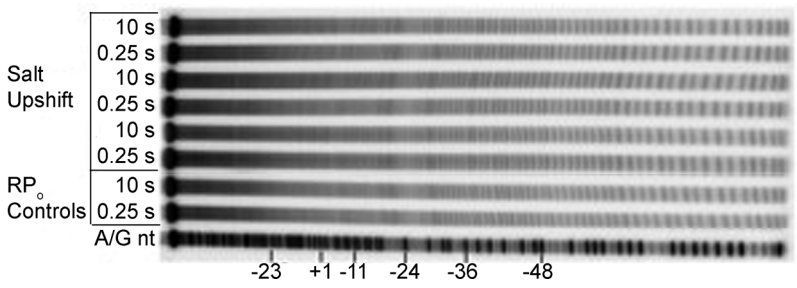
Salt
Upshift
RP$_o$
Controls
10 s
0.25 s
10 s
0.25 s
10 s
0.25 s
10 s
0.25 s
A/G nt
-23
+1
-11
-24
-36
-48

Figure 8.

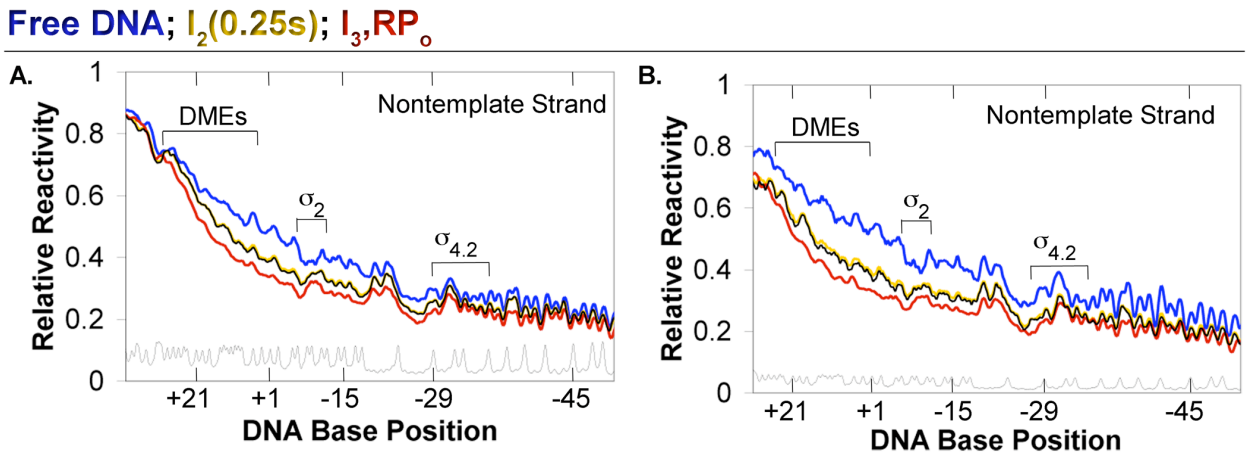
Free DNA; I2(0.25s); I3,RPo
A.
B.
Relative Reactivity
DMEs
Nontemplate Strand
σ2
σ4.2
1
0.8
0.6
0.4
0.2
0
+21
+1
-15
-29
-45
DNA Base Position

Figure 9.

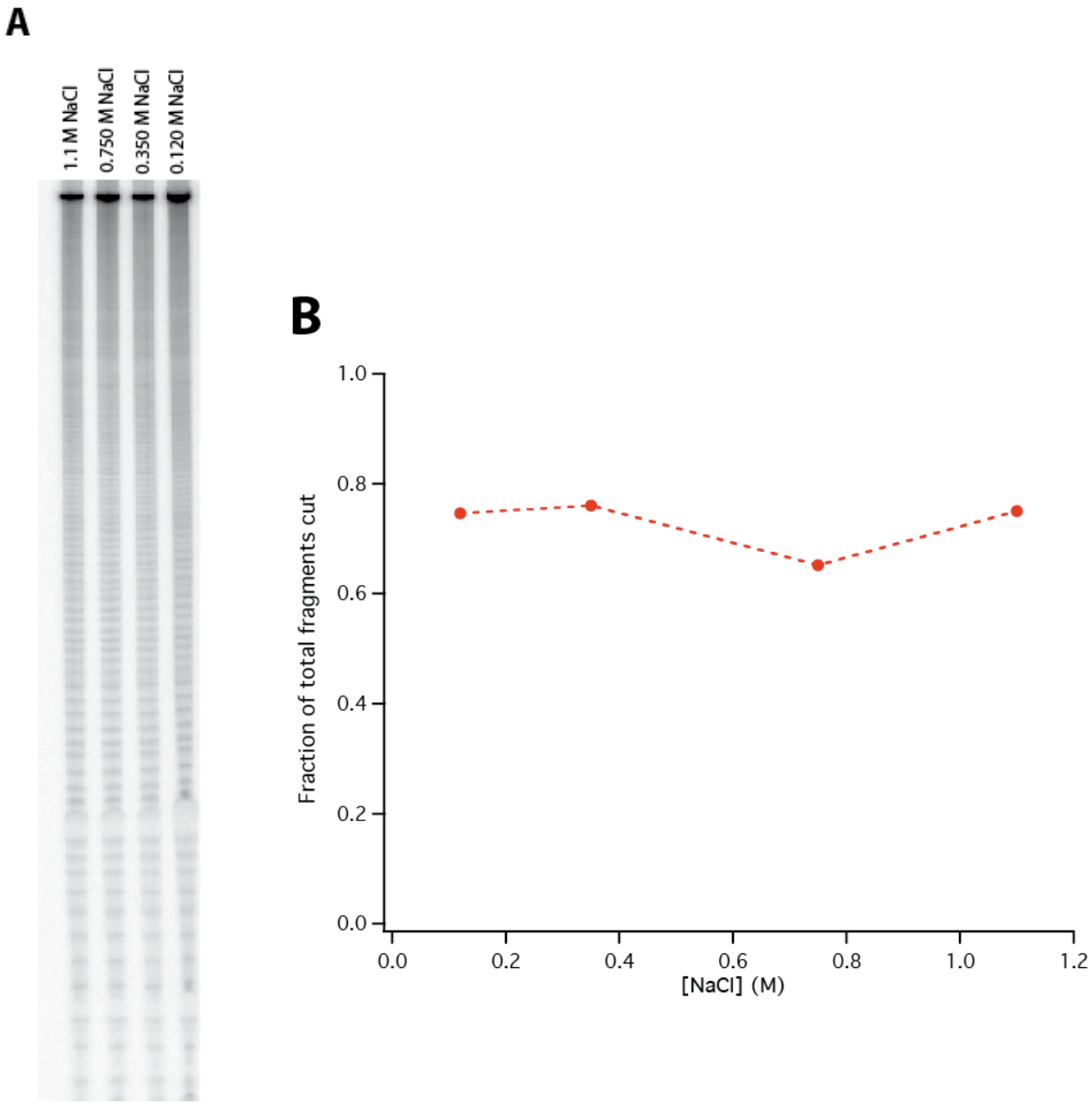
A
1.1 M NaCl
0.750 M NaCl
0.350 M NaCl
0.120 M NaCl
B
Fraction of total fragments cut
1.0
0.8
0.6
0.4
0.2
0.0
0.0
0.2
0.4
0.6
0.8
1.0
1.2
[NaCl] (M)

Chapter 3

Real-time and Equilibrium FRET Characterization of Promoter DNA Wrapping and Unwrapping in Closed and Open *E. coli* RNAP Transcription Initiation Intermediates

Preface: This chapter is a draft of a first-author manuscript, currently in preparation. My contributions include: primary design and execution of experiments, preparation of experimental materials, data fitting and interpretation, preparation of figures and manuscript writing. I thank Raashi Sreenivasan, Emily Lingeman, Kristin Zorn, and Natalie Gaio for their significant experimental contributions, Dr. Ruth Saecker and Prof. Ted Gries for preliminary FRET experiments, Prof. Robert Landick for providing me with the use of the stopped- flow spectrofluorimeter, Prof. Aaron Hoskins for discussions of FRET probes and FRET, and Prof. Irina Artsimovitch for discussions, preparation of figures and assistance with the manuscript.

Abstract

DNA bending is fundamental to many cellular processes. Here we report both real time and equilibrium FRET experiments during *E. coli* transcription initiation using Cy3-Cy5 labeled λP_R promoter DNA (dyes at -100 and +14, 134 bp fragment). We report equilibrium FRET titrations at low temperature (2°C) where the advanced closed intermediate (I_1) is the only promoter complex, and at 10, 19 and 37°C where there is a mixture of open complexes. We find that each of the on-pathway RNAP-λP_R promoter DNA complexes are highly wrapped with FRET efficiencies of approximately 0.4, yielding an prediction that the upstream and downstream end of promoter DNA are within 60A of each other. Real-time association FRET wrapping data at 19C was best fit to the sum of two exponentials, yielding a fast rate constant of approximately 10 s^{-1}, somewhat slower than that deduced for formation of the closed I_1 complex with an extended •HO downstream footprint. The second kinetic rate constant is about three orders of magnitude slower than the first phase, and is similar to the rate of isomerization of closed to open complexes obtained from filter binding and $KMnO_4$ assays at 19°C. We deduce that upstream wrapping occurs soon after formation of the initial, •HO-detected I_1 complex and is a precursor to base-flipping (-11A) and opening of the initiation bubble in the cleft. The experiments indicate that promoter DNA wrapping is initiated early during the formation of the advanced closed RNAP-promoter DNA complex and persists in open complexes. The use of this method has provided previously unattainable information about the nature of DNA wrapping during bacterial gene expression.

Introduction

E. coli RNA polymerase (RNAP) holoenzyme is a large multisubunit molecular machine (~450kDa, $\alpha_2\beta\beta'\omega\ \sigma^{70}$) that couples the free energy of binding to open the promoter DNA transcription bubble. Association of RNAP to most promoter sequences requires the sigma specificity factor σ^{70}. During initial binding of promoter DNA, RNAP bends the DNA, bringing the upstream and downstream ends of the DNA in relatively close proximity. The pathway for formation of open complexes at the phage λP_R promoter DNA (I_3, RP_o) is comprised of a series of large-scale conformational changes in both the RNAP and DNA machinery. The mechanism of this process is summarized by:

$$R + P \underset{\text{rapid equilibria}}{\overset{K_1}{\rightleftharpoons}} I_1 \underset{k_{-2}}{\overset{k_2}{\underset{\text{slow}}{\overset{\text{slow}}{\rightleftharpoons}}}} I_2 \underset{K_{-3}}{\overset{\text{rapid equilibria}}{\rightleftharpoons}} I_3 + RP_o$$

(Mechanism 1)

RNAP (R) binds to λP_R promoter DNA (P) in a series of steps that rapidly equilibrate on the time scale of the slow step, DNA opening. In the first kinetically significant intermediate I_1, the DNA is still duplex and is wrapped upstream to ~-80 (relative to the transcription start site +1) (Davis *et al.* 2007, Heitkamp and Drennan, unpublished). Subsequently, the DNA is opened during the transition from I_1 to the first open complex I_2. This is the bottleneck (slow) step in both the forward and reverse directions of the transcription initiation pathway. During this isomerization step, the +1 base of the template strand is specifically loaded into the RNAP active site as 13 base

pairs of promoter DNA are opened in a single step (-11 to +2 for the λP_R promoter) to form the first open intermediate I_2 (Gries *et al.* 2010). I_2 then rapidly converts to transcriptionally competent open complexes (I_3, RP_o) and upon binding of NTPs, these open complexes synthesize RNA from the promoter DNA template strand.

The largest dimensions of RNAP determined by EM are approximately 100 × 100 ×160 Å (Darst *et al.* 1989). However approximately 80-95 bases of promoter DNA are protected from cleavage by DNase I and hydroxyl radical footprinting agents in both I_1 (-81 to +20) and RP_o (-65 to +20) (Schicktor *et al.* 1990, Craig *et al.* 1995; Davis *et al.* 2007). This protection extends much farther than would be expected for linear binding of the promoter DNA and therefore it has been proposed that RNAP must bend and wrap promoter DNA. Various models have been proposed for extensive wrapping of promoter DNA on *E. coli* RNAP in both I_1 (Davis *et al.* 2007; Saecker et al. 2001) and RP_o (Rivetti *et al.* 1999a; Rivetti *et al.* 1999b; Heuman *et al.* 1988b, Meyer-Alme *et al.* 1994). For an early review of promoter DNA wrapping around eukaryotic and prokaryotic RNAP see Coulombe and Burton (1999).

E. coli RNAP has been found to induce bending of T7A1 promoter DNA in both open complexes and during transcription of RNA products up to 11 bases in length (Heuman *et al.* 1988a). Based on this work and evidence from neutron scattering and quantitative electrooptics, the DNA bend in RP_o at T7A1 was proposed to be centered at position -3 with regard to the +1 start site of transcription, with a bend angle 45° ± 5° (Heuman *et al.* 1988b, Meyer-Alme *et al.* 1994). RNAP-induced bending has also been demonstrated for σ^{70} RP_o at the *gal* promoter (Kuhnke *et al.* 1989) λP_L promoter (Rees *et al.* 1993) and for σ^{54} RP_o at the *glnA* promoter (Rippe *et al.* 1997). Fluorescence

assays demonstrated that rapid binding of T7 RNAP is followed by bending and opening of the DNA; bending was found to be coupled to opening (Tang and Patel 2006a and 2006b). Circular permutation assays support this DNA bending model for T7 RNAP (Ujvári and Martin 2000).

Open complexes formed by *E. coli* σ^{54} RNAP at the *glnA* promoter exhibited DNA contour lengths significantly shorter than that of free promoter DNA, suggesting that promoter DNA must wrap around the back side of RNAP (Rippe *et al.* 1997). AFM studies with *E. coli* σ^{70} RNAP found that formation of open complexes at the λP_R promoter resulted in a large DNA compaction (~30nm, ~90bp) that was interpreted in terms of wrapping of upstream promoter DNA (positions -100 to -40) around RNAP (Rivetti *et al.* 1999a, Rivetti *et al.* 1999b). In this work, the authors used a construct containing both the λP_R and λP_{RM} promoters; however the occupancy of RNAP was >90% at λP_R under the conditions studied. In support of their interpretation, they found that both the αCTD subunits of RNAP and an intact α-linker were required to maintain compaction, and that the extent of compaction and hence wrapping was dependent on the sequence of upstream promoter DNA.

Previous work from our lab indicated the importance of upstream DNA for the rate of association of RNAP with promoter DNA. Truncations of upstream DNA (truncated at -47 or -65; Davis *et al.* 2005 and Ruff, E., unpublished observations) greatly reduce the observed isomerization rate constant by affecting the rate of entry of the downstream DNA duplex into the RNAP cleft. Upstream DNA was found to wrap more extensively on RNAP in I_1 than in RP_o as evidenced by real-time •OH radical footprinting experiments. Protection of the DNA backbone was observed as far

upstream as -81 in I_1 but only to -65 in RP_o, whereas downstream protection of promoter DNA extends to approximately +20 in both complexes (Davis *et al.* 2007). Therefore we hypothesized that the upstream promoter DNA wrap around RNAP was more extensive in I_1 and that the extent of wrapping was reduced in the conversion to open complexes.

Promoter DNA has been proposed to remain wrapped during transcription initiation (Heuman *et al.* 1988a) and elongation (Rivetti *et al.* 2003). Transcription ternary complexes of *E. coli* RNAP stalled at positions +24, +70 and +379 had an average compaction of 22 nm as measured by AFM and a DNA deformation compatible with an approximate 180° DNA wrap around the enzyme. However this extent of wrapping was deduced to be less than that of open complexes. Yeast pol III stalled at position +377 showed a DNA compaction of 30 nm (Rivetti *et al.* 2003).

Here we report FRET experiments at equilibrium conditions (2°C) where the only RNAP-promoter DNA complex present is the I_1 closed complex (Craig *et al.* 1998) and also at 10, 19 and 37°C, where the majority of the population at equilibrium is open complexes (I_3 and RP_o). Cy3 and Cy5 FRET probes are an ideal choice for monitoring promoter DNA wrapping as they have been used extensively to monitor DNA bending by proteins (lac repressor: Morgan *et al.* 2005; *E. coli* SSB: Kozlov and Lohman 2002; NgoMIV endonuclease: Katiliene *et al.* 2003; the nucleosome: Bu *et al.* 2004; for an early review on the use of FRET in DNA bending studies see Parkhurst *et al.* 2001). The Forster distance, or the distance corresponding for 50% energy transfer is 50Å for freely rotating Cy3 and Cy5 dyes. Therefore, if the upstream and downstream ends of the DNA are within 10-100Å of each other, we should see FRET. Our experiments demonstrate wrapping of RNAP-promoter DNA complexes at each temperature,

suggesting that the DNA is wrapped early during formation of I_1 and remains wrapped during the DNA opening step and formation of stable open complexes. To monitor the kinetic time course of formation of the promoter DNA wrap around RNAP, we also performed real-time association assays at 19°C. These assays allow us to use the FRET signal from DNA wrapping to monitor the formation and isomerization of the initial wrapped closed complex.

Results

Design of Promoter DNA FRET Constructs

Cy3 and Cy5 probes were inserted in the upstream (-100, relative to the +1 start site of transcription) and downstream (+14) regions of the λP_R DNA promoter. Previously, we observed that promoter constructs containing fluorescent dyes located at the 5'-end were prone to nonspecific end binding by RNAP (Gries, T., unpublished). Because of this, dyes were incorporated five to ten base pairs in from each 5' end of the promoter. This was accomplished by purchasing PCR primers for the nontemplate (upstream) and template (downstream) strands containing internal Cy3 or Cy5 dyes (/iCy3/ and /iCy5/ modifications from Integrated DNA Technologies, Coralville, IA). The dyes are covalently attached so that they bridge the phosphate backbone of the 5' end of one base and the 3'-OH of the second base. Therefore these dyes are rigid and not freely rotating. Promoter DNA was either (*i*) double-labeled with Cy3 upstream (-100) and Cy5 downstream (+14), (*ii*) double-labeled with Cy5 upstream (-100) and Cy3 downstream (+14), or (*iii*) singly labeled with either Cy3 or Cy5 upstream (-100) or downstream (+14). The double-labeled DNA constructs were used to investigate DNA

wrapping around RNAP. The single-label DNA constructs were used as controls for dye sensitization, nonspecific end binding of RNAP, and dye photobleaching.

Equilibrium FRET Demonstrates Promoter DNA Wrapping around RNAP in the Closed Complex I_1:

We first tested the proposal of Davis *et al.* (2007) that the region of promoter DNA upstream of the -35 element (including both the DNA that interacts with the UP element and farther upstream) is wrapped on the back of RNAP in the first kinetically-significant closed complex at the λP_R promoter, I_1. Craig *et al.* (1996) found that near 0^oC, DNA opening is thermodynamically disfavored and I_1 is predicted to be the only observed LPR promoter complex at binding equilibrium. Footprinting of the 0^oC RNAP-promoter DNA complex revealed that it had an extended downstream backbone footprint (to +20) and was not permanganate-reactive, indicating that the downstream (-10 to +20) region of promoter DNA is bound in the active site cleft in this complex and that this DNA is closed; a model for the path of the downstream duplex in this complex was proposed by Saecker, Tsodikov *et al*. 2002 (see also Davis *et al.* 2007, and Vasseylev *et al.* 2002).

Equilibrium FRET measurements of the closed complex I_1 at 2°C in Figure 1A and 1B demonstrate very significant FRET effects that increase as the concentration of I_1 complexes increases, and which must result from DNA wrapping. For these studies, I_1 was formed by equilibrating *E. coli* RNAP holoenzyme with the λP_R promoter in standard transcription buffer for 1.5 hours at 2°C. The final concentrations of the samples contained 100nM promoter DNA (Cy3 -100, Cy5 +14; 134 bp construct from -112 to +22) and 50-150nM active RNAP holoenzyme. At 2°C the extrapolated value of

the I_1 binding constant is approximately 1 x 10^7 M^{-1}; therefore only a fraction of promoter DNA is present as I_1 even at 150 nM RNAP, and I_1 is deduced to be an equilibrium mixture of unwrapped and wrapped complexes so that only a fraction of I_1 is wrapped (see Ch. 4 and 5). Cy3 was excited at 515 and emission monitored from 550 to 650nm for Cy3 and 620 to 720nm for Cy5 (see Methods). The Cy3 excitation wavelength of 515nm was chosen so that direct excitation of Cy5 would be minimized.

Upon excitation of the donor dye, FRET causes an increase in emission from the acceptor dye and a decrease in emission from the donor dye. Figure 1 A (left top panel) and B clearly demonstrate these effects for the 2 °C RNAP complex; Cy5 emission increases (Fig 1A) and Cy3 emission decreases when RNAP is added to a Cy3 (-100) Cy5 (+14) doubly labeled λP_R promoter DNA, and these effects increase with increasing RNAP concentration. Cy5 (+14) promoter DNA bound to RNAP and lacking the Cy3 (-100) dye yielded no such increase (See Figure 2A). In the absence of Cy5 (+14), we find that there is no reduction in the emission of Cy3 (-100) promoter DNA upon mixing with RNAP (Figure 2B). In the absence of RNAP, no emission by Cy5 is seen for Cy3Cy5 promoter DNA when Cy3 is excited at 515nm (Figure 2C). As a control, we also tested whether core RNAP lacking the sigma70 specificity factor could give rise to FRET upon binding Cy3Cy5 LPR promoter DNA. Addition of core RNAP with Cy3(-100) Cy5 (+14) promoter DNA yielded no increase in Cy5 emission, consistent with the model that specific interactions of RNAP holoenzyme are required for the tight wrapping of promoter DNA around RNAP (Figure 2D). Experiments were also performed with Cy3 and Cy5 dyes in the opposite orientation (Cy3 +14, Cy5 -100; Figure 3A-C); these experiments yielded very similar results to those of Fig 1A.

FRET Demonstrates that Open Complexes Are Also Wrapped

At 10 and 19°C, where open complexes are stable, Figure 1 demonstrates that large increases in the equilibrium Cy5 FRET emission signal are also observed with increasing concentrations of RNAP, comparable to that observed for closed complexes at 2°C. However at 37°C the FRET signal is smaller than that observed at the lower temperatures, even at the highest [RNAP]. Experiments were performed identically as described above for the 2°C experiments. RNAP- promoter DNA complexes (50-150 nM active RNAP; 100nM LPR promoter DNA) were equilibrated at each temperature for 1.5 hours and the samples were then exited at 515nm. Each temperature experiment was performed on the same day as the 2°C experiments, with the same PMT settings and therefore the absolute amplitudes of the Cy3 and Cy5 emission peaks can be compared at the different temperatures. A total of five such determinations was performed with the Cy3(-100) Cy5 (+14) and with Cy3(+14) Cy5 (-100) promoter DNA constructs (Figures 1 and 3). Although the absolute fluorescence intensity values varied from day to day, the relative differences in fluorescence intensity were very similar from day to day for both dye orientations.

We find that the largest FRET signals are at 2, 10 and 19°C and that the smallest are at 37°C. Single dye controls with and without RNAP were also performed at each temperature in order to determine the effects of temperature on Cy3 and Cy5 emission. Interestingly, single dye controls (Cy3 promoter DNA or Cy5 promoter DNA bound to RNAP) exhibited fluorescence emission of both dyes that was temperature dependent, with the highest fluorescence intensity at 2°C and the least at 37°C (Figure 4A and 4B). The temperature dependence was identical in the presence and absence of RNAP

(data not shown). The fluorescence emission is plotted vs. temperature for each dye in Figures 4C and 4D. FRET efficiency can be calculated by the following:

$$E = \frac{I_D}{I_{AD}} \quad \text{(Equation 1)}$$

where I_D is the intensity of the donor dye in the absence acceptor and I_{AD} is the intensity of the acceptor when the donor is present. However, in order to determine the true FRET efficiency, the fluorophore intensities must be corrected for instrument effects, including leakage of excitation light into the donor channel ($\boldsymbol{\beta I_D}$), and photophysical effects, which include differences in detection efficiency for the donor and acceptor ($\boldsymbol{\gamma}$), and the quantum yield of each dye ($\boldsymbol{\varphi}$) (McCann *et al.* 2010).

Because we observed large changes in the intensity of both fluorophores as a function of temperature (Figure 4), we normalized the equilibrium experimental data to account for these changes. After temperature correcting the data, the FRET at 37°C is higher than that seen at 2, 10 and 19°C. Figure 5C depicts the temperature corrected fluorescence intensity of the Cy5 emission peak for 150nM RNAP, 100nM promoter DNA complexes at a wide range of temperatures from 2-37°C. In Figure 5D, the temperature corrected Cy5 FRET emission peaks at 660nm for complexes formed each temperature are plotted versus [RNAP]. From this temperature corrected data, it is clear that the lower signal observed at 37°C in the uncorrected data is not the result of a greater distance between the upstream and downstream regions of the DNA, but rather due to weaker fluorescence emission of both dyes at higher temperatures. We conclude that the promoter DNA wrap around RNAP is formed early in the closed complex I_1 and persists during formation of the open complex. FRET efficiencies were calculated using

the uncorrected donor emission quenching. The intensities of the donor dye in the presence and absence of the acceptor were compared in order to obtain approximate FRET efficiencies for the closed complexes at 2°C and for open complexes at 19°C. The FRET efficiencies are approximately 0.1 +/- 0.05 for 1:1 RNAP: promoter stoichiometries where most of promoter DNA is in an open complex. FRET efficiencies for a 1:1 RNAP promoter stoichiometry at 2 °C are in the range of 0.1 to 0.15, but for the concentrations studied, a 1:1 ratio of RNAP to promoter DNA corresponds to approximately 50% of promoter DNA in I_1 complexes, not all of which are wrapped. Therefore the intrinsic FRET efficiency of wrapped I_1 complexes at 2°C may be significantly higher than that of open complexes at higher temperature. This does not necessarily imply that I_1 complexes are more wrapped than open complexes, because the Cy3 and Cy5 dyes are not freely rotating and hence changes in orientation of one dye relative to the other may affect FRET efficiency as much or more as changes in interdye distance between closed and open forms. (These dyes are attached bridging the phosphate backbone of the 5' end of one base and the 3'-OH of the second base. This was done to avoid binding of RNAP to freely rotating dyes, which occurred in initial constructs that we designed and studied.)

Real-time Wrapping of the λP_R Promoter Around RNAP

Next, we monitored the kinetics of promoter DNA wrapping during association of RNAP with the λP_R promoter in real-time at 19°C using stopped-flow fluorescence. We rapidly mixed a high concentration of promoter DNA (100nM, Cy3 -100 and Cy5 +14) with 20-150nM active RNAP holoenzyme and monitored the changes in emission of the Cy3 (-100) and Cy5 (+14) dyes as a function of time (Figure 6). Use of two PMTs

allowed us to simultaneously monitor the change in the emission of both dyes. Samples were excited at 515 and the changes in fluorescence emission of each dye was monitored using filters selected to transmit only the emission wavelengths of the desired probe (See Methods). From one loading of reagents, typically data for 3-5 repeat shots was collected with 1000-2000 points uniformly collected on a log time scale. These data were then averaged to yield a single kinetic trace for each concentration within an experiment; reported rate constants are from the average of three or more independent experiments (Table 1). Uncertainties are reported as the standard deviation between these rates.

At 19°C, upon association of RNAP with Cy3(-100) Cy5 (+14) promoter DNA, the change in emission of both dyes is best fit to the sum of two exponentials. The Cy3 dye located at position -100 exhibits a rapid single exponential increase in fluorescence (positive amplitude), followed by a slower, single exponential decrease (negative amplitude) (Figure 6A, linear time scale, and 6B, log time scale). The initial increase in Cy3 emission is most likely due to a direct interaction of the Cy3 dye with RNAP or a local change in environment arising from the close proximity of RNAP with Cy3 after binding to promoter DNA. Cy3 can exhibit an increased quantum yield when bound directly to (Gruber *et al.* 2000) or near (Fischer *et al.* 2012) proteins. Protein binding changes the local environment of the probe and is thought to inhibit the photo-induced isomerization of Cy3 from the trans (photoactive) to cis (photoinactive dark state) conformation (Levitus and Ranjit, 2011). Previous work in our lab has shown that the downstream footprint of RNAP extends to approximately -81 in the early closed intermediate I_1 and to ~-65 in the final open complexes RP_o. Because of this, we

suggest that the increase in fluorescence emission for Cy3 (-100) seen here is due to a proximal binding effect of RNAP. In evidence of this effect, promoter DNA containing the Cy3 (-100) dye in the absence of Cy5 shows an identical increase in emission upon mixing with RNAP (Figure 6C). Promoter DNA lacking the Cy3 (-100) shows no emission decrease due to mixing with RNAP (Figure 6D).

In the double dye experiment (Cy3 -100 Cy5 +14 promoter DNA + RNAP), at longer times after mixing, Cy3 exhibits a large decrease in fluorescence emission. This decrease is not seen in the single dye control, even out to 600 seconds after mixing. Emission of the Cy5 dye during association of RNAP with Cy3 (-100) Cy5 (+15) promoter DNA with RNAP exhibits a biphasic increase in fluorescence (positive amplitude) that is best fit to the sum of two exponentials (Figure 6A,B). Rapid mixing of Cy5 (+14) promoter DNA lacking the Cy3 (-100) dye with RNAP exhibited no increase in fluorescence emission when excited at either 515 or 615nm (Figure 6D). From this, we conclude that the increase in Cy5 emission for the double dye FRET experiments can be attributed entirely to energy transfer from Cy3.

We conclude that the decrease in Cy3 occurs due to energy transfer between the Cy3 and Cy5 dyes, consistent with the upstream and downstream ends of promoter DNA coming in close proximity to each other. Like the equilibrium experiments detailed above, we estimate that the ends of the λP_R promoter DNA must be <100Å apart in order to FRET to be detectable with this dye pair. However, because the emission of the Cy3 dye is changing during the experiment because of a proximal binding effect of RNAP, and the dipole orientation of the dyes may be changing throughout the time

course (κ term in Equation 3), we have not attempted to determine FRET efficiencies during the association time course.

In order to determine the observed rates for the increase Cy5 emission, we averaged the kinetic traces for 3-5 shots from one loading of samples. The average traces were then fit using the equation for the sum of two exponentials:

$$F = F_0 + A_{fast}\{1 - \exp(-k_{fast}\, t)\} + A_{fast}\{1 - \exp(-k_{slow}\, t)\} \qquad \text{(Equation 4)}$$

where F_o is the initial fluorescence.

Single exponential fits to the data were insufficient, displaying systematic deviation in the fits to the residuals. Fits to the sum of three exponentials did not substantially improve the quality of the fit and in most cases did not produce three unique values for the observed rates. The rate constants k_{fast} and k_{slow} were determined from three independent experiments performed on separate days and averaged to produce the rates in Table 1. Uncertainties are reported as the standard deviation in k_{obs} between experiments.

In the transcription initiation mechanism for RNAP at the λP_R promoter, the closed complex I_1 is in rapid equilibrium with free RNAP and DNA (Davis *et al.* 2007, Ch. 2). I_1 is then slowly converted to I_2 and the DNA is opened. Therefore, to interpret the two exponentials observed in the FRET – detected kinetics of open complex formation, we propose that k_{fast} is a decay to equilibrium rate constant for forming the I_1 species detect by FRET ($k_{fast} = k_1\{[DNA]_{eq} + [RNAP]_{eq}\} + k_{-1}$), and that k_{slow} is the rate constant for converting this/ these I_1 species to open complexes.

At 100nM DNA, and 80nM RNAP, k_{fast} = 12.4 (± 4.9) s^{-1}, A_{fast}= 0.14 (± 0.04) (arbitrary units, fraction of total signal change) and k_{slow}= 0.015 (± 0.003) s^{-1}, A_{slow}= 0.86 (± 0.06). The value of k_{fast}, though at much high RNAP and DNA concentrations than those used in the HO• fast footprinting experiments (Ch. 2) is significantly smaller than that estimated as a lower bound for formation of the initial extended-footprint closed complex (> 20 s^{-1}; Ch 2). From this and more detailed analysis in progress (J. Murray), we propose that the wrapped species is not the first I_1 species to form, and that the fast phase of the FRET kinetics detects a decay to an equilibrium population of free promoter DNA and of wrapped and unwrapped I_1 species (see Ch. 4 and 5).

Because k_{fast} represents a decay to equilibrium from free promoter DNA and RNAP, k_{fast} should increase linearly with increases in the sum of equilibrium concentrations $\{[DNA]_{eq} + [RNAP]_{eq}\}$ in this initial kinetic phase, with a slope equal to k_1 and an intercept equaling k_{-1}. Therefore, we attempted to determine rates of association over a wide range of active [RNAP]. However, we found that at the high DNA concentration of our experiments, use of an excess of RNAP with respect to Cy3Cy5 promoter DNA resulted in a reduction of the FRET signal with increasing [RNAP], which we infer may be due to end binding of excess RNAP which disrupts the upstream wrap. In real-time kinetics experiments, under conditions of RNAP excess, the FRET signal appeared early but at longer times after mixing, the FRET signal appeared to be disrupted by the binding of a second RNAP to the promoter. Under conditions of a 1:1 active RNAP to promoter DNA ratio and also under conditions of DNA excess, no such effect was observed. Because we were unable to perform experiments over a wide range of [RNAP] and because the amplitude of k_{fast} was small in relation to the

amplitude of k_{slow}, we were unable to accurately determine the dependence of k_{fast} on [RNAP].

The amplitude of the fast phase A_{fast} is much smaller than the amplitude of the second exponential A_{slow}, with A_{slow} comprising >85% of the total change in signal. Two interpretations of the widely different relative amplitudes of the two phases are possible. One is that the FRET effect increases in the isomerization step forming open complexes, which would imply these open complexes are more wrapped. Alternatively, the initial phase is the decay to an equilibrium mixture of free promoter DNA and closed complexes, and the closed complex population appears to itself be a mixture of wrapped and unwrapped complexes, so the conversion of this mixture to open complexes in the slow phase involves much additional formation of wrapped complexes. As with the equilibrium FRET results, we can conclude that both closed and open complexes are wrapped, but we cannot yet conclude with certainty which complex is more wrapped. The large amplitude of the slow phase, with rate constant k_{slow}, allows us to determine that k_{slow} is independent of [RNAP]. This step occurs two orders of magnitude slower than the fast rate for formation of the transient equilibrium mixture of free promoter DNA and closed I_1 species, consistent with it being the conversion of this equilibrium mixture of I_1 species and free promoter DNA to open complexes.

As a control, real-time association assays were also performed with the dyes in the opposite orientation (Cy5 -100, Cy 3+14) (Figure 7). Upon mixing with Cy5 (-100) Cy3 (+14) promoter DNA with RNAP, Cy3 (+14) exhibits a rapid, double exponential increase, followed by a single exponential decrease in fluorescence (Figure 7A and 7B). Cy5 (-100) dye emission from Cy5 (-100) Cy3 (+14) promoter DNA construct exhibits a

triple exponential increase, with k_{fast}= 8.9 (± 3.6) s^{-1}, A_{fast}= 0.21 (± 0.03) (arbitrary units, fraction of total signal change); k_{slow}= 0.026 (± 0.003) s^{-1}, A_{slow}= 0.11 (± 0.06); and k_{third}= 0.002 (± 0.0002) s^{-1} A_{slow}= 0.67 (± 0.06). These results are semiquantitatively in agreement with those obtained using the Cy3 (-100) Cy5 (+14) promoter DNA construct. RNAP mixed with Cy3 (+14) promoter DNA exhibits a rapid, double exponential increase and RNAP mixed with Cy5 (-100) promoter DNA showed no changes in fluorescence emission when excited at both 515 and 615 nm (Figure 7C and 7D).

We also performed equilibrium and real-time FRET studies with promoter DNA containing the full-length wildtype P_RP_{RM} sequence (identical sequence as studied in Rivetti *et al.* 2002). Cy3 (+14) Cy5 (-100) P_RP_{RM} promoter DNA – RNAP equilibrium experiments performed at 2°C displayed a large Cy5 emission due to promoter DNA wrapping (Figure 8A). Real-time experiments with Cy3 (+14) Cy5 (-100) P_RP_{RM} at 19°C also displayed a biphasic increase in the Cy5 (-100) emission signal upon RNAP binding; the kinetics of the increase were qualitatively consistent with those determined for the P_R promoter: k_{fast}= 3.4 (± 1.9) s^{-1}, A_{fast}= 0.22 (± 0.04) (arbitrary units, fraction of total signal change) and k_{slow}= 0.008 (± 0.004) s^{-1}, A_{slow}= 0.88 (± 0.04) (Figure 8B). Therefore, we conclude that promoter DNA wrapping occurs for DNA containing both the λP_R and λP_RP_{RM} promoters.

Real-time Dissociation FRET Experiments Utilizing a High [Salt] Upshift Rapidly Disrupt Promoter DNA Wrapping

Next, we used high salt upshift “burst” experiments to destabilize open complexes and to monitor the changes in promoter DNA wrapping around RNAP. Use of a high salt or solute upshift generates a “burst” of the late intermediate I_2 by

destabilizing the final population of open complexes. Here, we generated a burst of the open complex I_2 by rapidly mixing open complexes with a high concentration of NaCl (1.1 M final concentration) at 19°C. We find that unwrapping of Cy3 (-100) Cy5 (+14) promoter DNA from RNAP occurs extremely rapidly with a k_{obs} = 40 s^{-1}; this is greater than an order of magnitude faster than that previously measured for DNA closing at λP_R (Figure 9, Kontur *et al.* 2008). Thus, it appears that the high salt upshift rapidly destabilizes the wrap faster than DNA closing occurs. This is consistent with previous work from our lab using upstream truncated (UT) LPR promoter DNA. Davis *et al.* 2005 found that truncation of promoter upstream of -47 had little effect on the rate of dissociation of open complexes. Here, the wrap is rapidly displaced by a high salt upshift, presumably by disrupting charged salt-bridge interactions of the polyanionic promoter DNA with positively charged RNAP amino acid side chains. However, disruption of the wrap must not weaken interactions of RNAP with the transcription bubble, as DNA closing occurs within the RNAP active site and is relatively salt insensitive (Kontur *et al.* 2008). Because DNA closing occurs within the protected environment of the RNAP cleft, it is less sensitive to perturbation by salt or solutes. However, outside of the transcription bubble, the duplex promoter DNA wraps around the backside of RNAP where it is more solvent-accessible to these agents.

Discussion

What are the major roles of the promoter DNA wrap around RNAP during transcription initiation? Numerous labs have proposed that promoter DNA is tightly wrapped in the preinitiation complex and/ or in the elongation complex for both *E. coli* RNAP (Rivetti *et al.* 1999a; Rivetti *et al.* 1999b; Heuman *et al.* 1988b, Meyer-Alme *et al.* 1994) and eukaryotic pol II (Coulombe and Burton, 1999, and references therein). The first steps of open complex formation discriminate promoter from nonpromoter DNA by establishing interactions between σ regions 4 and 2 and conserved 6 bp sequences at -35 and -10, respectively (Helmann and deHaseth, 1999). Formation of I_1 at the λP_R promoter creates an extensive interface with DNA that extends well beyond the -10 and -35 regions: protection from hydroxyl radical (•OH) or DNase I cleavage of the DNA backbone in I_1 extends to at least +20 at the λP_R and the λP_{RM} promoter (Davis *et al.* 2007; Craig *et al.* 1998, Li and McClure 1998); upstream protection from •OH cleavage at both the λP_R and T7A1 promoters extends to approximately -85 (Davis *et al.* 2007, Sclavi *et al.* 2005). These data, interpreted using structures of the free RNAP (Vassylyev *et al.* 2002; Murakami *et al*. 2002b) and a complex with a fork junction DNA [from −7 to −41 (Murakami *et al*. 2002a)], are consistent with a model in which upstream DNA is wrapped around RNAP and downstream DNA is bound in the active site channel created by the opposition of the β and β′ subunits. Here, we have shown that promoter DNA wraps around the backside of RNAP in the closed complex I_1, bringing the upstream and downstream regions of the DNA in close proximity.

In Davis et al. 2007, we modeled I_1 using •OH footprinting data and patterns of DNase I hypersensitive cleavage sites. In this model I_1, upstream promoter DNA is

wrapped around the outside of RNAP and a sharp DNA bend (≈90°) at position −11/−12 places downstream duplex DNA high in the channel (≈50 Å above the active site). Interestingly, •OH footprinting data at the T7A1 promoter suggests that the backbone is protected to −70 (nontemplate)/−82 (template) at early times, suggesting that wrapping of early intermediates at the T7A1 promoter may be similar to that of λP_R (Sclavi *et al.* 2008).

In order to investigate the extent of wrapping for open complexes I_3 and RP_o, we performed equilibrium FRET experiments at 10, 19 and 37°C. For RNAP-promoter DNA complexes formed at increasing temperatures (from 2 to 37°C) there appeared to be a decrease in the intensity of the FRET signal. However, single dye controls revealed that the fluorescence emission of both the Cy3 and Cy5 dyes is strongly temperature dependent; the emission of each dye is reduced at 37°C by approximately 2-fold relative to that at 2°C. After correcting the equilibrium FRET data to account for the temperature effects on the individual Cy3 and Cy5 fluorescence emission intensities, we find that there is a larger FRET signal at 37°C than at 10°C. Since in both cases we are dealing with relatively homogeneous populations of open complexes, this result indicates that either an increase in wrapping or a change in probe orientation occurs in open complexes with increasing temperature to increase the FRET signal.

In real-time association assays performed at 19°C, we observe a large increase in FRET emission upon mixing Cy3Cy5 promoter DNA with RNAP. The kinetics of the increase in promoter DNA wrapping are best-fit to the sum of two exponentials, consistent with wrapping occurring during the formation of the closed intermediate I_1 and then the conversion of I_1 to open complexes (I_3 and RP_o at this experimental

condition). For 100nM (-100) Cy3 (+14) Cy3 promoter DNA, and 80nM RNAP, k_{fast}= 12.4 (± 4.9) s^{-1}, A_{fast}= 0.14 (± 0.04) and k_{slow}= 0.015 (± 0.003) s^{-1}, A_{slow}= 0.86 (± 0.06). The amplitude of the second exponential phase comprises the majority of the total signal change, as discussed previously. Experiments performed with the dyes in the opposite orientation [Cy5 (-100) Cy3 (+14) promoter DNA] exhibits a triple exponential FRET increase, with k_{fast}= 8.9 (± 3.6) s^{-1}, A_{fast}= 0.21 (± 0.03) (arbitrary units, fraction of total signal change); k_{slow}= 0.026 (± 0.003) s^{-1}, A_{slow}= 0.11 (± 0.06); and k_{third}= 0.002 (± 0.0002) s^{-1} A_{slow}= 0.67 (± 0.06). These results are qualitatively consistent with those determined with Cy3 and Cy5 in the opposite orientations.

Previous characterizations of the extent of wrapping for open complexes at the λP_R promoter using AFM demonstrated a large DNA compaction (~30nm, ~90bp) interpreted as wrapping of upstream promoter DNA (positions -100 to -40) around RNAP (Rivetti *et al.* 1999a, Rivetti *et al.* 1999b). These results suggested that promoter DNA is wrapped in almost a complete turn around RNAP in the open complex at this promoter. Our FRET results are consistent with this model, and expand on it by providing evidence that the closed complex is highly wrapped as well.

Materials and Methods

E. coli PVS10 RNAP core and σ^{70} were both purified following the procedures in Belogurov *et al.* 2003. *E. coli* σ^{70} RNA polymerase was prepared by reconstituting PVS10 RNAP core with σ^{70} in a 1:2 (core: sigma) ratio in storage buffer at 37°C for 1 hour. RNAP holoenzyme was stored at -20°C and was used up to one month after reconstitution. Nitrocellulose equilibrium promoter binding activity assays indicated that reconstituted RNAP holoenzyme was >95% active. RNAP concentrations are therefore reported as total concentration.

Storage buffer for RNAP at -80 °C contained 10 mM Tris (pH 7.5 at 4°C), 6.85 M glycerol, 100 mM NaCl, 100 nM Na_2EDTA, and 100 nM DTT. Binding buffer used for all experiments was 40 mM Tris (pH 8 at 19°C), 10 mM $MgCl_2$, 120 mM NaCl, and 100 μg/mL BSA.

λP_R promoter DNA was amplified from a 963-bp-long DNA template P_R (wild type P_R sequence from −59 to + 34) using PCR and primers 'Fwd' (5'GTACGAATTCGATATCCAGCTATGACCATGATTACGCCAGC) and 'Rev' (5'CAGGACCCGGGGCGCGCTTAATTAACACTCTTATACATTATTCC).
Primers were custom synthesized (Integrated DNA Technologies, Coralville, IA) to contain an internal Cy3 or Cy5 dye at position -100 or +14 (relative to the transcription start site) and HPLC purified before use. All dyes were incorporated at least 5 base pairs in from the 5' end of the promoter DNA in order to inhibit end binding of the RNAP. The high fidelity DNA polymerase Pfx50 (Invitrogen, Carlsbad, CA) was used to create blunt ends during the PCR amplification. All DNA was purified using the Qiagen MinElute PCR cleanup kit and concentration determined by absorbance at 260nm. A

6% polyacrylamide gel was run for each DNA preparation in order to ensure purity. Stoichiometry of the active dye molecules was determined by comparing the concentration of each dye (Cy3 excited at 540nm, Cy5 excited at 615nm) with that of the double stranded DNA. Active dye stoichiometry ranged from 70-95%. We hypothesize that dye stoichiometries less than one are due to dark state inactivation of the dyes and not loss of the dye during the PCR reaction and cleanup steps.

Stable, open complexes between RNAP holoenzyme and λP_R promoter DNA were formed at room temperature by incubating RNAP in SB with promoter DNA at the temperature of interest for 1.5 hours. The final RNAP-promoter DNA complex contained 50-150 nM active RNAP and 50-100 nM DNA.

Equilibrium Fluorescence Measurements

Equilibrium FRET measurements were collected on a single beam fluorimeter (Photon Technology International) equipped with an 814 Photomultiplier Detection system and a peltier heating and cooling block connected to an external temperature control (Quantum Northwest). A nitrogen airflow system was also used at low temperatures (<10°C) to prevent condensation in the cuvette. Cy3 was excited at 515 and Cy5 was excited at 610. The Cy3 excitation wavelength was chosen in order to minimize direct excitation of Cy5. The Cy5 excitation was chosen such that it did not overlap with the dye's emission spectra. Cy3 emission was collected using the instrument monochromator from 550 to 650; Cy5 emission was collected from 620 to 720. Control experiments with Cy3 or Cy5 alone, with and without RNAP, were used as controls for dye sensitization, nonspecific end binding of RNAP, and dye photobleaching.

Stopped-flow Fluorescence Measurements

Real-time fluorescence measurements were taken on a Kintek SFX-300 stopped flow spectrometer (KinTek Corp., Austin, TX) equipped with computer-controlled motor-driven syringes and an external water bath. Equal volumes (20 μL) of RNAP (20-150nM final concentration) and promoter DNA (100nM final concentration) were rapidly mixed with an instrument data collection dead time less than 10 milliseconds. Cy3 was excited at 515 and Cy5 was excited at 610. The same emission filters were used as in Tims and Widom, 2007. For Cy3, emission light was collected after passing through both a 595AF60 band pass and 565 long pass emission filter. For Cy5, a 660nm long pass emission filter was used. Use of two PMTS allowed changes in emission for the Cy3 and Cy5 channels to be detected simultaneously. When possible, bleaching of both dyes was minimized by reducing the slit widths.

Kinetic Analysis

For all stopped-flow experiments, 1000-2000 data points were collected on a log time scale and data from 3-5 individual traces under identical conditions were averaged for each day. Data from at least three different days was collected for each reaction condition before being used in our analysis. The fluorescence time courses were fit to a sum of exponentials (either one or two) using Origin8 software according to the equation $F= \Sigma An \times \exp(-k_{obs,n}\, t) + C$, where F is the fluorescence at time *t*, *n* is the number exponential terms, A_n and $k_{obs,n}$ are the amplitude and the observed rate constants of the *n*th term, respectively. The uncertainties reported for the observed rates ($k_{obs,i}$) are the standard deviations. Other analyses of the data, including

simulations and fitting to appropriate kinetic or equilibrium models, were performed using Matlab.

References

Belogurov, G. A., Vassylyeva, M. N., Svetlov, V., Grishin, N. V., Vassylyev D., G., and Artsimovich, I. 2007. Structural basis for converting a general transcription factor into an operon-specific virulence regulator. *Mol Cell.* **26:** 117-29.

Coulombe, B and Burton, Z. F. 1999. DNA Bending and Wrapping around RNA Polymerase: a “Revolutionary” Model Describing Transcriptional Mechanisms. *Microbiology and Molecular Biology Reviews*. **63:** 457-478.

Craig, M. L., W. C. Suh, and M. T. Record, Jr. 1995. HO. and DNase I probing of E σ70 RNA polymerase--λPR promoter open complexes: Mg^{2+} binding and its structural consequences at the transcription start site. *Biochemistry*. **34:** 15624–15632.

Craig, M. L., Tsodikov, O. V., McQuade, K. L., Schlax, P. E., Jr, Capp, M. W., Saecker, R. M., and Record, M. T., Jr. 1998. DNA footprints of the two kinetically significant intermediates in formation of an RNA polymerase-promoter open complex: evidence that interactions with start site and downstream DNA induce sequential conformational changes in polymerase and DNA. *J Mol Biol.* **283:** 741-56.

Cellai, S., Mangiarotti, L., Vannini, N., Naryshkin, N., Kortkhonjia, E., Ebright, R.H., and Rivetti C. 2007. Upstream promoter sequences and alphaCTD mediate stable DNA wrapping within the RNA polymerase-promoter open complex. *EMBO.* **3:** 271-8.

Darst, S. A., Kubalek, E. W., and Kornberg, R. D. 1989. Three-dimensional structure of *Escherichia coli* RNA polymerase holoenzyme determined by electron crystallography. *Nature.* **340:** 730–732.

Fischer, C. J., Tomko, E. J., Wu, C. G., Lohman, T., M. 2012. Fluorescence methods to study DNA translocation and unwinding kinetics by nucleic acid motors. *Methods Mol Biol.* **875:** 85-104.

Gu Li , Marcia Levitus , Carlos Bustamante & Jonathan Widom. 2004. Rapid spontaneous accessibility of nucleosomal DNA. *Nature Structural & Molecular Biology* **12:** 46 – 53.

Gruber, H. J., Hahn, C., D., Kada, G., Riener C., K., Harms, G., S., Ahrer, W., Dax, T. G., Knaus, H., G. Anomalous fluorescence enhancement of Cy3 and cy3.5 versus anomalous fluorescence loss of Cy5 and Cy7 upon covalent linking to IgG and noncovalent binding to avidin. *Bioconjug Chem.* **11:** 696-704.

Heumann, H., Ricchetti, M., and Werel W. 1988a. DNA-dependent RNA polymerase of *Escherichia coli* induces bending or an increased flexibility of DNA by specific complex formation. *EMBO J.* **7:** 4379–4381.

Heumann, H., Lederer, H., Baer, G., May, R.P., Kjems, J.K., and Crespi, H.L. 1988b. Spatial arrangement of DNA-dependent RNA polymerase of *Escherichia coli* and DNA in the specific complex. A neutron small angle scattering study. *J Mol Biol.* **201:** 115–125.

Kapanidis, A. N., Margeat, E. M., Ho, S. O., Kortkhonjia, E., Weiss S., and Ebright, R. H. 2006. Initial Transcription by RNA Polymerase Proceeds Through a DNA-Scrunching Mechanism. *Science.* **314:** 1144-1147.

Katiliene, Z., Katilius, E., Woodbury, N.W. 2003. Single molecule detection of DNA looping by NgoMIV restriction endonuclease. *Biophys J.* **84:** 4053-61.

Kozlov, A.G., Lohman, T. M. 2002. Stopped-flow studies of the kinetics of single-stranded DNA binding and wrapping around the Escherichia coli SSB tetramer. *Biochemistry.* **41:** 6032-44.

Kuhnke, G., Theres, C., Fritz, H. J., and Ehring, R. 1989. RNA polymerase and *gal* repressor bind simultaneously and with DNA bending to the control region of the *Escherichia coli* galactose operon. *EMBO J.* **8:** 1247–1255.

Meyer-Alme, F. J., Heumann, H. and Porschke, D. 1994. The structure of the RNA polymerase–promoter complex: DNA bending by quantitative electrooptics. *J Mol Biol.* **236:** 1–6.

McMann, J. J., Choi, U. B., Zheng, L., Weninger, K., and Bowen, M. E. 2000. Optimizing Methods to Recover Absolute FRET Efficiency from Immobilized Single Molecules. *Biophys J.* **99:** 961–970.

Mukhopadhyay, J., Kapanidis, A. N., Mekler, V., Kortkhonjia, E., Ebright, Y. W., and Ebright, R. H. 2001. Translocation of σ^{70} with RNA polymerase during

transcription: fluorescence resonance energy transfer assay for movement relative to DNA. *Cell* **106:** 453–463

Murakami, K. S. and Darst, S. A. 2003. Bacterial RNA polymerases: The wholo story. *Curr Opin Struct Biol* **13:** 31–39.

Murakami, K. S., Masuda, S., Campbell, E. A., Muzzin, O., and Darst, S. A. 2002a. Structural basis of transcription initiation: An RNA polymerase holoenzyme-DNA complex. *Science* **296:** 1285–1290.

Murakami, K. S., Masuda, S., and Darst, S. A. 2002b. Structural basis of transcription initiation: RNA polymerase holoenzyme at 4 Å resolution. *Science* **296:** 1280–1284.

Lakowicz, J.R. 2006. Principles of Fluorescence Spectroscopy. Springer; New York.

Li, X. Y. and McClure, W. R. 1998. Characterization of the closed complex intermediate formed during transcription initiation by by *Escherichia coli* RNA polymerase. *J Biol Chem* **273:** 23549-23557.

Levitus, M., and Ranjit, S. 2011. Cyanine dyes in biophysical research: the photophysics of polymethine fluorescent dyes in biomolecular environments. *Q Rev Biophys.* **44:** 123-51.

Mangiarotti L, Cellai S, Ross W, Bustamante C, Rivetti C. 2009. Sequence-dependent upstream DNA-RNA polymerase interactions in the open complex with lambdaP_R and lambdaP_{RM} promoters and implications for the mechanism of promoter interference. *J Mol Biol.* **385:**748-60.

Morgan, M. A., Okamoto, K., Kahn, J. D., English, D., S. 2005. Single-molecule spectroscopic determination of lac repressor-DNA loop conformation. *Biophys J.* **89:** 2588-96.

Mukhopadhyay, J., Kapanidis, A. N., Mekler, V., Kortkhonjia, E., Ebright, Y. W., and Ebright, R. H. 2001. Translocation of σ^{70} with RNA polymerase during transcription: fluorescence resonance energy transfer assay for movement relative to DNA. *Cell* **106:** 453–463

Nickerson, C., A., and Achberger, E.,C. 1995. Role of curved DNA in binding of *Escherichia coli* RNA polymerase to promoters. *J Bacteriol.* **177:** 5756–5761.

Parkhurst, L. J., Parkhurst K., M., Powell, R., Wu, J., and Williams, S. 2001. Time-resolved fluorescence resonance energy transfer studies of DNA bending in double-stranded oligonucleotides and in DNA-protein complexes. *Biopolymers.* **61:** 180-200.

Polyakov, A., Severinova, E., and Darst, S. A. 1995. Three-dimensional structure of *E.coli* core RNA polymerase: promoter binding and elongation conformation of the enzyme. *Cell*. **83:** 365–373.

Rees, W. A., Keller, R. W., Vesenka, J. P., Yang, G., and Bustamante, C. 1993. Evidence of DNA bending in transcription complexes imaged by scanning force microscopy. *Science.* **260:** 1646–1649.

Rippe, K., Guthold, M., von Hippel, P. H., and Bustamante, C. 1997. Transcriptional activation via DNA-looping: visualization of intermediates in the activation pathway of *E.coli* RNA polymerase-σ54 holoenzyme by scanning force microscopy. *J Mol Biol.* **270:** 125–138.

Rivetti, C., Guthold, M., and Bustamante, C. 1996. Scanning force microscopy of DNA deposited on mica: equilibration versus kinetic trapping studied by polymer chain analysis. *J Mol Biol.* **264:** 919–932.

Rivetti, C., Walker, C., and Bustamante, C. 1998 Polymer chain statistics and conformational analysis of DNA molecules with bends or sections of different flexibility. *J Mol Biol.* **280:** 41–59.

Rivetti, C., Codeluppi, S., Dieci, G., and Bustamante, C. 2003. Visualizing RNA Extrusion and DNA Wrapping in Transcription Elongation Complexes of Bacterial and Eukaryotic RNA Polymerases. *J. Mol. Biol.* **326:** 1413–1426

Robert, F., Douziech, M., Forget, D., Egly, J. M., Greenblatt, J., Burton, Z. F., and Coulombe, B. 1998. Wrapping of promoter DNA around the RNA polymerase II initiation complex induced by TFIIF. *Mol Cell.* **2:** 341–351.

Roe J.H., Burgess, R.R., and Record M.T., Jr.1985. Temperature dependence of the rate constants of the *Escherichia coli* RNA polymerase λ_{PR} promoter interaction. Assignment of the kinetic steps corresponding to protein conformational change and DNA opening. *J Mol Biol,* **184:** 441–453.

Rogozina, A., Zaychikov, E., Buckle, M., Heumann, H., and Sclavi, B. 2009. DNA melting by RNA polymerase at the T7A1 promoter precedes the rate-limiting step at 37 °C and results in the accumulation of an off-pathway intermediate. *Nucleic Acids Res* **37:** 5390–5404.

Saecker, R. M. and Record, M. T., Jr. 2002. Protein surface salt bridges and paths for DNA wrapping. *Curr Opin Struct Biol* 12: 311–319.

Saecker, R. M. Record, M. T., and de Haseth, P. L. 2010. Mechanism of Bacterial Transcription Initiation: RNA Polymerase - Promoter Binding, Isomerization to Initiation-Competent Open Complexes, and Initiation of RNA Synthesis. *J Mol Biol* **4:** 754–771

Saecker, R. M., Tsodikov, O. V., McQuade, K. L., Schlax, P. E., Jr., Capp, M. W., and Record, M. T., Jr. 2002. Kinetic studies and structural models of the association of *E. coli* σ^{70} RNA polymerase with the λP_R promoter: Large scale conformational changes in forming the kinetically significant intermediates. *J Mol Biol* **319:** 649–671.

Schickor P., Metzger W., Werel W., Lederer H., and Heumann H. 1990. Topography of intermediates in transcription initiation of *E.coli. EMBO J*, **9**: 2215–2220.

Sclavi, B., Zaychikov, E., Rogozina, A., Walther, F., Buckle, M., and Heumann, H. 2005. Real-time characterization of intermediates in the pathway to open complex formation by *Escherichia coli* RNA polymerase at the T7A1 promoter. *Proc Natl Acad Sci (USA)* **102:** 4706–4711.

Tang G.Q., and Patel, S.S. 2006a. T7 RNA polymerase-induced bending of promoter DNA is coupled to DNA opening. *Biochemistry*. **45:** 4936-46.

Tang G.Q., and Patel, S.S. 2006b. Rapid binding of T7 RNA polymerase is followed by simultaneous bending and opening of the promoter DNA. *Biochemistry*. **45:** 4947-56.

Tims, H. S., and Widom, T. 2007. Stopped-flow Fluorescence Resonance Energy Transfer for Analysis of Nucleosome Dynamics. *Methods.* **41:** 296-30.

Travers, A. A. 1990. Why bend DNA? *Cell.* **60:** 177–180.

Ujvári A., and Martin C.T. 2000. Evidence for DNA bending at the T7 RNA polymerase promoter. *J Mol Biol.* **295:**1173-84.

Vassylyev, D. G., Sekine, S., Laptenko, O., Lee, J., Vassylyeva, M. N., Borukhov, S., and Yokoyama, S. 2002. Crystal structure of a bacterial RNA polymerase holoenzyme at 2.6 Å resolution. *Nature* **417:** 712–719.

Vassylyev, D. G., Vassylyeva, M. N., Perederina, A., Tahirov, T. H., and Artsimovitch, I. 2007. Structural basis for transcription elongation by bacterial RNA polymerase. *Nature* **448:** 157–162.

Table 1. Kinetic Rate Constants for Real-time FRET Experiments

	λP_R (-100 Cy3, +14 Cy5)	**λP_R (-100 Cy5, +14 Cy3)**	**$\lambda P_R P_{RM}$ (-100 Cy3, +14 Cy5)**
k_{fast}	12.4 (± 4.9) s^{-1}	8.9 (± 3.6) s^{-1}	3.4 (± 1.9) s^{-1}
A_{fast}	0.14 (± 0.04)	0.21 (± 0.03)	0.22 (± 0.04)
k_{slow}	0.015 (± 0.003) s^{-1}	0.026 (± 0.003) s^{-1}	0.008 (± 0.004) s^{-1}
A_{slow}	0.86 (± 0.06)	0.11 (± 0.06)	0.88 (± 0.04)
k_{third}	N/A	0.002 (± 0.0002)	N/A
A_{third}	N/A	0.67 (± 0.06).	N/A

All experiment performed at 19°C in transcription buffer. Rate constants and amplitudes for Cy5 FRET emission for different promoter DNA constructs. 100nM DNA and 80nM active RNAP were rapidly mixed and the fluorescence emission monitored as a function of time. Each experiment was performed a minimum of two times. The rates and amplitudes reported are the averages from each experiment; the uncertainties represent the standard deviation between replicates.

Figure Captions

Figure 1. Representative equilibrium FRET experiments for RNAP- promoter DNA complexes at 2, 10, 19, and 37°C (A). Complexes (50-150 nM active RNAP; 100nM Cy3 (-100) Cy5 (+14) λP_R promoter DNA) were equilibrated at each temperature for 1.5 hours. The samples were exited at 515nm and emission monitored using the instrument monochromator. Experiments at each temperature were performed on the same day and used the same PMT settings. Each experiment was performed a minimum of five times. Cy3 emission as a function of [RNAP] is shown in (B) at 2°C.

Figure 2. Representative equilibrium FRET control experiments at 2°C. RNAP- DNA complexes were formed 1.5 hours and then scanned in the PTI fluorimeter. (A) 100nM Cy5 (+15) λP_R promoter DNA, 100nM RNAP, Excitation: 515nm. (B) 100nM Cy3 (-100) promoter DNA, 100nM RNAP, Excitation: 515nm. (C) 100nM Cy3 (-100) Cy5 (+14) promoter DNA, no RNAP, Excitation: 515 nm. (D) 100nM Cy3 (-100) Cy5 (+14) promoter DNA, 100nM core RNA (lacking σ^{70}), Excitation: 515nm. Each experiment was performed a minimum of three times.

Figure 3. Representative equilibrium FRET experiments with dyes in the opposite orientation (Cy3 (+14) Cy5 (-100)). The complexes (100-250 nM active RNAP; 100 λP_R promoter DNA) were equilibrated at each temperature for 1.5 hours. The samples were exited at 515nm and emission monitored using the instrument monochromator. Experiments at each temperature were performed on the same day and used the same PMT settings. Each experiment was performed a minimum of five times. (A) 2°C, (B) 10°C, (C)19°C, and (D) 37°C.

Figure 4. Temperature dependence of Cy3 and Cy5 emission. Representative emission of (A) Cy3 and (B) Cy5 as a function of temperature (2-37°C). (C) Depicts the peak fluorescence emission of Cy3 at 565nm as a function of temperature. (D) Depicts the peak emission of Cy5 at 600nm a function of temperature. Red lines depict the best-fit line to a single exponential fit. Each experiment was performed a minimum of three

times. Errors are reported as the uncertainty in the determination of the emission intensities for the representative experiment.

Figure 5. Equilibrium FRET for 100nM RNAP- 100nM Cy3 (-100) Cy5 (+14) λP_R promoter DNA complexes as a function of temperature. (A) Raw data for FRET equilibrium studies at a range of temperature from 2-37°C. (B) Same data as in (A), but zoomed in on Cy5 emission. Normalized Cy5 FRET data for RNAP- promoter DNA complexes formed at each temperature. The normalized peak FRET fluorescence emission as a function of temperature is shown in (D). Samples contained 100nM Cy3 (-100) Cy5 (+14) promoter DNA and 150nM RNAP. Each experiment was performed a minimum of five times. Experiments performed with the dyes in the opposite orientation [Cy3 (+14) Cy5 (-100) promoter DNA] yielded an identical temperature effect.

Figure 6. Real-time DNA bending monitored by stopped-flow fluorescence at 19°C. 100nM Cy3 (-100) Cy5 (+14) λP_R promoter DNA was rapidly mixed with 80nM RNAP and the emission for both dyes was monitored simultaneously using two PMTs; samples were excited at 515nm and emission collected using 565 nm long pass and 595 nm band pass (Cy3 emission) or 660 nm long pass (Cy5 emission) filters. (■) Cy3 (-100) emission, (●) Cy5 (+14) emission. The data are plotted on both a (A) linear time scale (B) log time scale. A representative Cy3 (-100) promoter DNA emission control is shown in (C). 100nM Cy3 (-100) promoter DNA was rapidly mixed with 80nM RNAP and the emission monitored as a function of time. Samples were excited at 515 nm. (■) Cy3 (-100) emission. (D) Depicts a representative Cy5 (+14) emission control. 100nM Cy5 (+14) promoter DNA was rapidly mixed with 80nM RNAP and the emission monitored as a function of time. Samples were excited at 615. (■) Cy5 (+14) emission. Each experiment depicted in Figure 6 was replicated at least four times.

Figure 7. Reversal of FRET dye positions for real-time DNA bending monitored by stopped-flow fluorescence at 19°C. 100nM Cy3 (+14) Cy5 (-100) λP_R promoter DNA was rapidly mixed with 80nM RNAP and the emission for both dyes was monitored simultaneously using two PMTs; samples were excited at 515nm and emission

collected using glass filters. (■) Cy3 (+14) emission, (●) Cy5 (-100) emission. The data are plotted on both a (A) linear time scale (B) log time scale. A representative Cy3 (-100) emission control is shown in (C). 100nM Cy3 (-100) promoter DNA was rapidly mixed with 80nM RNAP and the emission monitored as a function of time. Samples were excited at 515 nm. (■) Cy3 (-100) emission. (D) Depicts a representative Cy5 (+14) emission control. 100nM Cy5 (+14) promoter DNA was rapidly mixed with 80nM RNAP and the emission monitored as a function of time. Samples were excited at 615. (■) Cy5 (+14) emission. Each experiment depicted in Figure 7 was replicated at least four times.

Figure 8. (A) Equilibrium and (B- C) real-time FRET experiments for RNAP- $\lambda P_R P_{RM}$ promoter complexes. In (A) complexes of 100nM RNAP and 100nM [Cy3 (+14) Cy5 (-100) $P_R P_{RM}$ promoter DNA were formed 1.5 hours at 2°C and then scanned in the PTI fluorimeter. Each experiment was replicated four times. In (B) linear time scale and (C) log time scale, 100nM Cy3 (+14) Cy5 (-100) $P_R P_{RM}$ promoter DNA was rapidly mixed with 80nM RNAP and the emission for both dyes was monitored simultaneously using two PMTs; samples were excited at 515nm and emission collected using glass filters. In each figure, the (■) Cy3 (+14) emission and (●) Cy5 (-100) emission are plotted as a function of time. Each experiment was replicated two times.

Figure 9. Rapid salt upshift “burst” experiment for characterizing the dissociation of the highly wrapped open complexes, I_3 and RP_o at 19°C. Cy3 (-100) Cy5 (+14) λP_R promoter DNA open complexes were formed at 19°C for a minimum of one hour and then rapidly upshifted to 1.1M NaCl (final concentration). (■) Cy5 (+14) emission is plotted as a function of time. The data was best described by a single exponential fit. The best-fit line is shown in red.

Figure 1. Equilibrium FRET for RNAP- Cy3 (-100) Cy5 (+14) promoter DNA Complexes Formed at Different Temperatures

A. Cy5 emission

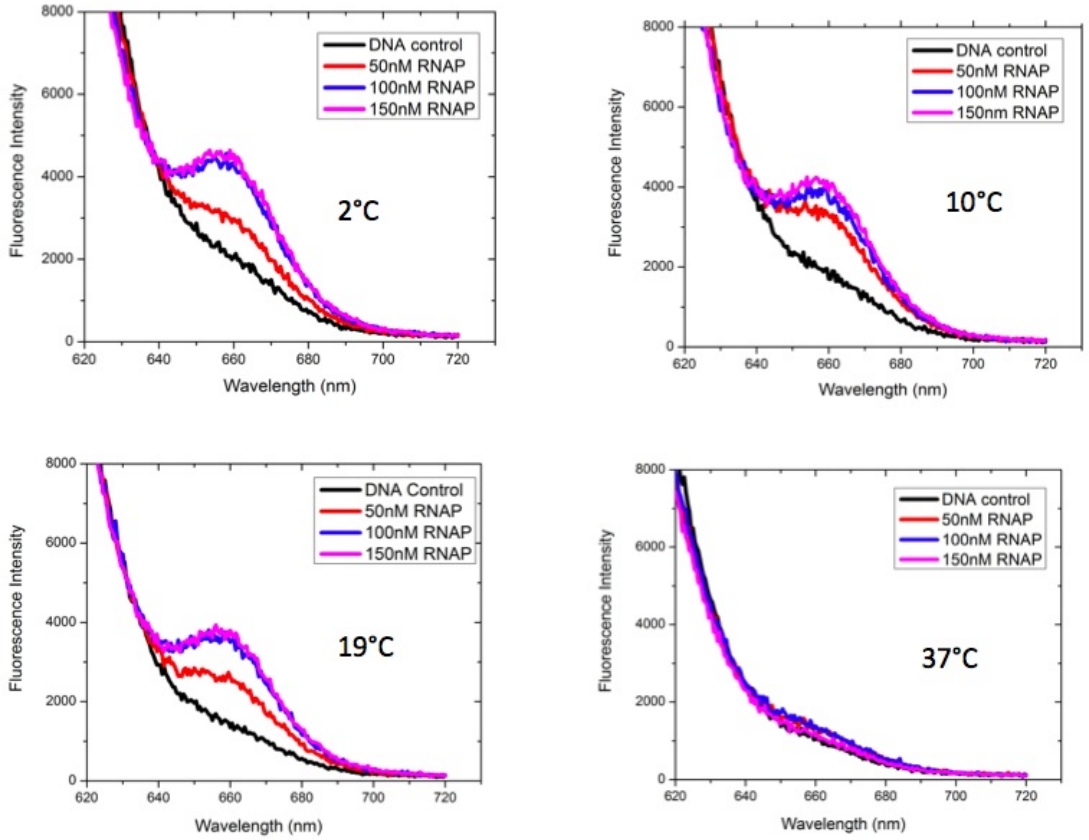

B. Cy3 emission at 2°C

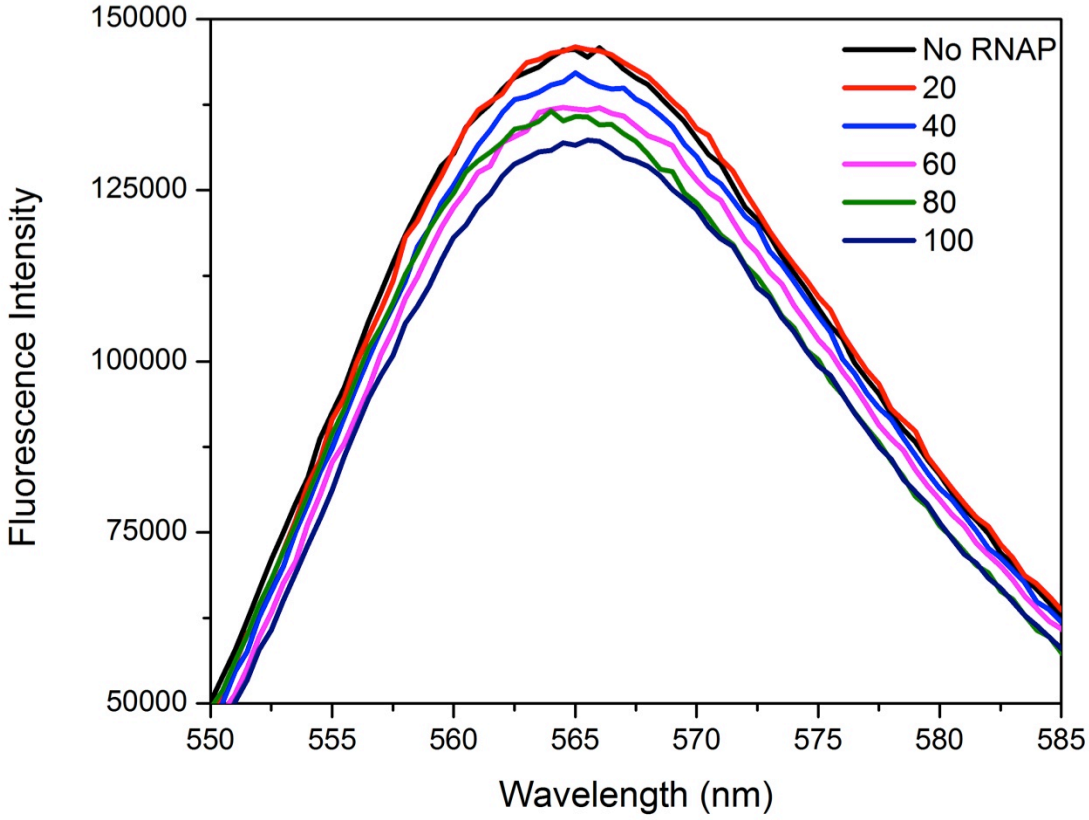

Figure 2. Equilibrium FRET Controls
A. 100nM Cy5 (+14) promoter DNA + 100nM RNAP Ex: 515

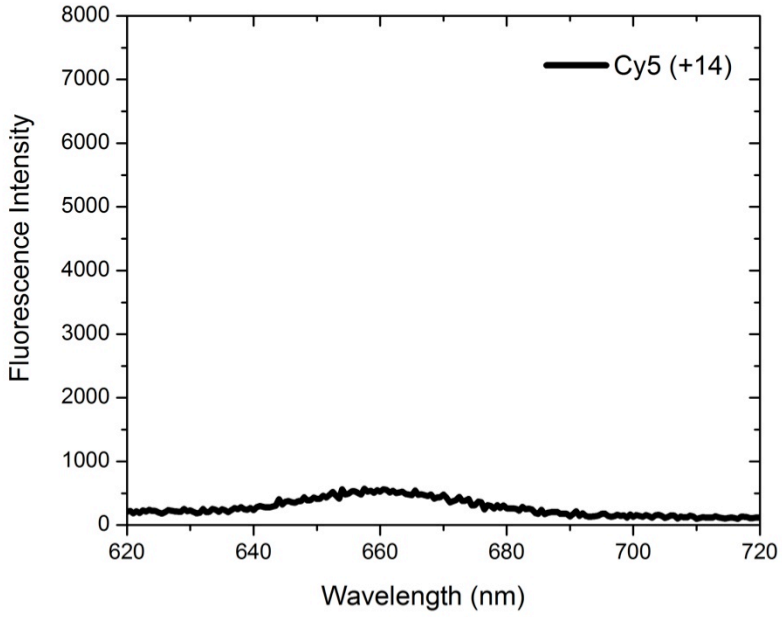

B. 100nM Cy3 (-100) promoter DNA + 100nM RNAP Ex: 515

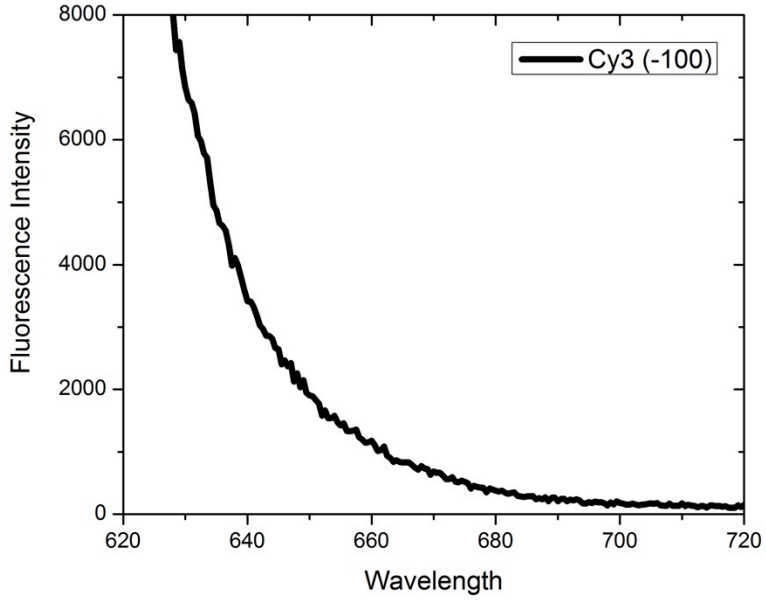

C. 100nM Cy3 (-100) Cy5 (+14) promoter DNA, no RNAP Ex: 515

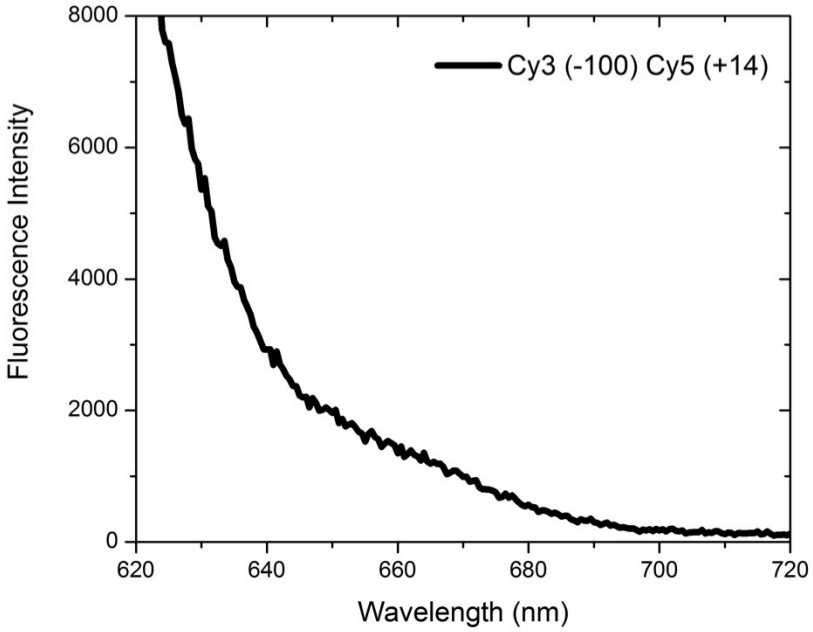

D. 100nM Cy3 (-100) Cy5 (+14) promoter DNA, 80nM core RNAP (no σ^{70}) Ex: 515

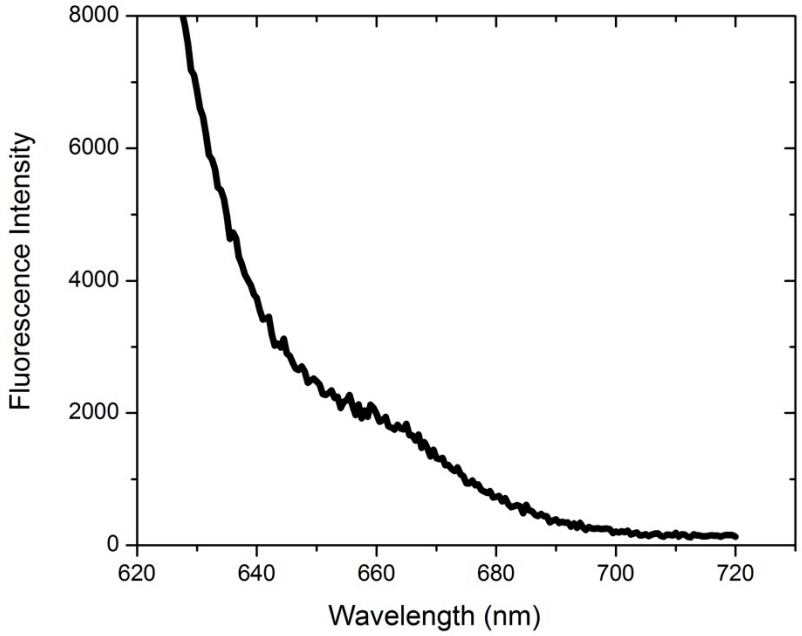

Figure 3. Equilibrium FRET for RNAP- Cy3 (+14) Cy5 (-100) promoter DNA
A. 2°C

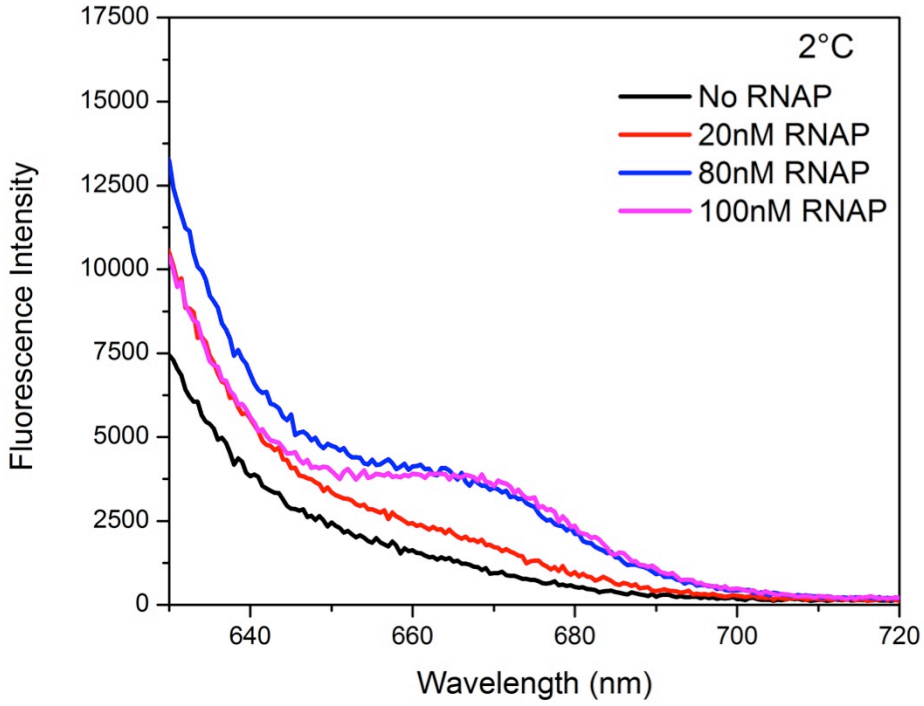

B. 10°C

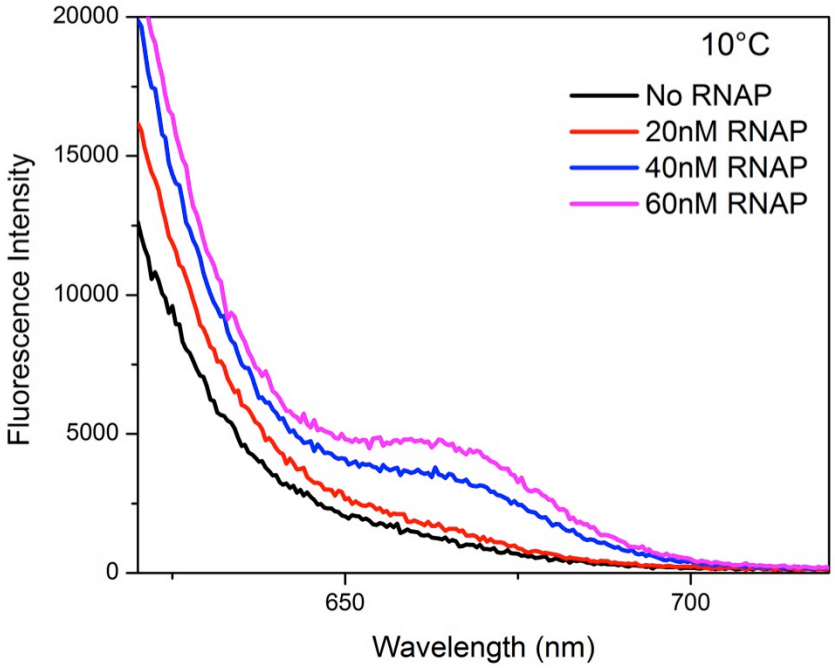

C. 19°C

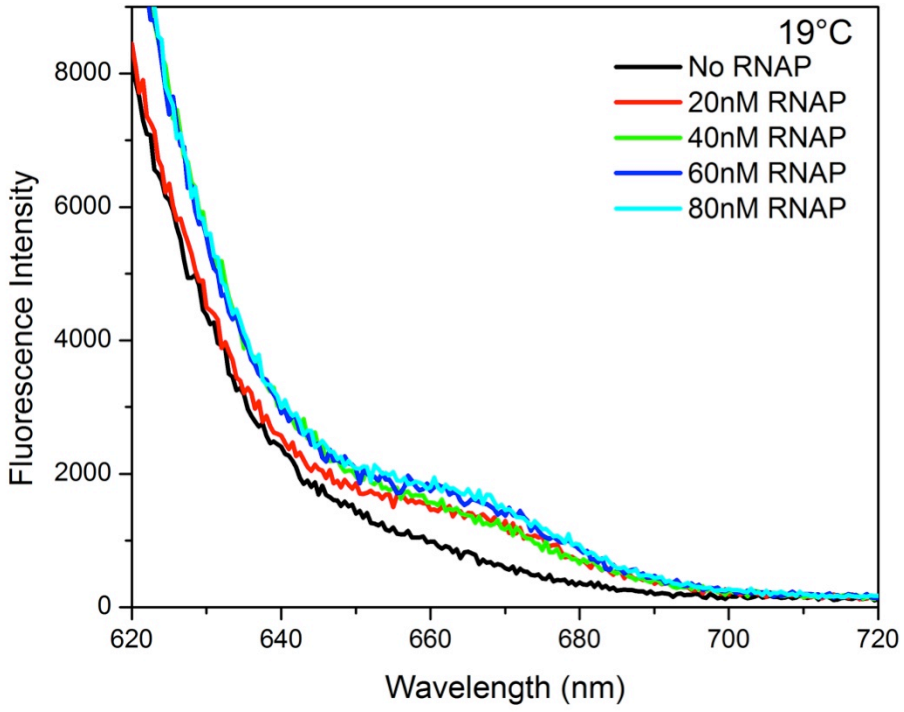
19°C
No RNAP
20nM RNAP
40nM RNAP
60nM RNAP
80nM RNAP
Fluorescence Intensity
0
2000
4000
6000
8000
620
640
660
680
700
720
Wavelength (nm)

D. 37°C

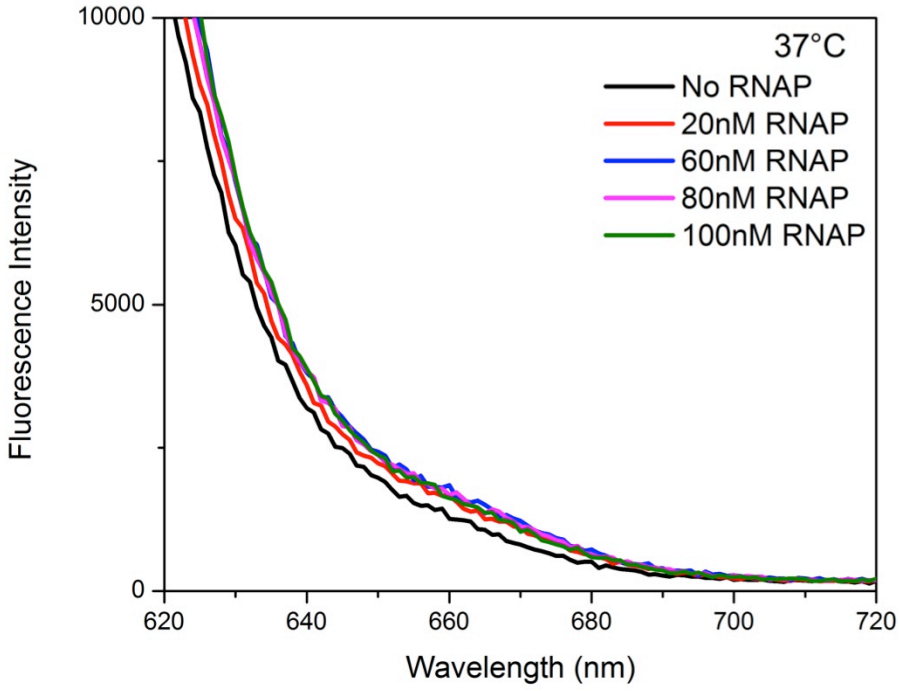
37°C
No RNAP
20nM RNAP
60nM RNAP
80nM RNAP
100nM RNAP
Fluorescence Intensity
0
5000
10000
620
640
660
680
700
720
Wavelength (nm)

Figure 4. Temperature dependence of Cy3 and Cy5 emission.
A.

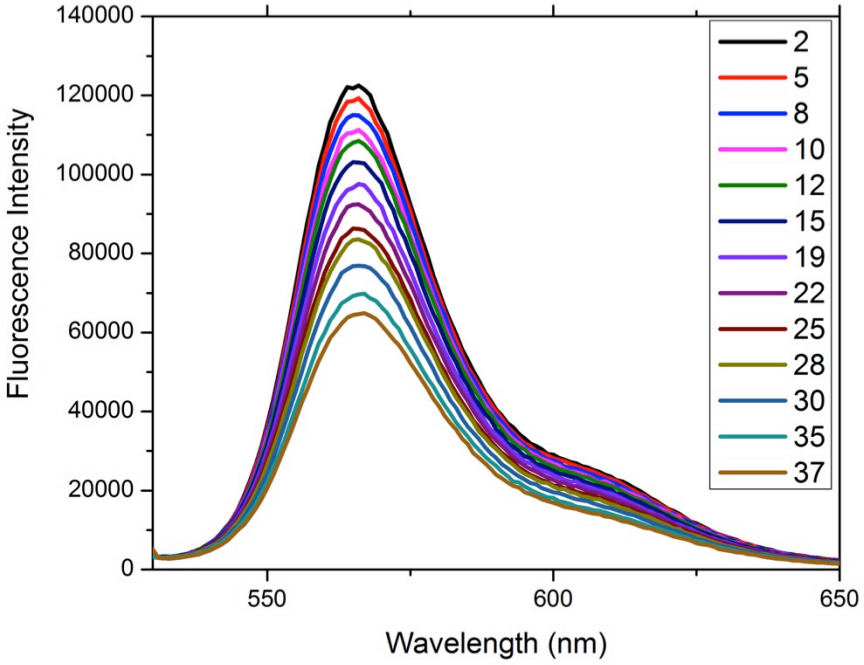

B.

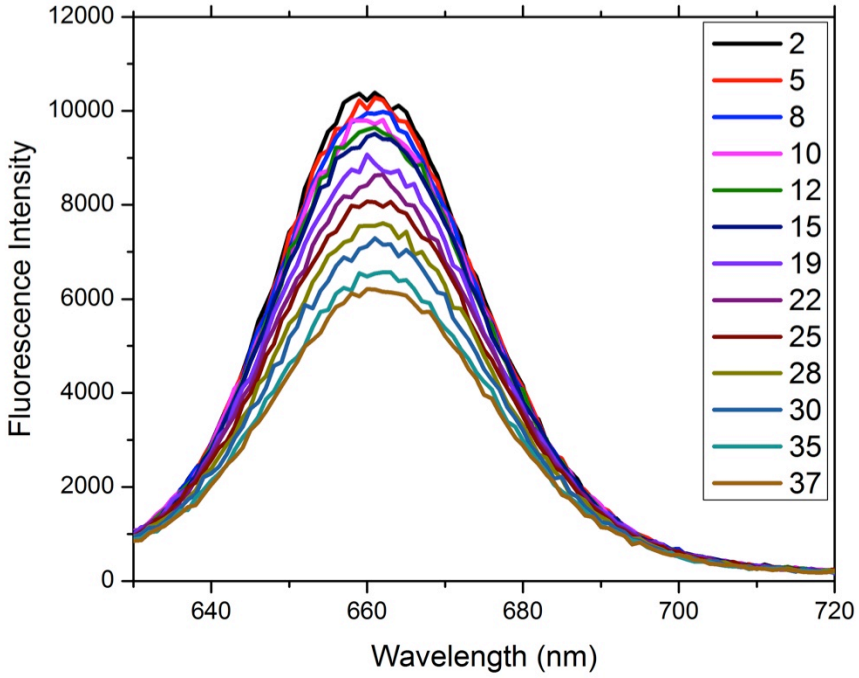

C.

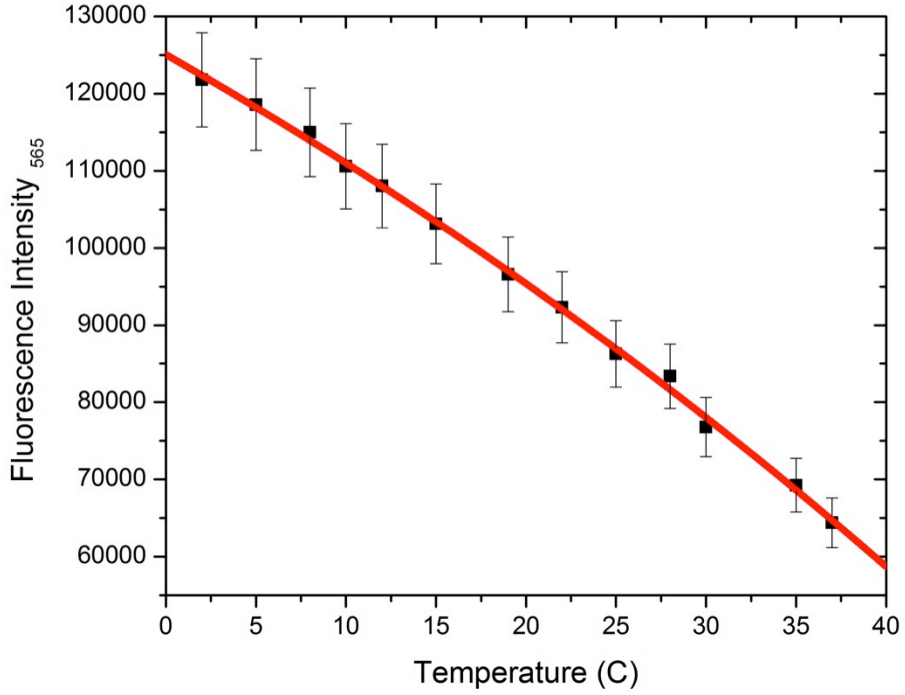
Fluorescence Intensity 565
130000
120000
110000
100000
90000
80000
70000
60000
0
5
10
15
20
25
30
35
40
Temperature (C)

D.

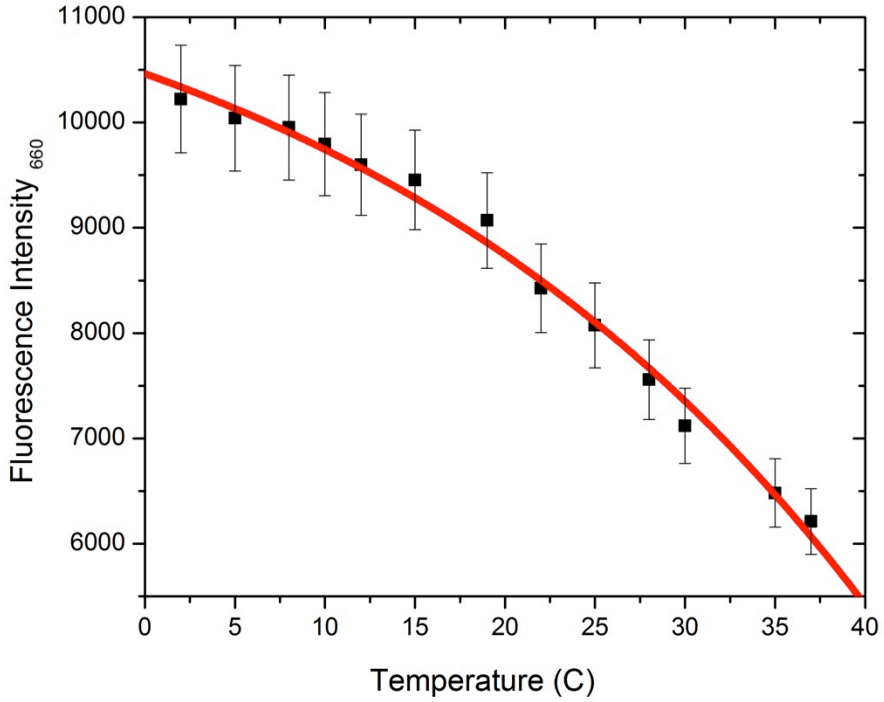
Fluorescence Intensity 660
11000
10000
9000
8000
7000
6000
0
5
10
15
20
25
30
35
40
Temperature (C)

Figure 5. Temperature dependence of equilibrium FRET measurements

A.

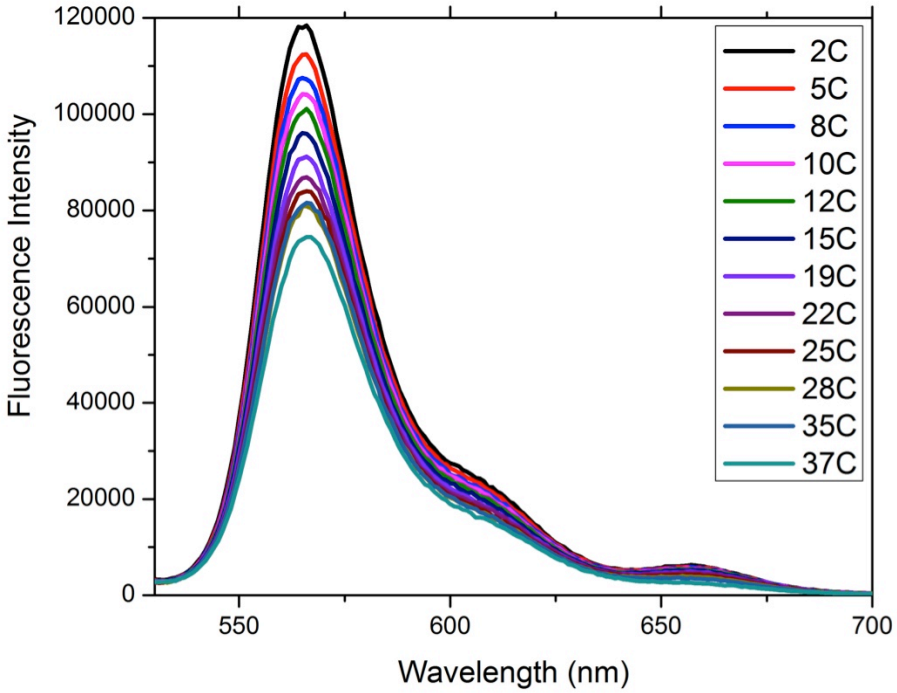

B.

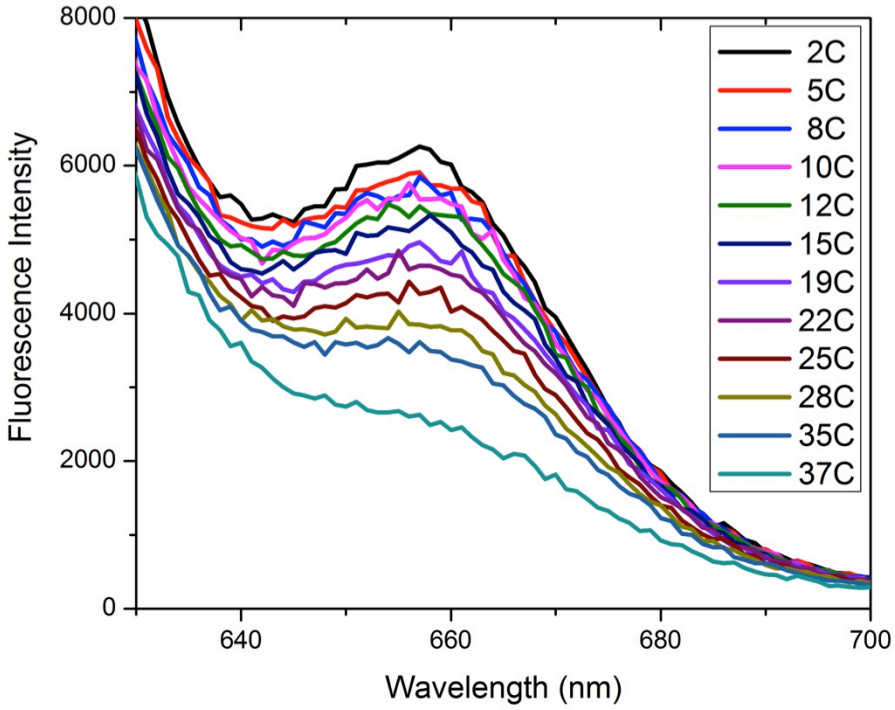

C.

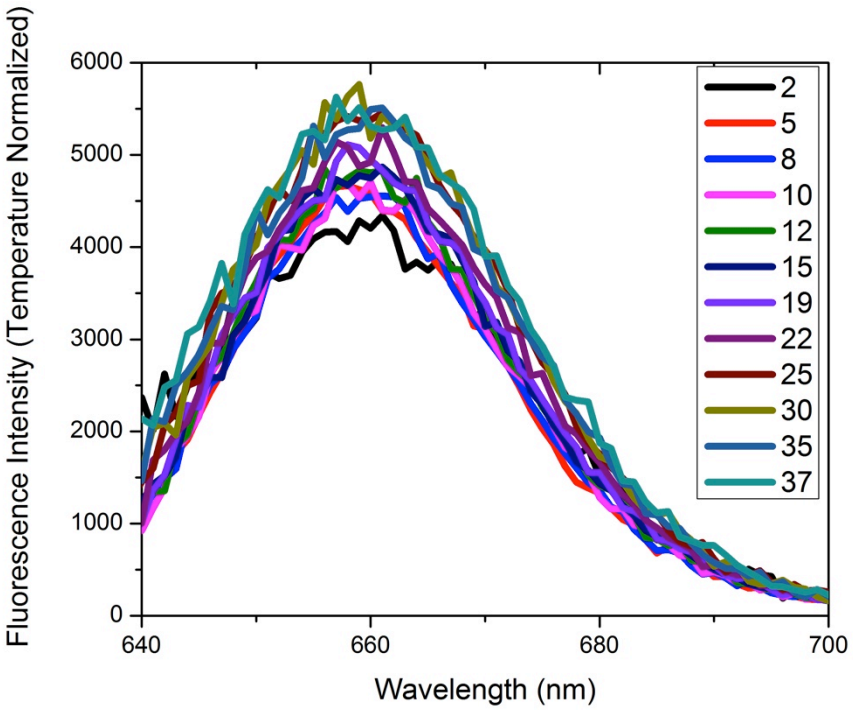
Fluorescence Intensity (Temperature Normalized)
Wavelength (nm)
2
5
8
10
12
15
19
22
25
30
35
37

D.

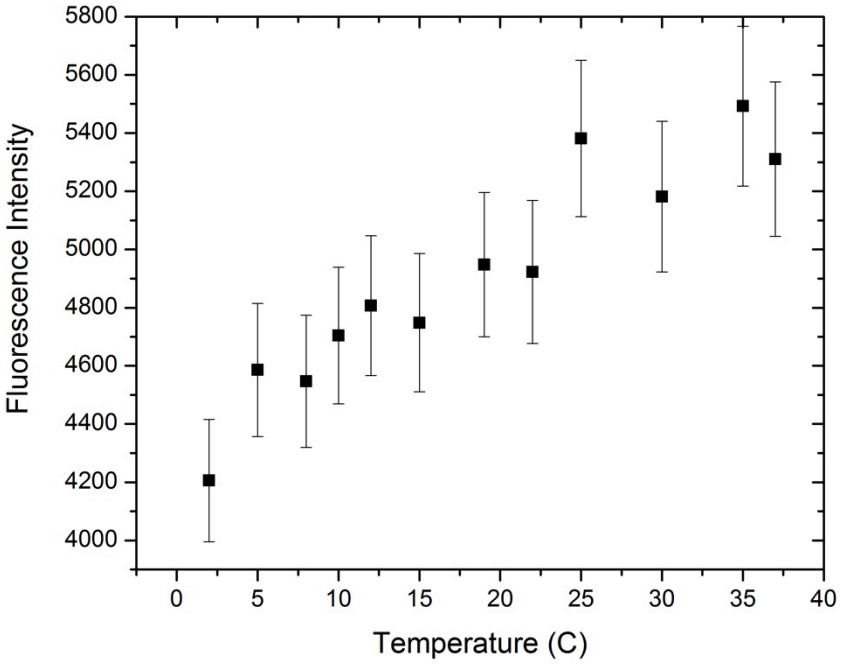
Fluorescence Intensity
Temperature (C)

Figure 6.
A. 100nM Cy3 (-100), Cy5 (+14) promoter DNA + 80nM RNAP 19°C

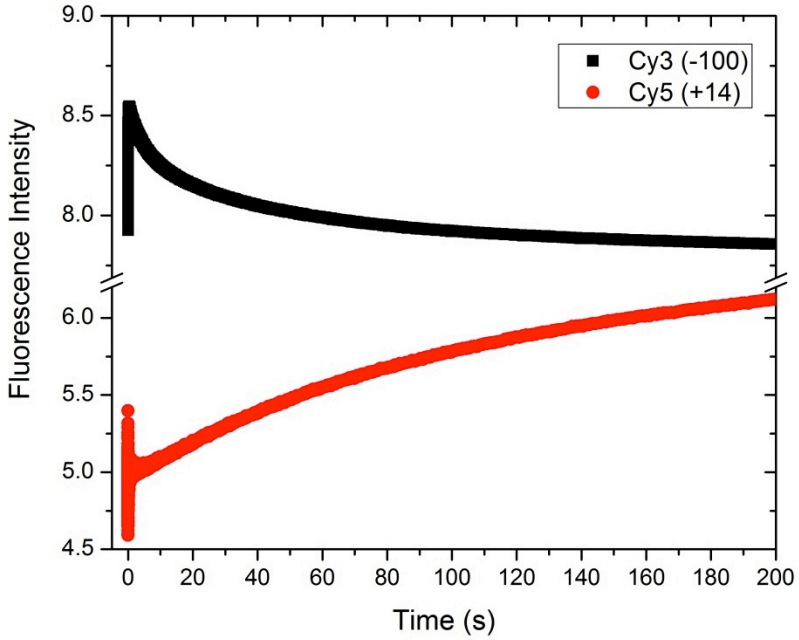

B.

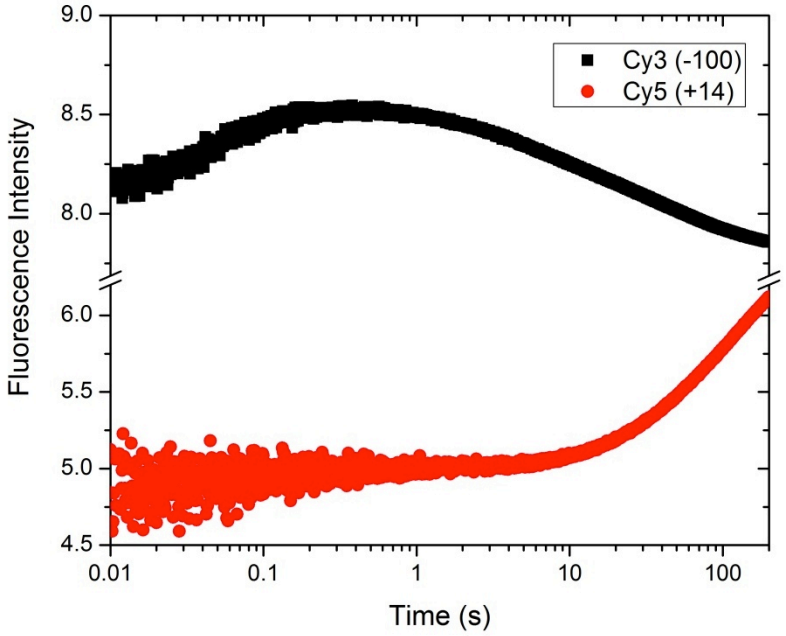

C. Control 100nM Cy3 (-100) promoter DNA + 100nM RNAP Ex: 515

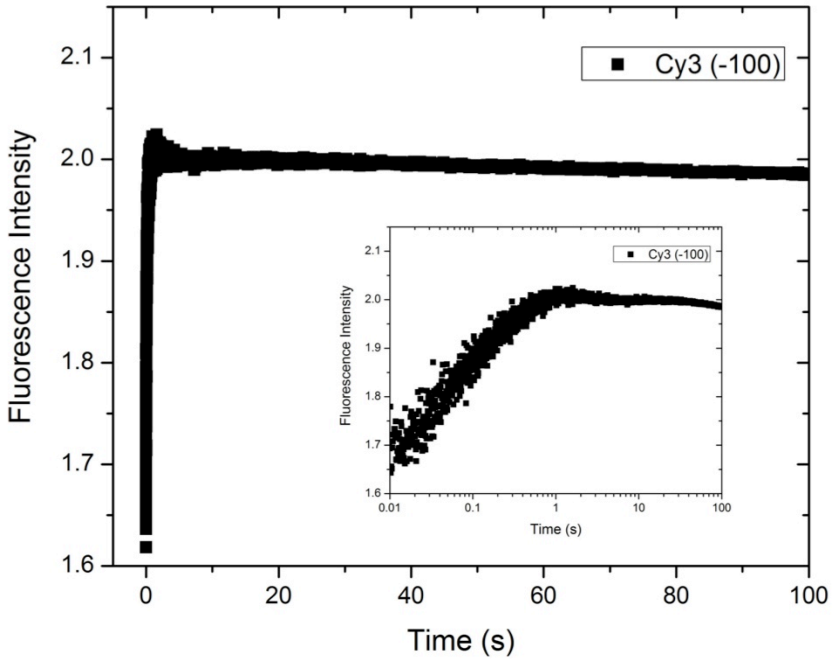

D. Control 100nM Cy5 (+14) promoter DNA + 100nM RNAP Ex: 615

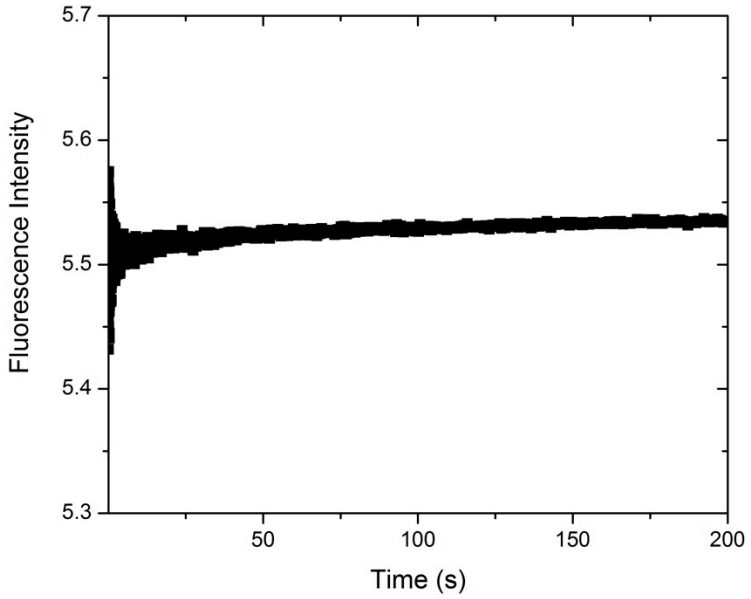

Figure 7. 100nM Cy3 (+14), Cy5 (-100) promoter DNA + 80nM RNAP 19°C
A.

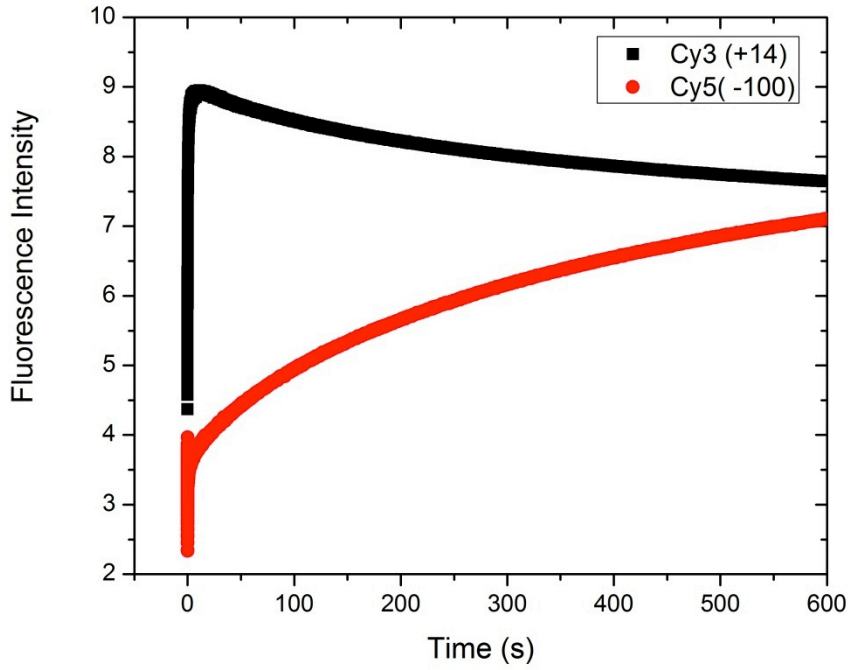

B.

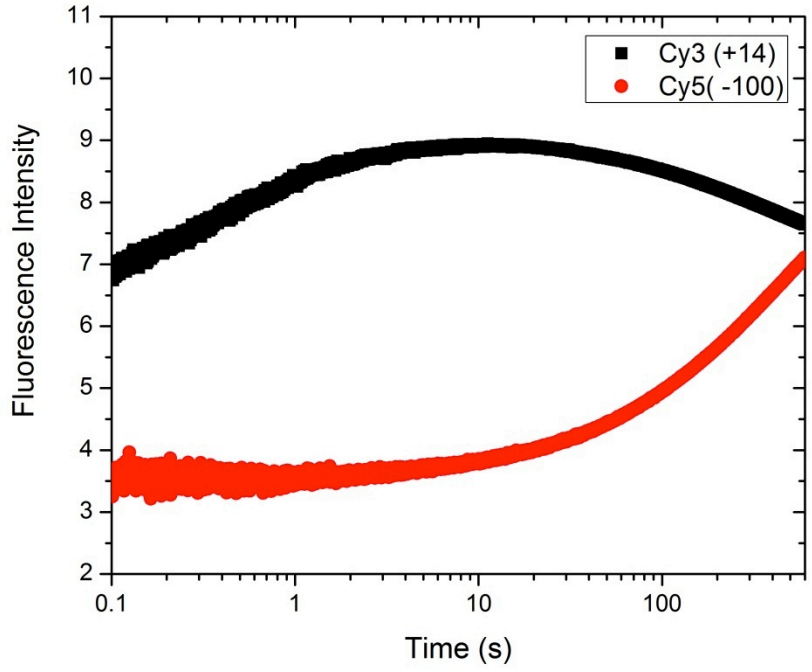

C. Control 100nM Cy3 (+14) promoter DNA + 100nM RNAP Ex: 515

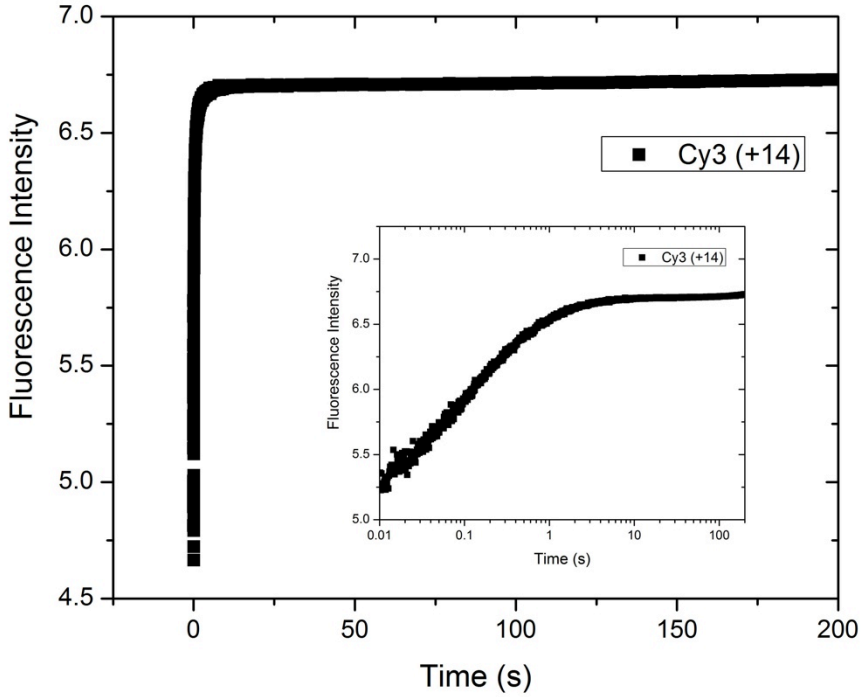

D. Control 100nM Cy5 (-100) promoter DNA + 100nM RNAP; Ex: 615

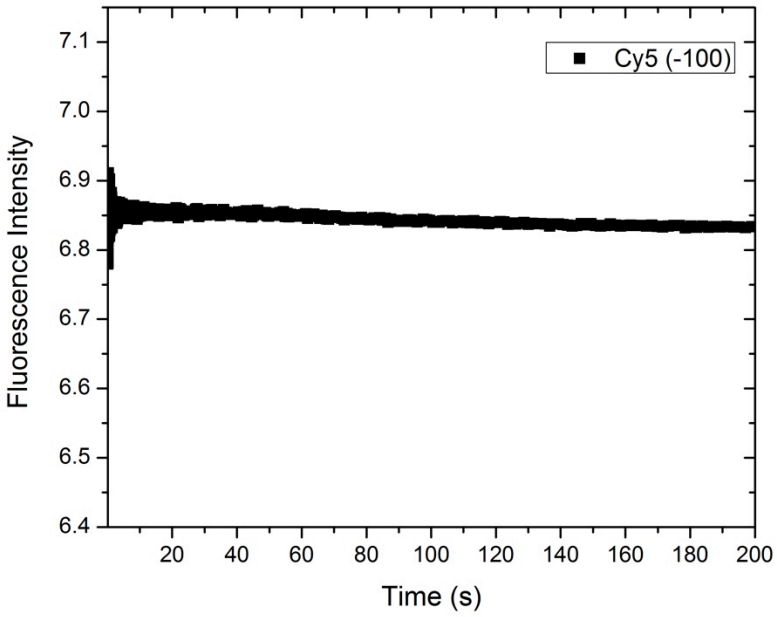

Figure 8. A. Equilibrium FRET for 100nM Cy3 (+14), Cy5 (-100) P_RP_{RM} promoter DNA + 100nM RNAP 2°C

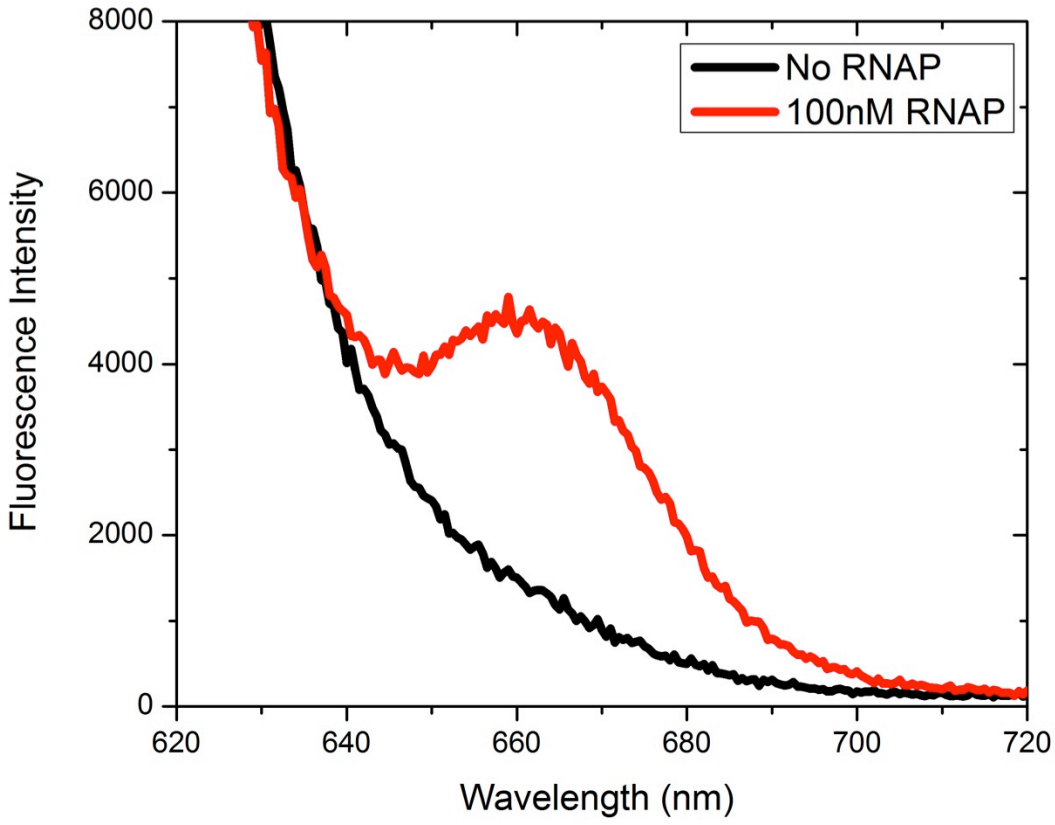

B. 100nM Cy3 (+14), Cy5 (-100) P_RP_{RM} promoter DNA + 80nM RNAP 19°C

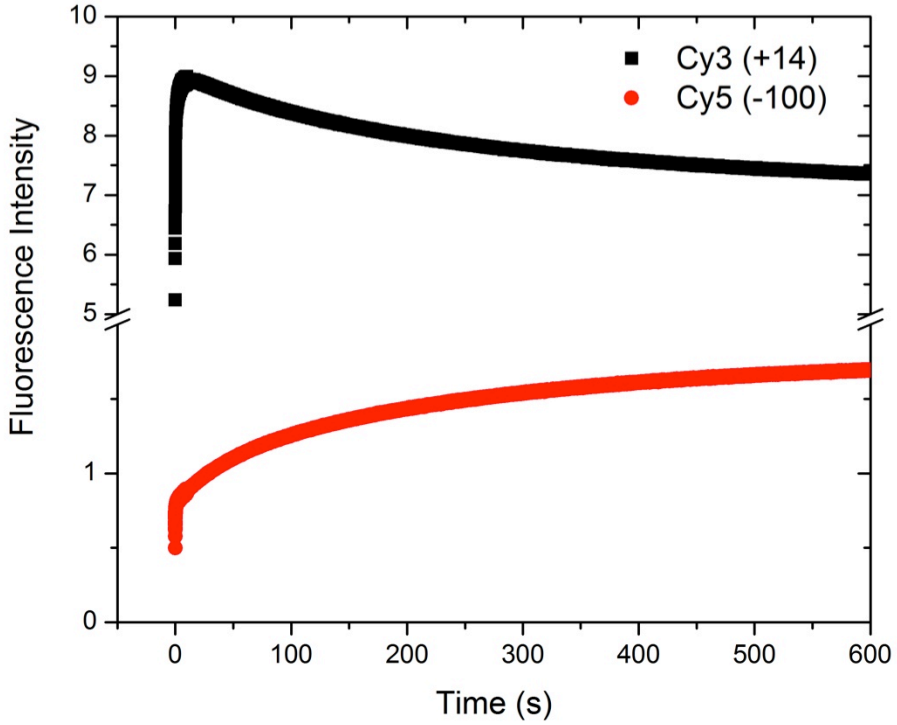

C. 100nM Cy3 (+14), Cy5 (-100) P_RP_{RM} promoter DNA + 80nM RNAP 19°C (log time scale)

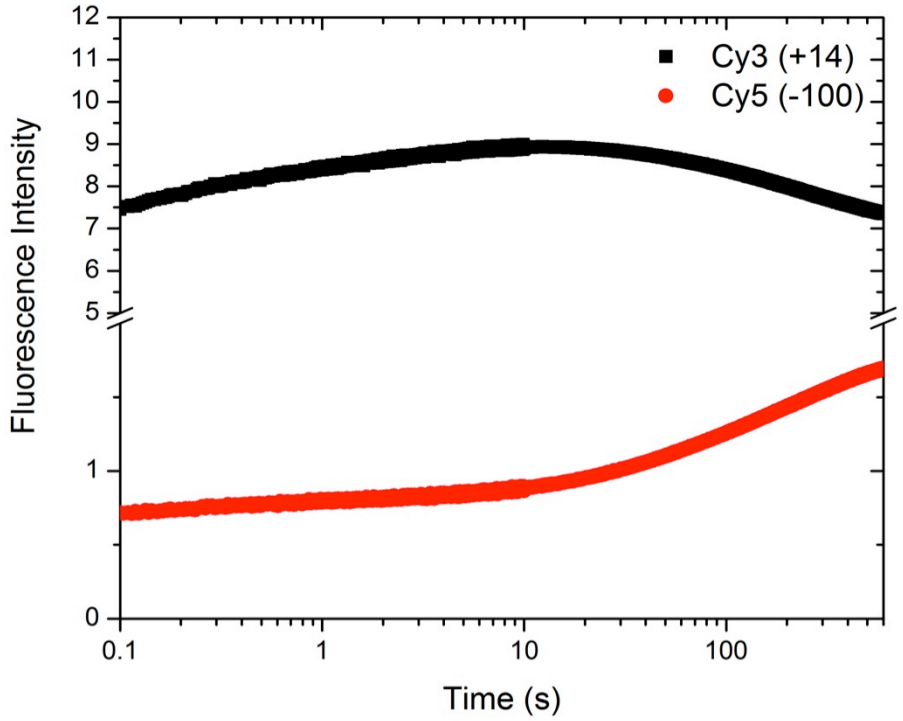

Figure 9. 100nM Cy3 (+14), Cy5 (-100) P_RP_{RM} promoter DNA + 80nM RNAP 19°C
k_{obs}= 40 s^{-1}

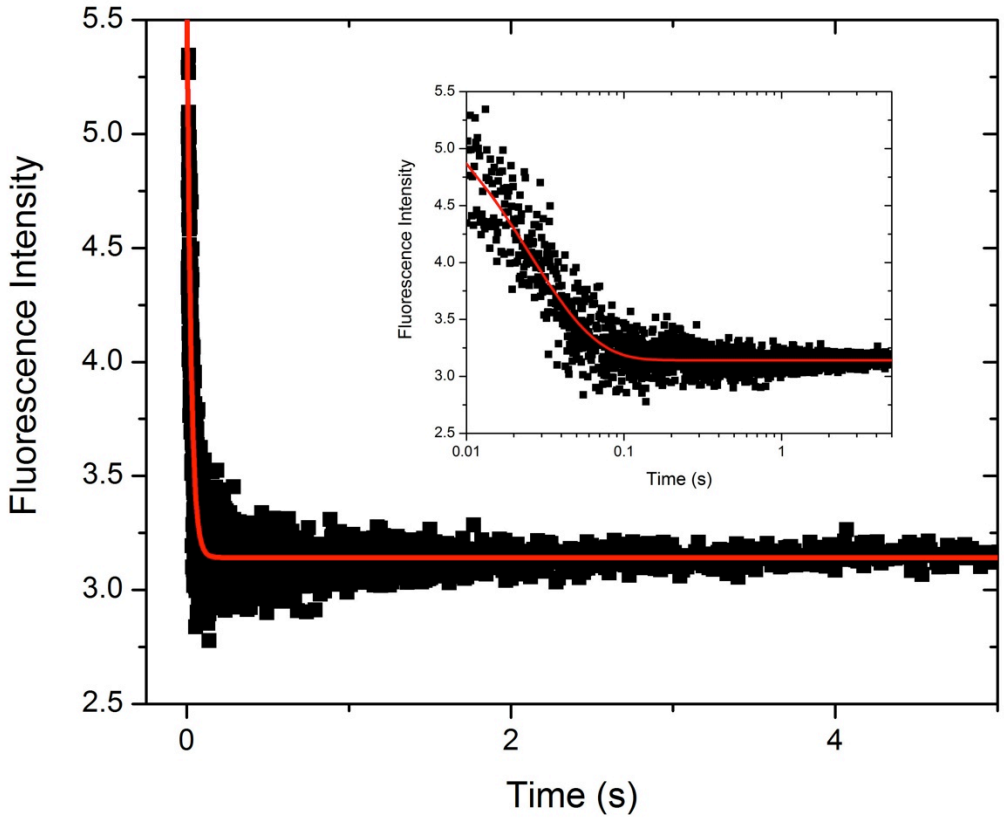

Chapter 4

Real-time DNA Base Flipping and Opening of the -10 Region of Promoter DNA Monitored by Intrinsic and "Beacon" Fluorescence of the Sigma70 Subunit of *E. coli* RNA Polymerase

Preface: This chapter is a draft of a first-author manuscript, currently in preparation. My contributions include: primary design and execution of experiments, preparation of experimental materials, data fitting and interpretation, preparation of figures and manuscript writing. I thank Emily Lingeman and Kristin Zorn for their significant experimental contributions, Ran Furman for experimental materials, and Emily Guinn for surface area calculations. I also thank Prof. Robert Landick for providing me with the use of the stopped flow spectrofluorimeter, Prof. Oleg Tsodikov for discussions, surface area calculations and data analysis, and Prof. Irina Artsimovitch for experimental materials, discussions, figures and assistance with the manuscript.

Abstract:

We report stopped-flow kinetic assays that monitor changes in fluorescence of the σ^{70} subunit of *E. coli* RNA polymerase (RNAP) in the steps of formation and dissociation of open complexes at the λP_R promoter. In these assays, we used both intrinsic (σ^{70} W433) and "beacon" (tetramethylrhodamine (TMR) adduct at σ^{70} residue 211) probes. In association experiments at 19°C, the kinetics of quenching of intrinsic fluorescence and the increase in beacon fluorescence are well fit by two exponentials of comparable amplitudes. For both probes, rate constants for the faster phase increase from approximately 0.15 s^{-1} to 0.3 - 0.4 s^{-1} with increasing [DNA]; rate constants for the slower phase are independent of [DNA] and in the range 0.01 – 0.03 s^{-1}. The first phase is much slower than in FRET experiments (10 s^{-1} at higher reactant concentrations; Ch 3) and even slower than the rate of formation of the initial downstream-extended closed complex estimated from fast •HO footprinting (>20 s^{-1}; Ch 2). The second phase is similar in rate to that observed by FRET (Ch 3) and to the "isomerization" rate (including DNA opening) determined from analysis of filter binding and $KMnO_4$ assays at 19°C. From these comparisons, we propose that the two exponential phases in intrinsic and TMR fluorescence represent 1) formation of an equilibrium distribution of the most advanced closed intermediate complex ($I_{1,F}$) in which base flipping at -11 A has occurred and earlier bent and wrapped but not flipped forms of I_1, and 2) slower opening of the upstream and downstream regions of the initiation bubble, converting the equilibrium mixture of I_1 to I_2.

Comparison of these kinetics with •HO and FRET kinetics reveals that bending of the downstream duplex toward the cleft to give a closed complex with an extended-

downstream HO footprint ($I_{1,B}$) occurs first, followed by upstream wrapping (forming $I_{1,W}$, detected by FRET) and then base flipping at -11 to form $I_{1,F}$ and nucleate subsequent large-scale opening step. RNAP σ^{70} variant W433A, which opens the closed complex at a much slower rate than WT RNAP, shows no detectable intrinsic fluorescence change in complex formation, providing evidence that W433 is the key residue required for base flipping and that quenching of W433 by the flipped base is the primary origin of the fluorescence changes. In the dissociation direction, salt upshift burst experiments demonstrate that there is no change in intrinsic or beacon fluorescence in conversion of the initial open complex (I_2) to the late open complex (RP_o).

Introduction

Promoter DNA bending, base flipping and opening in the -10 region are crucial steps for formation of transcriptionally-active RNAP open complexes. The *E. coli* RNAP core enzyme ($\alpha_2\beta\beta'\omega$ complex) recognizes promoter DNA by binding a specificity σ subunit, most commonly, the "housekeeping" σ^{70}. σ^{70} recognizes specific promoter elements centered at positions -10 (TATAAT consensus sequence) and -35 (TTGACA consensus) upstream of the transcription start site. Recognition and binding of the -10 promoter DNA element is mediated by a highly conserved region 2 of σ^{70} (σ_2). (Lonetto *et al.* 1992, Gribskov and Burgess 1986). σ_2 is involved in recognition of the -10 promoter DNA element ($\sigma_{2.4}$), nucleation of strand separation ($\sigma_{2.3}$), and formation of the open complex (Tomsic *et al.* 2001). Several basic residues in $\sigma_{2.3}$ are involved in promoter DNA binding and melting (De Haseth and Tsujikawa, 2003). Four aromatic residues (Y425, Y430, W433, and W434) protrude on approximately the same face of RNAP, where they can interact with promoter DNA (Malhotra *et al*, 1996, Murakami *et al.* 2002). Alanine substitutions of these amino acids render RNAP holoenzyme partially defective for DNA opening and transcription initiation below 20°C, where DNA opening is less favored. These results suggest that key amino acids in $\sigma_{2.3}$ mediate DNA opening. A recent structure of the *Thermus aquaticus* housekeeping σ^A containing regions 2 and 3 bound to ssDNA containing a partial -10 element shows that the nontemplate strand is bent -90° at the -11 and -10 bases and lays across a highly positively charged binding track on σ_2 (Feklistov and Darst, 2011). This structure reveals that, after DNA opening, $\sigma_{2.3}$ interacts directly with the nontemplate DNA strand; Y430 stacks on the -11A base, while W433 interacts with the backbones of the single

stranded -11A and the double stranded 12T. -11A and -7T are both flipped out of the DNA stack and are buried in RNAP hydrophobic pockets. This work provides key structural insights into the role of $\sigma_{2.3}$ in the isomerization steps of open complex formation

Extensive kinetic mechanistic investigations have yielded detailed information about the pathway for transcription initiation. Previously, the kinetic mechanism for *E. coli* RNAP and the λP_R promoter was known to include a minimum of four steps with three kinetically significant intermediates (Saecker *et al.* 2011 and refs therein):

$$R + P \underset{\text{rapid equilibria}}{\overset{K_1}{\rightleftharpoons}} I_1 \underset{\text{slow}}{\overset{k_2}{\underset{k_{-2}}{\rightleftharpoons}}} I_2 \overset{\text{rapid equilibria}}{\underset{K_{-3}}{\rightleftharpoons}} I_3 + RP_o$$

(Mechanism 1)

In Mechanism 1, RNAP binds to promoter DNA to form the initial complex I_1, which is in rapid equilibrium with free reactants on the time scale of the following rate-determining step converting I_1 to I_2. I_1 is found to be a closed complex in which downstream duplex promoter DNA, from the -10 region to +20, is bent toward and periodically protected on one face from cleavage by footprinting reagents by the RNAP active site cleft (Davis *et al.* 2007; Ch. 2).

During the conversion of I_1 to I_2, the downstream duplex DNA is opened in the active site cleft. This rate-determining step is highly temperature dependent (Saecker *et al.* 2002; Kontur *et al.* 2008; Kontur *et al.* 2010), although relatively insensitive to high concentrations of salt or solutes. In I_2, the template strand +1 thymine appears by MnO_4^-

footprinting to be in the RNAP active site. I_2 is unstable relative to I_1 and/ or I_3 at all temperatures and, above 10°C, rapidly and irreversibly converts to open complexes (Kontur *et al.* 2008). During this conversion, the nontemplate strand moves into its final position (Gries *et al.* 2010), and the downstream β' jaw/ clamp of RNAP is proposed to assemble on the downstream DNA (Kontur *et al.* 2008; Drennan *et al.* unpublished). The species designated RP_o represents the most stable form of the open complex at 37°C. Between 10°C and 19°C, evidence exists that the final population of open complexes may be a mixture of I_3 and RP_o; at lower temperatures (7 to 10°C), a mixture of I_1, I_3 and RP_o complexes coexists with free promoter and RNAP at equilibrium (Drennan *et al.* unpublished; Saecker *et al.* 2002; Kristi McQuade, PhD Thesis, 1996).

Both RNAP and promoter DNA must undergo a series of conformational changes in order to open the DNA and properly load the +1 transcription start site of the DNA into the RNAP active site cleft. The kinetic framework detailed above provides testable hypothesis regarding the roles of RNAP and DNA structural elements and the timing of key events during open complex formation. Previously, we proposed a "bind, bend, melt" mechanism for *E. coli* RNAP on λP_R (Saecker *et al.* 2011). How do interactions of $\sigma_{2.3}$ with the -10 promoter DNA elements regulate this process? What is the timing of bending of duplex DNA, base flipping of the -11 and -7 nontemplate strand bases and opening of the transcription bubble? How do the aromatic amino acids in $\sigma_{2.3}$ contribute to the process of binding, bending and opening of the DNA? The timing and mechanism of these events has remained ambiguous, due to the lack of real-time methods for monitoring specific regions of the RNAP and DNA. However, development of new fluorescent and chemical probes and the ability to monitor highly transient processes via

rapid quench flow or stopped-flow mixing has allowed for new investigations into these fundamental questions.

2-aminopurine (2-AP) is a fluorescent adenosine base mimic that is sensitive to changes in the base stacking/base pairing of duplex DNA. 2-AP substitutions in the upstream transcription bubble region (positions -11, -8, -4) were used to monitor conformational changes in a 65 bp (-45 to + 20) consensus promoter DNA during association with RNAP (Schroeder *et al.* 2011). Rate constants determined by 2-AP fluorescence (whether the 2-AP substitution is at −4, −8 or −11) were at least seven-fold greater than those detected by electrophoretic mobility shift assays (EMSA) for heparin-resistant complex formation, regardless of whether fit to single or double exponentials. The authors concluded that the 2-AP fluorescence assay detected a DNA conformational change that preceded formation of the EMSA-detected stable open complexes. Since 2-AP fluorescence emission reports on changes in the local environment of DNA bases, including the unstacking and melting of duplex DNA, the authors hypothesized that the observed changes reflect movements of the duplex DNA (bending and/or base flipping) prior to formation of the fully open transcription bubble.

Recently, an assay was developed that detects the interaction of $\sigma_{2.3}$ with promoter DNA, known as the RNAP “beacon” method (Mekler *et al.* 2011a). This assay takes advantage of the conserved aromatic amino acids in $\sigma_{2.3}$ that change their environment upon interaction with DNA. The RNAP beacon assay detects changes in the fluorescence emission of a tetramethylrhodamine (TMR) probe attached to a cysteine residue inserted at position 211 of the σ subunit (C-211). This residue is close in space to the highly conserved Trp and Tyr residues (W433, W434, Y425, Y430) of

$\sigma_{2.3}$. In free RNAP, TMR is thought to interact with these aromatic amino acids resulting in quenching of its fluorescence. Interactions of the -10 region of the nontemplate strand with $\sigma_{2.3}$ relieve this TMR quenching, causing a large increase in fluorescence intensity (Figure 1). This assay has been used to monitor RNAP interactions with both upstream and downstream fork junction promoter fragments and to investigate the role of Gp2 in regulating interactions of the *E. coli* RNAP β' jaw with downstream promoter DNA (Mekler *et al.* 2011a, Mekler *et al.* 2011b, Mekler *et al.* 2011c).

Changes in intrinsic fluorescence can also be used to monitor the interactions of RNAP with promoter DNA. Free RNAP in solution exhibits absorption and emission maxima at 280 and 340 nm, respectively, characteristic of the behavior of tryptophan amino acid side chains. However, tyrosine also absorbs well within this region and exhibits an emission maximum at 310 nm. Tyrosine emission can often be masked by that of tryptophan due to the much higher quantum yield (and therefore stronger fluorescence emission) of tryptophan residues (Lakowicz, 1983). Upon binding of promoter DNA, fluorescence emission of RNAP at 340 nm is dramatically reduced, due to a quenching interaction of the DNA with tryptophan(s) and/or tyrosine(s) in or near the DNA binding track. The obvious advantage to using intrinsic protein fluorescence is that it directly monitors RNAP conformational changes without introducing any extrinsic factors.

Johnson and Chester (1998) used intrinsic RNAP fluorescence to investigate the kinetics of association of *E. coli* RNAP with the T7A1 promoter. They found that association assays above 20°C exhibited biphasic kinetics that were best fit to the sum of two exponentials (referred to here as k_{fast} and k_{slow}). Below 20°C, the association

kinetics were best fit to a single exponential. At all temperatures, k_{fast} was promoter DNA-concentration dependent and, when detected, k_{slow} was promoter [DNA] independent. The authors concluded that these results are best explained by a two-step association mechanism in which RNAP and promoter DNA are in rapid equilibrium (k_{fast}) with the first closed intermediate and then slowly isomerize to form open complexes (k_{slow}). Below 20°C, the T7A1 promoter does not form open complexes, and therefore only k_{fast} is monitored. In this study, the authors had limited information about which specific tryptophans (and possibly tyrosines) were being detected by the intrinsic fluorescence assay and concluded that the assay monitored global effects arising from many tryptophan residues on RNAP. However, recent structural models of RNAP-DNA complexes provide a framework for a more detailed analysis of these questions (see Results).

Here, we monitor λP_R association kinetics in real-time by using both the beacon RNAP and intrinsic fluorescence assays. If both assays report on specific interactions within the same regions of σ and the promoter DNA -10 elements, we hypothesized that they would yield similar results (including observed rate constants and relative fluorescence amplitudes) for the kinetic pathway of transcription initiation. By performing experiments under identical conditions we are able to determine whether each method monitors the same or different processes within RNAP and to use the kinetic information to learn about the role of $\sigma_{2.3}$ and its interactions with DNA during early transient kinetic intermediates. Knowledge of structural differences between these early intermediates and the mechanism by which RNAP specifically recognizes the -10 element to bind,

bend, and open the DNA are essential for understanding the regulation of cellular activities of the RNAP molecular machine.

The previous chapters have provided evidence for two different conformational states of I_1. In the first, designated $I_{1,B}$ and detected by fast •HO footprinting, the promoter DNA is bent at the upstream end of the -10 region to direct the downstream duplex toward the cleft. In the second, designated $I_{1,W}$ and detected by fast FRET kinetics, the DNA upstream of -35 is bent and wrapped around the back of RNAP. In this chapter, we provide evidence for a third key conformational state of I_1, called $I_{1,F}$, which forms quite slowly from $I_{1,W}$. In $I_{1,F}$ the -11A base has flipped out to interact with and quench the fluorescence of W433. For the TMR adduct, we deduce that this base-flipping step causes the TMR fluorescence to increase.

Results and Analysis

Changes in Intrinsic and Beacon (Tetramethyl Rhodamine Adduct) RNAP Fluorescence on the Time Course of Open Complex Formation

In association of RNAP with the λP_R promoter, at high RNAP concentrations the first kinetically-significant intermediate I_1 forms in less than 100 ms at 19°C in transcription buffer and exists as the major species for ~15 seconds before a significant population of open complexes appear (Chapter 2). Therefore, it was essential that our assays monitor processes at least as fast at 10 s^{-1}, which is much faster than can be achieved by conventional bench top mixing. For this application, stopped-flow fluorescence is advantageous because it can monitor very fast processes and is excellent for separating rates of sequential processes that differ by at least one order of magnitude. Our instrument has a mixing dead time of less than 10 ms and can collect thousands of time points per second.

Figure 1 depicts a model of the "beacon" fluorescence assay. For the assay, we used a σ^{70} derivative in which a unique Cys residue introduced at amino acid position 211 was labeled with tetramethylrhodamine-5-maleimide (211TMR). In the absence of promoter DNA, $\sigma_{2.3}$ residues W433, W434 and Y430 quench the TMR fluorophore (Mekler *et al.* 2011a). However, during interaction of promoter DNA with $\sigma_{2.3}$, this quenching is relieved, causing a large increase in TMR fluorescence emission. Therefore, in our real-time assay, TMR provides a signal for the specific interactions of these aromatic residues of $\sigma_{2.3}$ with promoter DNA. Disruption of the interaction of TMR adduct with $\sigma_{2.3}$ residues W433, W434 and Y430 in base flipping may perturb the rate and equilibrium constants of this step.

The intrinsic fluorescence assay monitors tryptophan quenching in the steps of forming open promoter complexes. ASA calculations using a model of *E. coli* RNAP RP_o (PDB 3IYD) predict that only two of the nineteen tryptophan residues undergo large decreases in solvent accessibility upon RNAP binding to the promoter DNA: σ W433 (89 $Å^2$ buried) and β W183 (63 $Å^2$ buried). (This calculation assumes no conformational changes involving these W residues in open complex formation; see Methods). Also, calculations using a thermophilic holoenzyme (PDB 2A6E) to model the free RNAP, instead of obtaining it by removing the promoter DNA from the RP_o model, predict similarly large reductions in ASA for these two tryptophans in RP_o formation. W433 is located in the $\sigma_{2.3}$ aromatic cluster that interacts with the upstream end of the nontemplate strand in the open complex (Feklistov and Darst, 2011); this cluster is thought to initiate opening by serving as the binding pocket for the -11A when it is flipped out of the duplex (ref). β W183 is located near position -2 of the open nontemplate strand in the model of the E. coli open complex (PDB 3YID) and in the TEC (Opalka *et al.* 2010). Hence quenching of intrinsic tryptophan fluorescence is predicted from the ΔASA analysis to result from -11A base flipping (quenching W433) and subsequent opening of the initiation bubble (quenching β W183, and possibly quenching W433 further). An increase in TMR fluorescence is predicted to occur in the -11 A base flipping step, and possibly in subsequent opening of the initiation bubble.

RNAP holoenzyme (containing either wild-type σ^{70} or σ^{70}–211TMR) was rapidly mixed with λP_R at 19°C in transcription buffer using the Kintek SFX-300 stopped flow (see Methods), and the kinetics of the change in intrinsic or TMR fluorescence was monitored as a function of time. The kinetics of association were determined at a fixed

RNAP concentration of 20 nM (active) and a range of DNA concentrations from 20 to 300 nM. For intrinsic RNAP fluorescence experiments, the samples were excited at 280 or 295 nm and emission was monitored above 320 nm using a long-pass filter. (A representative kinetics experiment is shown in Figure 2A, plotted on both linear and log time scales.) For beacon RNAP (σ^{70}–211TMR) experiments, the samples were excited at 550 and emission monitored above 565 nm using a long-pass filter. A representative kinetic curve is shown in Figure 2B. The association of promoter DNA with RNAP decreases the intrinsic fluorescence of RNAP and increases the fluorescence of the TMR beacon probe. Thus, the amplitudes of beacon and intrinsic fluorescence kinetics are of opposite sign.

For one loading of reagents, three to five repeat shots are taken for each set of samples. Fitting to the individual kinetic traces is done using Origin 8 software using the equation for the sum of two exponentials:

$$F = F_o + A_{fast}\{1 - \exp(-k_{fast}\, t)\} + A_{slow}\{1 - \exp(-k_{slow}\, t)\} \qquad \text{(Equation 1)}$$

where F_o is the initial fluorescence. One-exponential fits were insufficient and three exponential fits were not significantly different from two-exponential fits at 19°C. Global fits of 3-5 replicate shots from each of at least three independent experiments on different days are averaged to determine the exponential decay rates (k_{fast} and k_{slow}) and amplitudes at each DNA concentration (see Supplementary Tables 1 and 2 for values of k_{fast} and k_{slow} and amplitudes A_{fast} and A_{slow}). For both assays, amplitudes of fast and slow kinetic phases are of comparable magnitude.

Analysis of Rate Constants k_{fast} and k_{slow} From the Two- Exponential Fits

Values of k_{fast} and k_{slow} from both intrinsic and TMR fluorescence assays are plotted as a function of [DNA] in Figure 3. For both assays, k_{fast} increases with increasing DNA concentration from approximately 0.15 s^{-1} at low DNA concentration to 0.4 s^{-1} at high DNA concentration. Compared at the same high DNA concentration, values of k_{fast} from the intrinsic assay are somewhat larger than from the TMR assay. Values of k_{slow} from both assays, while quite scattered, exhibit no systematic dependence on DNA concentration and average to 0.011 s^{-1} for the intrinsic fluorescence assay and 0.023 s^{-1} for the TMR fluorescence assay. Values of k_{slow} for the TMR- variant are systematically larger than those determined for the WT RNAP from the intrinsic fluorescence assay.

Values of k_{fast} from both assays are much slower than in FRET experiments (10 s^{-1} at higher reactant concentrations; Ch. 3) and even slower than the rate of I_1 formation estimated from fast •HO footprinting (>20 s^{-1}; Ch. 2). Values of k_{slow} are similar to those observed by FRET (Ch. 3) and to the isomerization (including DNA opening) rate constant determined by filter binding and $KMnO_4$- assays at 19°C; k_{slow} clearly represents an isomerization step to form open complexes here also. To interpret k_{slow}, it is necessary to understand k_{fast}.

What step(s) in the mechanism of open complex formation does k_{fast} represent? How is this decay rate constant best interpreted? Previous kinetic studies (Saecker *et al.* 2002; Gries *et al.* 2010; Ch. 2) found that the closed intermediate I_1 is in rapid equilibrium with reactants on the time scale of the rate-determining isomerization step that converts it to the initial open complex I_2. Therefore we propose to analyze k_{fast} as a decay-to-

equilibrium rate constant for the formation of a fluorescence-detected form of I_1 from free RNAP and promoter DNA:

$$R + P \rightleftarrows I_{1,F} \qquad \text{(Mechanism 2)}$$

where $I_{1,F}$, the form of I_1 detected in these assays, differs in intrinsic and beacon fluorescence from free RNAP. Since large-scale opening has not yet occurred in $I_{1,F}$, we propose that these differences in fluorescence of $I_{1,F}$ from free RNAP result from the flipping of -11A out of the bent duplex to interact with W433 in a pocket on $\sigma_{2.3}$; this quenches W433 fluorescence and, in the TMR variant RNAP, displaces TMR from this pocket to cause its fluorescence to increase. (Though $I_{1,F}$ is technically open at -11, -11T is not permanganate reactive in $I_{1,F}$ and by this operational definition $I_{1,F}$ is a "closed" complex.)

For the decay-to-equilibrium in Mechanism 2:

$$k_{fast} = k_1 ([DNA]_{eq} + [RNAP]_{eq}) + k_{-1} \approx k_1 [DNA]_{total} + k_{-1} \qquad \text{(Equation 3)}$$

The approximation that the sum of the equilibrium concentrations of reactants is approximately equal to the total DNA concentration ($[DNA]_{eq} + [RNAP]_{eq} \approx [DNA]_{total}$) is adequate since the DNA is in at least 2.5 fold excess over RNAP and the experimental error is as large as the error introduced by this approximation. Mechanism 3 and therefore Equation 3 are oversimplified because, as we discuss below, the fast •HO footprinting (Ch. 2) and FRET (Ch. 3) assays detect earlier forms of I_1 which appear to

be significantly populated and in equilibrium with both reactants and with $I_{1,F}$ in the time range from 0.1 s to 15 s.

Values of the forward rate constant k_1 and the back rate constant k_{-1}, obtained from the slopes and intercepts of the best-fit lines in Figure 3 are listed in Table 1. From the intrinsic fluorescence data, $k_1 = (1.5 \pm 0.6) \times 10^6$ M^{-1} s^{-1} and $k_{-1} = 0.11 \pm 0.04$ s^{-1} giving an estimate of the overall equilibrium constant $K_{1,F}$ for forming $I_{1,F}$ of approximately $(1.4 \pm 0.8) \times 10^7$ M^{-1}. From the TMR assay, $k_1 = (6.8 \pm 1.2) \times 10^5$ M^{-1} s^{-1} and $k_{-1} = 0.17 \pm 0.05$ s^{-1}, giving an estimate of the overall equilibrium constant $K_{1,F}$ for forming $I_{1,F}$ by this RNAP variant of approximately $4.0 \pm 1.6 \times 10^6$ M^{-1}. As noted above in a comparison of values of the first exponential k_{fast}, these second order rate constants for formation of $I_{1,F}$ (intrinsic $k_1 = (1.5 \pm 0.6) \times 10^6$ M^{-1} s^{-1}) are more than two orders of magnitude smaller than those estimated for forming the HO detected $I_{1,B}$ ($k_1 > 2 \times 10^8$ M^{-1} s^{-1}; Ch. 2) and the FRET detected $I_{1,W}$ ($k_1 \approx 6 \times 10^7$ M^{-1} s^{-1}; Ch. 3). This hierarchy of values of k_{fast} and k_1 is readily explained if these three forms of I_1 form sequentially and reversibly, so all are in equilibrium with one another and with free promoter on the time scale of the rate-determining DNA-opening step (see Ch. 5).

TMR-labeled RNAP binds less strongly than WT RNAP to fork junction promoter DNA probes (Mekler *et al.* 2011b). Our analysis of k_{fast} for TMR- adduct and WT RNAP is consistent with this finding; the presence of the TMR probe reduces the composite second order rate constant for forming $I_{1,F}$, increases the back rate constant and therefore reduces the equilibrium constant for formation of this intermediate from reactants, relative to WT RNAP.

If base flipping is the origin of the fluorescence signal for the fast kinetic phase, what is the origin of the fluorescence signal for the slow phase, and how should values of k_{slow} be interpreted. Since values of k_{slow} (0.025 ± 0.006 s^{-1} for the TMR adduct the TMR adduct and 0.011 ± 0.002 s^{-1} for WT RNAP) are comparable to one another and to rate constants of conversion of the equilibrium mixture of I_1 species to I_2 determined previously by analysis of filter binding and real-time permanganate footprinting data (Ch. 2), it appears likely that k_{slow} characterizes this process as well, and that the fluorescence change in the slow phase is largely from the same base flipping event as in the fast phase, occurring as the equilibrium mixture of I_1 species, much of which is in an unflipped state, converts by base flipping and subsequent opening to form I_2. This interpretation would indicate that k_{slow} detected by TMR should be smaller than that detected by intrinsic fluorescence, but the opposite is the case. This could mean that TMR selectively stabilizes the transition state for opening. Also, the interaction of β residue W183 with the downstream (-2) region of the nontemplate strand of the initiation bubble may contribute to the fluorescence quenching observed in the slow exponential phase for the WT RNAP.

Studies of the Role of W433 in Intrinsic RNAP Fluorescence

While ~80% of Trp residues on unbound *E. coli* RNAP are water- accessible as judged by acrylamide quenching (Sen and Dasgupta, 1994), only two are predicted to show a large reduction in water accessible surface area (ASA) in open complex formation, $\sigma_{2.3}$ W433 and β W183. As discussed above, W433 is likely to be quenched in the base-flipping step and W183 may be quenched in opening the downstream duplex.

As one way to examine the contribution of W433 to the observed change in intrinsic RNAP fluorescence in the initial phase of promoter DNA binding, we used the W433A variant studied previously (Panaghie *et al.* 2001, Tomsic *et al.* 2001). By performing promoter DNA binding experiments with RNAP-W433A holoenzyme, we examined (i) whether W433 was responsible for some or all of the change in intrinsic fluorescence (by exiting at 280 nm, where both tyrosine and tryptophan residues will absorb), (ii) whether more than one tryptophan was responsible for the fluorescence change (by exciting at 295 nm and comparing the relative emission intensity of wild type RNAP with that of W433A RNAP), and (iii) whether tyrosine residues were also involved in the fluorescence changes (by monitoring emission at 310 nm, outside of the range of tryptophan emission). We also determined whether W433A could bind and open the λP_R promoter DNA to form stable open complexes using permanganate footprinting at 19°C.

Complexes containing 50 nM RNAP-W433A and promoter DNA (<1 nM) were formed at 19°C for 1.5 hours and then challenged with heparin for 10 s before mixing with 6 mM MnO_4^- for 10 seconds. Addition of heparin removes any non-specific RNAP-promoter DNA complexes. We find that RNAP-W433A can open the promoter DNA transcription bubble and form complexes that are heparin stable; however, the permanganate reactivity of the thymine bases on the template strand is lower than that observed for wild type (Figure 4). From this, we conclude that W433A is not defective for DNA opening under our experimental conditions, although its open complex at 19°C appears “less open” than that formed by WT RNAP. Filter binding kinetic data (J. Murray, in progress) show that W433A exhibits much slower isomerization kinetics that

WT RNAP, but does completely convert promoter DNA to stable (competitor-resistant, presumably open) complexes in 1.5 hours at room temperature.

In stopped-flow fast mixing kinetic experiments, no change in intrinsic RNAP fluorescence was observed upon mixing with a high excess of promoter DNA (see Figure 5A) when we excited the samples at 295 nm. Since 295nm is well outside of the excitation maxima for tyrosine, we should only observe emission from tryptophan residues. Similarly, at an excitation of 280 nm where both tryptophan and tyrosine amino acid side chains can absorb, we observed no change in the fluorescence intensity of RNAP-W433A emission upon addition of DNA (Figure 5B). Although tyrosine has a much lower quantum yield than tryptophan and changes in its emission can therefore often be masked (Lakowicz, 1984), the lack of a change in signal upon DNA binding for the W433A substitution suggests that W433A is primarily responsible for the change in intrinsic RNAP fluorescence in the fast kinetic phase. Photobleaching and the slow kinetics of isomerization of W433A make it difficult to determine if there is a significant intrinsic fluorescence change in the slow phase by W433A RNAP at 19°C; experiments at higher temperature where opening is faster may determine if W183 contributes to the fluorescence quenching in this slow phase of the kinetics.

Real-time Fluorescence Salt Upshift Experiments on Stable Open Complexes Show That The Fluorescence Change Occurs With the Same Rate as DNA Closing

Next, we used high salt upshift “burst” experiments to destabilize the stable open complexes (RP_o and I_3) and to determine whether any additional changes in σ_2 fluorescence occur in converting the initial open complex (I_2) to the more stable open

complexes (RP_o and I_3, See Mechanism I). Previously, our lab demonstrated the power of salt and solute upshifts for creating a "burst" of the late intermediate I_2 in approximately 250 ms by destabilizing the final population of open complexes (Kontur *et al.* 2008, Gries *et al.* 2010). Here, we generated a burst of I_2 by rapidly mixing open complexes with a high concentration of NaCl (1.1 M final concentration) at 10, 22 or 37°C. No change in fluorescence is detected in the 250 ms time interval required to convert the stable open complexes to I_2, indicating that these steps do not affect the interaction of $\sigma_{2.3}$ with the -10 nontemplate strand.

We find that at both 37°C and 22°C, the changes in fluorescence emission due to the slow step of DNA closing for both the beacon (Figure 6A, 6B) and intrinsic RNAP fluorescence (Figure 7A, 7B) assays are best fit by a single exponential, with kinetics that are quantitatively the same as rates previously measured for DNA closing using nitrocellulose filter binding and permanganate footprinting (Refer to Tables 2 and 3). Here, we obtain k_{obs} =1.7 (±0.4) s^{-1} at 22°C and k_{obs} =4.1 (±1.2) s^{-1} at 37°C for the beacon assay and k_{obs} = 3.1 (±0.9) s^{-1} at 22°C and 6.4 (± 1.2) s^{-1} at 37°C for the intrinsic assay.

However for the beacon assay experiments at 10°C, the data was best fit to a sum of two exponentials (Figure 6C). The fast phase, k_{fast} comprising more than three-fourths of the total signal amplitude yielded a k_{fast}= 6.0 (± 0.9) × 10^{-1} s^{-1}, within error of the previously determined rate of DNA closing at this temperature (Kontur *et al.* 2008). The slow phase (k_{slow}), comprising less than 25% of the total signal change, was an order of magnitude slower than that expected for an on-pathway species, with k_{slow}= 4.9 (± 0.7) × 10^{-2} s^{-1}. Thus we conclude that there is a subpopulation of off-pathway beacon

RNAP-promoter DNA complexes at 10°C. For the intrinsic fluorescence assay at 10°C, the fluorescence increase is best fit to a single exponential with k_{obs} =7.1 (±1.4) × 10^{-1} s^{-1} (Figure 7C and Table 3).

Discussion

The most highly conserved region of all promoter DNA sequences is the -10 element (TATAAT consensus sequence), which is specifically recognized by σ_2. During RNAP association with promoter DNA, RNAP binds and bends duplex promoter DNA to form the closed complex, I_1. In I_1, the DNA is bent into the cleft and the -11A becomes flipped out of the DNA stack prior to DNA opening. Isomerization of RNAP converts the initial closed complex to a mixture of open complexes containing a transcription bubble that extends from the upstream -10 region down past the +1 transcription start site (-11 to +2 for λP_R promoter). Opening of the DNA is the rate-limiting step in this process. Interactions of σ_2 with the promoter DNA -10 element play a key role in promoter melting by stabilizing the nontemplate strand in the single-stranded state after opening. Key residues on the surface of σ_2 create a positively-charged "track" that buries over 1,000 $Å^2$ total molecular surface area upon binding to ssDNA in RP_o (Feklistov and Darst, 2011). Substitutions of conserved residues in $\sigma_{2.3}$ to alanines disrupt promoter melting at low temperature (Tomsic *et al.* 2001). Contacts between σ_2 and ssDNA are so strong that they have been shown to induce a pause at -10-like sequences in the nontemplate strand during early elongation (Ring *et al.* 1996) and are sufficient to enable σ recruitment to elongation complexes far downstream from a promoter (Mooney *et al.* 2005). Clearly, interactions of the -10 elements with $\sigma_{2.3}$ are important for specific recognition and opening of promoter DNA during transcription initiation; however until now, the timing of these steps was unclear.

All nucleotides in the promoter -10 region extensively interact with RNAP and two (-11 and -7) become flipped in the single stranded structure such that they are engulfed

within pockets on the RNAP (Feklistov and Darst, 2011). In the structure of *T. aquaticus* housekeeping σ^A regions 2 and 3, W433 interacts directly with both -12 and -11, implying a key role in both -11A base flipping and stabilization of the single stranded nontemplate strand.

Characterization of the Interaction of σ_2 with -10 Promoter DNA Elements

Here, we have used both the RNAP fluorescence beacon assay and changes in the intrinsic fluorescence of RNAP to directly monitor interactions of $\sigma_{2.3}$ with duplex and single stranded DNA during transcription initiation. This approach has allowed us to characterize the rates of -11A base flipping and opening of the transcription bubble. Our work provides an extension to previous nitrocellulose filter binding kinetic studies of open complex formation performed in excess RNAP over promoter DNA. In this assay, open complexes are retained on a nitrocellulose filter, while free RNAP and DNA are undetected. Use of the polyanionic DNA mimic heparin binds to free RNAP in solution. Therefore use of a heparin “quench” removes all closed complexes from solution, as the early closed complexes are in rapid equilibrium with free promoter DNA and RNAP. These experiments exhibited single exponential kinetics that were well described by a minimal mechanism involving at least one short-lived intermediate (I_1) that rapidly equilibrates with free RNAP and DNA on the time scale of its conversion to open complexes. At high concentrations of RNAP, all free promoter DNA is rapidly converted to I_1 such that k_{obs} becomes independent of [RNAP] and equal to the first order rate constant for the subsequent DNA opening step (k_2) from I_1 to I_2 . In these experiments, only the equilibrium constant for (K_1) but not the rate constants (k_1, k_{-1}) for the initial

formation of I_1 or the base flipping step, was determined from the RNAP-concentration dependence of formation of the final open complexes.

Real-time fast •OH footprinting experiements utilizing a high (55nM) concentration of active RNAP demonstrated that I_1 formed within 100ms and persists for ~15 seconds. It is during this extended lifetime of I_1 that the duplex DNA is wrapped and the -11A base is flipped out into a hydrophobic pocket on RNAP. However, •OH footprints were unable to distinguish between these different forms of I_1: $I_{1,B}$, $I_{1,W}$ and $I_{1,F}$.

Use of real-time fluorescence assays allow us to monitor the real-time base flipping of -11A and opening of promoter DNA during open complex formation in the absence of heparin. Stopped-flow experiments monitoring changes in either RNAP intrinsic fluorescence or the RNAP "beacon" TMR probe at 19°C yield data that is best fit by the sum of two exponentials. The fast observed rate constant (k_{fast}) is promoter DNA- concentration dependent while the slow observed rate constant (k_{slow}) is promoter DNA-concentration independent. From analysis of the DNA concentration dependence of k_{fast} (see above) we determined the overall second order rate constant k_1 for forming $I_{1,F}$, the most advanced closed complex with -11 A flipped into the pocket involving W433. We also determined the reverse rate constant k_{-1} for coverting $I_{1,F}$ to $I_{1,B}$ from the intercept. This is the first dissection of these important steps of the early (preopening) mechanism, an understanding of which is required to understand regulation of DNA opening by upstream acting factors and ligands in transcription initiation.

The ratio of k_1/ k_{-1} yields K_1, the equilibrium binding constant for the first kinetically-significant intermediate I_1. For the intrinsic assay $K_1 = (1.4 \pm 0.5) \times 10^7\ M^{-1}$, consistent with previously published determinations of K_1 at the λP_R promoter from

nitrocellulose filter binding assays in our lab. For the beacon assay K_1 = (4.02 ± 1.6) × 10^6 M^{-1}, qualitatively consistent with the intrinsic assay, although the TMR probe may be slightly perturbing.

The rate constant for the second exponential phase, k_{slow} , represents the concentration-independent isomerization of the equilibrium mixture of closed complexes to open complexes. We obtain k_{slow}= 0.011 ± 0.002 s^{-1} for WT RNAP and k_{slow}= 0.025 ± 0.006 s^{-1} for the TMR-variant RNAP. These are both similar to rates of isomerization of closed to open complexes determined for this promoter and conditions by other assays. In Feklistov and Darst (2011) the authors concluded from the structure and from biochemical data that σ^A region 2.3 captures the nontemplate strand after the DNA is opened; however here we have indirect evidence that specific interactions of sigma region 2 with the -10 region of duplex promoter DNA must occur early, since they must be responsible for initial bending of the downstream duplex toward the cleft in $I_{1,B}$. $\sigma_{2.3}$ subsequently provides the binding pocket for the -11A base when it is flipped out of the duplex. We hypothesize that wrapping of upstream DNA to form $I_{1,F}$ from $I_{1,B}$ allows additional bending at -11 and entry of the downstream duplex into the cleft, and that this additional bending, by distorting the duplex, favors base flipping to slowly form $I_{1,F}$, which is nucleated for subsequent opening of the initiation bubble in the conversion of $I_{1,F}$ to I_2.

DNA Closing

Previous kinetic mechanistic analysis showed that the conversion of the I_1 and I_2 intermediates, involving DNA opening (I_1 to I_2) and closing (I_2 to I_1), is the rate-limiting step in the forward and reverse directions of the kinetic pathway for transcription

initiation at the λP_R promoter. Here, we used a 1.1M salt upshift to rapidly destabilize open complexes formed at 10, 22, and 37°C and induce dissociation. k_2 is independent of [salt] and therefore a rapid high [salt] upshift generates a burst in the population of I_2 in 250 ms after mixing. Use of nitrocellulose filter binding experiments to monitor the kinetics of decay of the transient population of I_2 to I_1 yielded a rate constant k_{-2} for DNA closing.

After high [salt] upshifts at 10, 22 and 37°C, we find that the observed rates at all temperatures for both the beacon and intrinsic assay yield rate constants consistent with steps occurring during DNA closing. Therefore all fluorescence effects occur in forming I_1 and converting it to I_2 and no fluorescence changes occur during the conversion of I_2 to late open complexes I_3 and RP_o. Thus, contacts between $\sigma_{2.3}$ and the promoter DNA -10 element must be formed early (during formation of I_1 and I_2) in the mechanism, remain largely unchanged during the transition of I_2 to RP_o. When open complexes are rapidly destabilized, contacts between $\sigma_{2.3}$ and the promoter DNA are not broken in the fast conversion of RP_o to I_2, but rather during the rate-limiting conversion of I_2 back to I_1 and to free RNAP and promoter DNA. Here we have shown that contacts of $\sigma_{2.3}$ with the -10 promoter DNA element are some of the first to be formed and last to be broken during association and dissociation, respectively.

Comparison of RNAP Beacon and Intrinsic Fluorescence Results to Previous 2-AP Fluorescence Studies

Previously, the fluorescence increase for association of RNAP with a 65 bp consensus promoter DNA containing a 2-AP substitution at -11 was found to be single exponential, with a rate constant $k_1 = 0.39 \pm 0.02\ s^{-1}$ and amplitude $a_1 = 0.03$ fluorescence units

(arbitrary units) at 25°C (Schroeder *et al.* 2009). Interestingly, 2-AP substitution at -4 yielded double exponential kinetics with k_1= 0.53 ± 0.080 s^{-1}, a_1=0.07 ± 0.01, k_2 =0.15 ± 0.03 s^{-1}, and a_2=0.2 ± 0.01. The amplitude of fluorescence change for the second step was more than double that of the first, consistent with our finding that the majority of the fluorescence change for both beacon and intrinsic fluorescence occurs in the second step. However, our experiments here using the beacon and intrinsic fluorescence assays yield a rate constant for k_2 that is within error of previous measurements of the rate-limiting DNA opening step and conversion of I_1 to I_2 measured using nitrocellulose filter binding and permanganate footprinting (Saecker *et al.* 2001, Chapter 2). Thus, we are able to monitor both the -11A base flipping step, along with DNA opening. In the 2-AP assay, the initial closed complex is "silent" such that the only fluorescence signal comes from distortions of the DNA. However, because 2-AP fluorescence is sensitive to changes in the stacking interactions of duplex DNA, it is reasonable to conclude that the 2-AP experiments were able to detect movements of the DNA occurring before DNA opening, including flipping of -11A on the nontemplate strand into the RNAP pocket and unstacking of the bases prior to opening. This would explain the apparent discrepancies between the rates observed with EMSA and the 2-AP fluorescence assay, and would support our hypothesis that the fast kinetic phase we monitored via the intrinsic and beacon assay is due to structural changes in the DNA including DNA bending and base flipping.

Comparison with Previous Intrinsic Fluorescence Studies on the T7A1 Promoter

Previously, intrinsic RNAP tryptophan fluorescence was used to investigate the kinetics and equilibrium of open complex formation at the T7A1 promoter (Johnson and

Chester, 1998). Association of RNAP with T7A1 was best described by the sum of two exponentials over the temperature range of 25-37°C. At 20°C the data was best described by a single exponential. The authors concluded that $k_{obs,1}$ represents the bimolecular association of RNAP with T7A1 to form the initial closed complex:

$$R + P \rightleftarrows RPc \qquad \text{(Mechanism 4)}$$

k_{isom} represents the unimolecular isomerization of the closed complex to open complexes:

$$RPc \longrightarrow RPo \qquad \text{(Mechanism 5)}$$

Above 25°C, both $k_{obs,1}$ and k_{isom} are monitored; at 20°C at the T7A1 promoter no open complexes are formed and only $k_{obs,1}$ is detected. At 37°C, the authors reported $k_{1,\,app}$ = 4.0 (±0.6) × 10^7 (M^{-1} s^{-1}) and k_{isom} = 0.26 (± 0.02) s^{-1} (under somewhat different experimental conditions than those used here: 10mM Hepes, 0.05M KCl, 10mM $MgCl_2$, 0.1M EDTA, 10% glycerol, 0.1mM DTT at pH 8.0). At 20°C, the authors report $k_{1,\,app}$ = 0.05 (±0.03) × 10^7 (M^{-1} s^{-1}). These findings are consistent with those reported here; $k_{1,\,app}$ is two to three orders of magnitude slower than observed for facilitated binding (~10^{10} M^{-1} s^{-1}, von Hippel *et al.* 1984) and for a diffusion-limited process (~10^8 M^{-1} s^{-1},von Hippel *et al.* 1984). Therefore, the intrinsic fluorescence assay does not detect formation of the collision complex, or of an early closed complex that forms prior to the DNA base-flipping step. Rather, the intrinsic fluorescence assay must be monitoring the conversion of a bent, closed complex to the base-flipped closed complex, and then to the open complex.

Role of W433

A σ^{70} variant containing the $\sigma_{2.3}$ W433A substitution has previously been shown to be able to form a stable complex with core RNAPand to bind duplex DNA; however, W433A holoenzyme exhibited a ~40% reduction in the amount of transcription products in run-off transcription gels at 37°C (Panaghie *et al.* 2001). Likewise, reduced permanganate reactivity is seen for W433A open complexes at 19°C (Figure 6). However, W433A holoenzyme- was able to bind and open a 65 bp consensus promoter DNA with 2-AP substitutions at either the -11, -8 or -4 positions (Schroeder *et al.* 2010). Taken together, this suggests that W433 plays a critical role in opening the DNA, recognizing the single stranded region of the -10 element and for stabilizing RP_o.

Y430 participates in a base stacking interaction with the -11A base once it is flipped out of the DNA duplex (Schroeder *et al.* 2010; Fenton et al. 2000), a conclusion confirmed by structural analysis (Feklistov and Darst, 2011). Substitution of Y430 to alanine greatly increased the fluorescence of DNA with 2-AP at -11 during association with RNAP, and this process was found to be single-order, indicating that it was occurring after DNA binding. Our data also suggests that the majority of the signal change of the intrinsic RNAP fluorescence is due to the interactions of W433 with the nontemplate strand. The first step, k_{fast}, monitors base flipping of -11A into the RNAP pocket prior to DNA opening. Because the RNAP beacon assay exhibits nearly identical kinetics as the intrinsic assay, it too must monitor base flipping in the first step of association of RNAP with promoter DNA.

Conclusion

The intrinsic and beacon RNAP fluorescence assays monitor the interactions of $\sigma_{2.3}$ with the nontemplate strand of the -10 region of promoter DNA. During real-time association of RNAP with promoter DNA, these assays are used in real-time to characterize the rate of -11A base flipping and DNA opening at 19°C. During formation of the first kinetically-significant closed complex I_1, the promoter DNA is bent into the RNAP active site cleft. Prior to DNA opening, the -11A base of the nontemplate strand is flipped out of the DNA base stack and into a hydrophobic pocket on RNAP. This step is the first that is observed in the intrinsic and beacon fluorescence assays. After the -11A base is flipped out of the DNA base stack, the DNA is opened in the subsequent, rate-determining step. Conversion of the equilibrium mixture of closed (flipped and unflipped) complexes to the initial open complex is the slow phase in both intrinsic and beacon fluorescence assays. Here we have determined the rate constants and the timing of promoter DNA bending, base flipping and opening in real-time for the first time.

Materials and Methods

Reagents

All reagents were of the highest purity commercially available and were purchased from Sigma or Fisher. Enzymes were purchased from NEB; all DNA oligonucleotides were ordered from IDT.

Buffers

Storage buffer for RNAP at -80 °C contained 10 mM Tris (pH 7.5 at 4°C), 6.85 M glycerol, 100 mM NaCl, 100 nM Na_2EDTA, and 100 nM DTT. Binding buffer used for all beacon experiments was 40 mM Tris (pH 8 at 19C), 10 mM $MgCl_2$, 120 mM NaCl, 100 μg/mL BSA and 0.02% Tween. Binding buffer used for all intrinsic fluorescence experiments was identical with the exception that the BSA was omitted. BSA also absorbs at 280 nm and significantly increases the background fluorescence signal in the intrinsic assay.

DNA Preparation and purification

The λP_R promoter DNA was amplified from a 963-bp-long DNA template P_R (wild type P_R sequence from −59 to + 34) using PCR and primers 'Fwd' (5'GTACGAATTCGATATCCAGCTATGACCATGATTACGCCAGC) and 'Rev' (5'CAGGACCCGGGGCGCGCTTAATTAACACTCTTATACATTATTCC) (primers and template were the gifts of Wilma Ross). This 963-bp-long DNA template P_R was previously obtained by PCR from plasmid pPR59 using primers NEB_FOR (5′-AAAACCTCTGACACATGCAGC) and NEB_REV (5′-GCTGCCCTTTTGCTCACATG).

The high fidelity DNA polymerase Pfx50 (Invitrogen, Carlsbad, CA) was used to create blunt ends during the PCR amplification. All DNA was purified using the Qiagen

MinElute PCR cleanup kit and concentration determined by absorbance at 260nm. A 6% polyacrylamide gel was run for each DNA preparation in order to ensure purity.

RNAP Preparation and purification

E. coli PVS10 RNAP core and σ^{70} were both purified following the procedures in Belogurov *et al.* 2007. σ^{70}-W433A was prepared and purified as in Sevostyanova *et al.* 2008. *E. coli* σ^{70} RNA polymerase was prepared by reconstituting PVS10 RNAP core with σ^{70} in a 1:2 (core: sigma) ratio in storage buffer at 37°C for 1 hour. *E. coli* σ^{70} W433A RNA polymerase was prepared in the same way. RNAP holoenzyme was stored at -20°C and was used up to one month after reconstitution. Nitrocellulose equilibrium promoter binding activity assays indicated that reconstituted wt RNAP holoenzyme was greater than 95% active. RNAP concentrations are therefore reported as total concentration.

E. coli RNA polymerase holoenzyme containing the σ^{70} derivative labeled at position 211 with fluorescent label 5-tetramethylrhodamine ((211Cys-TMR) σ^{70}) was prepared as in Mekler *et al.* (2011a). RNAP σ^{70}–211TMR holoenzyme was stored at -20°C and was used up to two weeks after reconstitution. Long-term storage of RNAP σ^{70}–211TMR (> 1 month) resulted in greatly decreased binding activity. RNAP σ^{70}–211-Atto488 was also used for real-time association assays, but had a much smaller (~0.5-fold) observed fluorescence change for λP_R open complexes than RNAP σ^{70}–211-TMR. However, RNAP σ^{70}–211-Atto488 was stable up to 2 months at -20°C with no observed decrease in binding activity.

For the real-time association assays, the final solutions contained 10-20 nM (intrinsic fluorescence) or 5-10nM (beacon assay) active RNAP and 50-300 nM DNA, depending on the experiment.

Intrinsic Fluorescence

Equilibrium fluorescence measurements

Intrinsic fluorescence measurements were taken on a single beam fluorimeter (Photon Technology International) equipped with an 814 Photomultiplier Detection system connected to an external temperature control (Quantum Northwest). The excitation wavelength was either 280 or 295 nm with 3nm slit widths, and emission light was collected from 320 to 400nm using the instrument monochromator and 5nm slit widths. The beacon assay equilibrium experiments were performed on the same instrument, using 550nm excitation and 3nm slit width. Emission light was collected from 565 to 595 nm with 5nm slit widths. We note that all equilibrium emission spectra were corrected for inner-filter effects due to absorption by DNA, therefore changes in the solution emission can be attributed solely to a decrease in RNAP emission and not to increased absorption by the DNA. Raman scattering also contributes to the emission signal at 330nm, therefore, all emission spectra were also compared to a water-only reference sample.

Stopped flow fluorescence measurements

Real-time fluorescence measurements were taken on a Kintek SFX-300 stopped flow spectrometer (KinTek Corp., Austin, TX) equipped with computer-controlled motor-driven syringes and an external water bath. For intrinsic fluorescence experiments, equal volumes (20 μL) of RNAP (20nM) and promoter DNA (20-300nM) were rapidly

mixed at 19°C with an instrument data collection dead time less than 10 ms. The excitation wavelength was either 280 or 295 nm and the slit widths were 0.280 mm. Light emitted from the sample was collected after passing through a 320nm long pass filter. Controls with promoter DNA only indicated that absorption by the nucleic acid was unchanged over the time course of interest for data collection.

Bleaching of the RNAP was minimized by decreasing the slit widths and using an excitation wavelength of 295nm, instead of 280nm, the absorbance maxima for tryptophan. For the association experiments, bleaching (less than 15% of the total signal amplitude) was determined from RNAP-only controls. RNAP was rapidly mixed with binding buffer and the decrease in signal due to bleaching was monitored out to 600 seconds. The best-fit line to the bleaching time course was used to correct the experimental data. For the dissociation (salt upshift) experiments, bleaching of RNAP was minimal due to the fast kinetics of this process. Therefore, this data is presented uncorrected for bleaching.

For the beacon assay, reconstituted holoenzyme containing 211Cys-TMR σ^{70} was excited at 550nm and emission collected using a 565 nm long pass filter. The slit widths were 1.280 mm. Equal volumes (20uL) of holoenzyme 211Cys-TMR σ^{70} (5nM) and LPR DNA (100nM) were rapidly mixed at 19°C. Bleaching of TMR was insignificant under the time range (10-1000 seconds) investigated, as confirmed by RNAP 211Cys-TMR σ^{70} control reactions.

For all stopped-flow experiments, 600-2000 data points were collected and data from 2-5 traces under identical conditions was collected. Each individual trace was fit was fit to the equation

$$F = \Sigma A_n \times \exp(-k_{obs,n}\, t) + C \quad \text{(Equation 2)}$$

where F is the fluorescence at time *t*, *n* is the number exponential terms, A_n and $k_{obs,n}$ are the amplitude and the observed rate constants of the *n*th term, respectively. The data were fit to the sum of one, two, or three exponentials.

Single exponential fits to the data were insufficient, displaying systematic deviation in the fits to the residuals. Fits to the sum of three exponentials did not substantially improve the quality of the fit and in most cases did not produce three unique values for the observed rates. All individual traces were visually inspected before being included in further analysis. Not all of the individual traces were of sufficient quality to be included in the final analysis, due to sample air bubbles and protein sticking within the cuvette.

Next, the individual traces for a given experiment were globally fit using Origin 8 software. From these global fits, we determine the rate constants k_{fast} and k_{slow} and the amplitudes A_{fast} and A_{slow}. Experimental replicates from at least two separate days were averaged to produce the rates in Table 1. Uncertainties are reported as the standard deviation between experiments.

ASA calculations

Accessible surface calculations were done with Surface Racer (van der Waals radius set 2, probe radius 1.4 Angstroms) and using the EM structure of RP_o (PDB structure 3YID) with or without DNA. *E. coli* RNAP contains 19 Trps; of these 19 approximately 10 Trp residues are highly accessible in both structures. Two of these 10 Trp residues change their accessibility to a significant degree upon binding of promoter

DNA, W183 in beta (chain C) and W433 in sigma (chain F). Their accessibilities double upon DNA removal, going from 44 $Å^2$ to 81 $Å^2$ and from about 60 $Å^2$ to 120 $Å^2$, respectively. Accessible surface calculations were also done comparing the EM structure of RP_o (PDB structure 3YID) with DNA and the crystal structure of free thermus RNAP (PDB structure 2A6E). 3 Trps are known to be conserved between the two organisms (*E.coli* $\sigma_{2.3}$ W433 and W434 and β W183). Two Trp residues change their accessibility to a significant degree upon binding of promoter DNA, W183 and W433. Their accessibilities more than double upon DNA removal, going from 40 $Å^2$ to 102 $Å^2$ and from about 62 $Å^2$ to 151 $Å^2$, respectively.

References

Buc, H. and McClure, W.R. 1985. Kinetics of open complex formation between *Escherichia coli* RNA polymerase and the *lac* UV5 promoter. Evidence for a sequential mechanism involving three steps. *Biochemistry*. **24**: 2712-2723.

Craig, M. L., Tsodikov, O. V., McQuade, K. L., Schlax, P. E., Jr., Capp, M. W., Saecker, R. M., and Record, M. T., Jr. 1998. DNA footprints of the two kinetically significant intermediates in formation of an RNA polymerase-promoter open complex: Evidence that interactions with start site and downstream DNA induce sequential conformational changes in polymerase and DNA. *J Mol Biol* **283:** 741–756.

Davis, C. A., Bingman, C. A., Landick, R., Record M. T., Jr., and Saecker, R. M. 2007. Real-time footprinting of DNA in the first kinetically significant intermediate in open complex formation by *Escherichia coli* RNA polymerase. *Proc Natl Acad Sci* (USA) **104:** 7833- 7838.

Fenton, M. S., Lee, S. J., and Gralla, J. D. 2000. *Escherichia coli* promoter opening and −10 recognition: mutational analysis of σ70. *EMBO J.* **19:** 1130–1137.

Feklistov A., and Darst S. A. 2011. Structural basis for promoter-10 element recognition by the bacterial RNA polymerase σ subunit. *Cell.* **147:** 1257-69.

Gries, T. J., Kontur, W. S., Capp, M. W., Saecker, R. M., and Record, M. T., Jr. 2010. One-step DNA melting in the RNA polymerase cleft opens the initiation bubble to form an unstable open complex. *Proc Natl Acad Sci (USA)* **107:** 10418-10423.

Helmann, J. D. and deHaseth, P. L. 1999. Protein-nucleic acid interactions during open complex formation investigated by systematic alteration of the protein and DNA binding partners. *Biochemistry* **38:** 5959–5967.

Johnson R.S., and Chester R.E. 1998. Stopped-flow kinetic analysis of the interaction of Escherichia coli RNA polymerase with the bacteriophage T7 A1 promoter. *J Mol Biol.* **283:** 353-70.

Kontur W.S., Capp, M.W., Gries, T.J., Saecker, R.M., and Record, M.T., Jr. 2010. Probing DNA binding, DNA opening, and assembly of a downstream clamp/jaw

in Escherichia coli RNA polymerase-lambdaP(R) promoter complexes using salt and the physiological anion glutamate. *Biochemistry.* **49:** 4361-73.

Kontur, W. S., Saecker, R. M., Capp, M. W., and Record, M. T., Jr. 2008. Late steps in the formation of *E. coli* RNA polymerase-λP_R promoter open complexes: Characterization of conformational changes by rapid [perturbant] upshift experiments. *J Mol Biol* **376:** 1034–1047.

Kontur, W. S., Saecker, R. M., Davis, C. A., Capp, M. W., and Record, M. T., Jr. 2006. Solute probes of conformational changes in open complex (RP_o) formation by *Escherichia coli* RNA polymerase at the λP_R promoter: Evidence for unmasking of the active site in the isomerization step and for large-scale coupled folding in the subsequent conversion to RP_o. *Biochemistry* **45:** 2161–2177.

Lakowicz, J. R. 1983. Protein Fluorescence. *Principles of Fluorescence Spectroscopy.* pp 341- 379. Plenum Press, New York.

Mekler V., Pavlova O., and Severinov K. 2011a. Interaction of Escherichia coli RNA polymerase σ70 subunit with promoter elements in the context of free σ70, RNA polymerase holoenzyme, and the β'-σ70 complex. *J Biol Chem.* **286:** 270-9.

Mekler V., Minakhin L., and Severinov K. 2011b. A critical role of downstream RNA polymerase-promoter interactions in the formation of initiation complex. *J Biol Chem.* **286:** 22600-8

Mekler V., Minakhin L., Sheppard C., Wigneshweraraj S., and Severinov K. 2011c. Molecular mechanism of transcription inhibition by phage T7 gp2 protein. *J Mol Biol.* **413:** 1016-27.

Panaghie, G., Aiyar, S.E., Bobb, K., Ll, K., Hayward, R.S., and de Haseth, P.L. 2000. Aromatic amino acids in region 2.3 of Escherichia coli sigma 70 participate collectively in the formation of an RNA polymerase-promoter open complex. *J Mol Biol.* **200:**1217-30.

Roberts, C. W., Roberts, J. W. 1996. Base-specific recognition of the nontemplate strand of promoter DNA by *E. coli* RNA polymerase. *Cell* **86:** 495–501

Roe, J. H., Burgess, R. R., and Record, M. T., Jr. 1984. Kinetics and mechanism of the interaction of *Escherichia coli* RNA polymerase with the λP_R promoter. *J Mol Biol* **176:** 495–522.

Saecker, R. M. Record, M. T., and de Haseth, P. L. 2010. Mechanism of Bacterial Transcription Initiation: RNA Polymerase - Promoter Binding, Isomerization to Initiation-Competent Open Complexes, and Initiation of RNA Synthesis. *J Mol Biol* **4:** 754–771

Saecker, R. M., Tsodikov, O. V., McQuade, K. L., Schlax, P. E., Jr., Capp, M. W., and Record, M. T., Jr. 2002. Kinetic studies and structural models of the association of *E. coli* σ^{70} RNA polymerase with the λP_R promoter: Large scale conformational changes in forming the kinetically significant intermediates. *J Mol Biol* **319:** 649–671.

Schroeder, L. A., Choi, A.J., and deHaseth, P. L. 2007. The −11A of promoter DNA and two conserved amino acids in the melting region of σ^{70} both directly affect the rate limiting step in formation of the stable RNA polymerase-promoter complex, but they do not necessarily interact. *Nucleic Acids Res*. **35:** 4141–4153.

Schroeder, L. A., Gries, T. J., Saecker, R. M., Record, M. T., Jr., Harris, M. E., and DeHaseth, P. L. 2009. Evidence for a tyrosine-adenine stacking interaction and for a short-lived open intermediate subsequent to initial binding of *Escherichia coli* RNA polymerase to promoter DNA. *J Mol Biol* **385:** 339–349.

Schroeder, L. A., Karpen, M. E., and deHaseth, P. L. 2008. Threonine 429 of *Escherichia coli* σ^{70} is a key participant in promoter DNA melting by RNA polymerase. *J Mol Biol* **376:** 153–165.

Sevostyanova, A., Svetlov, V., Vassylyev, D. G., and Artsimovitch, I. 2008. The elongation factor RfaH and the initiation factor σ bind to the same site on the transcription elongation complex. *Proc Natl Acad Sci U S A.* **105:** 865–870.

Tomsic, M., Tsujikawa, L., Panaghie, G., Wang, Y., Azok, J., and deHaseth, P. L. 2001. Different roles for basic and aromatic amino acids in conserved region 2 of *Escherichia coli* σ^{70} in the nucleation and maintenance of the single-stranded DNA bubble in open RNA polymerase-promoter complexes. *J Biol Chem* **276:**

31891–31896.

Tsodikov, O. V. and Record, M. T., Jr. 1999. General method of analysis of kinetic equations for multistep reversible mechanisms in the single-exponential regime: Application to kinetics of open complex formation between $E\sigma^{70}$ RNA polymerase and λP_R promoter DNA. *Biophys J* **76:** 1320–1329.

Von Hippel, P. H., Bear, D. G., Morgan, W. D., and McSwiggen, J. A. 1984. Protein-nucleic acid interactions in transcription: a molecular analysis. *Annu. Rev. Biochem.* **53:** 389-446.

Table 1.

Assay	k_1 (M^{-1} s^{-1})	k_{-1} (s^{-1})	K_1 (M^{-1})	k_2 (s^{-1})
Beacon RNAP	6.8 (± 1.2) × 10^5	0.17 (±0.05)	4.0(±1.6) × 10^6	0.023 (± 0.005)
Intrinsic RNAP	1.5 (±0.6) × 10^6	0.11 (±0.04)	1.4 (±0.5) × 10^7	0.011 (± 0.002)

Rate and equilibrium constants for the beacon and intrinsic fluorescence assays during formation of open complexes at the λP_R promoter. All experiments performed at 19°C, 20 nM active RNAP and variable [DNA] in transcription buffer. k_1 represents the slope and k_{-1} represents the intercept for best-fit lines to the data shown in Figure 3. K_1 is determined from the ratio k_1 / k_{-1}. The approximation that the sum of the equilibrium concentrations of reactants is approximately equal to the total DNA concentration ($[DNA]_{eq} + [RNAP]_{eq} \approx [DNA]_{total}$) is adequate since the DNA is in at least 2.5 fold excess over RNAP and the experimental error is as large as the error introduced by this approximation.

Table 2. Dissociation Rates for RNAP "Beacon" Open Complexes Upshifted to 1.1M Salt

Temp °C	k_1 (s^{-1})	A_1 (fraction of total signal)	k_2 (s^{-1})	A_2 (fraction of total signal)	No. Replicates	Previously Published Value (s^{-1})
10	6.0 (±0.9) × 10^{-1}	0.76	4.9 (±0.7) × 10^{-2}	0.24	2	7.3 (±0.6) × 10^{-1}
22	1.7 (±0.4)	1.0			2	N/A
37	4.1 (±1.2)	1.0			4	3.3±0.2

Observed rate constants for dissociation of "beacon" RNAP from the λP_R promoter following a rapid high salt upshift. The data were best fit to either a single or double exponential (Equation 1). No change in fluorescence is detected in the 250 ms time interval required to convert the stable open complexes to I_2, indicating that these steps do not affect the interaction of $\sigma_{2.3}$ with the -10 nontemplate strand.

Table 3. Intrinsic Fluorescence Dissociation Rates for RNAP Open Complexes Upshifted to 1.1M Salt

Temp °C	k_1 (s^{-1})	A_1 (fraction of total signal)	No. Replicates	Previously Published Value (s^{-1})
10	7.1 (±1.0) × 10^{-1}	1.0	3	7.3 (±0.6) × 10^{-1}
22	3.1 (±0.9)	1.0	4	N/A
37	6.4 (±1.2)	1.0	4	3.3 ±0.2

Observed rate constants for dissociation of RNAP from the λP_R promoter following a rapid high salt upshift as monitored by intrinsic fluorescence. The data were best fit to a single exponential (Equation 1). No change in fluorescence is detected in the 250 ms time interval required to convert the stable open complexes to I_2, indicating that these steps do not affect the interaction of $\sigma_{2.3}$ with the -10 nontemplate strand.

Figure Captions

Figure 1. (A) Cartoon model and (B) structural model based on PDB 3YID depicting the RNAP "beacon" assay. The assay detects changes in the fluorescence emission of a probe attached to a unique C-211 residue. This residue is spatially close to the highly conserved Trp and Tyr residues (W433, W434, Y430) of $\sigma_{2.3}$. In free RNAP, these aromatic amino acids participate in photo-electronic transfer to the dye, resulting in fluorescence quenching. However, interactions of the -10 element within the DNA-binding track of $\sigma_{2.3}$ relieves quenching, causing a large increase in fluorescence intensity. C211 is in lime green, $\sigma_{2.3}$ residues W433, W434, Y430 are in light blue, promoter DNA is in navy blue (nontemplate strand) and black (template strand), the flipped -11A base on the nontemplate strand is in red.

Figure 2. Representative kinetic data for formation of open complexes at the λP_R promoter. 100nM λP_R promoter DNA (final concentration) was rapidly mixed with 10nM active RNAP holoenzyme at 19°C using a Kintek SFX-300 stopped-flow spectrophotometer. For each loading of sample reagents, 3-5 replicate shots were averaged to generate the curves depicted. The data best fit a sum of two exponentials (Equation 1); the best-fit line to the data is shown in red. (A) A representative "beacon" RNAP σ^{70}211-Cys-TMR experiment; samples were excited at 550nm and emission monitored using a 565 long pass filter. The same data is plotted on a log time scale in the insert. (B) Representative intrinsic RNAP σ^{70} experiments; the insert depicts the same data on a log time scale. Samples were excited at 280 nm and emission monitored using a 320 long pass filter.

Figure 3. Rate constants k_{fast} and k_{slow} quantifying the fast and slow components of two exponential fits to the intrinsic and TMR kinetic data (see Fig 1) plotted as a function of the promoter DNA concentration (50-300 nM). Values of k_{fast} and k_{slow} at each [DNA] are the average of 2-4 independent sets of experimental (replicate) determinations; the reported uncertainties are the standard deviations of these averages. Best-fit lines are shown. (A) k_{fast} for (●) intrinsic RNAP σ^{70} and (■) beacon RNAP σ^{70}211-Cys-TMR; the slopes and intercepts of these fits, interpreted by Eq 3 for the rapid equilibrium forming

the species of I_1 detected by these assays, yield the second order rate constant for formation of this I_1 and the first order rate constant for its dissociation. (B) for (●) intrinsic RNAP σ^{70} and (■) beacon RNAP σ^{70}211-Cys-TMR; as expected, k_{slow} is independent of promoter [DNA] and represents the rate constant for conversion of the I1 species detected to open complexes Values of the slopes and intercepts are reported in Table 1.

Figure 4. Permanganate reactivity of wild type and W433A RNAP- promoter DNA complexes. Complexes (50nM active RNAP, <1nM promoter DNA) were equilibrated at 19°C for 1.5 hours and then mixed with 6mM $NaMnO_4^-$ for 10 seconds. Reactions were quenched using a 2.4M beta-mercaptoethanol and 6.25M NH_4OAc solution, ethanol precipitated and resuspended. The solutions were reacted with 1M piperidine, ethanol precipitated, resuspended in loading buffer and run on an 8% polyacrylamide sequencing gel.

Figure 5. Representative kinetic data for the association of 10nM (total) RNAP σ^{70}-W433A with 100nM λP_R promoter DNA. Samples were excited at (A) 280 nm and (B) 295 nm and the emission monitored using a 320nm glass filter. The best-fit line to the data is shown the red.

Figure 6. Representative kinetic data for dissociation of beacon RNAP σ^{70}211-Cys-TMR open complexes (I_3, RP_o) following a 1.1M NaCl upshift. Open complexes containing 100nM total RNAP σ^{70}211-Cys-TMR and 50nM λP_R promoter DNA were equilibrated at the temperature of interest for a minimum of one hour. Open complexes were then rapidly mixed with 1.1M NaCl (final concentration), which destabilizes the final open complexes (RP_o and I_3) and creates a burst (transient near-homogeneous population) of the early open complex, I_2. The samples were excited at 550nm and the emission of TMR monitored using a 565 LP filter. Representative kinetic curves are shown for experiments performed at (A) 37°C, (B) 22°C, and (C) 10°C. The best-fit line to the data is shown the red and the inserts depict the same data plotted on a log time

scale. Curves at 37°C and 22°C were best fit to a single exponential; curves at 10°C were best fit to the sum of two exponentials.

Figure 7. Representative kinetic data for dissociation of RNAP σ^{70} open complexes following a 1.1M NaCl upshift as monitored by intrinsic RNAP fluorescence. Open complexes containing 100nM total RNAP and 50nM λP_R promoter DNA were equilibrated at the temperature of interest for a minimum of one hour. Open complexes were then rapidly mixed with 1.1M NaCl (final concentration), which destabilizes the final open complexes (RP_o and I_3) and creates a burst (transient near-homogeneous population) of the early open complex, I_2. Representative kinetic curves are shown for experiments performed at (A) 37°C, (B) 22°C, and (C) 10°C. Inserts depict the same data plotted on a log time scale. The best-fit line to the data is shown the red. Curves at all temperatures were best fit to a single exponential.

Figures

Figure 1. A.

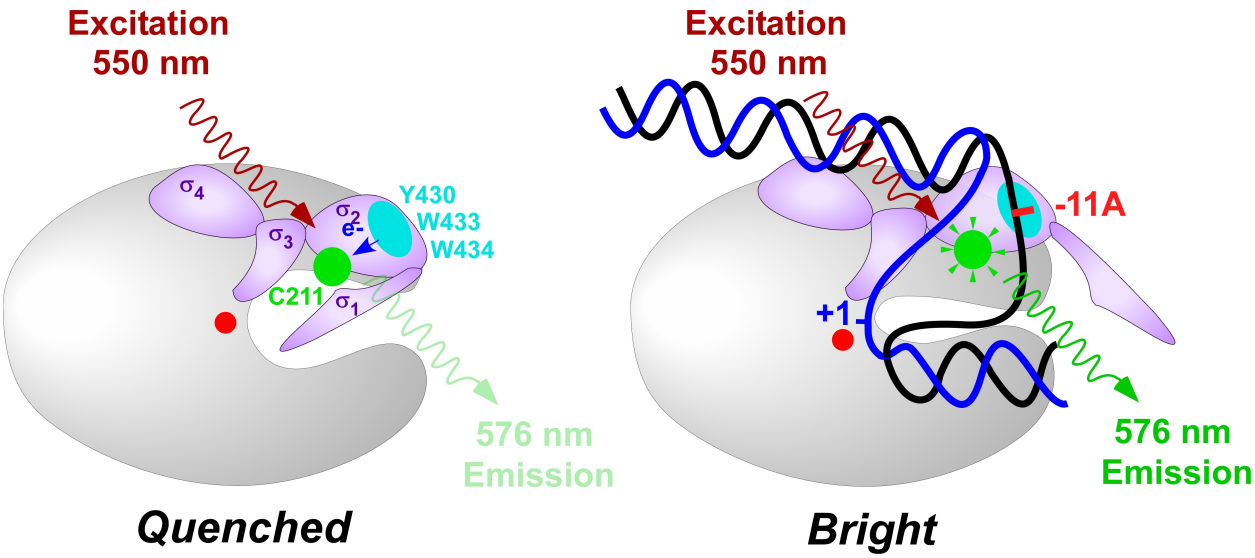

B.

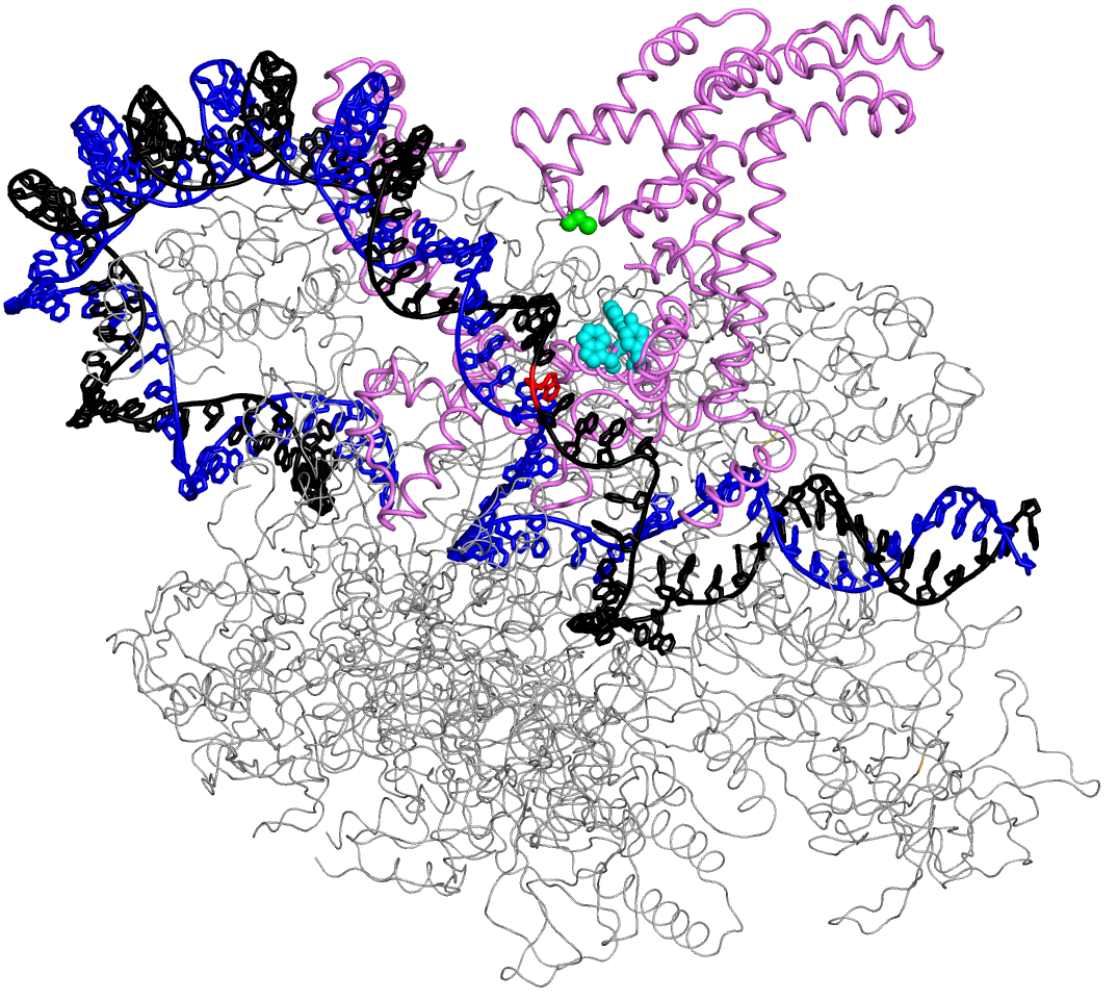

Figure 2. A.

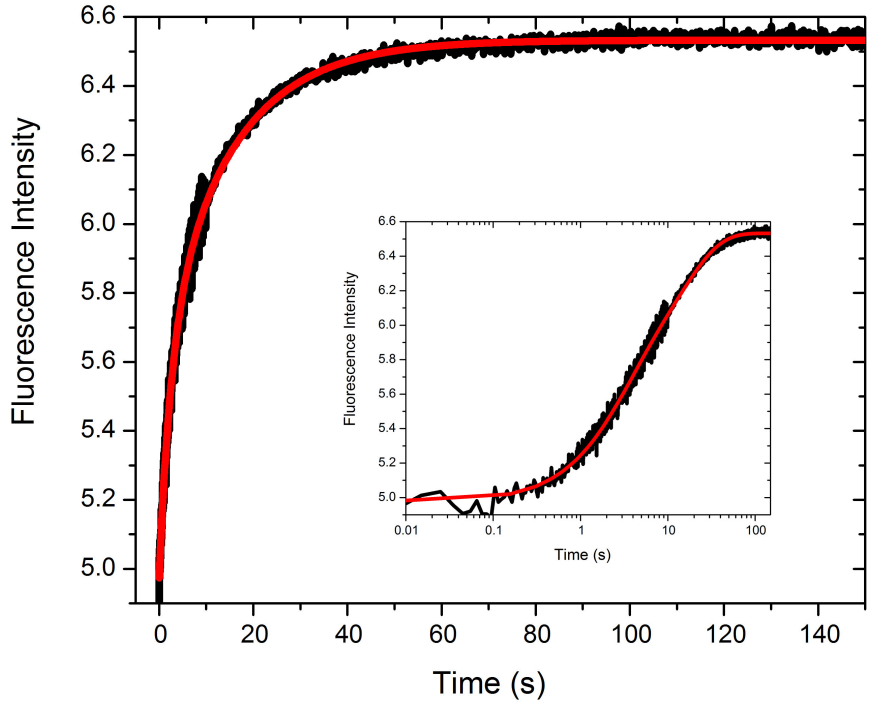
Fluorescence Intensity
Time (s)
Fluorescence Intensity
Time (s)

B.

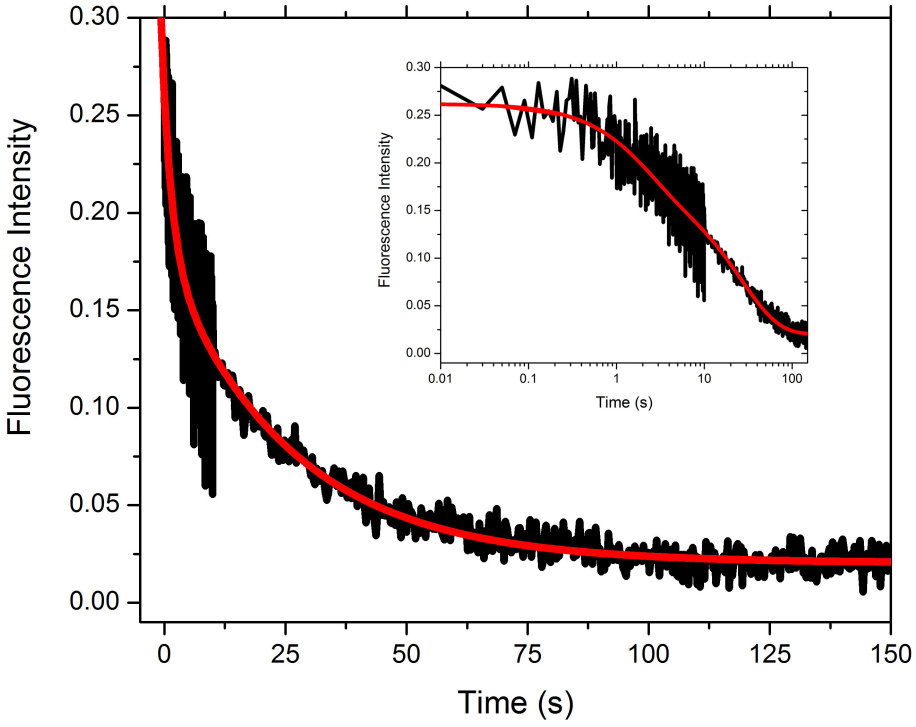
Fluorescence Intensity
Time (s)
Fluorescence Intensity
Time (s)

Figure 3.
A.

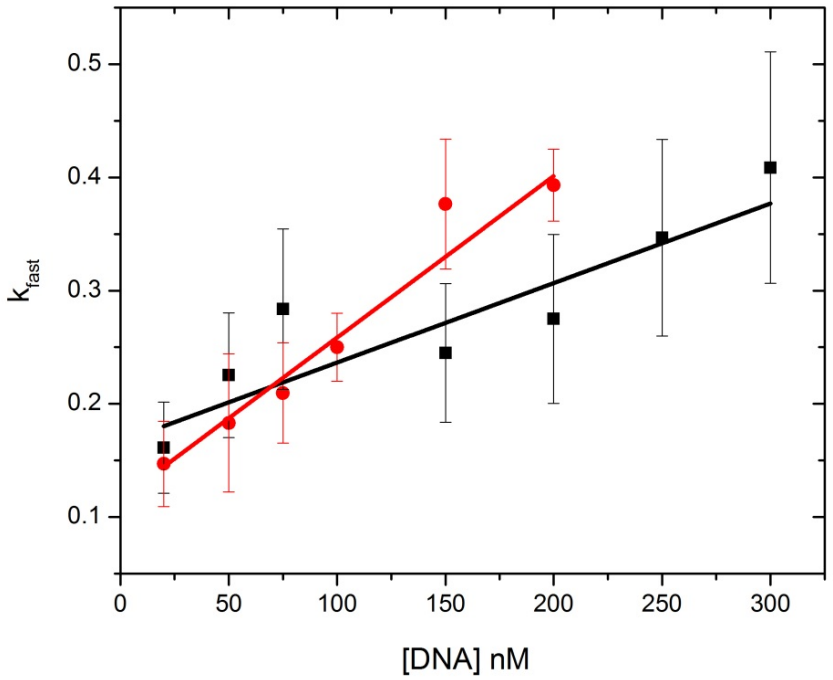
0.5
0.4
0.3
0.2
0.1
k_{fast}
0
50
100
150
200
250
300
[DNA] nM

B.

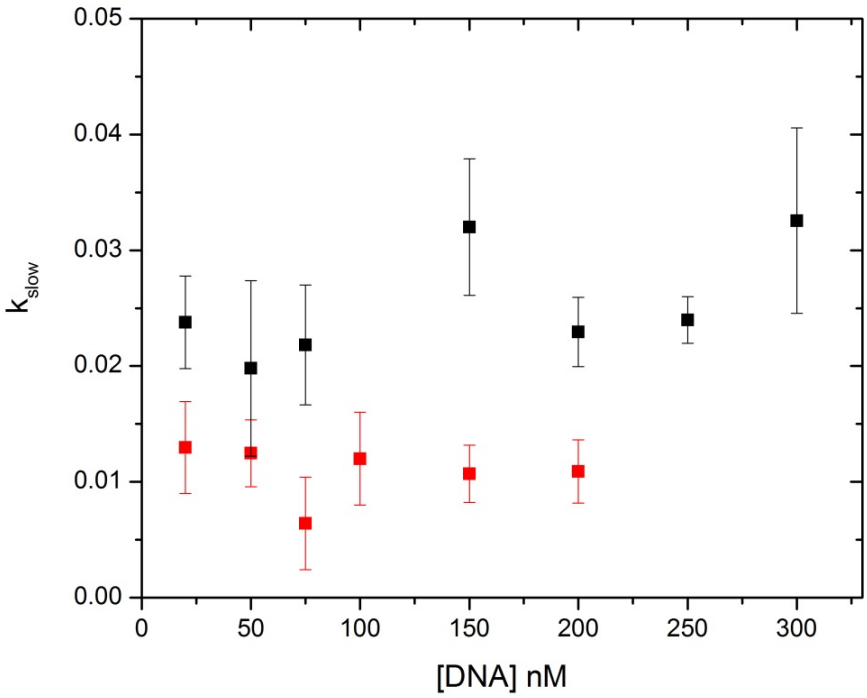
0.05
0.04
0.03
0.02
0.01
0.00
k_{slow}
0
50
100
150
200
250
300
[DNA] nM

Figure 4. MnO_4^- reactivity of the RNAP W433A- DNA complex

Figure 5.

A.

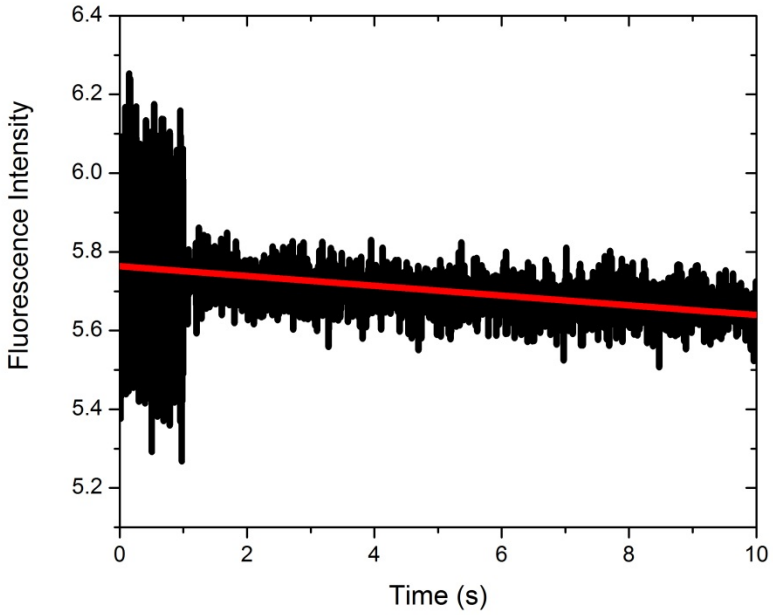
Fluorescence Intensity
6.4
6.2
6.0
5.8
5.6
5.4
5.2
0
2
4
6
8
10
Time (s)

B.

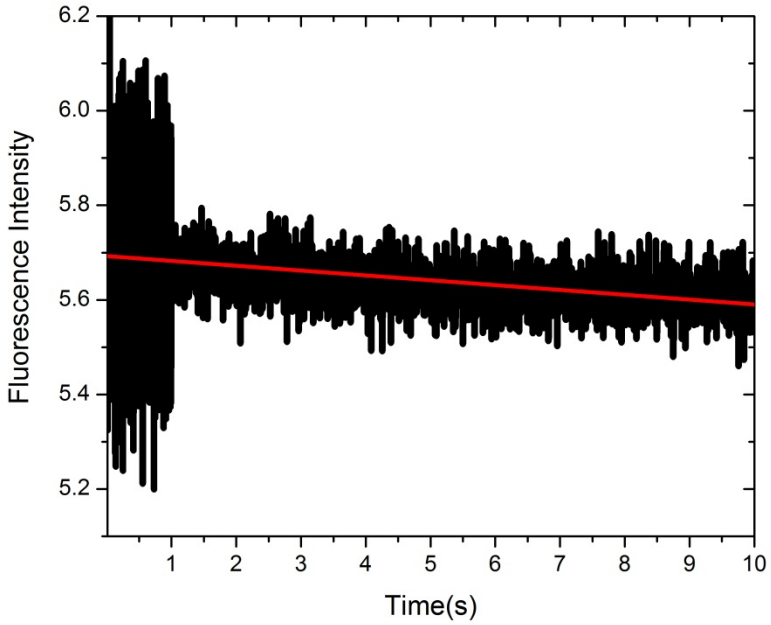
Fluorescence Intensity
6.2
6.0
5.8
5.6
5.4
5.2
1
2
3
4
5
6
7
8
9
10
Time(s)

Figure 6.

A. RNAP beacon open complexes + 1.1M salt at 37°C

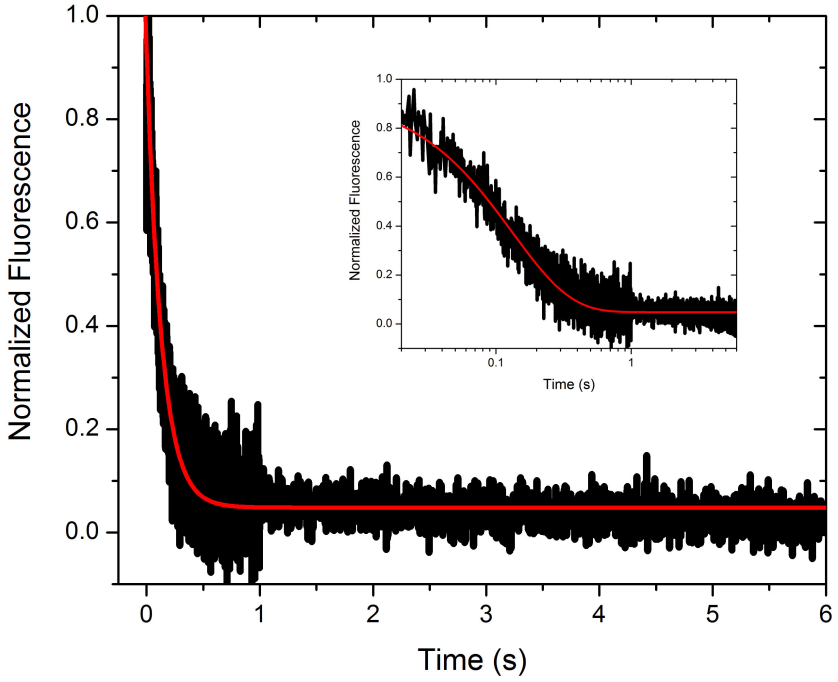

B. RNAP beacon open complexes + 1.1M Salt at 22°C

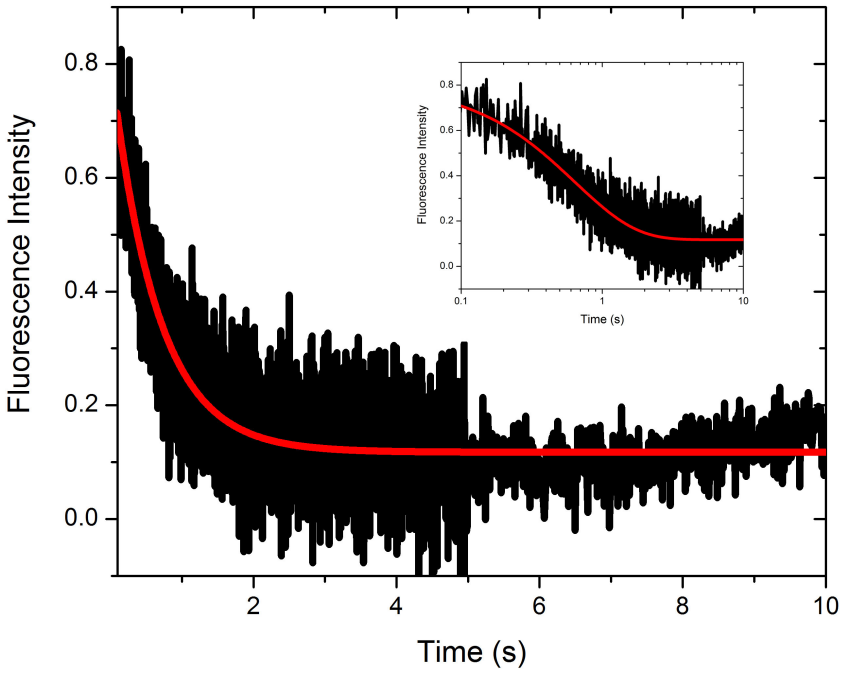

C. RNAP beacon open complexes + 1.1M salt at 10°C

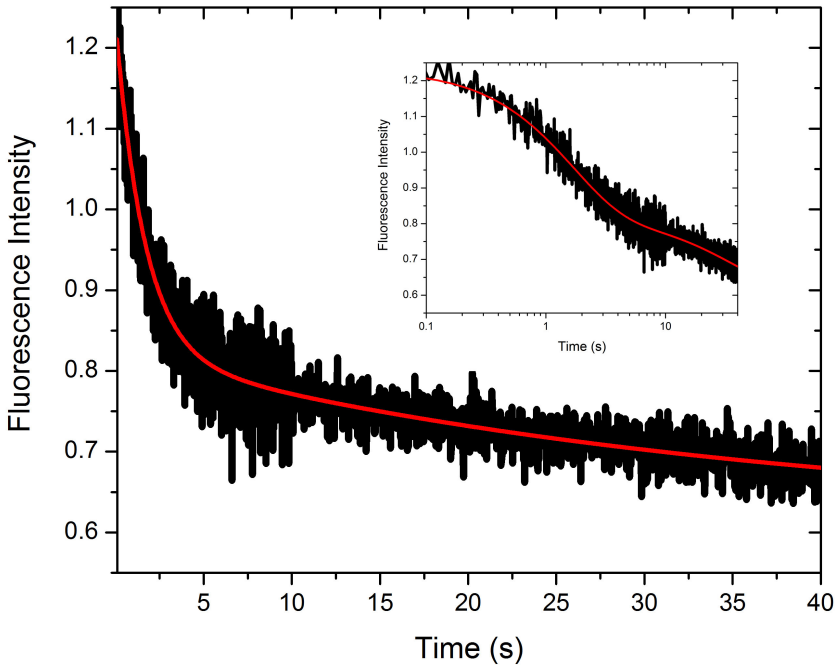

Figure 7.

A. Intrinsic fluorescence- RNAP open complexes + 1.1M salt at 37°C

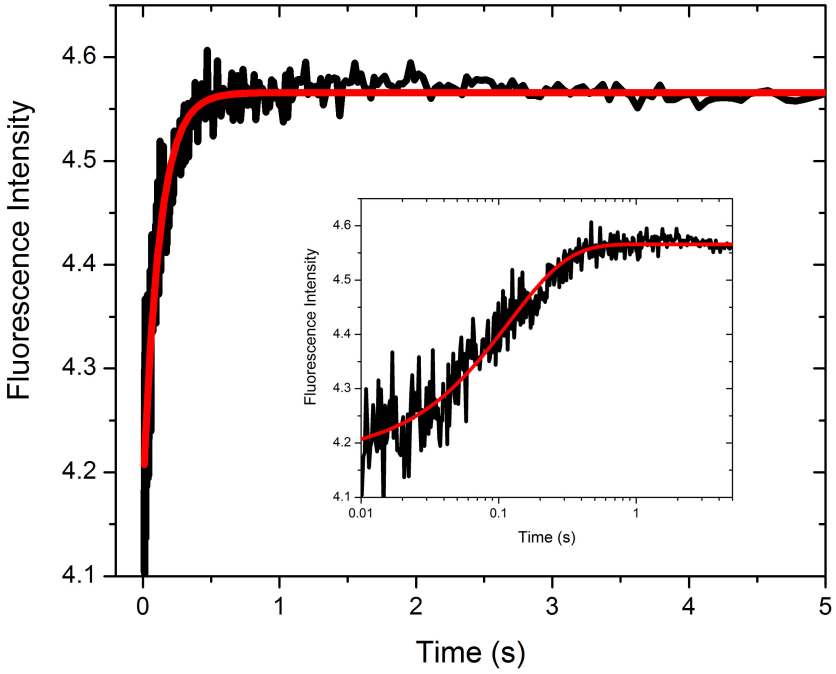

B. Intrinsic fluorescence- RNAP open complexes + 1.1M salt at 22°C

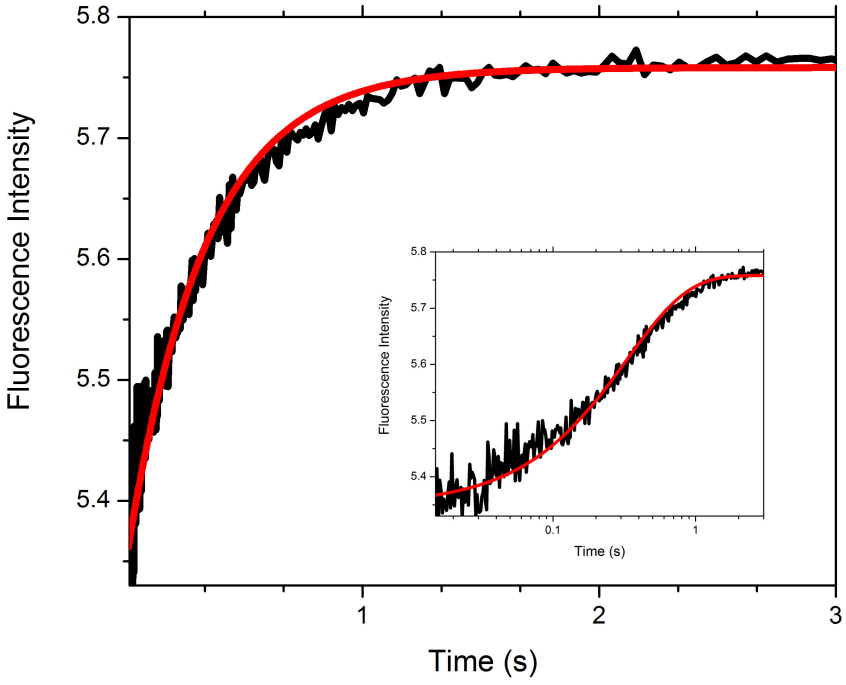

C. Intrinsic fluorescence- RNAP open complexes + 1.1M salt at 10°C

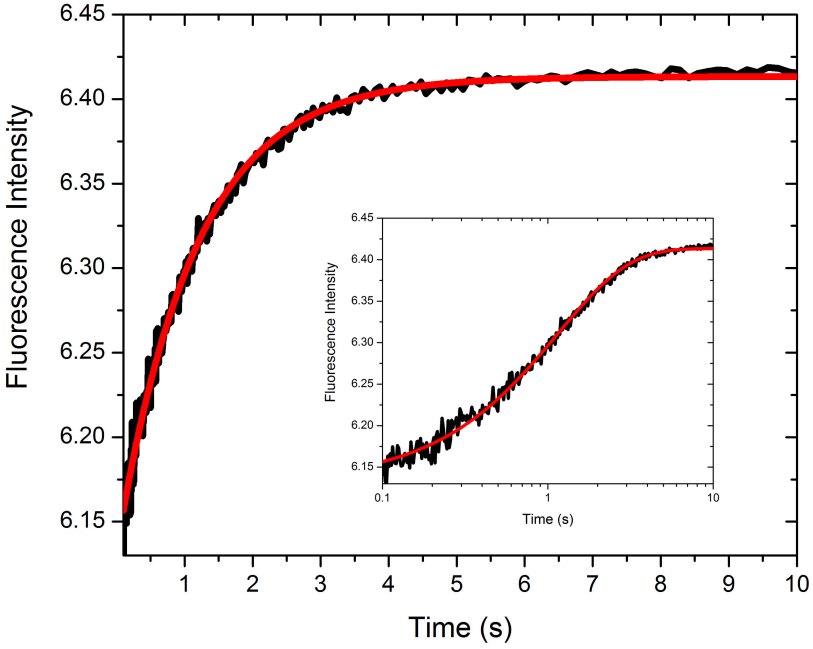

Supplemental Table 1. Compiled Kinetic Data for Intrinsic Fluorescence Experiments

[DNA] nM	k_{fast} (s^{-1})	A_{fast}	k_{slow} (s^{-1})	A_{slow}
20	0.36	0.16	0.016	0.16
20	0.12	0.11	0.010	0.16
20	0.11	0.13	0.013	0.16
50	0.86	0.16	0.016	0.17
50	0.14	0.11	0.012	0.14
50	0.14	0.068	0.012	0.08
50	0.18	0.089	0.008	0.17
50	0.27	0.050	0.014	0.08
75	0.11	0.082	0.006	0.12
75	0.22	0.078	0.011	0.10
75	0.32	0.097	0.014	0.10
100	0.58	0.15	0.015	0.18
100	0.50	0.067	0.016	0.13
100	0.41	0.22	0.016	0.11
150	0.37	0.28	0.013	0.17
150	0.44	0.18	0.011	0.10
150	0.20	0.10	0.008	0.11
200	0.35	0.20	0.010	0.06
200	0.34	0.08	0.0057	0.15
200	0.42	0.22	0.021	0.11
200	0.22	0.08	0.009	0.15
200	0.39	0.14	0.005	0.12
200	0.27	0.11	0.018	0.09

Supplemental Table 2. Compiled Kinetic Data for Beacon Fluorescence Experiments

[DNA] nM	k_{fast} (s^{-1})	A_{fast}	k_{slow} (s^{-1})	A_{slow}
20	0.16	0.35	0.024	0.24
20	0.16	0.38	0.021	0.37
50	0.38	0.48	0.024	0.32
50	0.33	0.51	0.024	0.21
50	0.11	0.62	0.011	0.22
75	0.31	0.55	0.015	0.38
75	0.28	0.63	0.016	0.26
75	0.29	0.51	0.021	0.44
150	1.41*	0.73	0.031	0.39
150	0.28	0.86	0.045	0.54
150	0.22	0.66	0.0046	0.44
200	0.34	0.91	0.057	0.51
200	0.24	1.04	0.031	0.43
200	0.24	0.97	0.023	0.54
250	0.25	1.11	0.022	0.33
250	0.36	1.09	0.025	0.65
250	0.32	0.98	0.024	0.50
300	0.32	1.05	0.11*	0.44
300	0.50	1.09	0.033	0.69

* Indicates an outlier not used in the final analysis

Chapter 5

Summary

Previously most of the information regarding the kinetics and mechanism of forming and stabilizing transcriptionally-capable open complexes between *E. coli* RNAP and the λP_R promoter was derived from filter binding assays for long-lived (open) complexes. Analysis of the behavior of the association and dissociation rate constants as a function of RNAP concentration, salt and solute concentrations and temperature demonstrated that there are a minimum of three intermediates (I_1, I_2, I_3), and that the rate determining step in both directions is the interconversion of I_1 and I_2. These kinetic data provide information about conditions and time ranges where a majority population of a single intermediate (I_1, I_2) is obtained, as well as conditions where the I_1 closed complex is thermodynamically stable.

Real time footprinting of I_1 at 17^{o}C by manual mixing (Davis *et al.* 2007) and equilibrium footprinting at 2^{o}C, using DNase, HO•, and MnO_4^- (Craig *et al.* 1995, Craig *et al.* 1998, Chapter 4), was consistent with it being an advanced closed complex, although the results were complicated by the presence of a significant subpopulation (<30%) of open complexes in the real-time experiments and by a low MnO_4^- dose in the 2^{o}C experiments. These experiments also provided the first footprinting (structural) evidence that far upstream DNA is wrapped on the backside of RNAP and that the downstream duplex was bent toward or into the cleft in this intermediate.

MnO_4^- footprinting of a burst population of I_2 (by fast mixing) demonstrated that it was the initial (unstable) open complex, in which the full 13 bp transcription bubble is formed (Chapter 2). MnO_4^- reactivities of I_2 compared to that of RP_o reveal that the template strand in I_2 may be correctly placed in the active site, but show that the discriminator region of the nontemplate strand is not yet in its final track. Effects of

stabilizing and destabilizing solutes and salts on the dissociation rate constant demonstrated that I_2 is converted to the final open complex at λP_R (designated RP_o) in at least two steps of folding/assembly/tightening of a group of DME (downstream mobile elements) on the promoter duplex downstream of the initiation bubble (Kontur et al. 2006, Kontur et al 2008, Gries *et al.* 2010).

In this thesis, I have applied four different fluorescence fast-kinetic assays together with HO• and MnO_4^- fast footprinting kinetic assays to investigate the mechanism of transcription initiation and to structurally characterize I_1 and I_2 (Chapter 2-4). Results of these assays, combined with and interpreted in the context of the previous kinetic data summarized above, lead to a proposed extension of the previously proposed mechanism to interpret irreversible forward direction kinetic data:

Previous status:

$$R + P \overset{K_1}{\leftrightarrow} I_1 \overset{k_2}{\rightarrow} I_2 \cdots\cdots \rightarrow RP_o$$

New proposal:

$$R + P \overset{K_{1,B}}{\leftrightarrow} I_{1,B} \overset{K_{B,W}}{\leftrightarrow} I_{1,w} \overset{K_{W,F}}{\leftrightarrow} I_{1,F} \overset{k_2}{\rightarrow} I_2 \cdots\cdots \rightarrow RP_o$$

(Subscript B indicates DNA bent near -11 and -38, W - bent as in B and also wrapped upstream, and F - bent and wrapped as above and also flipped at -11A.)

To obtain the above mechanism we used the following experimental results:

A) Forming The Family of I_1 Closed Complexes:

1.) Fast HO• footprinting shows that a complex with the downstream-extended, periodic protection of I_1 is formed in < 0.1 s at 19 °C, 55 nM RNAP. To obtain 90% completion of the reaction in < 0.1 s, this translates into a relaxation rate constant for establishing this equilibrium of > 23 s^{-1}. If the equilibrium constant for this first I_1 species is about 1.8 x 10^7 M^{-1} (18 μM^{-1}, see below), then the second order association rate constant for this earliest form of this intermediate is at least 2.1 x 10^8 $M^{-1}s^{-1}$ and the off rate is at least 11 s^{-1}. We use these lower bounds in the following discussion.

2.) The faster exponential rate constant k_{fast} for Cy3Cy5 FRET (either dye orientation-Chapter 3) and for the Cy3 single dye fluorescence change at +14 or +29 is 11 s^{-1} at 100 nM λP_R, 80 nM RNAP (Appendices). We hypothesize that this FRET signal originates from wrapping of DNA in the I_{1W} complex and that the decay to equilibrium process of forming this complex from reactants has a smaller relaxation rate constant than that needed to explain the formation of the •HO-observed-I_1 in 0.1 s (11 s^{-1} vs. 23 s^{-1}), even though the FRET experiment is performed at higher reactant concentrations. Assuming the equilibrium constant for formation of this bent and wrapped form of I_1 is 1.2 x 10^7 M^{-1} (i.e. 12 μM, see below), we then find that $[P]_{eq}$ = 0.065 μM, $[R]_{eq}$ = 0.045 μM, and from the decay to equilibrium equation find a second order rate constant for forming this wrapped form of I_1 from reactants of 5.8 x 10^7 M^{-1} s^{-1} and k_{-BW} = 4.7 s^{-1}. The ratio of second order rate constants for FRET and HO• is the ratio of forward and back rate constants for the $I_{1,B}$ complex: k_{BW}/k_{-B} = 0.28 but from the •HO footprint results we have found a lower bound on k_{-B} of 11 s^{-1}. If k_{-B} = 11 s^{-1} then k_{BW} = 3.2 s^{-1} and K_{BW} = 3.2/4.7 = 0.67.

3) The fast component of intrinsic ($\sigma_{2.3}$ W433) fluorescence quenching. We propose that this intrinsic signal arises due to -11A base flipping which converts I_{1W} to I_{1F}. From fitting the [DNA] dependence of the first exponential decay rate constant, we obtain a composite second order rate constant of 1.5 x 10^6 M^{-1} s^{-1} and a reverse rate constant of 0.11 s^{-1}. Values obtained by the beacon assay are similar but slightly less favorable for flipping: a composite second order rate constant of 6.8 x 10^5 M^{-1} s^{-1} and a reverse rate constant of 0.18 s^{-1}. As above, the ratio of second order rate constants for Intrinsic fluorescence and FRET is the ratio of forward and back rate constants for the $I_{1,F}$ complex: k_{WF}/k_{-BW} = 0.026. From FRET kinetics, we estimate that k_{-BW} = 4.7 s^{-1} so k_{WF} = 0.12 s^{-1} and K_{WF} = 0.12/0.11 = 1.1.

Summary (I_1): These I_1 intermediates form a nested set of equilibria, each established rapidly on the time scale of the next step, which is consistent with the observation of single exponential forward kinetics of open complex formation by filter binding (and permanganate footprinting):

$R + P \leftrightarrow I_{1,B}$: $k_{1,B} > 210\ \mu M^{-1}\ s^{-1}$; at 55 nM RNAP, $K_{1,B}[R] > 1.0$; $k_{-1,B} > 11\ s^{-1}$

$I_{1,B} \leftrightarrow I_{1,w}$: $k_{BW} = 3.2\ s^{-1}$; $k_{-BW} = 4.7\ s^{-1}$; $K_{BW} = 0.67$

$I_{1,w} \leftrightarrow I_{1,F}$: $k_{WF} = 0.12\ s^{-1}$; $k_{-WF} = 0.11\ s^{-1}$; $K_{WF} = 1.1$

Therefore we propose that a) in the time range of the relatively constant HO• footprint (0.1 s – 15 s) there exists an equilibrium mixture of these three forms of I_1, that b) bending of the downstream DNA toward/into the cleft may precede/trigger movement of the DME relay to contact the upstream wrap, and then c) once the upstream wrap is made, the -11A can flip and form $I_{1,F}$ which is poised (nucleated) to be opened in the

cleft by binding free energy. Figure 1 below incorporates these three proposed forms of I_1 into the mechanism of forming and stabilizing the open complex in transcription initiation. These hypotheses will be tested in future experiments. Simulations of these kinetics for the conditions of the experiment of this thesis are in progress (J. Murray) to test the validity of the above analysis, extend it to the interpretation of isomerization rate constants from filter binding experiments, permanganate fast footprinting experiments (Ch. 2) and the second, slow exponential phase of fluorescence kinetics experiments (Ch. 3, 4).

Figure 1. Mechanism of Formation and Stabilization of Open Complexes Between *E. coli* RNA Polymerase and Promoter DNA

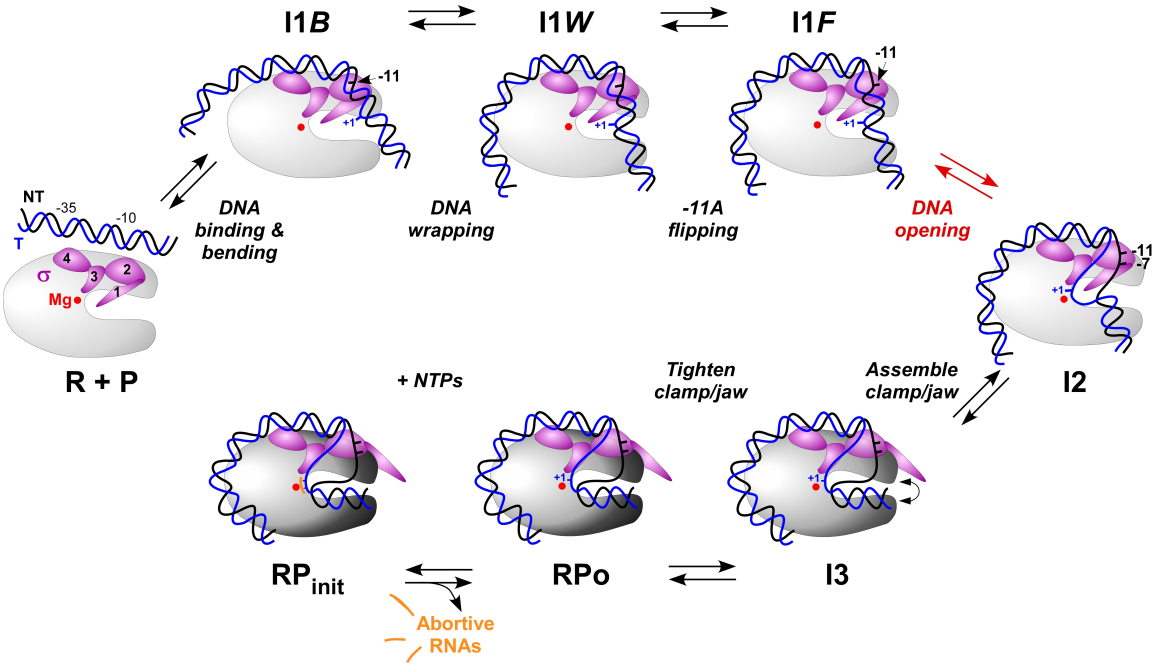

In the mechanism of Figure 1, duplex promoter DNA is first bound and bent at the upstream end of the -10 recognition region by RNAP in less than 0.1 s under the conditions investigated here. Bending places the downstream duplex (-5 to +20) in

contact with elements of RNA polymerase at the top of the active site cleft (Saecker *et al.* 2002) to form the initial I_1 complex, designated $I_{1,B}$, detected by fast HO footprinting. In the next step, on a time scale of a few tenths of a second and detected by FRET, upstream promoter DNA is tightly wrapped around the backside of RNAP to form $I_{I,W}$. Wrapping of promoter DNA is proposed to engage an upstream-downstream relay system (Davis *et al.* 2007) which allows the downstream duplex to more fully enter the RNAP active site cleft, increasing the distortion at the upstream end of the -10 region. This distortion facilitates base flipping of -11A to form $I_{1,F}$, on a time scale of a few seconds and detected by sigma W433 and TMR (beacon) fluorescence. Base flipping in turn nucleates DNA opening within the RNAP active site cleft, which occurs on a time scale of about 100 s at 19°C. All three I_1 species are in rapid equilibrium with one another and with free RNAP and promoter DNA on the time scale of DNA opening, and each I_1 intermediate appears to be in rapid equilibrium with the preceding one on the time scale of its conversion to the next. This allows the interpretation of the first exponential decay rate constant as a decay to equilibrium, used in the analysis in Chapters 3 and 4.

I_2 is the initial open complex, in which the +1 base of the template strand appears to be positioned in the environment of the active site (Gries *et al.* 2010). I_2 is relatively unstable and rapidly converts to I_3 and then RP_o. During this process downstream mobile elements of RNAP assemble on the downstream promoter DNA and the discriminator region of the melted nontemplate strand moves into its final binding track in the RNAP cleft (Drennan *et al.* submitted, Gries et al. 2010). These steps are irreversible under the solution conditions used to study the association kinetics, but can

be reversed and investigated in dissociation kinetic experiments induced by addition of a polyanionic competition like heparin or by rapid destabilization of open complexes with high salt or urea, which produces a transient burst of I_2.

References

Craig, M. L., Suh, W. C., and Record, M. T., Jr. 1995. HO• and DNase I probing of $E\sigma^{70}$ RNA polymerase-λP_R promoter open complexes: Mg^{2+} binding and its structural consequences at the transcription start site. *Biochemistry* **34:** 15624–15632.

Craig, M. L., Tsodikov, O. V., McQuade, K. L., Schlax, P. E., Jr., Capp, M. W., Saecker, R. M., and Record, M. T., Jr. 1998. DNA footprints of the two kinetically significant intermediates in formation of an RNA polymerase-promoter open complex: Evidence that interactions with start site and downstream DNA induce sequential conformational changes in polymerase and DNA. *J Mol Biol* **283:** 741–756.

Davis, C. A., Bingman, C. A., Landick, R., Record M. T., Jr., and Saecker, R. M. 2007. Real-time footprinting of DNA in the first kinetically significant intermediate in open complex formation by *Escherichia coli* RNA polymerase. *Proc Natl Acad Sci* (USA) **104:** 7833- 7838.

Gries, T. J., Kontur, W. S., Capp, M. W., Saecker, R. M., and Record, M. T., Jr. 2010. One-step DNA melting in the RNA polymerase cleft opens the initiation bubble to form an unstable open complex. *Proc Natl Acad Sci (USA)* **107:** 10418-10423.

Kontur W.S., Capp, M.W., Gries, T.J., Saecker, R.M., and Record, M.T., Jr. 2010. Probing DNA binding, DNA opening, and assembly of a downstream clamp/jaw in Escherichia coli RNA polymerase-lambdaP(R) promoter complexes using salt and the physiological anion glutamate. *Biochemistry.* **49:** 4361-73.

Kontur, W. S., Saecker, R. M., Capp, M. W., and Record, M. T., Jr. 2008. Late steps in the formation of *E. coli* RNA polymerase-λP_R promoter open complexes: Characterization of conformational changes by rapid [perturbant] upshift experiments. *J Mol Biol* **376:** 1034–1047.

Kontur, W. S., Saecker, R. M., Davis, C. A., Capp, M. W., and Record, M. T., Jr. 2006. Solute probes of conformational changes in open complex (RP_o) formation by *Escherichia coli* RNA polymerase at the λP_R promoter: Evidence for unmasking of the active site in the isomerization step and for large-scale coupled folding in the subsequent conversion to RP_o. *Biochemistry* **45:** 2161–2177.

Saecker, R. M., Tsodikov, O. V., McQuade, K. L., Schlax, P. E., Jr., Capp, M. W., and

Record, M. T., Jr. 2002. Kinetic studies and structural models of the association of *E. coli* σ^{70} RNA polymerase with the λP_R promoter: Large scale conformational changes in forming the kinetically significant intermediates. *J Mol Biol* **319:** 649–671.

Appendices

1. Temperature dependence of equilibrium “beacon” RNAP fluorescence and of permanganate reactivity for RNAP-λP_R promoter DNA complexes at a range of temperatures from 2-37°C
2. Preliminary determinations of the association kinetics of RNAP with the λP_R promoter utilizing Cy3 fluorescent probes located at (-100), (+14) or (+29) relative to the start site of transcription
3. Preliminary determinations of the association and dissociation kinetics of RNAP with the T7A1 promoter at 19°C and 37°C using the RNAP “beacon” assay
4. Preliminary determinations of the association kinetics of RNAP with the *rrnB* P1 promoter in the presence and absence of initiating nucleotides ATP and CTP at 37°C using the RNAP “beacon” assay

5. Determination of the rates of GTP incorporation at the +3 position at the λP_R promoter at 5, 10, 25, and 37°C using thin layer chromatography
6. Effect of nucleotides and of heparin on promoter DNA wrapping around RNAP as monitored by equilibrium and real-time FRET
7. Comparison of amounts of long and short transcripts produced by WT RNAP at the λP_R promoter under single round conditions at 10°C and 37°C

Appendix 1

Temperature dependence of equilibrium "beacon" RNAP fluorescence emission and of permanganate reactivity for RNAP-λP_R promoter DNA complexes at a range of temperatures from 2-37°C.

Are there significant differences in the nature of the open complex at different temperatures? Dissection of the kinetics of dissociation of λP_R open complexes at 10°C and 37°C revealed that the much larger dissociation rate constant at 10°C resulted from a much smaller stabilization of the initial open complex by assembly of the downstream jaw/clamp and rearrangement of the discriminator region of the nontemplate strand in the cleft at 10°C than at 37°C (Kontur *et al.* 2008). This reduced stabilization at 10°C is similar to the loss of stabilization of the initial open complex when the downstream jaw is deleted (Drennan *et al.* in preparation) and with that of the late open intermediate I_3. Equilibrium FRET experiments at temperatures from 2°C to 37°C (Chapter 3), after correction for large temperature dependences of the fluorescence of both Cy3 and Cy 5, reveal that the FRET effect increases with increasing temperature, which could result from a reduction in distance between the FRET probes with increasing temperature. The experiments in this and some subsequent appendices (5, 6, 8) were performed in part to test whether there are other significant differences between the 10°C and 37°C open complexes.

Here, we monitor the equilibrium beacon fluorescence of RNAP- λP_R complexes at equilibrium at a range of temperatures from 2-37°C (Figure 1). We also use constant-dose permanganate footprinting to characterize the population of open complexes (with reactive thymines on the template strand in the transcription bubble) formed under

equilibrium conditions at four different temperatures in this range: 2, 10, 19 and 37°C (Figure 2). In previous (unpublished) studies, M. Capp in our laboratory determined the temperature dependence of the second order rate constant for the reaction of permanganate with TMP; this rate constant is very small (on the order of 1 – 10 M^{-1} s^{-1}) and increases with increasing temperature, with an activation energy of ~9 kcal/ mole or an increase in the rate constant of nearly 2-fold for every 10°C. In our permanganate footprinting experiments as a function of temperature, concentrations of MnO_4^- were adjusted to provide the same dose of permanganate at each temperature (dose= rate constant × [MnO_4^-] × time) allowing us to directly compare the extent of opening at different temperatures, and compare these results with those obtained by TMR (beacon) fluorescence and other assays.

Results

Temperature Dependence of TMR Fluorescence in RNAP-Promoter Complexes

In the salt-upshift dissociation TMR (beacon) kinetic experiments at 19°C, no change in fluorescence is observed in the rapid conversion of the stable open complexes (I_3, RP_o) to the unstable open intermediate I_2 (Chapter 4). Hence the TMR fluorescence of I_2 is that same as that of I_3 and RP_o. How does the TMR fluorescence signal of open complexes change with temperature?

Figure 1 shows that there is an increase in beacon fluorescence as a function of temperature. We find that the beacon probe can detect three populations of fluorescent complexes. The first is formed at temperatures from 2-10°C and exhibits the lowest fluorescence emission intensity. The second population occurs from >10°C to approximately 30°C and has an intermediate fluorescence value. The last population

occurs at >30°C to 37°C and has the highest fluorescence intensity. We speculate that these three fluorescence phases may in fact represent the different populations of RNAP-promoter DNA complexes (I_1, I_2, I_3, and RP_o). From Chapter 4, we know that I_1 and I_2 have different "beacon" RNAP fluorescence intensities, due to structural differences in the -10 promoter DNA. In $I_{1,\ flipped}$, the -11A base is flipped out of the base stack, where it interacts with W433. During formation of the early open complex I_2, movements of the nontemplate strand result in a second, equally large, fluorescence increase. However, from the equilibrium temperature series, we hypothesize that late open complexes I_3 and RP_o may have different interactions and/or conformations of $\sigma_{2.3}$ with the -10 element than I_1 or I_2, at least at temperatures > 30°C. Our lab is currently investigating these findings.

At 2°C, where I_1 is the only promoter complex, we find that there is no permanganate reactivity, confirming that the promoter DNA is closed in this complex (Figure 2, Lanes 2-4). For promoter complexes formed at 10, 19 and 37°C, permanganate reactivity is observed for all four thymines on the template strand (-11, -9, -8, and +1). The extent of the reactivity for all four thymines increases significantly from 10°C to 19°C and also from 19°C to 37°C. We interpret these changes as a shift in the population of open complexes from a majority of I_3 (10°C) to a majority RP_o (37°C). At 19°C the open complex population is a mixture of I_3 and RP_o.

Methods

Beacon fluorescence experiments

Equilibrium fluorescence measurements were collected on a single beam fluorimeter (Photon Technology International) equipped with an 814 Photomultiplier

Detection system and a peltier heating and cooling block connected to an external temperature control (Quantum Northwest). A nitrogen airflow system was also used at low temperatures (<10°C) to prevent condensation in the cuvette. The samples were excited at 550 and sample emission was collected using the instrument monochromator from 555 to 700 nm.

Permanganate footprinting

Permanganate footprinting of RNAP- promoter DNA complexes was performed as described in Davis *et al.* 2007, with the modification that a range of [$NaMnO_4^-$] were used in order to provide a constant dosage of permanganate reactivity (2mM at 37°C, 6mM at 19°C, 8mM at 10°C, and 10-12mM at 2°C). Briefly, RNAP-promoter DNA complexes were formed at the temperature of interest for 1.5 hours and then challenged with 50ug/ mL heparin (final concentration) for 10 seconds before mixing with $NaMnO_4^-$ for 10 seconds. The reactions were quenched using a 2.4M beta-mercaptoethanol and 6.25 M NH_4OAc

solution, ethanol precipitated, reacted with 1M piperidine, and were resuspended in gel loading buffer and run on an 8% polyacrylamide sequencing gel. The gels were analyzed using ImageQuant software.

Figure Captions

Figure 1. Fluorescence of beacon RNAP- promoter DNA complexes as a function of temperature. Complexes (100nM RNAP σ^{70}211-Cys-TMR, 200nM LPR promoter DNA) were equilibrated for 1.5 hours and then emission scans were performed as a function of temperature. The emission spectra at each temperature was normalized relative to a control experiment containing RNAP only (no promoter DNA) at each temperature in order to adjust for differences in TMR emission at each temperature (A). Two experimental replicates were averaged to produce the curves shown. The averaged normalized peak emission at 572 is plotted as a function of temperature in (B).

Figure 2. Permanganate reactivity of RNAP- promoter DNA complexes. Complexes (50nM active RNAP, <1nM promoter DNA) were equilibrated at the temperature of interest for 1.5 hours and then mixed with $NaMnO_4^-$ for 10 seconds. The concentration of $NaMnO_4^-$ was titrated in order to keep the reactivity dosage constant. Reactions were quenched using a 2.4M beta-mercaptoethanol and 6.25M NH_4OAc solution, ethanol precipitated and resuspended. The solutions were reacted with 1M piperidine, ethanol precipitated, resuspended in loading buffer and run on an 8% polyacrylamide sequencing gel.

Figure 1

A.

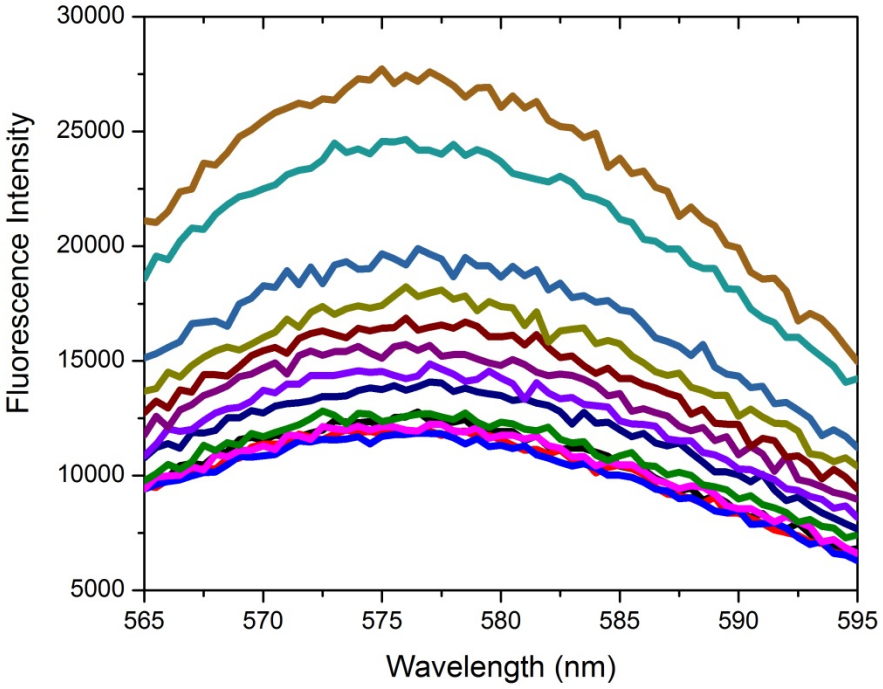
Fluorescence Intensity
30000
25000
20000
15000
10000
5000
565
570
575
580
585
590
595
Wavelength (nm)

B.

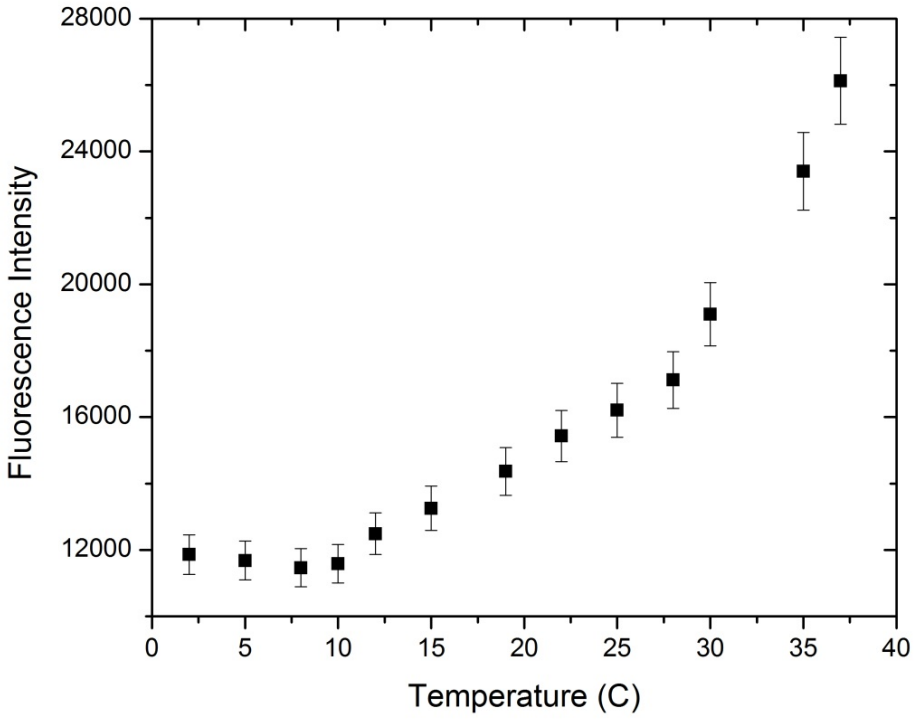
Fluorescence Intensity
28000
24000
20000
16000
12000
0
5
10
15
20
25
30
35
40
Temperature (C)

Figure 2. MnO_4^- footprinting of RNAP-promoter DNA complexes at different temperatures

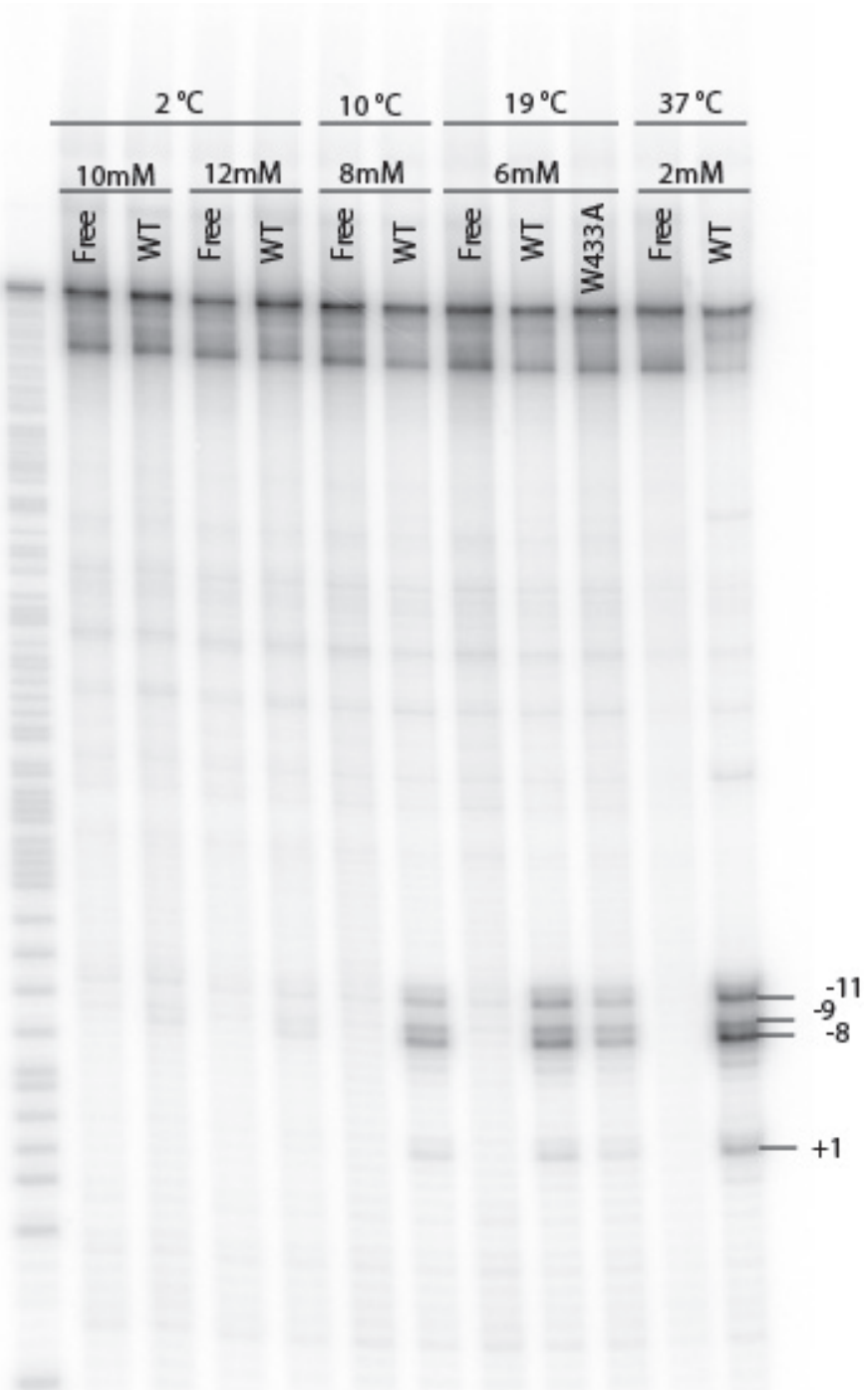

Appendix 2

Preliminary determinations of the association kinetics of RNAP with the λP_R promoter utilizing Cy3 fluorescent probes located at (-100), (+14) or (+29) relative to the start site of transcription

In Chapter 3, I found that Cy3 dyes located in or near the RNAP binding track (-100 or +14) on promoter DNA exhibit a large fluorescence emission increase due to RNAP binding. The effects are large and specific; the initial increase in Cy3 emission is most likely due to a direct interaction of the Cy3 dye with RNAP or a local change in environment arising from the close proximity of RNAP with Cy3 after binding to promoter DNA. Cy3 can exhibit an increased quantum yield when bound directly to (Gruber *et al.* 2000) or near (Fischer *et al.* 2012) proteins. Protein binding changes the local environment of the probe and is thought to inhibit the photo-induced isomerization of Cy3 from the trans (photoactive) to cis (photoinactive dark state) conformation (Levitus and Ranjit, 2011). Previous work in our lab has shown that the downstream footprint of RNAP extends to approximately -81 in the early closed intermediate I_1 and to ~-65 in the final open complexes RP_o.

We sought to use Cy3 probes to detect specific RNAP-promoter DNA interactions in different regions (upstream and downstream) of the promoter DNA. We designed λP_R promoter DNA constructs with a single Cy3 dye located at either (-100), (+14) or (+29) relative to the start site of transcription. This was accomplished by purchasing PCR primers for the nontemplate (upstream) and template (downstream) strands, one of which contained an internal Cy3 dye (/iCy3/ modification from Integrated DNA Technologies, Coralville, IA). The dyes are covalently attached so that they bridge

the phosphate backbone of the 5' end of one nucleotide and the 3'-OH of the second base. Therefore these dyes are rigid and not freely rotating.

We monitored the kinetics of promoter DNA-RNAP association in real-time at 19°C using stopped-flow fluorescence. We rapidly mixed a high concentration of RNAP (800nM final concentration) with 100nM λP_R promoter DNA (final concentration) and monitored the changes in emission of the Cy3 dye as a function of time. Association kinetics for all Cy3 dye positions exhibit a rapid double exponential increase in fluorescence (positive amplitude) (Figure 1A-C, Table 1).

We find that the fastest rate of association occurs with the -100 Cy3 probe and the slowest with +29 labeled promoter DNA. This may indicate that interactions of RNAP with promoter DNA originate on the upstream end of the DNA and proceed in the upstream to downstream direction. However, given that we show in Chapter 2, that I_1, with both the upstream and downstream DNA regions bound to RNAP, is detected as early as 100 milliseconds after mixing 55nM of RNAP with <1nM promoter DNA, is it surprising that we are able to monitor any difference in the rates of association for the upstream and downstream DNA regions. However, it is possible that the Cy3 fluorophores are able to pick up changes in the interactions of RNAP with promoter DNA that are undetectable in the fast footprinting assays. Our lab is currently pursuing experiments utilizing a range of [RNAP] in order to investigate the kinetics of association with each promoter DNA position (-100, +14 and +29).

Figure 1.

A. Association of 80nM RNAP with -100 Cy3 promoter DNA (100nM) at 19°C

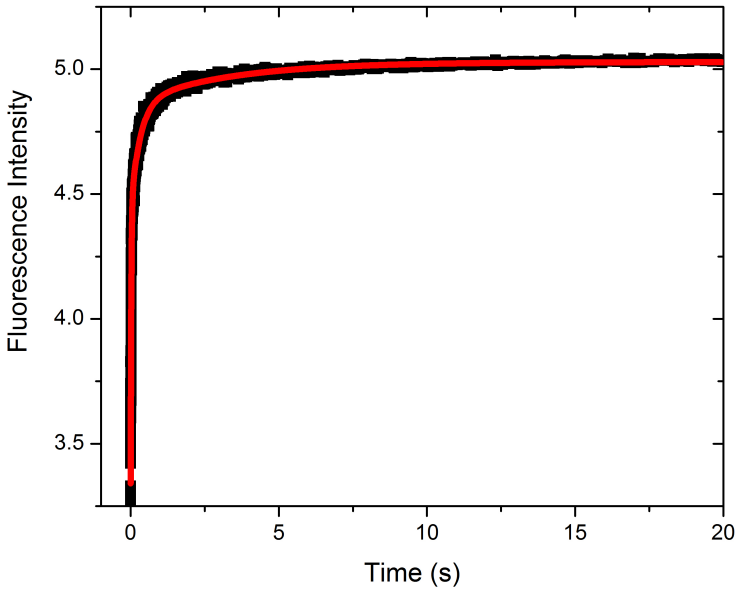

B. Association of 80nM RNAP with +14 Cy3 promoter DNA (100nM) at 19°C

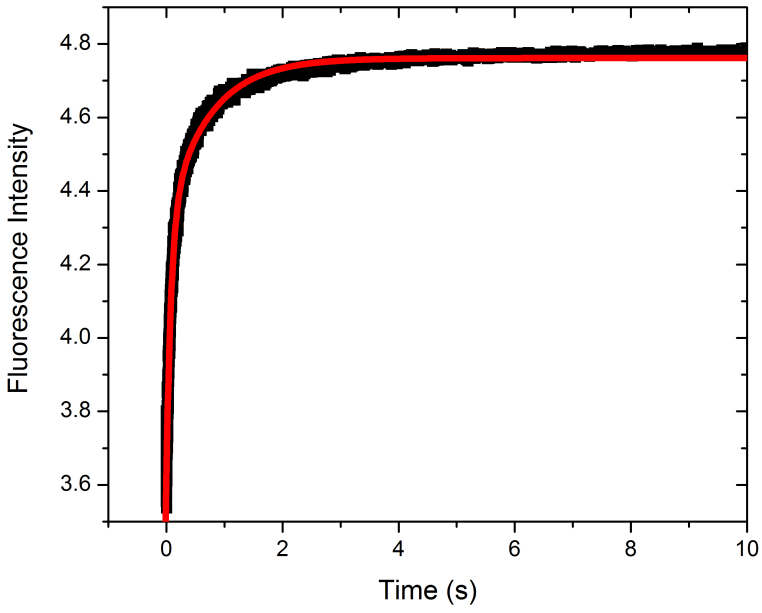

C. Association of 80nM RNAP with +29 Cy3 promoter DNA (100nM) at 19°C

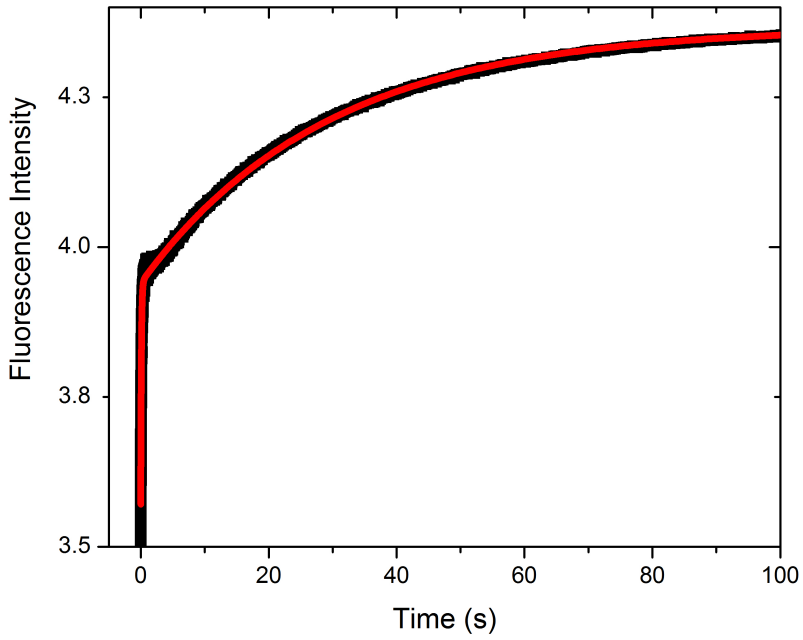

Table 1. Rates of Association for 80nM RNAP and 100nM Cy3 labeled promoter DNA at 19°C for various Cy3 positions

Cy3 Position	k_{fast} (s^{-1})	k_{slow} (s^{-1})
-100	50 (± 8.0)	1.58 (± 0.9)
+14	12.5 (± 3.2)	1.39 (± 0.6)
+29	10.4 (± 2.2)	0.03 (± 0.05)

Appendix 3

Preliminary determinations of the association and dissociation kinetics of RNAP with the T7A1 promoter at 19°C and 37°C using the RNAP "beacon" assay

During normal cellular function, *Escherichia coli* RNA polymerase (RNAP) binds the specificity unit σ^{70} to constitute an active transcription molecular machine leading to the synthesis of specific structural and messenger RNA essential to life. Other sigma factors in *E. coli* direct cellular adaption to a variety of environmental conditions and stresses (e.g. σ^{54} in nitrogen utilization, σ^{32} heat shock response, etc.). Regulation of bacterial gene expression is tightly controlled at all levels. A first level of regulation is provided by promoter-specific rates of recognition and initiation. Further levels of regulation are afforded by a variety of other DNA binding proteins (e.g. *lac* repressor), which can modify promoter accessibility, or effector proteins (e.g. ppGpp and DksA), which can modulate the activity of RNAP itself. However, much less known about the key parameters leading to intrinsic differences in rates of initiation at various promoters.

Studies of transcription initiation at the λP_R promoter suggest that a minimum of three steps with at least two kinetically significant intermediates are required to form a stable open complex that initiates transcription on addition of nucleotides (Saecker *et al.* 2011 and references therein). The process begins with promoter recognition and association of RNAP with promoter DNA. The first complex, typically called RP_c, represents an initial collision complex. This complex may involve contacts of the -35 and -10 promoter DNA elements with RNAP σ^{70} regions 4 and 2, and/or contacts between the α subunit C-terminal domains (αCTD) and upstream DNA. RP_c rapidly interconverts with the closed intermediate I_1 in which contacts between the σ^{70} subunit and the -10

region of the promoter create a ~90˚ bend in promoter DNA. As a result, downstream duplex DNA (to at least position +20) is directed into the active site cleft of RNAP (Davis *et al.* 2007). In the next step, 13 base pairs of DNA from the -10 region to the start site of transcription (+1) are opened to form the relatively unstable open complex I_2; this step is the rate-limiting step of the overall process at λP_R. Subsequently I_2 rapidly converts to the stable open complex RP_o, which is able to initiate RNA synthesis upon the addition of nucleotides. After making (and often releasing) a short RNA transcript, RNAP breaks free from the promoter to begin processive elongation.

Crucial to regulation of transcription initiation is a detailed understanding of the rate-limiting step during the process of forming transcription-competent complexes. At the λP_R promoter, melting of 13 base pairs of DNA (-11 to +2) occurs in this step. Currently, the general mechanism of DNA opening is not well understood. Two models have been proposed to describe this process. The active model, based on work at the λP_R promoter, proposes that RNAP actively nucleates DNA after the duplex DNA has been bound inside the RNAP active site cleft. In this model, base flipping at position -11 occurs after binding DNA into the cleft in I_1. DNA opening then occurs in one step within the cleft through interactions with RNAP. An alternative model, based upon molecular dynamics simulations (Chen *et al.* 2010) and work at the T7A1 promoter (Rogozina *et al.* 2009) suggests that DNA opening is passive and occurs outside the active site cleft of RNAP via thermal breathing. In the active model, DNA melting is proposed to be rate-limiting. In the passive model, capture of single-stranded non-template DNA by the σ subunit and/or entry of single-stranded template DNA into the active site cleft are presumed to be rate-limiting.

Differences in sequence between the λP_R and T7A1 promoters do not easily explain the experimental results leading to these two models. Both T7A1 and λP_R are strong $E\sigma^{70}$ promoters capable of forming stable open complexes without the need of accessory proteins (Saecker *et al*. 2011, Rogozina *et al.* 2009). λP_R has a near consensus -10 element (GATAAT); in contrast, the T7A1 promoter has -10 element sequence GATACT in addition to an AT rich UP element. Also, the length of the discriminator (region between -10 element and start site) and sequence differ. The λP_R discriminator is more like the consensus 7 bp $E\sigma^{70}$ discriminator whereas T7A1 has a poor 6 bp discriminator. It is possible that these differences in sequence in or near the -10 hexamer affect the mechanism of DNA opening at these two promoters.

Here, we have used real-time stopped-flow “beacon” RNAP association assays with the T7A1 promoter in order to determine the timing of promoter DNA bending and opening. RNAP is rapidly mixed with the T7A1 promoter and the kinetics of the change in fluorescence was monitored as a function of time (Figure 1). The kinetics of association of the beacon RNAP (σ70–211TMR) with the T7A1 promoter are determined for a range of DNA concentrations from 50 to 250nM. RNAP holoenzyme (containing σ70–211TMR) is rapidly mixed with LPR at 19°C or 37°C in transcription buffer using the Kintek SFX-300 stopped flow (see Methods). The samples are excited at 550 and emission monitored above 565 nm using a long-pass filter. A representative kinetic curve is shown in Figure 1. The association of promoter DNA with RNAP increases the fluorescence of the TMR beacon probe.

For one loading of reagents, three to five repeat shots are taken for each set of samples. The shots were then averaged to increase the signal to noise ratio of the data.

Fitting to kinetic traces is done using Origin 8 software using the equation for the sum of two exponentials:

$$F = F_0 + A_{fast} \exp(-k_{fast} t) + A_{slow} \exp(-k_{slow} t) \qquad \text{(Equation 1)}$$

After determining the observed k_{fast} and k_{slow} from the fits to each kinetic trace, the observed rates were plotted as a function of [DNA] (Table 1, Figure 2). The data at both temperatures are best described by a fit to the sum of two exponentials, with an observed fast phase (k_{fast}) that is DNA- concentration dependent and a slower phase (k_{slow}) that is also DNA-concentration dependent.

At 19°C, the best-fit line to k_{fast} vs. [DNA] is $y = 8.2 \times 10^5\ M^{-1}\ s^{-1} + 0.107\ s^{-1}$. This yields a $K_1 = 7.7 \times 10^6\ M^{-1}$ and a $k_{-1} = 0.107\ s^{-1}$ (Table 3). k_{slow} vs. [DNA] also yielded a linear increase with the best-fit line $y = 8.0 \times 10^4\ M^{-1}\ s^{-1} + 0.018\ s^{-1}$; therefore $K_2 = 4.4 \times 10^6\ M^{-1}$ and a $k_{-2} = 0.018\ s^{-1}$. Although it is somewhat surprising that both k_{fast} and k_{slow} are [DNA]- dependent, this may be because there are a series of nested rapid equilibria, with two complexes that are in rapid equilibrium with free promoter DNA and RNAP.

At 37°C, the best-fit line to k_{fast} vs. [DNA] is $y = 2.3 \times 10^6\ M^{-1}\ s^{-1} + 0.374\ s^{-1}$. This yields a $K_1 = 6.3 \times 10^7\ M^{-1}$ and a $k_{-1} = 0.374\ s^{-1}$ (Table 3). k_{slow} vs. [DNA] also yielded a linear increase with the best-fit line $y = 2.7 \times 10^5\ M^{-1}\ s^{-1} + 0.047\ s^{-1}$; therefore $K_2 = 5.9 \times 10^6\ M^{-1}$ and a $k_{-2} = 0.047\ s^{-1}$. These experiments are intriguing, but require replication and also comparison to fast footprinting and nitrocellulose filter binding experiments with the T7A1 promoter in order to deduce the complete mechanism of isomerization of RNAP and to compare it with the mechanism at λP_R.

Figure Captions

Figure 1. Association of 10nM beacon RNAP with 100nM T7A1 at 19°C. Representative kinetic data for formation of open complexes at the T7A1 promoter. 100nM T7A1 promoter DNA (final concentration) was rapidly mixed with 10nM active RNAP σ^{70}211-Cys-TMR at 19°C using a Kintek SFX-300 stopped-flow spectrophotometer. For each loading of sample reagents, 3-5 replicate shots were averaged to generate the curves depicted. The data were best fit to a sum of two exponentials; the best-fit line to the data is shown in red. The same data is plotted on a log time scale in the insert.

Table 1. Association rates (k_{fast} and k_{slow}) at 19°C. Observed forward rate constants k_{fast} and k_{slow} as determined from the best-fit lines to association kinetic data at a range of T7A1 promoter [DNA] (50-250 nM).

Figure 2. Observed forward rate constants k_{fast} and k_{slow} as a function of T7A1 promoter [DNA] at 19°C Observed forward rate constants k_{fast} and k_{slow} were determined from the best-fit lines to association kinetic data for beacon RNAP σ^{70}211-Cys-TMR at a range of T7A1 promoter [DNA] (50-250 nM). Best fit lines are shown. (A) k_{fast} and (B) k_{slow}.

Figure 3. Association of 10nM beacon RNAP with 100nM T7A1 at 37°C. Representative kinetic data for formation of open complexes at the T7A1 promoter. 100nM T7A1 promoter DNA (final concentration) was rapidly mixed with 10nM active RNAP σ^{70}211-Cys-TMR at 19°C using a Kintek SFX-300 stopped-flow spectrophotometer. For each loading of sample reagents, 3-5 replicate shots were averaged to generate the curves depicted. The data were best fit to a sum of two

exponentials; the best-fit line to the data is shown in red. The same data is plotted on a log time scale in the insert.

Table 2. Association of 10nM beacon RNAP with T7A1 at 37°C

Observed forward rate constants k_{fast} and k_{slow} as determined from the best-fit lines to association kinetic data at a range of T7A1 promoter [DNA] (50-225 nM).

Figure 4. Observed forward rate constants k_{fast} and k_{slow} as a function of T7A1 promoter [DNA] at 37°C Observed forward rate constants k_{fast} and k_{slow} were determined from the best-fit lines to association kinetic data for beacon RNAP σ^{70}211-Cys-TMR at a range of T7A1 promoter [DNA] (50-225 nM). Best-fit lines are shown. (A) k_{fast} and (B) k_{slow}.

Figure 5. Dissociation of RNAP from T7A1 at 37°C. Representative kinetic data for dissociation of beacon RNAP σ^{70}211-Cys-TMR open complexes following a 1.1M NaCl upshift. Open complexes containing 100nM total RNAP σ^{70}211-Cys-TMR and 50nM T7A1 promoter DNA were equilibrated at 37°C for a minimum of one hour. Open complexes were then rapidly mixed with 1.1M NaCl (final concentration), which destabilizes the final open complexes (RP_o and I_3) and creates a burst in the population of the early open complex, I_2. The samples were excited at 550nm and the emission of TMR monitored using a 565 LP filter. The best-fit line to the data is shown the red and the inserts depict the same data plotted on a log time scale. Curves were best fit to a single exponential.

Table 3. Compiled Kinetic Data for T7A1. Rate and equilibrium constants for the association of RNAP with T7A1 at 19°C and 37°C

Figure 1. Association of 10nM "beacon" RNAP with 100nM T7A1 at 19°C

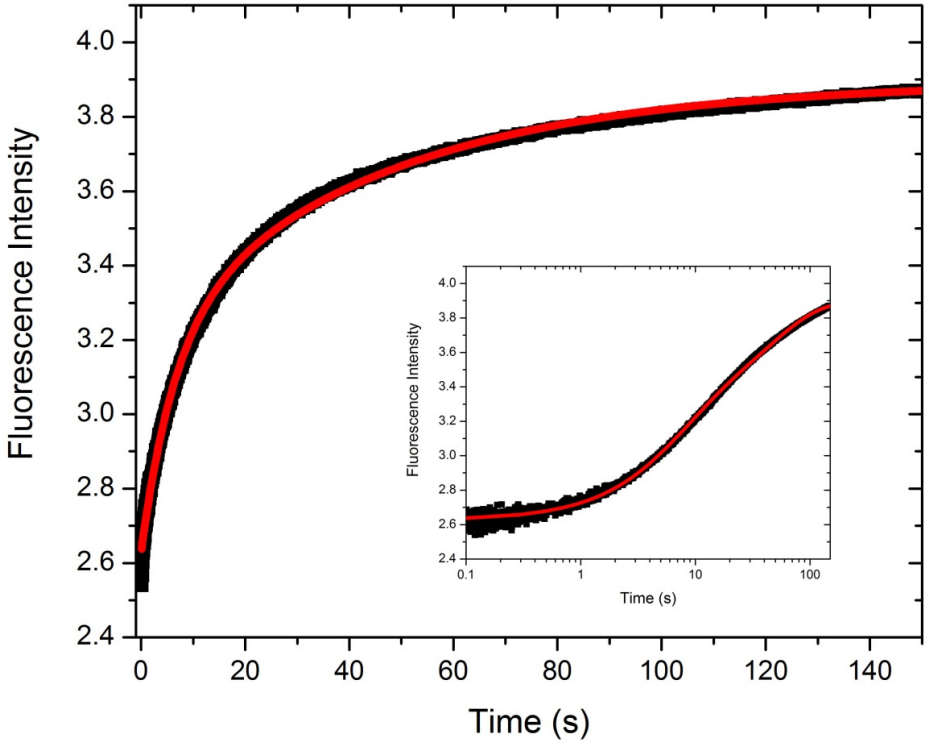

Table 1. Association kinetics of RNAP with the T7A1 promoter at 19°C

T7A1 promoter [DNA] nM	k_{fast} (s^{-1})	A_{fast}	k_{slow} (s^{-1})	A_{slow}
50	0.17	0.47	0.027	0.76
100	0.16	0.58	0.022	0.68
200	0.36	0.55	0.035	1.3
250	0.30	0.66	0.041	1.2

Figure 2

A.

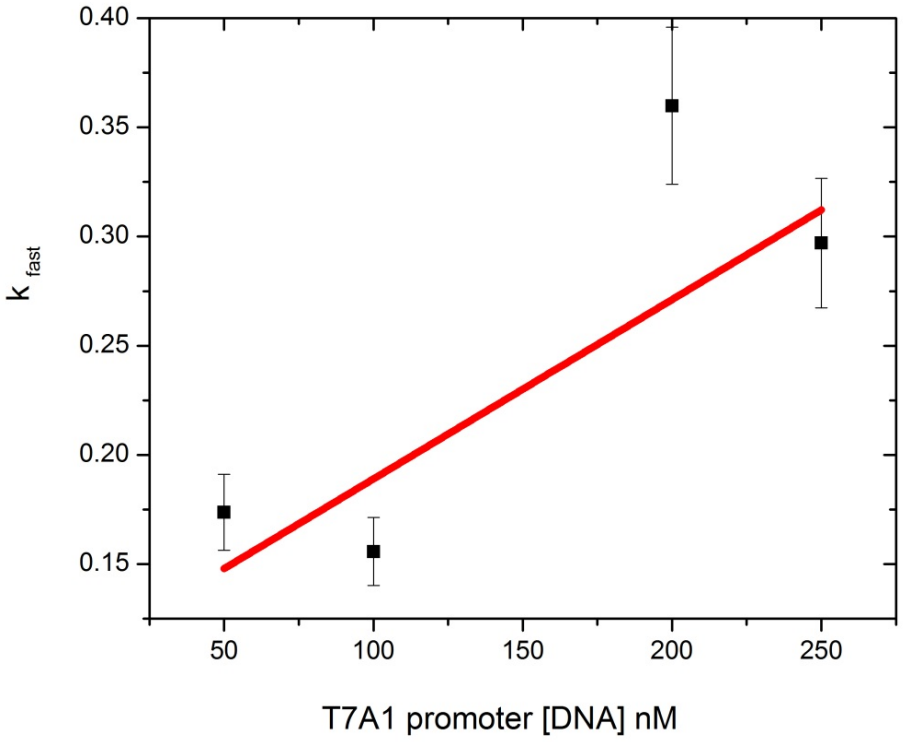
0.40
0.35
0.30
0.25
0.20
0.15
k fast
50
100
150
200
250
T7A1 promoter [DNA] nM

B.

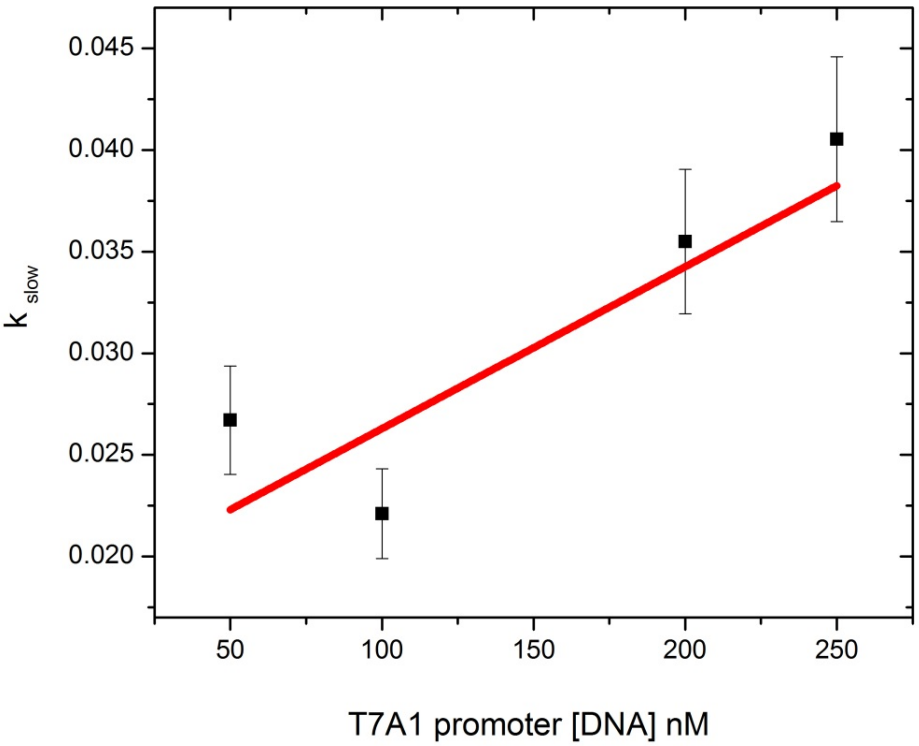
0.045
0.040
0.035
0.030
0.025
0.020
k slow
50
100
150
200
250
T7A1 promoter [DNA] nM

Figure 3. Association of 10nM "beacon" RNAP with 100nM T7A1 at 37°C

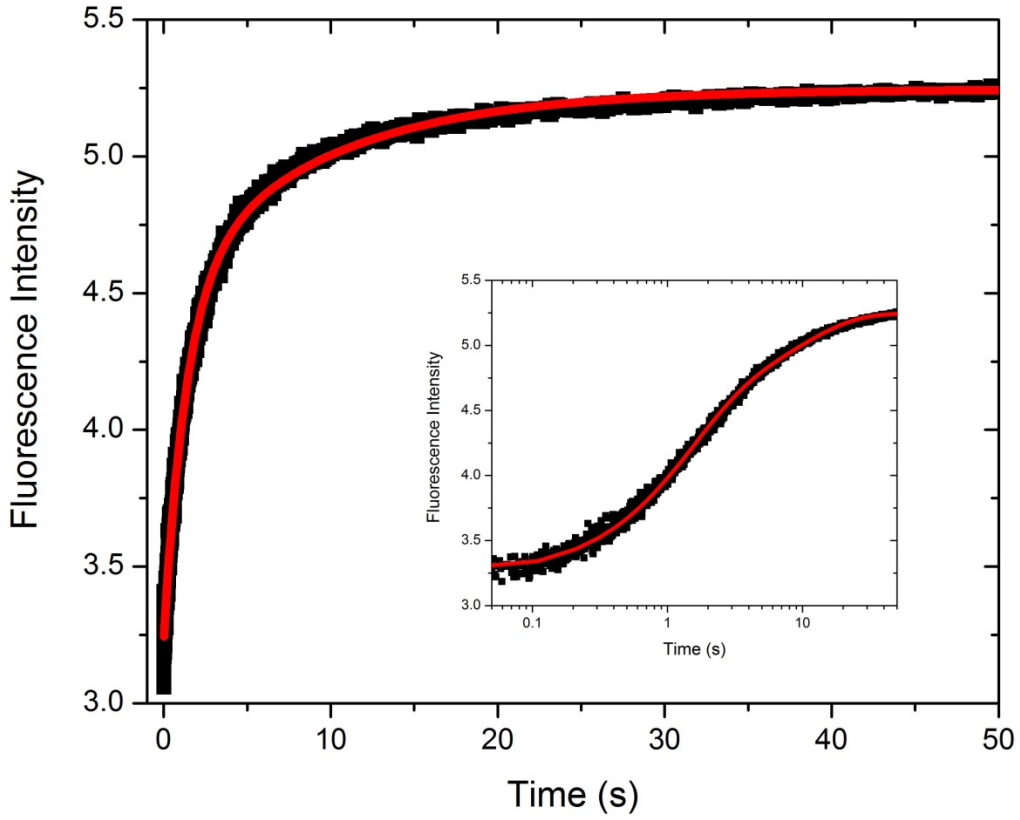

Table 2. Association kinetics of 10nM "beacon" RNAP with T7A1 at 37°C

T7A1 promoter [DNA] nM	k_{fast} (s^{-1})	A_{fast}	k_{slow} (s^{-1})	A_{slow}
50	0.51	1.4	0.070	0.99
100	0.65	1.3	0.090	0.68
125	0.58	1.6	0.059	0.45
150	0.73	1.3	0.11	0.72
200	0.86	1.8	0.10	0.73
225	0.95	1.4	0.14	0.88

Figure 4.
A.

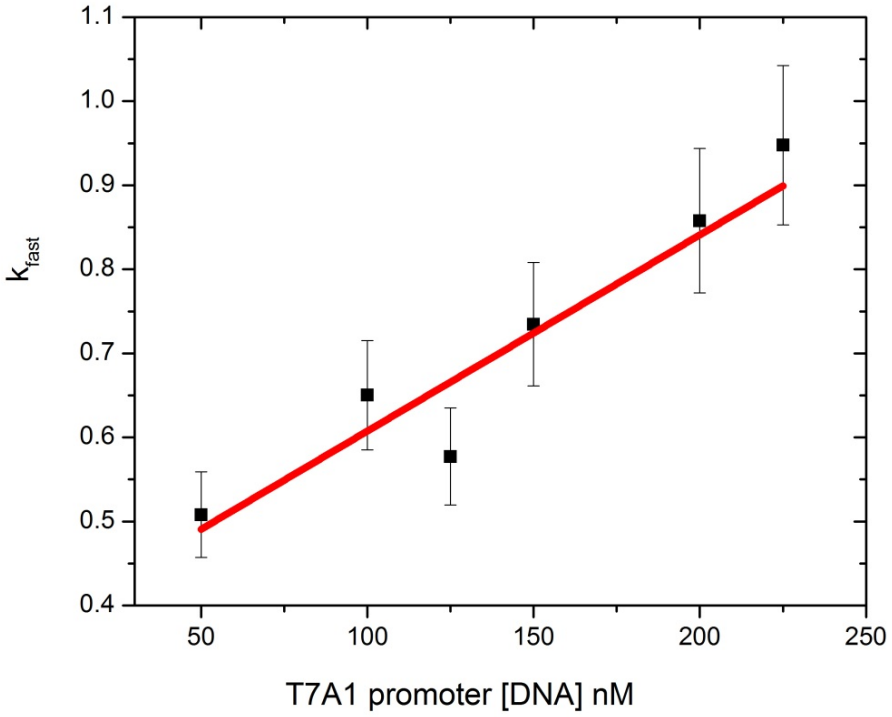
1.1
1.0
0.9
0.8
0.7
0.6
0.5
0.4
k_{fast}
50
100
150
200
250
T7A1 promoter [DNA] nM

B.

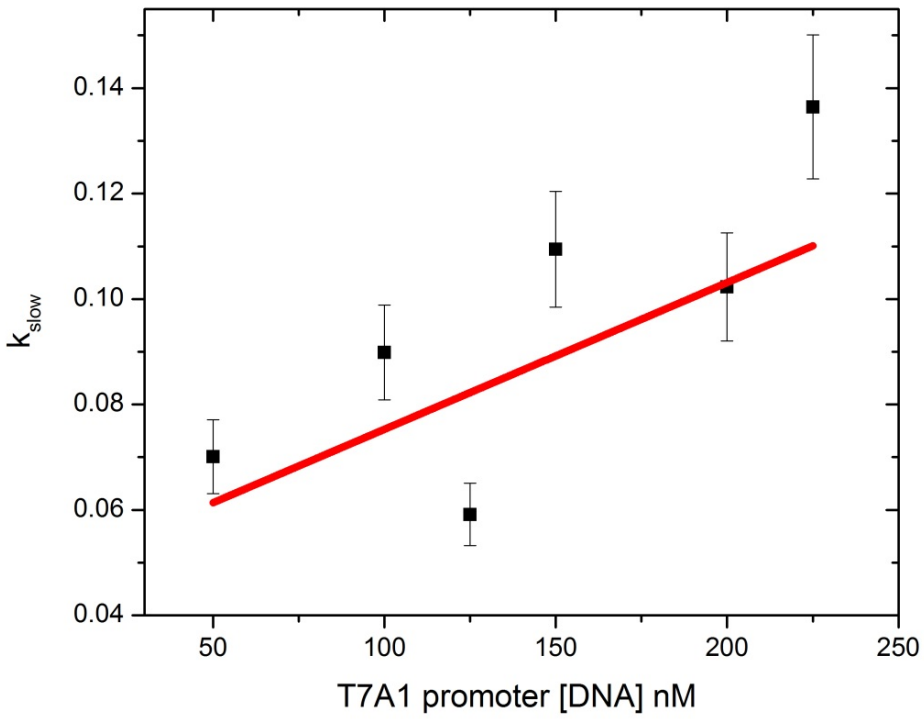
0.14
0.12
0.10
0.08
0.06
0.04
k_{slow}
50
100
150
200
250
T7A1 promoter [DNA] nM

Figure 5. Dissociation of RNAP from the T7A1 promoter at 37°C

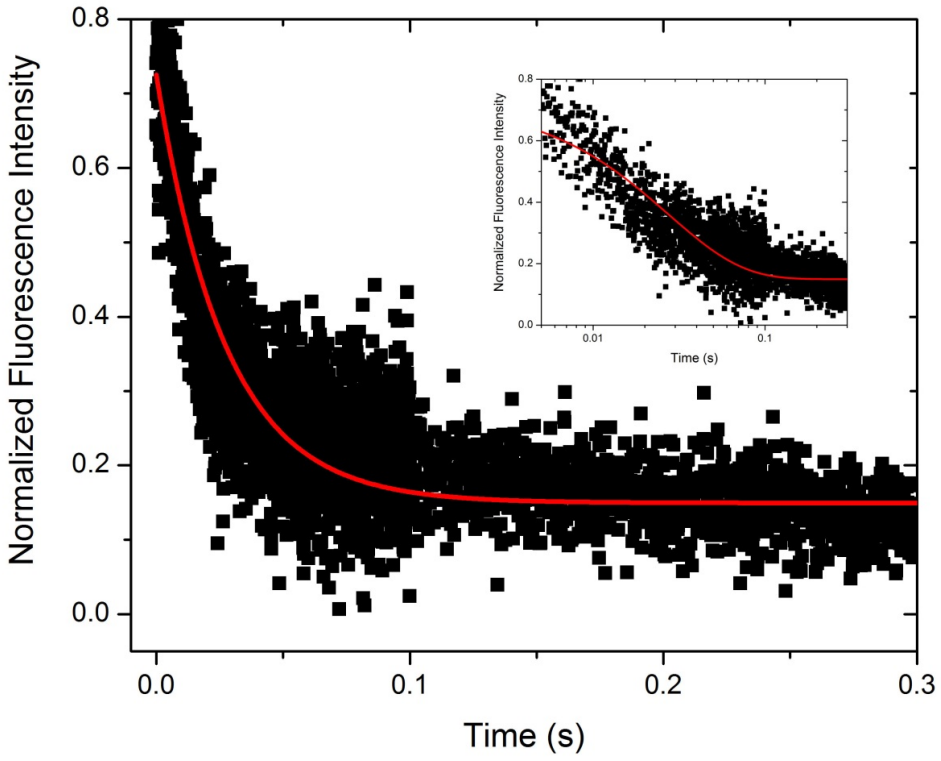

Table 3. Compiled Kinetic Data for T7A1. Rate and equilibrium constants for the association of RNAP with T7A1 at 19°C and 37°C

	19°C	**37°C**
$\mathbf{K_1}$	$7.7 \times 10^6\ M^{-1}$	$6.3 \times 10^7\ M^{-1}$
$\mathbf{k_{-1}}$	$0.107\ s^{-1}$	$0.374\ s^{-1}$
$\mathbf{K_2}$	$4.4 \times 10^6\ M^{-1}$	$5.9 \times 10^6\ M^{-1}$
$\mathbf{k_{-2}}$	$0.018\ s^{-1}$	$0.047\ s^{-1}$
$\mathbf{k_{obs,\ salt}}$	N/A	$40\ s^{-1}$

Appendix 4

Preliminary determinations of the association kinetics of RNAP with the rrnb P1 promoter in the presence and absence of initiating nucleotides ATP and CTP at 37°C using the RNAP "beacon" assay

Introduction

Cellular ribosome synthesis is rate-limited by ribosomal RNA production by RNA polymerase. Transcription of ribosomal RNA is highly NTP dependent and can constitute the majority of all cellular RNAP activity during log phase growth (Paul *et al.* 2004 and references therein). Because of the large metabolic expense of synthesizing ribosomal components, ribosome biogenesis is finely tuned to cellular nutrient levels. There are seven rRNA operons which are transcribed from two promoters, *rrn* P1 and *rrn* P2. These promoters are separated by ~120 base pairs of DNA. *rrn* P1 promoters require unusually high concentrations of the initiating nucleoside triphosphates (ATP or GTP, depending on the promoter) for maximal transcription *in vitro* (Schneider *et al.* 2002).

Results

RNAP- rnbp1 promoter DNA association kinetics were investigated in real-time using the RNAP "beacon" assay at the transcription buffer salt (0.12 M KCl) condition in the presence and absence of initiating nucleotides ATP (300 uM) and CTP (30 uM) at 37°C. Previous work has show that RNAP- rnbp1 interactions are weak at high salt and in the absence of initiation NTPs (Bartlett *et al.* 1998).

We find that the kinetic curves describing the data are best fit to the sum of two exponentials. in the presence of ATP and CTP, we find that RNAP- rnbp1 association kinetics are much faster than without initiating nucleotides (Figures 1 and 2). In the presence of ATP and CTP, the observed rates k_{1obs} and k_{2obs} are both approximately 3-fold higher than in the absence of nucleotides. This is consistent with previous findings that nucleotides can “pull” the unstable RNAP- rnbP1 closed complex to the more stable open complex. However, much more work remains to characterize the kinetic pathway of RNAP isomerization at the rnbP1 promoter.

Methods

RNAP and promoter DNA

E. coli RNA polymerase holoenzyme containing the σ^{70} derivative labeled at position 211 with fluorescent label 5-tetramethylrhodamine ((211Cys-TMR) σ^{70}) was prepared as in Mekler *et al.* 2011a. rnbP1 promoter DNA was amplified from the plasmid p1616 using PCR and primers “3038” (upstream primer) 5’-CCGCGGATCCGTATCACGAGGCCCTTTCG-3’ and “1620” (downstream primer) 5’- GCGCTACGGCGTTTCACTTC-3’ (gifts of Jared Winkelman) to yield a 226 bp product, from -121 to +105, with -88 to +50 wt rrnB P1 sequence. The high fidelity DNA polymerase Pfx50 (Invitrogen, Carlsbad, CA) was used to create blunt ends during the PCR amplification. All promoter DNA was purified using the Qiagen PCR cleanup kit (MD) and concentration determined by absorbance at 260nm.

Stopped-flow measurements

Real-time fluorescence measurements were taken identically as in Chapter 4.

Figure Captions

Figure 1. Association of RNAP with the rrnB P1 promoter in the presence and absence of initiating nucleotides ATP and CTP. 10nM (211Cys-TMR) σ^{70} RNAP holoenzyme (final concentration) was rapidly mixed with 100nM rnbP1 promoter DNA in the presence (A) and the absence (B) of and the initiating nucleotides ATP and CTP (300uM and 30uM, final concentration). The samples were excited at 550 nm and the increase in fluorescence emission was monitored over time using a 565 long pass glass filter. From one loading of reagents, 3-5 sample “shots” were taken and averaged. Data acquired on two different days were combined to obtain the curves shown. The kinetic curves were best fit to the sum of three exponentials.

Figure 1. A.

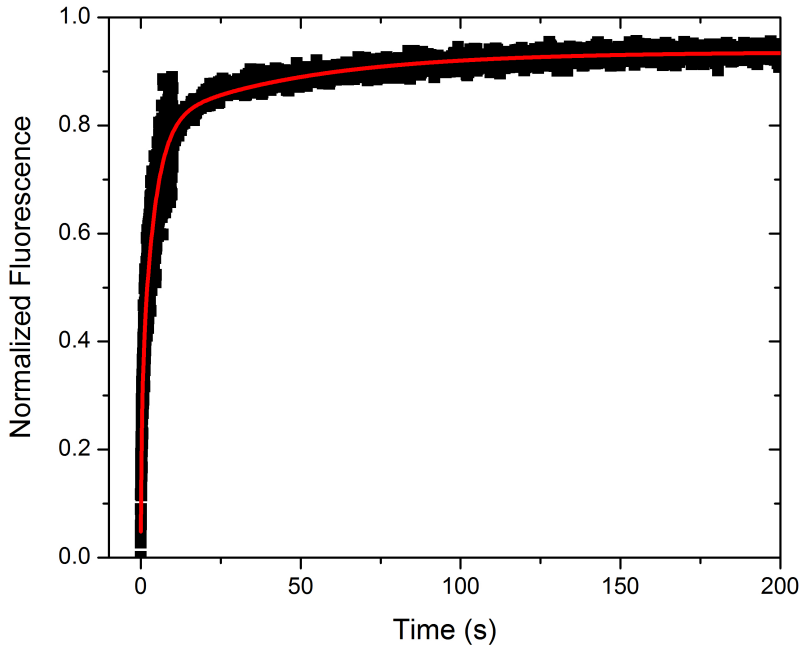
Normalized Fluorescence
1.0
0.8
0.6
0.4
0.2
0.0
0
50
100
150
200
Time (s)

B.

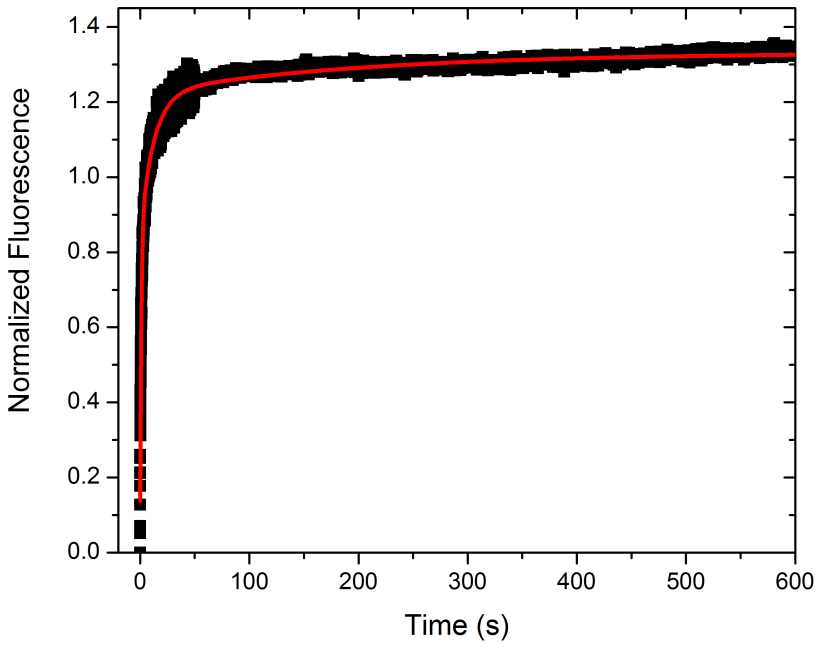
Normalized Fluorescence
1.4
1.2
1.0
0.8
0.6
0.4
0.2
0.0
0
100
200
300
400
500
600
Time (s)

Table 1. Comparison of Observed Rates for RNAP- rnbP1 promoter DNA association. (211Cys-TMR) σ^{70} RNAP (10nM) was rapidly mixed with 100nM rnbP1 promoter and the fluorescence change monitored as a function of time (See Figure 1 A and B). Observed rate constants were determined from the best fit of the kinetic curves to a sum of three exponentials. Amplitudes are reported as the fraction of the total change in fluorescence.

	$k_{1,obs}$ (s^{-1})	A_1	$k_{2,obs}$ (s^{-1})	A_2	$k_{3,obs}$ (s^{-1})	A_3
- NTPs	0.88	0.6	0.08	0.31	0.005 s^{-1}	0.09
+ NTPS	2.4	0.27	0.25	0.58	0.04 s^{-1}	0.33

Appendix 5

Preliminary determination of the rates of GTP incorporation at the +3 position at the λP_R promoter using thin layer chromatography

Transcription is the process whereby RNA polymerase catalyzes the synthesis of RNA using a promoter DNA template. At many promoters, *E. coli* RNAP performs repeated rounds of abortive cycling prior to transitioning to processive transcription of full-length RNA products. This abortive cycling occurs both *in vitro* and *in vivo* (Goldman *et al.* 2009). However, the cellular role of these short abortive products is currently unknown.

During RNA synthesis, RNAP catalyzes the incorporation of an NTP into the growing RNA strand, which causes cleavage of the bond between the alpha and beta phosphates of the NTP, allowing the NMP to be incorporated and the PPi to be released. Here we use thin layer chromatography to separate the PP_i product from the unincorporated NTP and thereby quantitate the fraction of NMP incorporated into the growing RNA strand. Use of the initiating dinucleotide ApU (+1, +2 relative to the start site of transcription) and γ-^{32}P- labeled GTP (+3) allows us to quantitate the rate of incorporation of GTP at the +3 position on the λP_R promoter at different temperatures (5, 10, 25, and 37°C).

Methods

Reagents and Buffers

All reagents and buffers were identical to Chapter 2.

TLC Transcription Assay

RP_o was formed at the λP_R promoter by *E. coli* RNAP in standard binding buffer [40 mM Tris (pH 8), 10 mM $MgCl_2$, 120 mM KCl, 100 μg/mL BSA, and 1 mM DTT, 3.125% (v/v) glycerol] at the temperature of interest (5, 10, 25, or 37°C) and allowed to equilibrate for at least one hour. At time zero, a mixture containing the ApU dinucleotide (which binds to +1, +2 on the promoter DNA) along with cold GTP and ^{32}P- labeled GTP (which incorporates at position +3) was mixed with RP_o. The final concentrations were 100nM λP_R promoter, 120nM active RNAP, 100uM ApU, and 80uM GTP total (containing 1uL of ^{32}P- labeled GTP). At different times during the reaction, 10uL aliquots of the transcription reaction were taken out and quenched using 5uL of 5M formic acid. Formic acid stops the reaction by denaturing RNAP. As a result, any GMP-PPi not yet released from the RNAP active site cleft will be unable to incorporate into the growing RNAP chain. In contrast, use of an $EDTA^{4-}$ quench stops the reaction by chelating all free Mg^{2+} in solution. Therefore, GMP-PPi in the active site cleft still has the ability to be incorporated, although a new GTP molecule will be unable to bind to RP_o. These two differing quench types can yield the same or different kinetic results, depending on the kinetic mechanism for NTP incorporation of the enzyme (Anand *et al.* 2006).

Reaction time points collected out to 20 minutes and then 1uL of each quenched sample was spotted onto a PEI-cellulose TLC plate that had been pre-run with

deionized water. Samples were shown to migrate up the plate better when the plates had first been prerun with deionized water (data not shown). The plates were placed into a glass TLC chamber containing 0.4M K_2HPO_4 pH 3.6 solvent buffer that had been filled to just below the sample line on the TLC plate. The plates were run for 1 hour, dried, and then exposed to a phosphorimaging screen and imaged using either a Typhoon 9410 Variable Mode Imager (Amersham Biosciences) or a Typhoon FLA-9000 (GE Healthcare), and analyzed using Image Quant TL.

Results

Figure 1 depicts the raw data from a TLC incorporation assay at 37°C. The circles at the very bottom of the TLC plate represent the unincorporated GTP and the smaller circles above represent the PPi product released due to incorporation of GMP. Because the GTP is ^{32}P-labeled on the gamma phosphate, the GMP is “silent” such that it cannot be visualized on the TLC plate.

Figures 2A-C contain the quantified data from the TLC plate assays performed at 10, 25 and 37°C. Each temperature was replicated a minimum of two times. At 5°C, no incorporation products above background were detected. The data have been corrected to account for the small amount of GMP and GDP (and therefore Pi and PPi) initially present in the γ-^{32}P-GTP stock solution. The data were normalized to the number of products per promoter and plotted versus time in order to obtain the best-fit line, the slope of which represents the number of products per promoter per second. Error bars represent the standard deviation in the number of products per promoter determined at each time point from 2-6 independent experiments.

The results from this analysis are plotted in Tables 1 and 2. At 5°C, no incorporation products above background were detected. However, complexes formed at 10, 25 and 37°C all yielded products and the rate of incorporation increased with increasing temperature, suggesting that the k_{cat} for incorporation is strongly temperature dependent. Plotting the log k_{cat} vs. 1/T yields an activation enthalpy of 17 kcal, consistent with previous determinations from our lab (Sigrid Leirmo, PhD dissertation).

One limitation of this assay is that the TLC protocol utilized a solvent separation system that was optimized for visualizing P_i and not PPi. Because of its larger size, under these solvent conditions the PPi did not migrate very far up on the plate relative to the position of the unincorporated GTP. Therefore, under conditions of low incorporation (for example at low temperature or at low concentrations of open complexes) it was difficult to quantitate the concentration of PPi products produced relative to total GTP due to the strong signal coming from unincorporated GTP. Future studies will be needed to determine the optimum separation solvent and assay conditions for quantitating the amount of GTP incorporation.

Figure Captions

Figure 1. Representative TLC plate for incorporation of γ-^{32}P GTP at +3. Open complexes were formed at 37°C for one hour and then mixed with a solution containing the initiating dinucleotide ApU along with cold GTP and ^{32}P- labeled GTP (which incorporates at position +3). The final concentrations were 100nM λP_R promoter, 120nM active RNAP, 100uM ApU, and 80uM GTP total (containing 1uL of ^{32}P- labeled GTP). For each time point, 10uL aliquots of the transcription reaction were taken out and quenched using 5uL of 5M formic acid. 1uL of each sample was spotted onto a PEI-cellulose TLC plate and the plates were run in a glass TLC chamber containing 0.4 M K_2HPO_4 pH 3.6 solvent buffer. The plates were run for 1 hour, dried, and then exposed to a phosphor imager screen and imaged.

Figure 2. Incorporation of GTP at +3 for λP_R. The number of products per promoter is plotted versus time. The error bars reflect the standard deviations in the number of products per promoter determined from 2-6 independent replicates. (A) 37°C. Fitting the data to the best-fit line yielded a k_{cat} of 0.151 ± 0.004 products per promoter per second. (B) 25°C. Fitting the data to the best-fit line yielded a k_{cat} of 0.032 ± 0.001 products per promoter per second. (C) 10°C. The best-fit line to the data yielded a k_{cat} of 0.0079 ± 0.00056 products per promoter per second.

Figure 1.

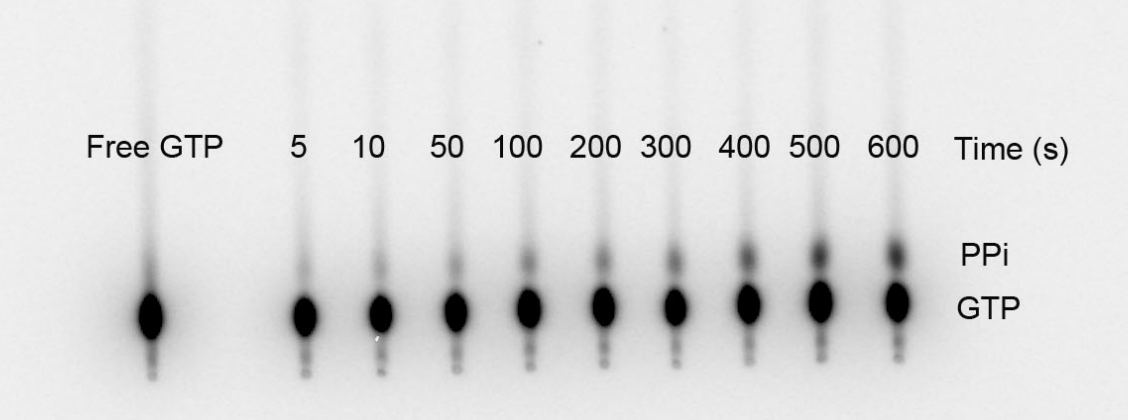

Figure 2.

A.

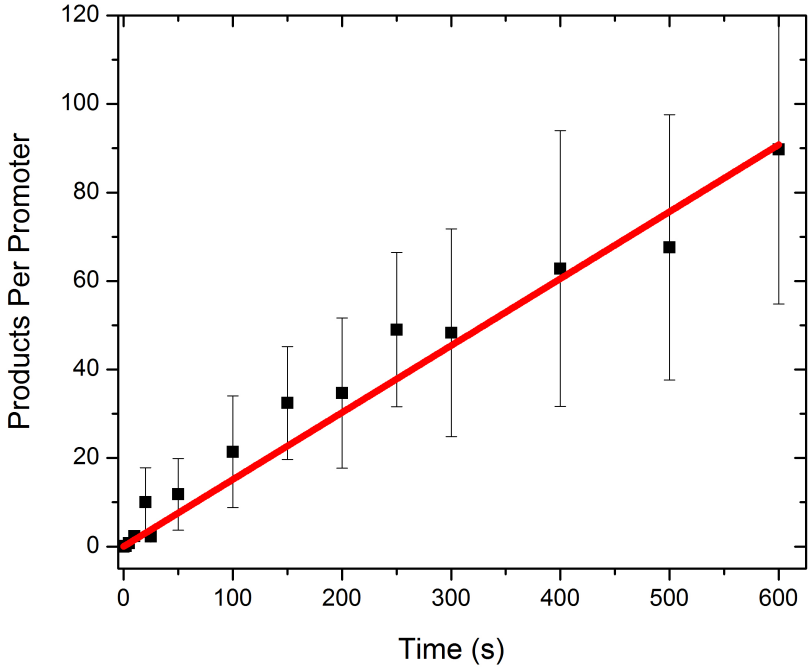
Products Per Promoter
Time (s)
0
20
40
60
80
100
120
0
100
200
300
400
500
600

B.

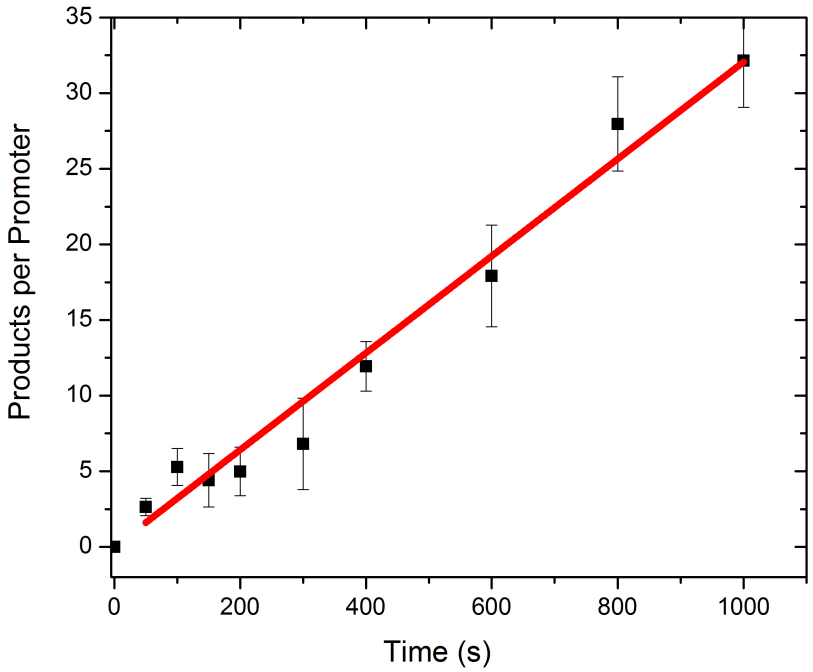
Products per Promoter
Time (s)
0
5
10
15
20
25
30
35
0
200
400
600
800
1000

Figure 2C.

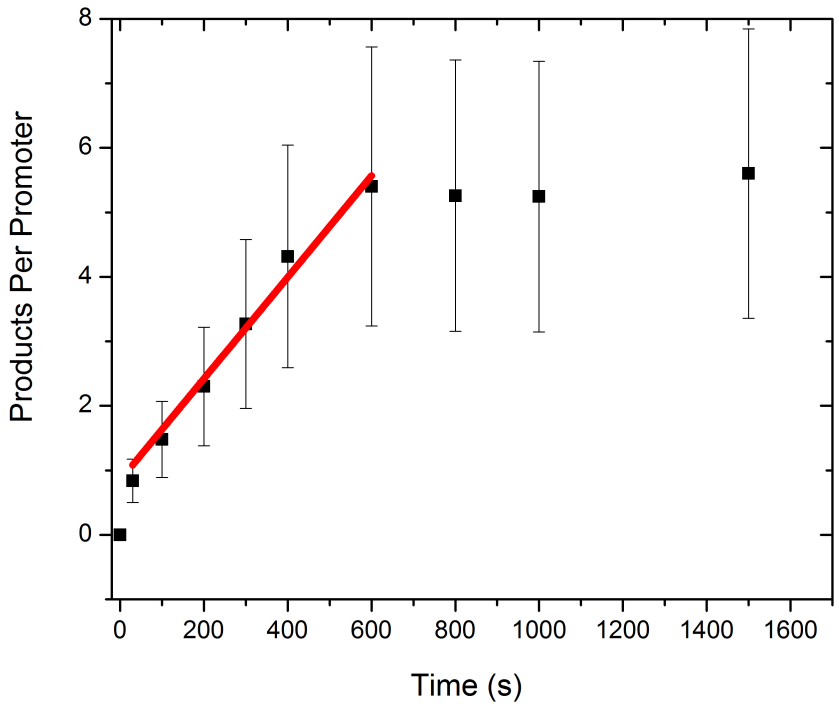
Products Per Promoter
Time (s)
0
2
4
6
8
0
200
400
600
800
1000
1200
1400
1600

Table 1. Rates of Incorporation of GTP at +3 At Different Temperatures for Open Complexes formed at LPR. The rates of incorporation were determined from the slope to the best-fit line of products per promoter versus time. Each rate reflects an average of 2-6 independent experimental replicates.

Temperature (°C)	Rate (products promoter^{-1} second $^{-1}$)	Error
5	N/A	N/A
10	0.0079	± 0.0006
25	0.032	± 0.001
37	0.151	± 0.004

Appendix 6.

Effect of nucleotides on promoter DNA wrapping around RNAP in open complexes at 19°C as monitored by real-time FRET; Effect of heparin on RNAP-DNA wrapping as detected by equilibrium FRET at 2, 10, and 19°C

In Chapter 3, I reported Forster Resonance Energy Transfer (FRET) experiments on equilibrium RNAP- promoter DNA complexes as a function of temperature and also in real-time during association at 19°C. These investigations show that promoter DNA is wrapped completely around RNAP during formation of the closed complex I_1 and that the wrap persists during DNA opening.

To further develop testable models about the regulatory role of the promoter DNA wrap, I investigated the extent of promoter DNA wrapping during abortive cycling and elongation. However, one caveat to the results presented below is that the downstream Cy5 dye is located at +14, and the end of the promoter fragment is +22. Therefore, not only is the Cy5 dye located in the region known to contact RNAP during assembly of the downstream mobile elements (DMEs), but the initially transcribed region of the DNA is only 23 nucleotides long. Upon addition of all four nucleotides, RNAP will translocate to the end of the fragment and dissociate. This dissociation will cause unwrapping of the promoter DNA. Therefore, caution should be used in over-interpreting these results. Although there is a reduction in the FRET signal as a function of time, this could be due to dissociation of RNAP from the end of the promoter.

First, I tested whether the addition of saturating NTPs would change the FRET signal at 19°C. Open complexes containing 50 nM active RNAP and 50 nM Cy3 (-100) Cy5 (+14) promoter DNA were equilibrated at 19°C for 1 hour and then rapidly mixed with

saturating NTPs (300 μM each of ATP, UTP, GTP, and CTP) using the Kintek SFX-300 stopped flow. Addition of saturating NTPs to open complexes at 19°C resulted in a biphasic decrease in the Cy5 (+14) emission and a biphasic increase in the Cy3 (-100) fluorescence emission consistent with a decrease in FRET due to unwrapping of the DNA during transcription (Figure 1A and 1B), but also consistent with RNAP dissociation from the DNA. The Cy5 (+14) FRET decrease was best fit to the sum of two exponentials, with k_1= 0.038 s^{-1}, A_1=0.43 and k_2=0.0032 s^{-1}, A_2=1.89. The observed rate constant k_1 is an order of magnitude smaller than previously determined rates of NTP incorporation during initiation at λP_R (~0.2 second $^{-1}$ at 19°C for incorporation of NTPs at +2 or +3 at λP_R, unpublished observations, Heitkamp, Lingeman and Poulos). Simplistically, if the transition to elongation occurs near +10, we estimate that the observed rate constant for the transition to elongation would occur at ~0.02 s^{-1}. Therefore, if we are monitoring FRET changes due to translocation of RNAP during elongation (and not due to RNAP dissociation), the k_1 observed here would be most simply explained as monitoring the transition from initiation to elongation. The second observed rate constant k_2, is an order of magnitude slower than k_1. Optimistically, we hypothesize that the second observed rate constant may be monitoring dissociation of RNAP from the end of the promoter and that the first rate constant monitors a change in FRET efficiency arising from movements of the DNA during elongation.

Control experiments were performed by monitoring the changes in fluorescence intensity for each individual dye upon addition of saturating nucleotides to open complexes. Results for open complexes containing promoter DNA labeled with a single Cy5 (+14) or Cy3 (-100) dye are shown in Figure 1C and 1D. Complexes containing

Cy5 (+14) promoter DNA did not exhibit any change in the fluorescence emission of Cy5 upon NTP addition. Complexes containing Cy3 (-100) promoter DNA displayed a small increase in fluorescence intensity upon mixing with saturating NTPs, however the total signal amplitude was only 25% of that seen in the double dye FRET experiment. We hypothesize that the increase seen in the single dye Cy3 (-100) experiment may be due to rebinding of dissociated RNAP to the promoter DNA over the course of the experiment, or of movements of the RNAP upon addition of NTPs that change the local environment of the Cy3 dye. Further control experiments will need to be done in order to determine which FRET changes arise due to RNAP-dye interactions and separate those from FRET changes due to movements of promoter DNA during transcription.

Next, we wanted to determine whether the promoter DNA wrap would be affected by abortive cycling. During transcription initiation, RNAP performs repeated rounds of abortive cycling, producing short (<10 bases) RNA products while still bound to the promoter. During the transition from initiation to elongation, RNAP breaks free from the promoter and begins to processively produce full-length products. It has been hypothesized that DNA “scrunching” contributes to this process by causing the buildup of a stressed intermediate; this accumulated DNA-unwinding and DNA-compaction stress is then used by RNAP to break free from the promoter and also from transcription factors upstream of the promoter recognition site (Kapanidis *et al.* 2006).

We used the initiating dinucleotide CpA (-1, +1) and the +3 position, UTP, to monitor changes in DNA wrapping during production of the RNA product CpApU. Open complexes containing 50 nM Cy3 (-100) Cy5 (+14) promoter DNA and 50 nM RNAP were formed at 19°C for a minimum of one hour and then rapidly mixed with 300 μM of

both CpA and UTP in the Kintek SFX-300 stopped flow. We find that there is no change in the emission of either dye, even out to times as long as 600 seconds (Figure 2A and 2B). Control experiments showed no change in fluorescence of the single dyes. From this, we conclude that abortive cycling does not change the extent of wrapping or the positions of the upstream and downstream regions of promoter DNA relative to each other.

In preliminary experiments, we also investigated the effects of adding heparin to pre-formed Cy3 (-100) Cy5 (+14) promoter DNA- RNAP complexes at 2, 10, and 19°C. Complexes containing 100nM DNA, 100nM RNAP were formed at the temperature of interest for a minimum of 1.5 hours. The samples were excited at 515nM and the emission of Cy5 monitored using the instrument monochromator. In the presence of RNAP, there is a large increase in the FRET efficiency (Chapter 3, and Figure 2A-C). Upon addition of 100 µg/ mL heparin (final concentration) to each sample, the FRET efficiency at all temperatures is decreased, suggesting a dramatic decrease in the extent of wrapping. Heparin is a polyanionic DNA mimic; these results suggest that heparin may be able to disrupt the promoter DNA wrap, even in open complexes. Further investigation of these findings is currently being conducted in our lab.

Conclusion

Addition of the initiating dinucleotide CpA and UTP (-1, +1, +2) to form a 3mer RNA product resulted in no unwrapping of promoter DNA in open complexes at 19°C, but addition of all four NTPs at saturating concentrations results in unwrapping of the DNA at a rate consistent with the transition from initiation to elongation. However further control experiments need to be performed in order to separate true FRET changes from

RNAP-dye interactions. One future direction for this project would be to move the FRET dye probes to position on the DNA further away from the RNAP wrapping footprint, where they are less likely to be influenced by the local environment of RNAP. We have identified positions -115, +29, +35, and +40 as good candidates for dye positioning. By determining the FRET efficiency for a range of dye positions, we would also be able to more accurately determine the distances between the upstream and downstream regions of the DNA.

Heparin appears to displace the promoter DNA wrap in complexes formed at low (2°C) and higher (19°C) temperatures. However, the mechanism of this displacement is currently unknown.

Figure Captions

Figure 1. Open complexes containing 50 nM active RNAP and 50 nM Cy3 (-100) Cy5 (+14) promoter DNA were equilibrated at 19°C for 1 hour and then rapidly mixed with saturating NTPs (300 μM each of ATP, UTP, GTP, and CTP) using the Kintek SFX-300 stopped flow. The emission for both dyes was monitored simultaneously using two PMTs; samples were excited at 515nm and emission collected using glass filters. (A) (■) Cy3 (-100) emission, (B) (●) Cy5 (+14) emission. Each experiment depicted in Figure 1 was replicated three times.

Figure 2. Open complexes containing 100 nM active RNAP and 100 nM Cy3 (-100) Cy5 (+14) promoter DNA were equilibrated at the temperature of interest for a minimum of 1.5 hours. The samples were excited at 515nM and the emission of Cy5 monitored using the instrument monochromator. (A) 2°C, (B) 10°C, and (C) 19°C. Each experiment depicted in Figure 1 was replicated one time.

Figure 1. Cy3 (-100) Cy5 (+14) promoter DNA + 300uM of ATP, UTP, CTP and GTP.
A.

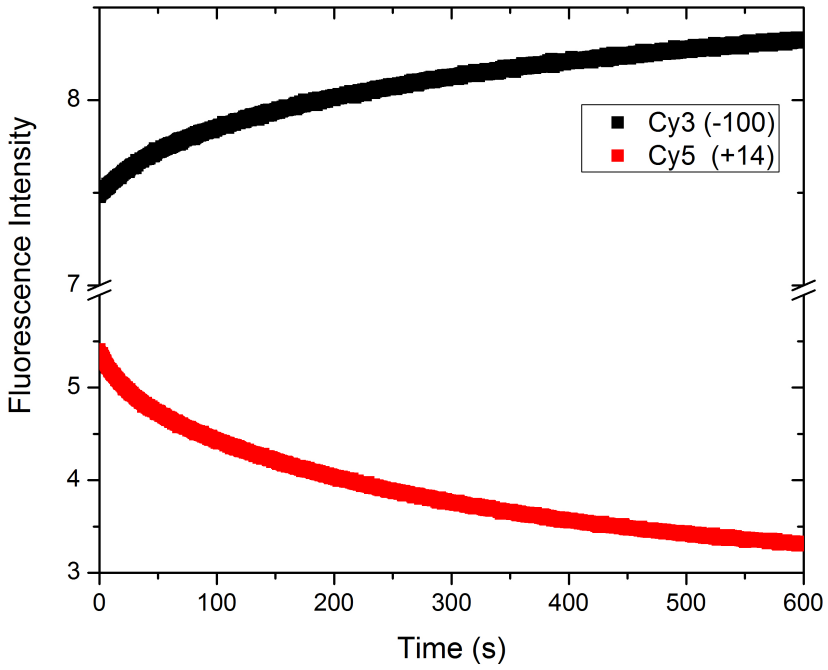

B.

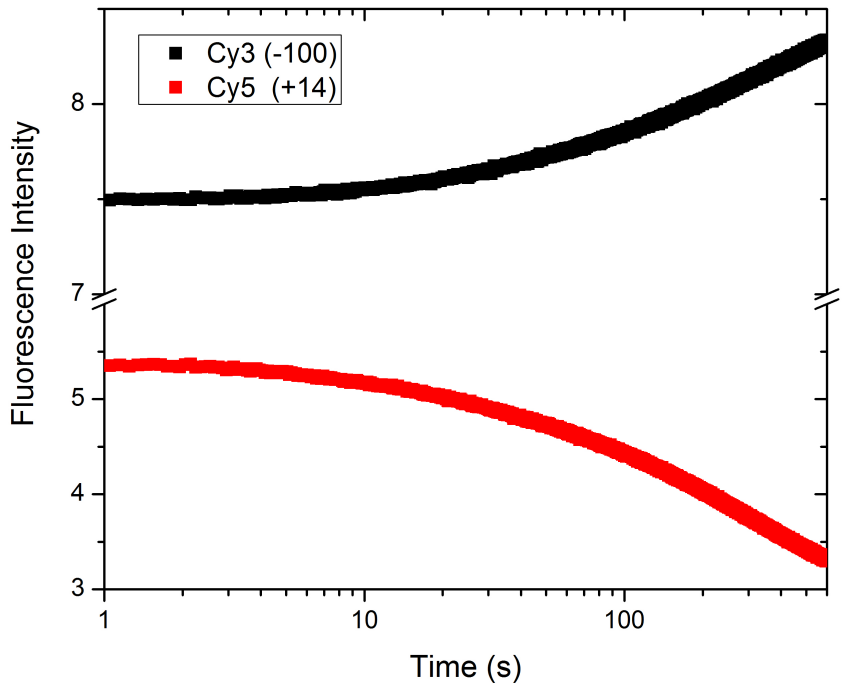

Figure 2. Cy3 (-100) Cy5 (+14) promoter DNA + 300uM CpA, 300uM UTP

A. Cy3 emission

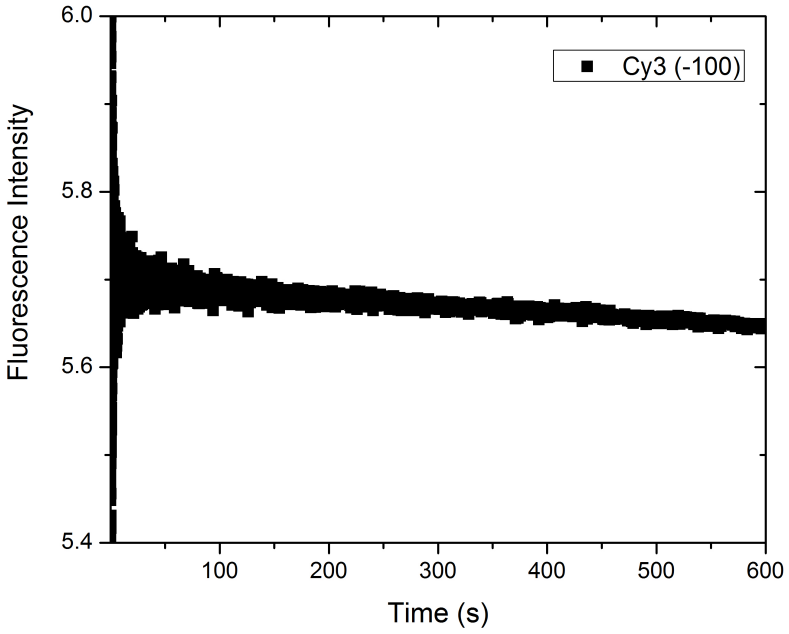

B. Cy5 emission

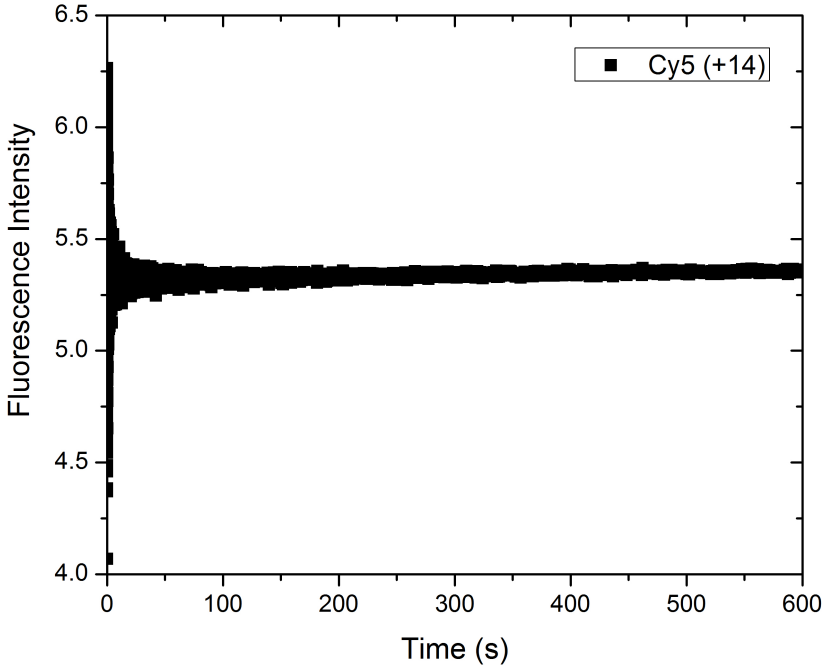

Figure 3. A.

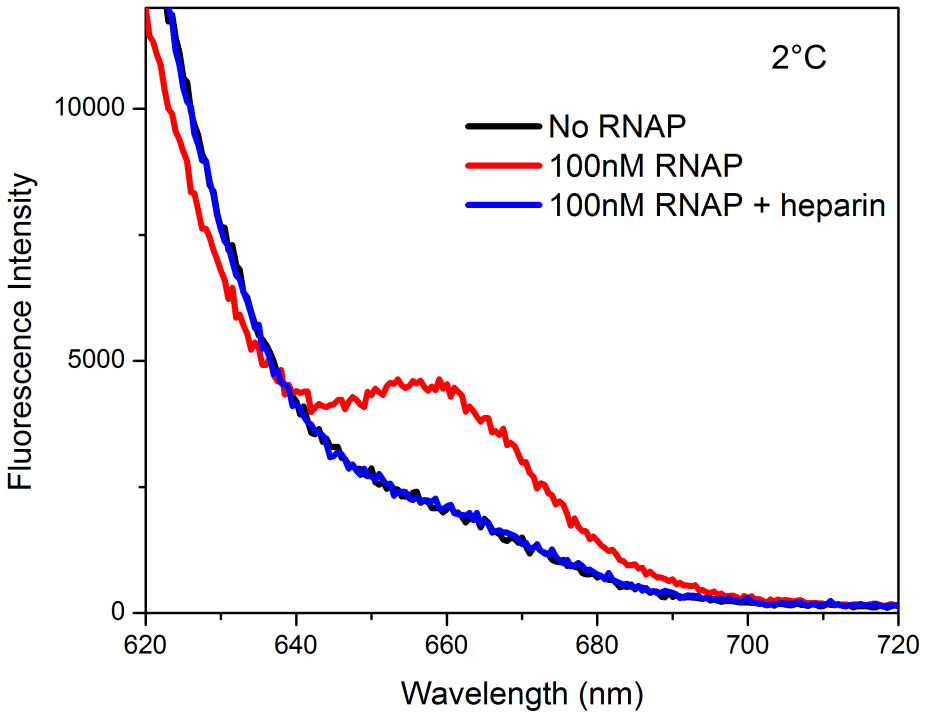
2°C
No RNAP
100nM RNAP
100nM RNAP + heparin
Fluorescence Intensity
10000
5000
0
620
640
660
680
700
720
Wavelength (nm)

B.

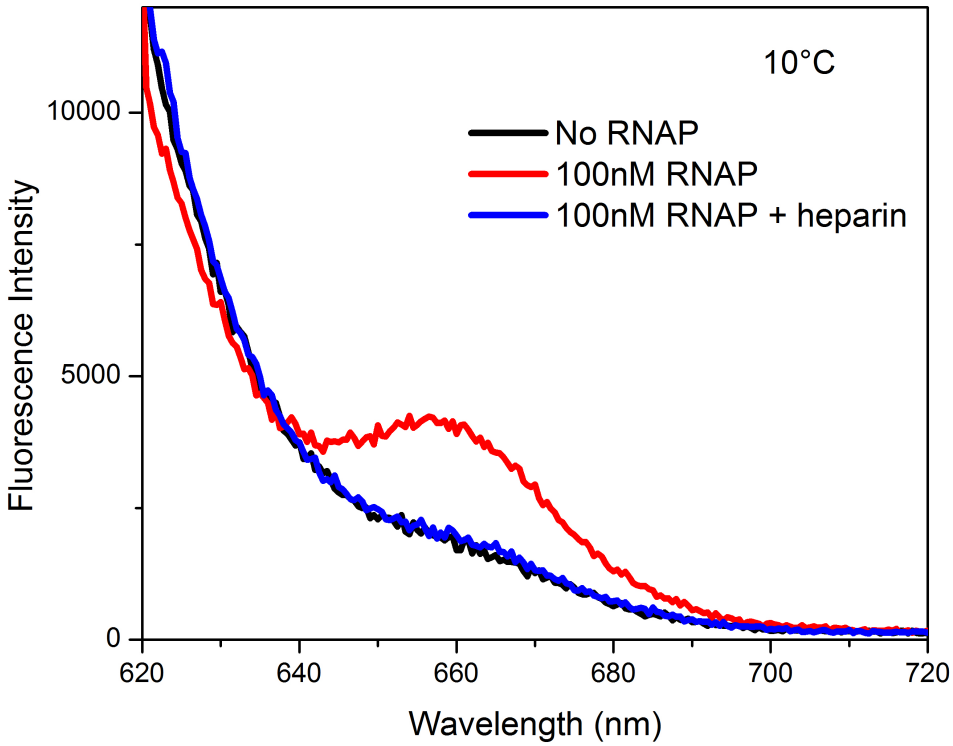
10°C
No RNAP
100nM RNAP
100nM RNAP + heparin
Fluorescence Intensity
10000
5000
0
620
640
660
680
700
720
Wavelength (nm)

C.

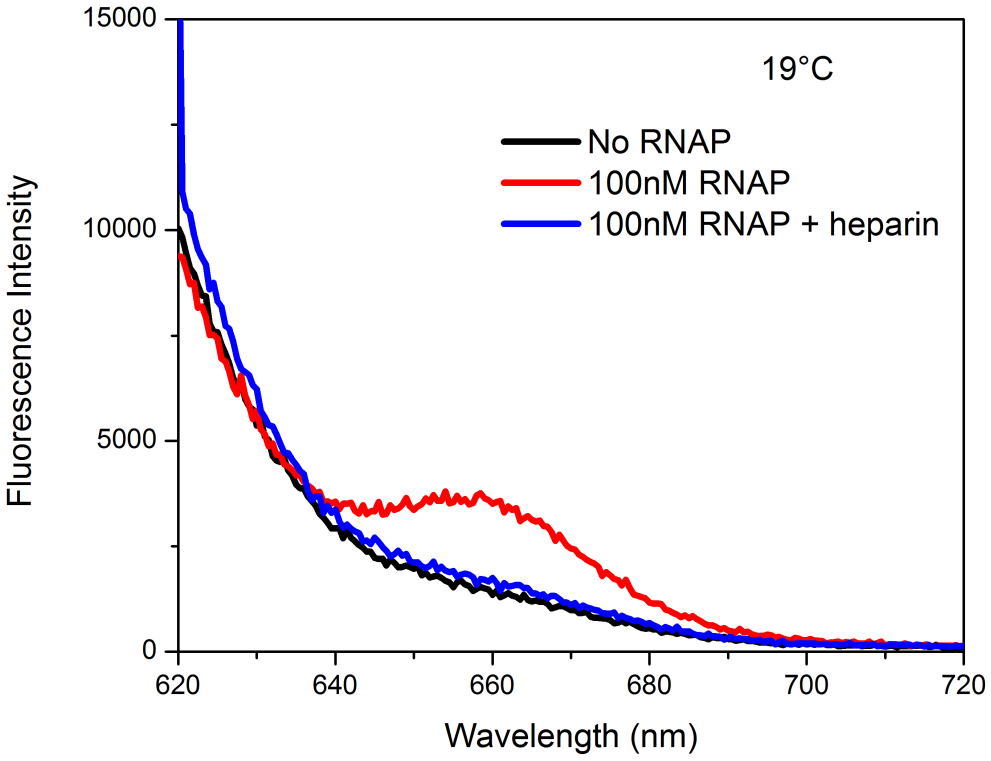
19°C
No RNAP
100nM RNAP
100nM RNAP + heparin
Fluorescence Intensity
Wavelength (nm)
15000
10000
5000
0
620
640
660
680
700
720

Appendix 7:

Preliminary comparison of transcription product for the λP_R promoter at 10°C and 37°C with WT RNAP indicates that the low temperature (10°C) open complex, in which the late (post-opening) downstream interactions are much weaker than at 37°C and which may be like the I_3 open intermediate, has a higher ratio of long (productive) to short (abortive) transcripts than the 37°C open complex.

Previous work in our lab has shown that there are three different forms of the open complex populated at the λP_R promoter: I_2, I_3, and RP_o (Roe *et al.* 1984, Saecker *et al.* 2002, Kontur *et al.* 2008). After promoter DNA is opened in a single step in the transition from I_1 to I_2, the template strand is loaded into the RNA polymerase active site in I_2, and assembly of the downstream jaw/clamp occurs during the I_2 to RP_o transition. Based on the result that the dissociation of RP_o to I_2 exhibits a large negative activation energy, Kontur *et al* proposed the existence of a third intermediate, I_3 (Kontur *et al.* 2008). The conversion of I_3 to RP_o is believed to exhibit a large positive change in enthalpy, suggesting that the RNA polymerase downstream jaw/clamp is assembled in this step, or possibly that the single stranded promoter DNA is becoming unstacked (Kontur *et al.* 2010). These open complexes also differ in the amount permanganate reactivity of the nontemplate strand; in I_2, the permanganate reactivity is only 50% of that of RP_o (Gries *et al.* 2010). This suggests that the nontemplate strand is reassembled in the cleft during the conversion of I_2 to I_3 and RP_o and that movements of the nontemplate strand are coupled to assembly of the downstream β' jaw and other downstream mobile elements (DMEs) on downstream duplex DNA (Kontur *et al.* 2008, Kontur, Capp and Gries *et al.* 2010, Drennan *et al.* in submission)

Our hypothesis based on these results is that each of the three open complexes (I_2, I_3 and RP_o) represent different assembly states of the downstream jaw/clamp and we propose to compare the properties of each intermediate during transcription initiation. How does I_3 differ from I_2? From analysis of the effects of solutes on the kinetics of dissociation of RNAP from λP_R promoter DNA, our lab determined that approximately 80 amino acid residues are buried during the conversion of I_2 to I_3 (or to the $(I_2\text{-}I_3)^{\ddagger}$ transition state) and that approximately 40 additional amino acid residues are buried during the subsequent isomerization of I_3 to RP_o (Kontur, *et al.* 2010). We hypothesize that the β' clamp and/or β lobe assemble in the I_2 to I_3 transition and that the jaw and downstream mobile elements (DME) assemble on the +10 to +20 distal DNA during the conversion of I_3 (or the $I_2\text{-}I_3^{\#}$ transition state) to RP_o. In our lab, Drennen and collaborators have been using both a jaw deletion mutant of the RNA polymerase (Δjaw = Δ1149-1190) and a downstream truncated form of the λP_R promoter (truncated at +12) which lacks the DNA scaffold required for clamp/jaw assembly(+12 to +20) to determine if either of these mutants behave similarly to I_3. The DT+12 λP_R promoter variant can form open complexes, but they are less stable than complexes with full-length λP_R, indicating that the downstream clamp cannot fully assemble and suggesting that this species is more like I_3. Mutations in the RNAP downstream jaw also produce less stable open complexes, which may be I_3- or I_2-like (Mike Capp, unpublished observations, Drennan *et al*. 2012).

Here, we have used temperature to shift the population of open complexes from a majority RP_o (at 37°C) to a mixture of I_3 and RP_o (at 10°C) and performed single-round transcription assays. The addition of heparin (which is a mimic of single stranded

DNA) prevents any RNAP that dissociates from the promoter during transcription initiation from rebinding. Although it is difficult to estimate the exact amounts of each population of open complexes at these temperatures, we have evidence that there is a shift in the extent of clamp/jaw assembly at low temperatures, Also, at low temperature, the conversion of I_3 to RP_o has a large positive activation enthalpy and this indicates that there is proportionately much more I_3 populated at equilibrium at low temperatures such as 10°C than at 37 °C (Kontur *et al.* 2008).

Methods

Reagents

All reagents were of the highest purity commercially available and were purchased from Sigma or Fisher. Enzymes were purchased from NEB; all DNA oligonucleotides were ordered from IDT.

Buffers

All reagents were made up in transcription buffer containing 0.12M KCl, 40mM Tris pH 8, 10mM MgCl2 and 100ug/mL BSA or low salt transcription buffer (LSTB). Transcription quench buffer (TQB) contains 8 M urea, 0.5X TBE, 15 mM Na_2EDTA, 0.05% (w/v) xylene cyanol, and 0.05 % (w/v) bromophenol blue.

RNA Polymerase Preparation

E. coli WT RNAP holoenzyme was endogenously expressed and purified from *E. coli* MG1655 (Burgess, 1975, with modifications). Briefly, *E. coli* MG1655 cells were grown in a fermentor and cells were harvested in the late log phase of growth. A polyamine p precipitation was used, followed by a cibacron blue on sepharose FF column, then a BioGel A1.5M size exclusion column, and finally a phosphocellulose

column run in 50% glycerol. Two different preps of RNAP were used; prep #28 (68% active) and prep #29 (23% active). RNAP activity was determined using an equilibrium promoter DNA binding assay.

Transcription Assays for WT RNAP at 10 and 37ºC

The λP_R promoter DNA was amplified from a 963-bp-long DNA template P_R (wild type P_R sequence from −59 to + 34) using PCR and primers 'Fwd' (5'GTACGAATTCGATATCCAGCTATGACCATGATTACGCCAGC) and 'Rev' (5'CAGGACCCGGGGCGCGCTTAATTAACACTCTTATACATTATTCC) (primers and template were the gifts of Wilma Ross). This 963-bp-long DNA template P_R was previously obtained by PCR from plasmid pPR59 using primers NEB_FOR (5′-AAAACCTCTGACACATGCAGC) and NEB_REV (5′-GCTGCCCTTTTGCTCACATG).

Open complexes were made at the experimental temperature of interest for a minimum of one hour and contained 40nM λP_R promoter DNA and 40nM active RNAP; a second solution was made up containing 2mM ATP, 1mM CTP and GTP, 100uM cold UTP, and 50nM α-^{32}P UTP. The NTP solution also contained 100ug/mL of heparin as competitor for free RNAP, ensuring that RNAP that dissociated from the promoter could not rebind and re-initiate. These solutions were rapidly mixed using a Kintex 3-syringe quench flow mixer in equal volumes and so the final concentrations were half that of the original solutions. After mixing for the desired period of time, the samples were quenched with a solution of 15mM Na_2EDTA and ejected into a collection tube containing 1mL of ethanol, 2uL of 2mg/ml glycogen, and 25uL of 5M NaCl. The samples were then precipitated in this solution for at least 16 hours at -20°C. Sample precipitation times longer than 8 hours were observed to result in higher recoveries of

the α-^{32}P UTP (Capp, unpublished observations) and increased the sensitivity and detectability of products in the bottom of the gel and in particular the 2-mer RNA product.

After washing and drying, the pellets were resuspended in 6uL of TE buffer, and were then mixed with a mid-sized pellet of urea and 5uL of sample loading buffer to a final sample volume of 18uL. The samples were then run on a 15% polyacrylamide gel (19:1 acrylamide: bis-acrylamide ratio) containing 8M urea, 1x TBE buffer, 100uL of 100mM ammonium bisulfite and 100uL of TEMED. Band identification was determined using a set of RNA size standards from USB that were end-labeled with γ-^{32}P-ATP using polynucleotide kinase.

Gel Imaging and Analysis

After electrophoresis, each transcription gel was exposed to a phosphorimager screen and imaged using either a Typhoon 9410 Variable Mode Imager (Amersham Biosciences) or a Typhoon FLA-9000 (GE Healthcare)), and analyzed using Image Quant TL.

Results

Comparison of Amounts of Long and Short Transcripts Produced by WT RNAP at the λP_R Promoter At Different Temperatures under Single Round Conditions

We performed single- round transcription assays at both 10°C and 37°C, in order to compare the ratios of processive (long, >11 nucleotides) to abortive (short, < 11 nucleotides) transcription products at each temperature and to determine whether I_3 or RP_o open complexes were responsible for processive RNA production. We find that at 10°C, although the overall amount of transcription is lower than at 37°C, that the ratio of

long to short products is approximately 8 fold higher than that measured at 37°C for reaction times longer than 200 seconds (See Figures 1 and 2). This different is independent of choice of cutoff length (11-15) for defining the abortive products. These results suggest that I_3 and not RP_o is the open complex responsible for processive transcription. However, another explanation for the differences in product length at low temperatures could be due to a difference in the amount of scrunching or in the affinity of RNAP open complexes for NTPs and/or the promoter DNA (Kapanidis *et al.* 2006).

What is the mechanism of long transcript production by WT RNAP at λP_R, where RP_o is extremely stable with respect to I_3? Previous proposals invoked strong interactions in a "stressed" intermediate that had to be released for the open complex to escape abortive initiation and synthesize a full-length product (Hsu, 2002, Straney and Crothers 1987, Revyakin *et al.* 2006; Kapanidis *et al.* 2006). We find that deletion of the downstream mobile jaw accomplishes this, and therefore propose that the species with the strong interactions that need to be released is actually RP_o (the very stable open complex), that the productive complex is I_3 (the less stable open intermediate in RP_o formation at λP_R), and that productive initiation from WT RNAP at λP_R may require release of the jaw from downstream DNA, perhaps driven by scrunching or steps of NTP binding and production of short transcripts.

Figure Captions

Figure 1. Representative gel of transcription products at 10 and 37°C. Open complexes were formed at either 10°C (I_3 and RP_o) or 37°C (RP_o) for a minimum of one hour and then rapidly mixed with NTPs (2mM ATP, 1mM CTP and GTP, 100uM cold UTP, and 50nM 32-P UTP) and 100ug/mL heparin to prevent rebinding of dissociated RNAP. Transcription reactions were then quenched with 15mM Na_2EDTA, ethanol precipitated, and run on a 15% polyacrylamide 8M urea denaturing gel. Lanes 1-6 contain time points for 10°C and Lanes 7-12 contain 37°C data. “A” and “B” designate the long and short products, respectively. Transcript lengths are numbered on the left-hand side of the gel.

Figure 2. Ratio of long (>11 nucleotides) to short (<11 nucleotides) transcription products plotted as a function of time for both 10C (■) and 37C (●). The data for 10°C is an average of two experiments and the data at 37°C is an average of six experiments. The error bars reflect the standard deviation in the determinations of the ratio of long to short products at each time point. The length of each product was determined using a ^{32}P- end labeled single stranded RNA ladder run on the same gel.

Figure 1.

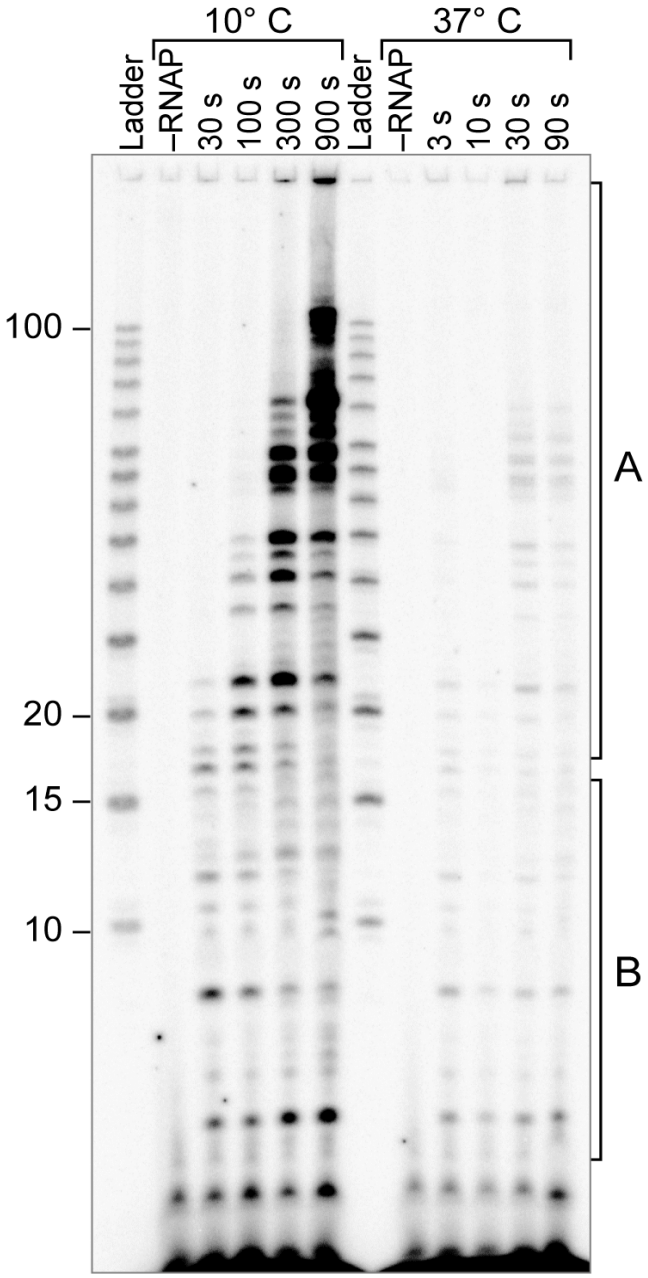
10° C
37° C
Ladder
–RNAP
30 s
100 s
300 s
900 s
Ladder
–RNAP
3 s
10 s
30 s
90 s
100
20
15
10
A
B

Figure 2.

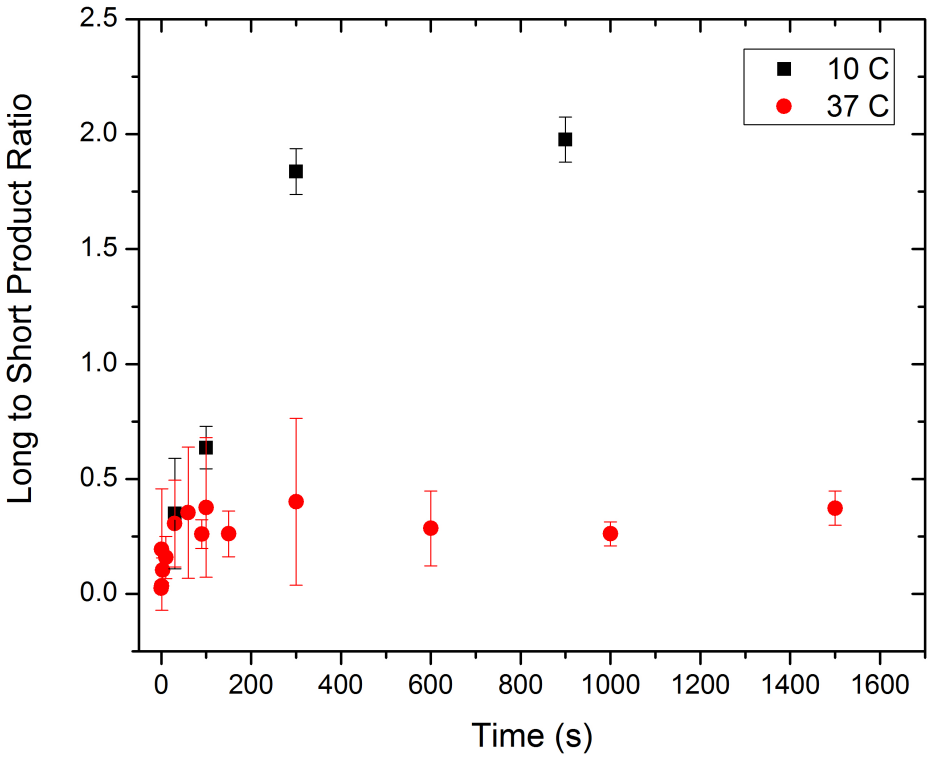
Long to Short Product Ratio
Time (s)
10 C
37 C
0.0
0.5
1.0
1.5
2.0
2.5
0
200
400
600
800
1000
1200
1400
1600

References

Anand, V. S., and Patel, S. S. 2006. Transient state kinetics of transcription elongation by T7 RNA polymerase. *J Biol Chem.* **47:** 35677-85.

Bartlett, M. S., Gaal, T., Ross, W., and Gourse, R. L. 1998. RNA polymerase mutants that destabilize RNA polymerase-promoter complexes alter NTP-sensing by rrn P1 promoters. *J Mol Biol* **279:** 331–345.

Bertrand-Burggraf, E., Lefèvre, J. F., Daune, M. 1984. A new experimental approach for studying the association between RNA polymerase and the tet promoter of pBR322. *Nucleic Acids Res*. **12:** 1697-706.

Burgess, R. R., and Jendrisak, J. J. 1975. A procedure for the rapid, large-scall purification of Escherichia coli DNA-dependent RNA polymerase involving Polymin P precipitation and DNA-cellulose chromatography. *Biochemistry* **21:** 4634-8.

Cámara, B., Liu, M., Reynolds, J., Shadrin, A., Liu, B., Kwok, K., Simpson, P., Weinzierl, R., Severinov, K., Cota, E., Matthews, S., and Wigneshweraraj, S.R. 2010. T7 phage protein Gp2 inhibits the Escherichia coli RNA polymerase by antagonizing stable DNA strand separation near the transcription start site. *Proc Natl Acad Sci U S A.* **107:** 2247-52.

Chen, J., Darst, S. A., and Thirumalai, D. (2010) Promoter melting triggered by bacterial RNA polymerase occurs in three steps, *Proc Natl Acad Sci U S A 107*, 12523-12528.

Goldman, S. R., Ebright, R. H., and Nickels, B. E. 2009. Direct detection of abortive RNA transcripts *in vivo. Science* **324:** 927–928

Davis, C. A., Bingman, C. A., Landick, R., Record, M. T., Jr., and Saecker, R. M. 2007. Real-time footprinting of DNA in the first kinetically significant intermediate in open complex formation by *Escherichia coli* RNA polymerase. *Proc Natl Acad Sci (USA)* **104:** 7833–7838.

Fischer, C. J., Tomko, E. J., Wu, C. G., Lohman, T., M. 2012. Fluorescence methods to study DNA translocation and unwinding kinetics by nucleic acid motors. *Methods Mol Biol.* **875:** 85-104.

Gries, T. J., Kontur, W. S., Capp, M. W., Saecker, R. M., and Record, M. T., Jr. 2010. One-step DNA melting in the RNA polymerase cleft opens the initiation bubble to form an unstable open complex. *Proc Natl Acad Sci (USA)* **107:** 10418-10423.

Gruber, H. J., Hahn, C., D., Kada, G., Riener C., K., Harms, G., S., Ahrer, W., Dax, T. G., Knaus, H., G. Anomalous fluorescence enhancement of Cy3 and cy3.5 versus anomalous fluorescence loss of Cy5 and Cy7 upon covalent linking to IgG and noncovalent binding to avidin. *Bioconjug Chem.* **11:** 696-704.

Hsu, L. M. 2002. Promoter clearance and escape in prokaryotes. *Biochim Biophys Acta.* **2:**191-207.

Kapanidis, A. N., Margeat, E., Ho, S. O., Kortkhonjia, E., Weiss, S., and Ebright, R. H. 2006. Initial transcription by RNA polymerase proceeds through a DNA-scrunching mechanism. *Science* **314:** 1144-1147.

Kontur W.S., Capp, M.W., Gries, T.J., Saecker, R.M., and Record, M.T., Jr. 2010. Probing DNA binding, DNA opening, and assembly of a downstream clamp/jaw in Escherichia coli RNA polymerase-lambdaP(R) promoter complexes using salt and the physiological anion glutamate. *Biochemistry.* **49:** 4361-73.

Kontur, W. S., Saecker, R. M., Capp, M. W., and Record, M. T., Jr. 2008. Late steps in the formation of *E. coli* RNA polymerase-λP_R promoter open complexes: Characterization of conformational changes by rapid [perturbant] upshift experiments. *J Mol Biol* **376:** 1034–1047.

Kontur, W. S., Saecker, R. M., Davis, C. A., Capp, M. W., and Record, M. T., Jr. 2006. Solute probes of conformational changes in open complex (RP_o) formation by *Escherichia coli* RNA polymerase at the λP_R promoter: Evidence for unmasking of the active site in the isomerization step and for large-scale coupled folding in the subsequent conversion to RP_o. *Biochemistry* **45:** 2161–2177.

Levitus, M., and Ranjit, S. 2011. Cyanine dyes in biophysical research: the photophysics of polymethine fluorescent dyes in biomolecular environments. *Q Rev Biophys.* **44:** 123-51.

Leirmo, S. 1989. The Mechanism of Interaction of *E. coli* RNA Polymerase with Bacteriophage and Bacterial Promoters. Ph.D. Thesis, Department of Biochemistry, University of Wisconsin, Madison, WI.

Mekler V., Pavlova O., and Severinov K. 2011a. Interaction of Escherichia coli RNA polymerase σ70 subunit with promoter elements in the context of free σ70, RNA polymerase holoenzyme, and the β'-σ70 complex. *J Biol Chem.* **286:** 270-9.

Mekler V., Minakhin L., and Severinov K. 2011b. A critical role of downstream RNA polymerase-promoter interactions in the formation of initiation complex. *J Biol Chem.* **286:** 22600-8

Mekler V., Minakhin L., Sheppard C., Wigneshweraraj S., and Severinov K. 2011c. Molecular mechanism of transcription inhibition by phage T7 gp2 protein. *J Mol Biol.* **413:** 1016-27.

Paul, B. J., Ross, W., Gaal, T., Gourse, R. L. 2004. rRNA Transcription in *Escherichia coli. Annu Rev Genet*. **38:** 749-70.

Revyakin, A., Liu C., Ebright, R.H., Strick, T.R. 2006. Abortive initiation and productive initiation by RNA polymerase involve DNA scrunching. *Science* **314:** 1139-43.

Roe, J. H., Burgess, R. R., and Record, M. T., Jr. 1984. Kinetics and mechanism of the interaction of *Escherichia coli* RNA polymerase with the λP_R promoter. *J Mol Biol* **176:** 495–522.

Saecker, R. M., Tsodikov, O. V., McQuade, K. L., Schlax, P. E., Jr., Capp, M. W., and Record, M. T., Jr. 2002. Kinetic studies and structural models of the association of *E. coli* σ^{70} RNA polymerase with the λP_R promoter: Large scale conformational changes in forming the kinetically significant intermediates. *J Mol Biol* **319:** 649–671.

Schneider, D. A., Gaal, T., and Gourse, R. L. 2002. NTP-sensing by rRNA promoters in Escherichia coli is direct. *Proc Natl Acad Sci U S A.* **99:** 8602-7.